Universität Rostock

Traditio et Innovatio

Synthesis and Properties of Ullazine Derivatives

Cumulative Dissertation

To acquire the academic degree

Doctor rerum naturalium (Dr. rer. nat.)

of the Faculty of Mathematics and Natural Sciences

at the University of Rostock

Submitted by Jonas Polkaehn, born on 20.02.1997 in Lübeck

Rostock, 07.08.2024

https://doi.org/10.18453/rosdok_id00005264

The present work was completed in the period from October 2021 to July 2024 at the Institute of Chemistry of the University of Rostock at the Chair of Organic Chemistry in the working group of Prof. Dr. Dr. h. c. mult. Peter Langer.

1. Gutachter: Prof. Dr. Dr. h.c. mult. Peter Langer, Universität Rostock

2. Gutachter: Prof. Dr, Thomas J. J. Müller, Heinrich-Heine-Universität Düsseldorf

Tag der Einreichung: 07.08.2024

Tag der Verteidigung: 03.06.2025

Declaration

1. The opportunity for this doctoral project was not arranged for me commercially. commercially. In particular, I did not contact any organization that seeks supervisors for the preparation of dissertations for a fee, or that performs all or part of the duties incumbent upon me with regard to or partially for me.
2. I hereby declare in lieu of an oath that I have written this thesis independently and without outside help. I have not used any aids or sources other than those specified by me, and I have marked the passages taken from the works used in terms of content and verbatim as such.

Erklärung

1. Die Gelegenheit zum vorliegenden Promotionsvorhaben ist mir nicht kommerziell vermittelt worden. Insbesondere habe ich keine Organisation eingeschaltet, die gegen Entgelt Betreuerinnen/Betreuer für die Anfertigung von Dissertationen sucht oder die mir obliegenden Pflichten hinsichtlich der Prüfungsleistungen für mich ganz oder teilweise erledigt.
2. Ich versichere hiermit an Eides statt, dass ich die vorliegende Arbeit selbstständig angefertigt und ohne fremde Hilfe verfasst habe. Dazu habe ich keine außer den von mir angegebenen Hilfsmitteln und Quellen verwendet und die den benutzten Werken inhaltlich und wörtlich entnommenen Stellen habe ich als solche kenntlich gemacht.

Rostock,

Jonas Polkaehn

Danksagung

Zunächst möchte ich bei Herrn Prof. Dr. h.c. mult. Peter Langer für die Aufnahme in seinen Arbeitskreis, der Bereitstellung dieses interessanten Themas, der benötigten Arbeitsmittel sowie die damit verbundene Möglichkeit diese Arbeit anzufertigen, bedanken.

Meinen besonderen Dank spreche ich Herrn Dr. Peter Ehlers für die Betreuung bei den durchgeführten Projekten und für die Hilfestellungen beim Auftreten von Problemen aus.

Zusätzlich möchte ich mich bei allen anderen Mitarbeitern von Prof. Langer bedanken. Dr. Holger Feist und Dr. Martin Hein danke ich für diverse Tipps und Hilfestellungen bei den durchgeführten Labortätigkeiten. Jana Unger, Maximilian Quasdorf, Alexander Klotzek und Adelgunde Fifelski danke ich für die Unterstützung bei und neben der Labortätigkeit.

Den Kollegen der Analytischen Abteilungen der Universität Rostock sowie des Leibniz Instituts für Katalyse möchte ich für das Vermessen der zahlreichen Proben danken.

Des Weiteren gilt mein Dank den Doktoranden von Prof. Dr. h.c. mult. Peter Langer sowie dem Fachbereich der Organischen Chemie für das harmonische Miteinander und die angenehme Arbeitsatmosphäre. Besonderen Dank möchte ich hierbei Ricardo Molenda und Franziska Spruner von Mertz, für die Zusammenarbeit an diversen Projekten und Publikationen, entgegenbringen. Fortsetzend möchte ich mich bei Richard Thom bedanken, der während seiner Masterarbeit unter meiner Aufsicht einen wesentlichen Beitrag zu dieser Arbeit liefern konnte.

Außerdem möchte ich mich bei allen meinen Freunden, meiner Familie insbesondere meiner Schwester und meinen Eltern für den Rückhalt, die Unterstützung und den Zusammenhalt in schweren Zeiten bedanken.

Aus tiefsten Herzen möchte ich zuletzt meiner Freundin Anna für ihre Unterstützung, Geduld, Zuspruch und Rückhalt danken.

Vielen Dank!

Summary

This thesis regards the synthesis, characterization and investigation of the properties of novel ullazine derivatives. The initial focus was on the synthesis of the molecules and the optimization of the individual synthesis steps. Various modifications such as substitution, π-expansion and nitrogen doping were used. The new structures were examined using UV-vis spectroscopy, cyclic voltammetry and calculations *via* density functional theory. On the one hand, the focus was on evaluating the substitution pattern of the final products. On the other hand, the influence of the modifications was assessed and compared with ullazine structures already known from the literature.

Zusammenfassung

Die vorliegende Arbeit beschäftigt sich mit der Synthese, Charakterisierung und Untersuchung der Eigenschaften neuartiger Ullazin-Derivate. Der Schwerpunkt lag zunächst auf der Synthese der Moleküle sowie der Optimierung der einzelnen Syntheseschritte. Dabei kamen verschiedene Modifikationen wie Substitution, π-Expansion und Stickstoffdotierung zum Einsatz. Die neuen Strukturen wurden mit Hilfe von UV-vis-Spektroskopie, Zyklovoltammetrie und Berechnungen mittels Dichtefunktionaltheorie eingehend untersucht. Dabei lag der Schwerpunkt einerseits auf der Bewertung des Substitutionsmusters der Endprodukte, anderseits wurde der Einfluss der Modifikationen eingehend mit bereits aus der Literatur bekannten Ullazin- Strukturen verglichen und analysiert.

Table of Contents

List of abbreviations

ACM	alkyne-carbonyl-metathesis
AcOH	acetic acid
Ar	aryl-group
ATR	attenuated total reflection
cataCXium A	Di-(1-adamantyl)-*n*-butylphosphin
Cp*	1,2,3,4,5-Pentamethylcyclopentadiene
CV	cyclic voltammetry
DCE	1,2-dichloroethane
DCM	dichloromethane
DDQ	2,3-dichloro-5,6-dicyanobenzoquinone
DFT	Density-functional theory
DIPEA	*N*,*N*-diisopropylethylamine
DMA	*N*,*N*-Dimethylacetamide
DMF	*N*,*N*-Dimethylformamide
DMP	Dess–Martin periodinane
DMSO	dimethyl sulfoxide
dppm	Methylenebis-(diphenylphosphane)
Et	ethyl-group
Et_2O	diethyl ether
EWG	electron withdrawing group
et al.	*et alii/aliae*
eq.	equivalents
HOMO	highest occupied Molecular orbital
*i*Pr	*iso*-propyl-group
IR	Infrared
ICT	intramolecular charge transfer
LED	light-emitting diode
LUMO	Lowest unoccupied molecular orbital
m	*meta*
Me	methyl-group
MeCN	acetonitrile
MeOH	methanol
Mes	mesityl-group
n-BuLi	*n*-butyllithium
NMR	nuclear magnetic resonance
NTOs	natural transition orbitals
o	ortho
OAc	acetoxy-group
OTf	triflate-group
OMe	methoxy-group
p	para
Ph	phenyl-group
PL	Photoluminescence
*p*TsOH	*p*-Toluenesulfonic acid
R	organic residue
Rho-6G	rhodamine 6G
rt	room temperature
*t*Bu	*tert*-butyl-group
TFA	trifluoroacetate-group
TFAA	Trifluoroacetic anhydride
THF	tetrahydrofuran
TMEDA	tetramethyl ethylenediamine
Tol	tolyl-group
UV-vis	Ultraviolet–visible

1 Introduction

Polycyclic aromatic hydrocarbons (PAHs) constitute a class of organic compounds prevalent in the environment due to natural and anthropogenic activities.[1,2] Natural sources include combustion processes, such as wild fires and volcanic eruptions, while anthropogenic sources are combustion processes during waste incineration, fuel combustion or other industrial processes, which is why they are often regarded as environmental pollutants.[1–5]

In recent decades, PAHs have garnered substantial interest in materials science.[6–8] The compounds are characterized by multiple fused aromatic rings, forming planar structures with delocalized π-electrons. This unique feature imparts PAHs with high thermal stability, strong UV and visible light absorption, and distinct electronic properties.[9–11] Consequently, PAHs are highly demanded for applications in organic electronic devices such as organic light emitting diodes (OLEDs)[8,12,13] organic field effect transistors (OFETs)[8,14,15] and organic photovoltaics.[8,13,16]

Organic synthesis focuses intensively on preparing these systems and precisely modifying their optoelectronic properties through methods like substitution or expansion.[10,17] Another effective approach to customize their optical and electronic characteristics involves incorporation of heteroatoms such as nitrogen, oxygen, boron, and sulfur.[18–20] This modification can control the energy levels of frontier orbitals, stabilize charges and radicals, impact the energy gap, optical characteristics, and redox behavior.[17–19,21,22] Nitrogen is particularly effective as a dopant due to the ease of synthesis and the resulting chemical stability of N-doped PAHs.[20,23] Furthermore, nitrogen doping enhances electron features such as charge transfer properties, while the molecular structure of the PAH can be preserved .[18] Therefore, nitrogen-containing PAHs are highly demanded for applications in organic electronic devices.[24]

1.1 Ullazine

Indolizino[6,5,4,3-*ija*]quinoline (ullazine) is such a representative of a nitrogen doped hetero-PAH, that consists of four condensed rings with 16-π electrons, thus it is isoelectronic to pyrene (Figure 1).[24] Unlike pyrene, ullazine contains an internal, iminium like nitrogen which leads to structural modification.[20] Instead of a benzene ring, ullazine has a five-membered pyrrole ring in its backbone. Besides the structural alteration, the nitrogen donates electron density, forming an electron-accepting iminium center surrounded by an electron-donating annulene.[24] The planar π-system with push-pull properties, which are extensively modifiable, makes ullazine highly attractive for use in organic electronic devices, particularly in dye-sensitized solar cells (DSCs).[24,25]

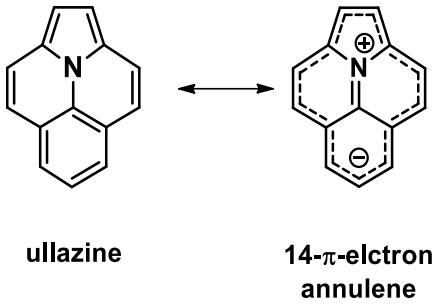

Figure 1: Ullazine with the 14-π resonance structure.

1.1.1 Synthesis

Balli and Zeller first synthesized ullazine in 1983 while searching for new donor systems for organic dyes (Scheme 1).[26] Starting from known Ester **1** they carried out a CLAUSSON-KAAS reaction to form a pyrrole-ring (**2**).[27] Reduction of the Ester (**2**) with $LiAlH_4$ followed by a reaction with PBr_3 gave brominated **4**. Nucleophilic acylation with various substituted 1,3-dithianes gave compound **5**, which was hydrolyzed with $HgCl_2$ in $MeOH/H_2O$, resulting in double ring closure to form ullazines (**6**). The yields depended highly on the introduced residue. While the unsubstituted product was obtained in 30% yield, the introduction of an alkyl chain led to lower yields. Best result gave Ph-substituted **6** with 75%. Due to the fact that **1** is not commercially available nowadays, the sequence would be extended to nine reaction steps with an expected total yield of 19%.[24]

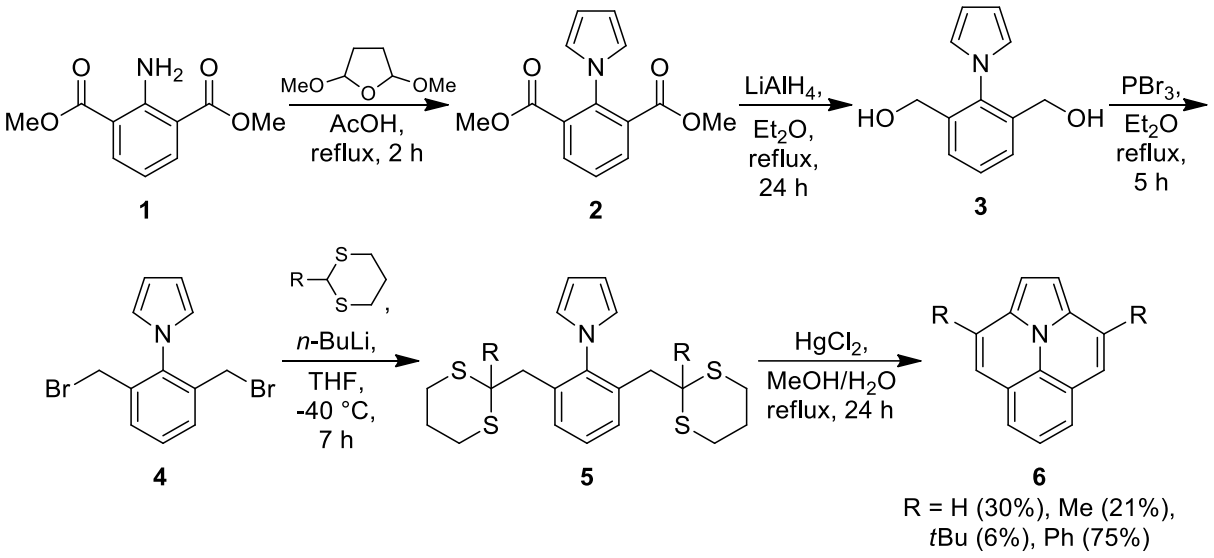

Scheme 1: Initial synthesis of ullazine by Balli and Zeller.

The approach of Takashi's working group from 2005 involves a stepwise construction of the ullazine scaffold. First, a lithiation of the phenylpyrrole (**7**) with a subsequent benzannulation reaction with hex-3-yne and $CrCl_3$ was performed to synthesize the pyrroloquinoline **8** (Scheme 2).[28] The transformation into the ullazines (**9**) was achieved in a similar manner using a variety of alkynes. The yields ranged from 39% for *tetra*-ethyl-ullazine to the best yield of 55% for the Ph-substituted derivative.

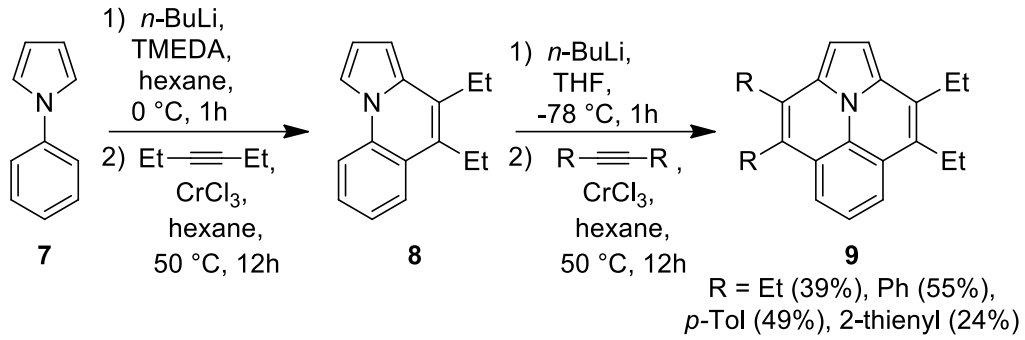

Scheme 2: Synthesis of ullazines by the working group of Takahashi in 2005.

A more convenient method with a good overall yield of 55% was established by the Gräzel group in 2013.[24] First, dibromoaniline (**10**) was converted into **11** *via* CLAUSSON-KAAS reaction, followed by functionalization with terminal alkynes using SONOGASHIRA reaction. The final step was promoted by LEWIS-acid mediated intramolecular cycloisomerization, forming **13** in 80% yield. The simple implementation is the reason why this method has since become the predominant approach for synthesizing ullazine structures.[29–33]

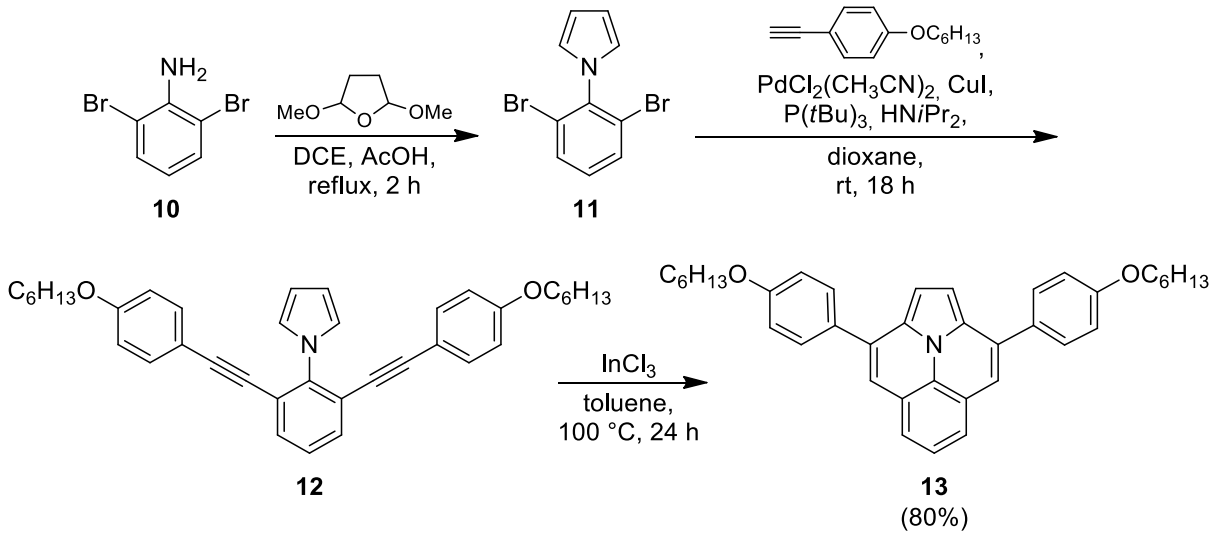

Scheme 3: Synthetic approach by the working group of Grätzel.

You's group and the group of König independently reported a one pot synthesis of ullazines starting from **11** in 2016, since Grätzel's methodology requires an additional reaction step (SONOGASHIRA reaction).[34,35] You's approach employed Pd-catalyzed direct C-H cyclization with diverse alkynes (Scheme 4).[34] Remarkably, this reaction exhibits tolerance towards a diverse array of functional groups, yielding ullazines in the range between 27% and 80% (some examples are displayed in Scheme 4).

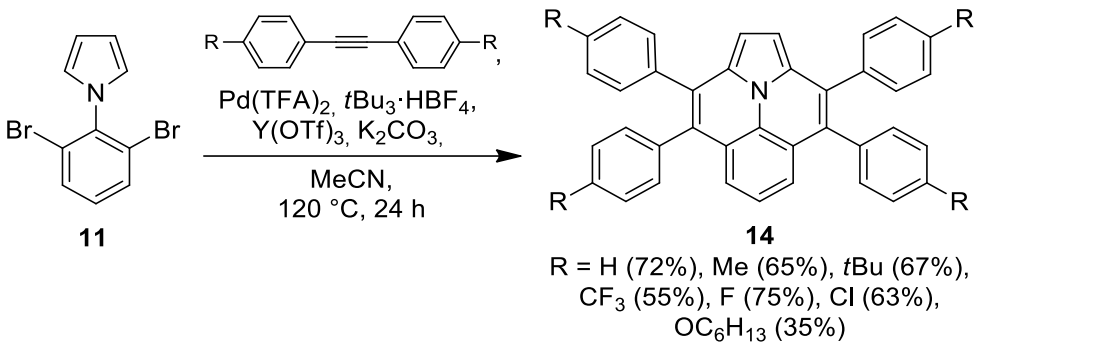

Scheme 4: Palladium-catalyzed direct C−H cyclization by the working group of You.

Moreover, König and colleagues pioneered the first photocatalytic synthesis of ullazines, employing Rho-6G as the photocatalyst (Scheme 5).[35] Despite yielding **15** at a moderate range of 30% - 45%, the synthesis stands out for the absence of transition metal catalysts, strong bases, ligands and high temperatures.

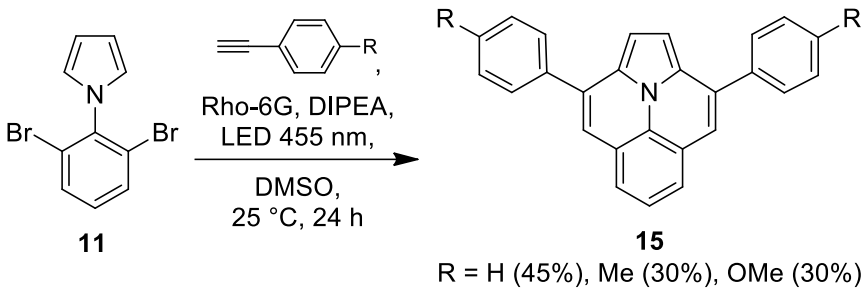

Scheme 5: Photocatalytic synthesis of ullazines by the working group of König.

Recently, the working group of Zhou demonstrated a Rh-catalyzed synthesis.[36] Similar to the approach of Takahashi, the ullazine is assembled in two steps. Initially, a Rh-catalyzed intramolecular annulation of aromatic *o*-alkynyl amino ketones (**16**) was executed, yielding the intermediate pyrroloquinoline (**17**). The ullazine core (**21**) was completed through a Rh-catalyzed oxidative annulation of diphenylacetylene, demonstrating good yields regardless of the substituents on the pyrroloquinoline (**17**).

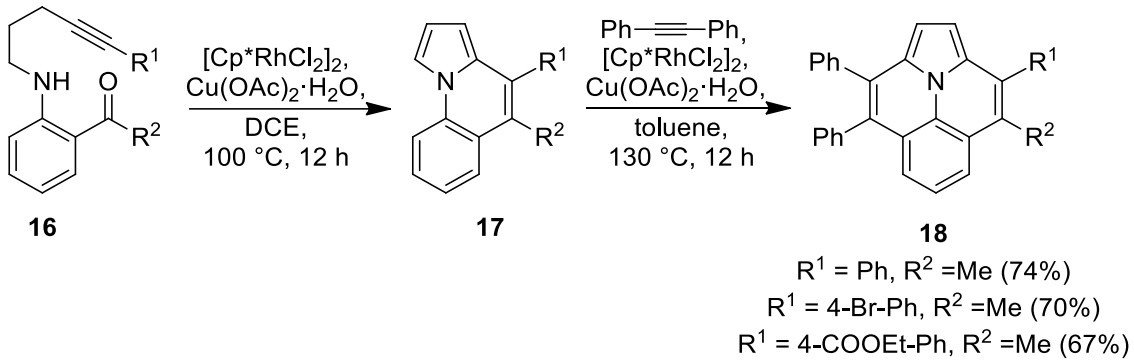

Scheme 6: Rhodium catalyzed synthesis of ullazines by the working group of Zhou.

In 2024, the working group of Saá developed a Rh-catalyzed construction of ullazines in one step starting from phenyl-pyrroles (**19**) (Scheme7).[37] Twofold CH-activation/oxidative annulation of **19** provides the ullazines (**20**) in yields around 60%, a remarkable efficiency for constructing the ullazine core in one step starting from phenylpyrroles.

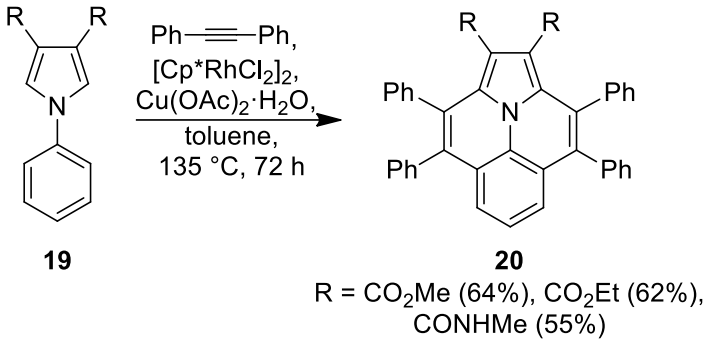

Scheme 7: Rhodium catalyzed synthesis of ullazines by the working group of Saá.

1.1.2 Properties

Among all ullazines, 3,9-diphenylullazine (**21**) is characterized by a minimal degree of substitution and it's properties have been extensively investigated (Figure 2).[26,29,32,38] Easy accessible *via* the synthesis route of Grätzel, the final cyclization is promoted in up to 90% yield.[29,32,38]

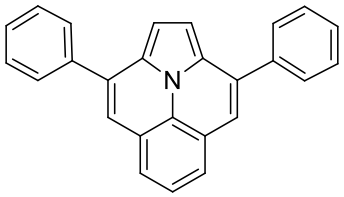

21

Figure 2: 3,9-diphenylindolizino[6,5,4,3-*ija*]quinoline (3,9-diphenylullazine)

Investigation on the optoelectronic properties of **21** with UV-vis and PL spectroscopy as well as CV measurements were performed by the groups of Nazeerudin[29], Gros[32] and Liu[38]. The combined data are provided in Table 1.

Table 1: Combined spectroscopic data of **21**.

compound	UV-vis/fluorescence			CV	
	$\lambda_{abs.}$[a] [nm]	$\lambda_{em.}$[a] [nm]	Θ_{PL}[c]	$E_{Ox.}$ [V]	$E_{Red.}$ [V]
21	291, 374[b], 391, 440[b]	478[b], 513, 553[b]	0.19	0.75	-2.22
[a] measured in cyclohexane; [b] indicated as shoulder; [c] measured in DCM					

The absorption of **21** is characterized by a strong absorption band in the range of 250-300 nm, which is attributed to a π-π^*-transition.[29] Furthermore, a more structured low-energy band is apparent at 350-400 nm. Gros's working group performed DFT calculations on the transitions.[32] The associated NTOs reveal that this $S_0 \rightarrow S_2$ excitation is a local π-π^*-transition as well. However, the $S_0 \rightarrow S_1$, indicated as shoulder at 440 nm, featuring a rearrangement of the electron density and a very low oscillator strength, which reflects the low absorption very

well. Furthermore, the HOMO of **21** is delocalized around the periphery, whereas the LUMO is located on the central nitrogen and carbon atoms.[24,32] The emission spectrum of **21** exhibits a structured profile, which is corresponding to the $S_1 \rightarrow S_0$ transition.[32] The quantum yield is rather moderate with 19%.[38] Nazeerudin's working group furthermore studied the solvatochromic properties of **21** and found that no significant effects, such as bathochromic/hypsochromic shifts and change in fine structure, occurred with increasing polarity of the solvents (cyclohexane, THF and acetonitrile) (Figure 3).[29] During CV measurements **21** shows a distinct oxidation peak at 0.75 V as well as a reduction peak at -2.22 V.[29]

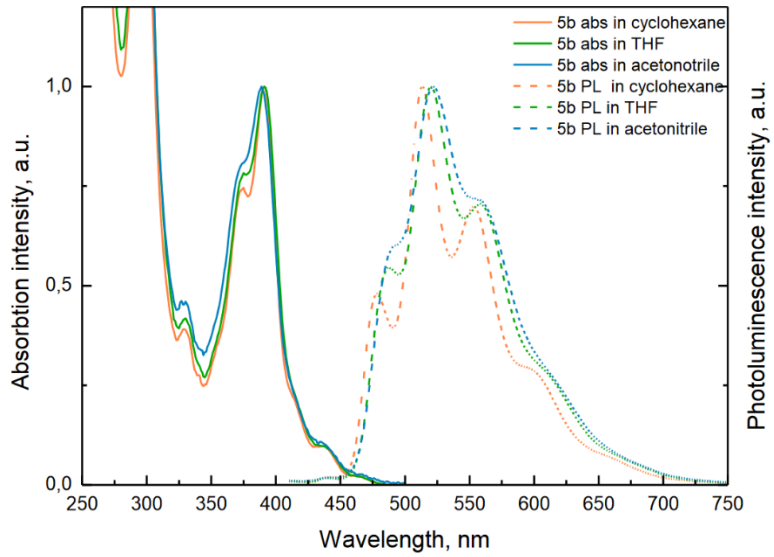

Figure 3: UV-vis (solid) and fluorescence (dashed) spectra normalized at peak value of **21** (equals **5b**) in cyclohexane, THF and acetonitrile. Reprinted from supporting information of Ref. [29] with permission from Prof. Nazeerudin.

1.2 Modifications of Ullazine

The ullazine core itself provides fascinating properties, in the last decade modifications of this hetero-PAH gained interest, since the possibility of application in organic electronics was reported in 2013 by Grätzel's group.[24] Various molecular designs of ullazines are accessible through different synthetic strategies, resulting in diverse modification possibilities that lead to an improvement of the optoelectronic properties and various applications.[25]

1.2.1 Substitution pattern

Most ullazines are constructed starting from phenylpyrroles.[24,26,28,34,35] Due to benzannulation reactions in the final step, substitution with aryl residues in 3,9- or/and 4,8-position are common. Those substituents hardly effect the properties of the ullazine core. However, substitution in 3,9-position increases the stability of the molecules as shown by Gerson and Metzger.[39] The nomenclature of the substitution positions is displayed in Figure 4.

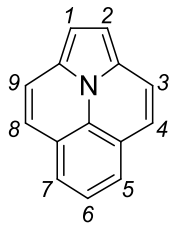

ullazine

Figure 4: Substitution positions on the ullazine core.

Moreover, simple functionalization can be implemented through the use of substituted phenylpyrroles.[30,32] Thus, substitutions in position 6 are easy accessible by using *para*-substituted phenylpyrroles.[29,30,32,34] In addition to various substituents such as Ph, Me, OMe, CN, CF_3, and others, halogens can be introduced in this position, allowing for subsequent cross-coupling reactions.[24,29,32,34] Due to the fact that position 6 lies in the nodal plane of the ullazine, the introduced residues only have a minimal influence on the properties, making this type of substitution less significant.[24,29,30,32]

Utilizing substituted 2,5-dimethoxytetrahydrofuran offers the possibility to functionalize the pyrrole unit during the CAUSSON-KAAS reaction. In this way 1-formyl-ullazine (**24**) can be isolated after the final cyclization in good yield (Scheme 8).[29]

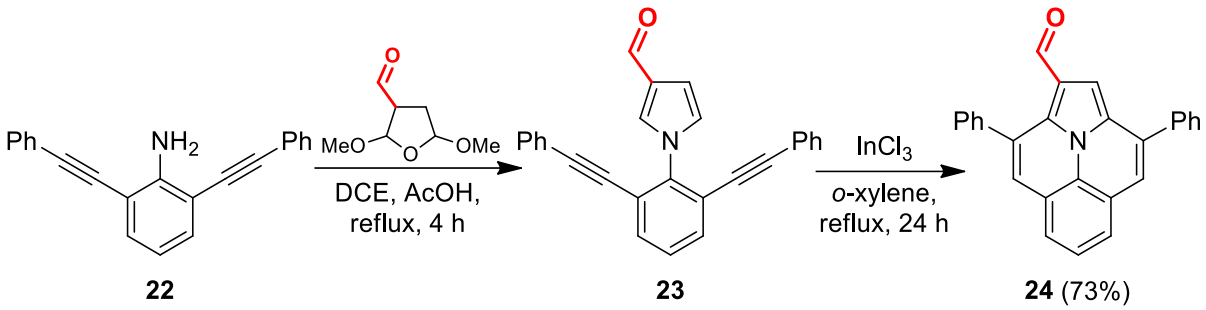

Scheme 8: Synthesis of 1-formyl substituted ullazine.

In addition to pre-functionalization, it's possible to functionalize the existing ullazine core through the reaction with electrophiles. Using the VILSMEIER-HAACK reaction, substitutions in the 1-, 4- and 5-position can be achieved.[24,29,34] The reaction produces a mixture of three isomers in which the 5-formyl-ullazine (**26**) is the major product (Scheme 9).[29] Additionally, isomer **24** is obtained in moderate yields.

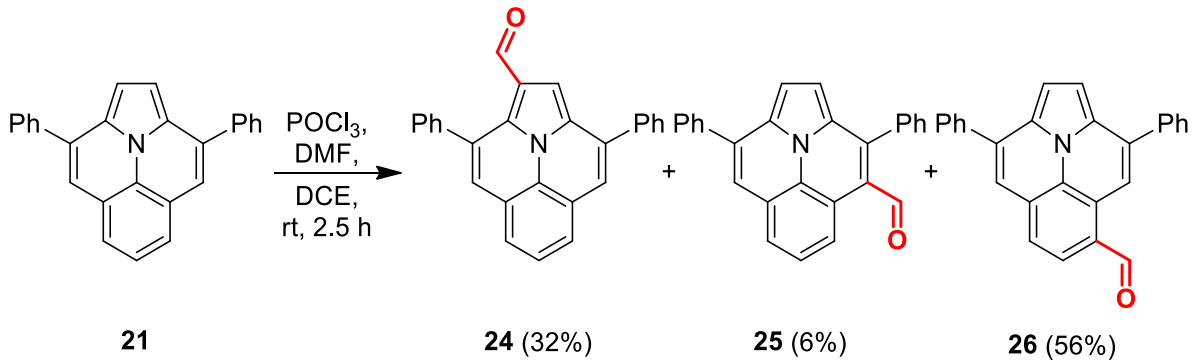

Scheme 9: Isomers of VILSMEIER-HAACK reaction for **21**.

Isomer **25**, on the other hand, delivers a very unsatisfactory yield, therefore the synthesis can be carried out by means of an iodocyclization yielding **28**, which is transformed into the formylated **29** and then cyclized to 4-formyl-ullazine (**26**) in very good yield (Scheme 10).[29,30,40] In addition to conversion into a formyl group, the iodine can be replaced by acceptor- or donor-bearing aryl and aryl-ethynyl moieties by cross-coupling reactions, such as SONOGASHIRA and SUZUKI-MIYAURA, as well as into a cyano-group *via* ROSENMUND-VON-BRAUN reaction as shown by the group of Chan.[30]

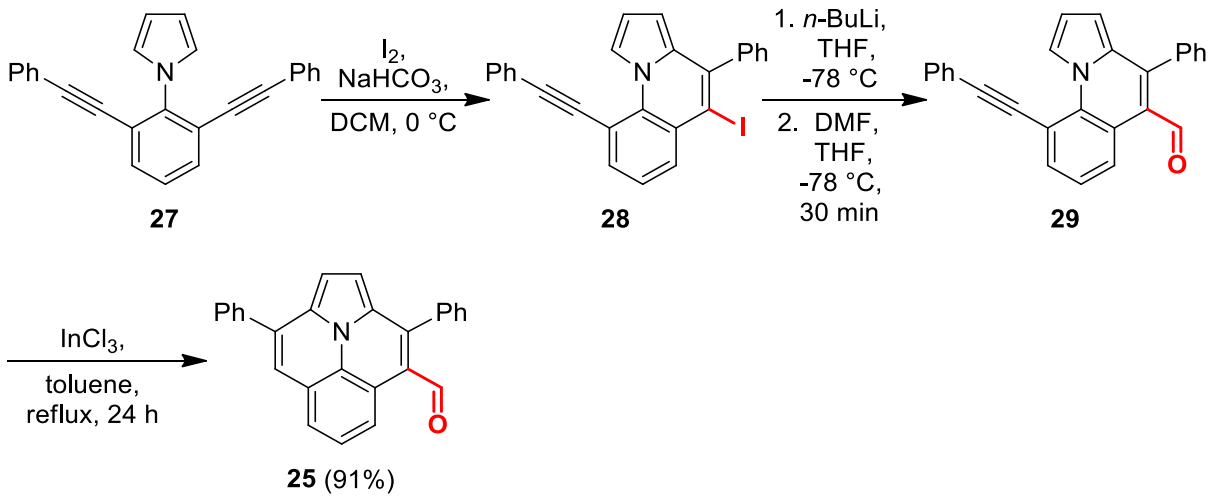

Scheme 10: Synthesis of 4-formyl substituted ullazine.

The group of Nazeerudin analyzed the impact of the substitution positions on the ullazine core in detail. For this purpose, they converted the isomers **24-26** into the acceptor-substituted products **30-32** *via* KNOEVENAGEL condensation (Scheme 11).[29] The Ullazine **31** shows similar absorption bands as **21**, however the ICT shoulder has stronger absorption values. Dyes **30** and **32** have weaker π-π*-transitions and a stronger and broadened ICT band, bathochromic shifted by 30 nm (**30**) and 80 nm (**32**) respectively. The energies of the ICT bands are in accordance with the expected electron donation strength on the different peripheral sites of the ullazine core, with position 5 being the strongest, followed by 1-, 4- and 6-position.[24,29] PL spectra revealed vibronic structures for **30** and **32** similar to **21**, however **31** is broadened. While the maxima of **31** and **32** are red shifted compared to **21** (~15 nm), the maximum of **30** is blue shifted by 10 nm. Electrochemically, attachment of the acceptor stabilizes the HOMO level of **30-32** by 100–200 mV, correlating with their photophysical data.[29]

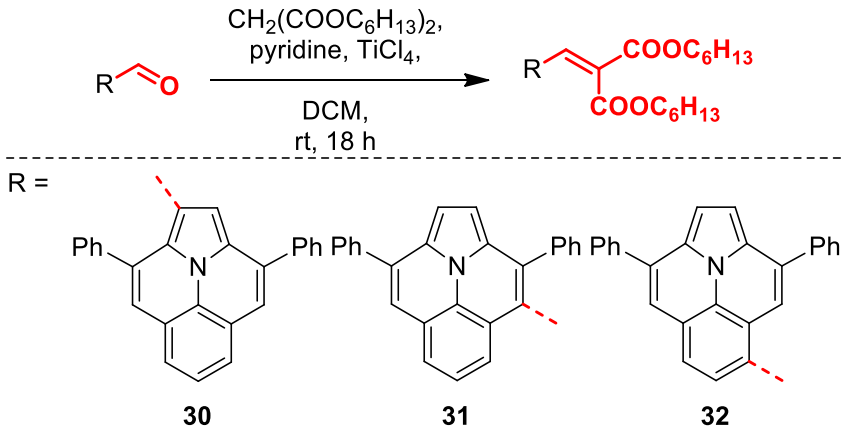

Scheme 11: Synthesized substituted ullazine dyes by the group of Nazeerudin.

These investigations demonstrate how substitution patterns influence the optical and electronic properties of ullazine, highlighting the potential for acceptor substitution in 5-position of the ullazine. Therefore, this position is widely used to modify the properties of ullazine.[24,34,41–43] Examples of those are displayed in Figure 5.

The absorption spectra of the 5-substituted-ullazines with the residues **33-37** show a strong absorption band similar to **21** in the range of approx. 300 nm, which can be attributed to a π-π* transition.[42] Moreover, all spectra display a lower energy band between 400 and 600 nm (λ_{abs} = 530 nm (**33**); λ_{abs} = 480 nm (**34**); λ_{abs} = 490 nm (**35**)), attributable to an ICT between the ullazine donor and the respective acceptor. The hypsochromic shift of **34** and **35** compared to **33** was explained by the double bonds within the π-spacers (thiophene and benzene) as well as the weaker acceptor properties of the carboxylic acid compared to the cyanoacrylic acid. Notably, compared to **21**, the absorption maxima experience a bathochromic shift, furthermore all compounds exhibit a distinct red shift of the PL maxima (λ_{abs} = 638 nm (**33**); λ_{abs} = 583 nm (**34**); λ_{abs} = 614 nm (**35**)). Ullazine with residue **36** exhibits analogous characteristics. In contrast to compound **33**, the introduction of alkyne-cyclopentadithiophene moieties resulted in broadened and bathochromic shifted absorption spectra with particularly strong absorption in the high energy region. Again, the first transition is described by an ICT between donor and acceptor entities with a maximum at 549 nm.[43]

The characteristic of the absorption spectrum of the molecule with the porphyrin substituent (**37**) is rather characterized by the absorption of the porphyrin itself, a comparison with **21** is therefore difficult.[41] However, the ullazine donor showed an improvement in visible light absorption compared to a related porphyrin structure.

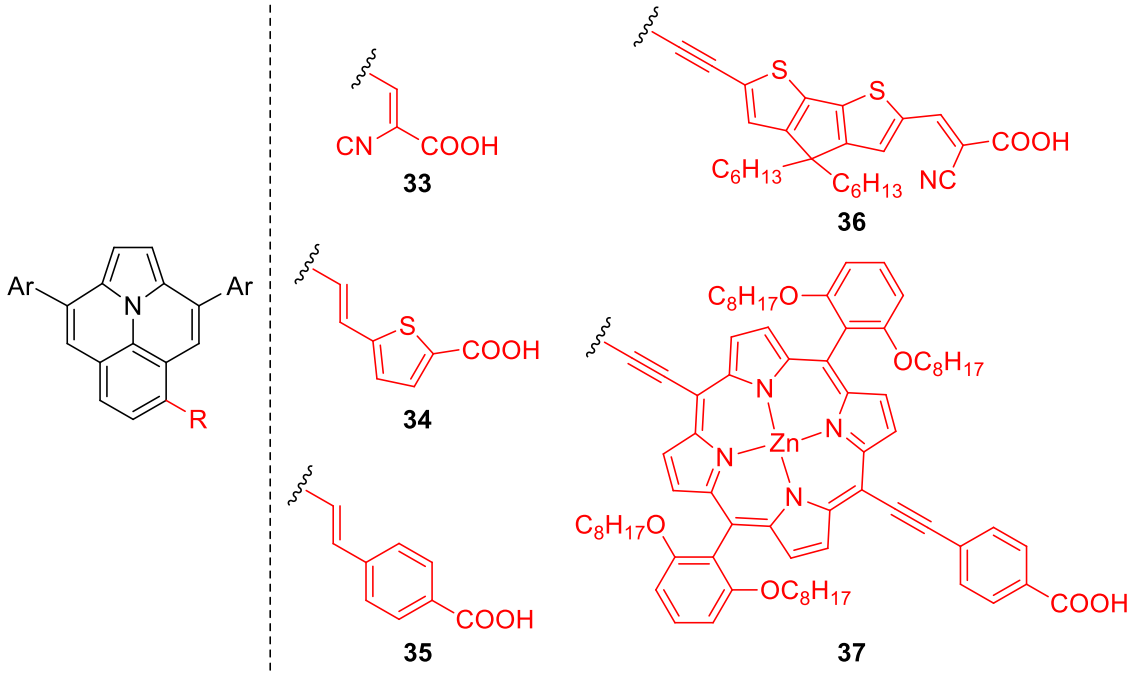

Figure 5: Examples of substituents in position 5 of the ullazine for the application in organic devices.

Based on these optical properties, such donor-acceptor molecules are of great interest for applications in organic electronic devices.[25,44] These push-pull systems exhibit unique optoelectronic properties due to their low energy charge transfer.[45] Accompanied by bathochromic shifts, the increased light-harvesting efficiency is particularly valuable for applications in DSCs.[44,45] In this manner these ullazines are of high interest for such applications, as the introduction of acceptor in 5-position is easily accessible.[24,25,34,41–43,46,47] Some of the presented examples in Figure 5 show great performance in DSCs (**33**, **36** and **37**) (Table 2).[24,41,43]

Besides several theoretical studies on the DSC performance of ullazine based dyes,[48–50] the working group of Grätzel was the first to use ullazines as dyes for DSCs.[24] Despite testing 4-, 5-, and 6-substituted ullazines, the 5-substituted ullazines proved to be the most promising. On the one hand, 4-substituted ullazines have a significantly decreased ICT band which was attributed to the loss of planarity due to the substituent in this position. On the other hand, substitution at the 6-position has a negligible effect due to the nodal plane, as discussed earlier. In Grätzel's study dye **33** achieved the best performance among the 5-substituted ullazines with an incident photon-to-electron conversion efficiency (IPCE) ranging from 400 nm to 730 nm with a maximum of 95% at 520 nm. However, the IPCE range of **33** is broader compared to its absorption in dichloromethane, suggesting aggregation within the device. The performance of dye **33** is characterized by a power conversion efficiency (PCE) of 8.4%, a short circuit current

density (J_{sc}) of 15.4 mA cm^{-2}, an open-circuit voltage (V_{oc}) of 730 mV, and a fill factor (FF) of 0.75 (Table 2). Furthermore, the performance of dye **33** was tested in a solid-state DSC.[46] However, the PCE only achieves a value of 4.2% in this case.

Delcamp's group synthesized a variety of novel ullazine-based dyes featuring an alkyne linker between the donor and acceptor, forming D-π-A-systems.[43]. The stronger absorption in the high energy bands are of particular interest, as improved DSC performance can be attributed to the enhanced absorption.[51] Among the studied dyes, **36** demonstrated the best performance. Achieving a broad IPCE spectrum between 350 nm and 800 nm with a peak value of 65% at approximately 530 nm. The PCE was determined at 5.6%, with a V_{oc} of 559 mV, a J_{sc} of 14.1 mA cm^{-2} and a FF of 0.67.

As previous mentioned, the group of Grätzel worked on an ullazine-porphyrin dye **37**.[41] The dye exhibits improved absorption of green (~550 nm) and red (>700 nm) light compared to other D-π-A-porphyrin dyes, highlighting the significant impact of the ullazine moiety. Thus, the IPCE is at 60-65% between 360 nm and 760 nm with a dip to 55% at 600 nm. The DSC performance showed slightly diminished PCE of 7.4% compared to a dimethylaniline-porphyrin dye (PCE = 8.5%). This reduction was attributed to significant aggregation in solution due to its large aromatic structure.

Table 2: DSC performance of selected ullazine dyes.

Compound	V_{OC} [mV]	J_{SC} [mA cm^{-2}]	FF	PCE [%]
33[24]	730	15.4	0.75	8.4
33 (solid-state)[46]	743	8.5	0.66	4.2
36[43]	559	14.1	0.67	5.6
37[41]	700	14.4	0.73	7.4

1.2.2 Heteroatom doping

Heteroatom doping is a common tool for modification of PAHs. In this context nitrogen is by far the most commonly used heteroatom.[18,20,52] Especially, pyridine-like nitrogen is of interest because it can be introduced into the molecules without changing the structure, but improves the optical and electronical properties.[18,23,53,54] Consequently, nitrogen is the most common heteroatom incorporated into the ullazine backbone (Figure 6).[31–33,55–62] For the sake of clarity, only the synthesis of the Ph-derivatives is presented below, although significantly more derivatives were produced.

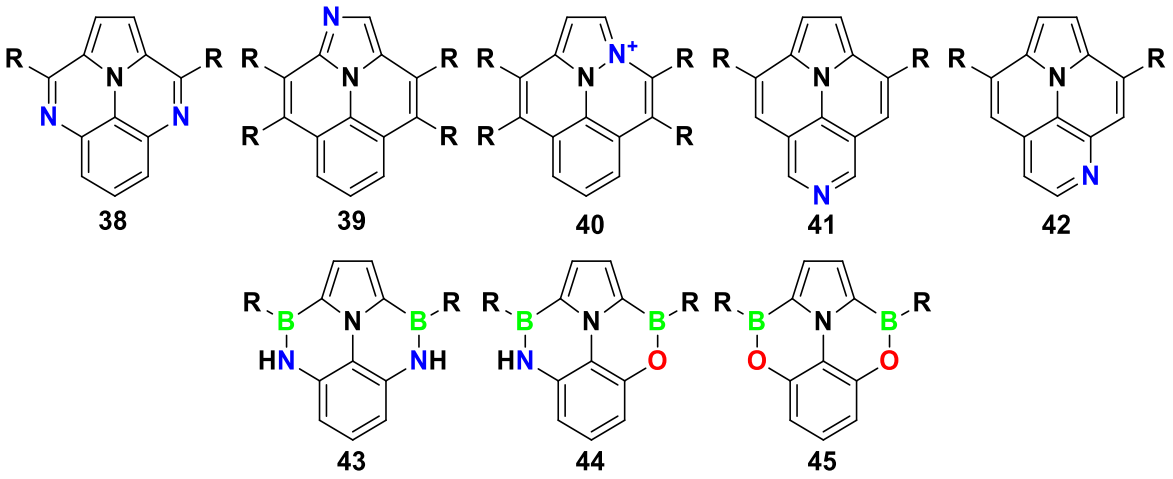

Figure 6: Overview of heteroatom-doped ullazines.

Balli and his coworker Hou were the first, who synthesized a nitrogen doped ullazine (**38**) in 1992 (Scheme 12).[55] Starting from **46** they performed CLAUSSON-KAAS reaction to form 1-(2,6-dinitrophenyl)-1*H*-pyrrole (**47**). The nitro-groups were converted into amines using RANEY-nickel and hydrazine hydrate. The amide **49** was then synthesized through the conversion with benzoyl chloride and pyridine. Cyclization was achieved with polyphosphoric acid in the final step with moderate yields of the 4,8-diazaullazine (**50**).

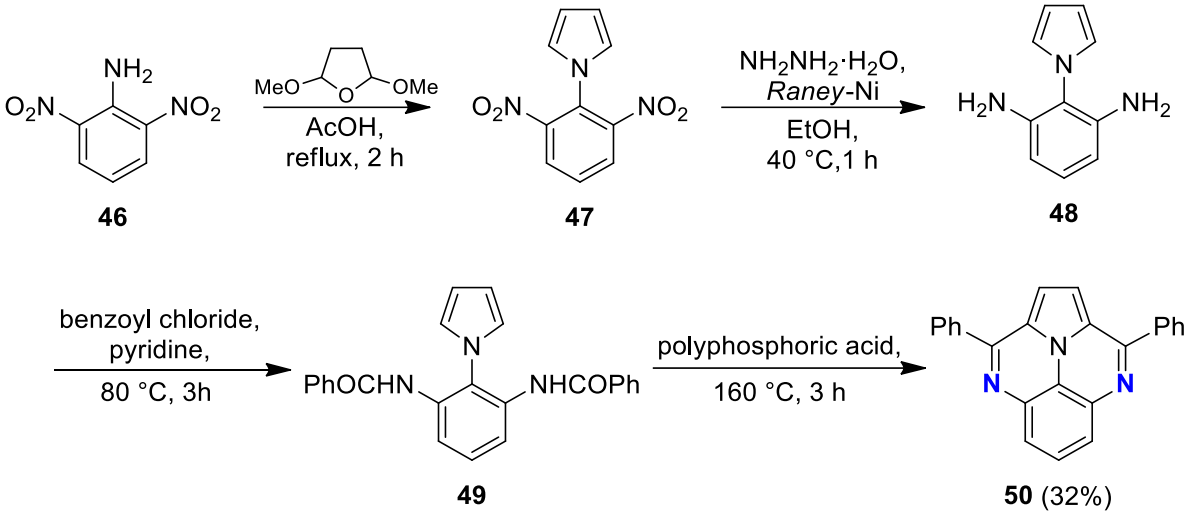

Scheme 12: Synthesis of 4,8-diazaullazine by Balli and Hou.

As the reaction gave an overall yield of 14% for **50**, Sanz and coworkers in 2017 reported an improved synthesis (Scheme 13).[56,59] Using the same starting material as Balli, the conversion of **47** into **50** was performed with secondary glycol (**51**) under Mo-catalysis in one step with a yield of 50%. However, the influence of nitrogen doping on the optoelectronic properties was not investigated by either group.

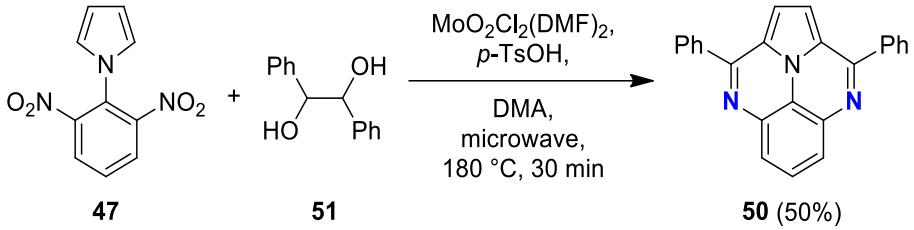

Scheme 13: Synthesis of 4,8-diazaullazine by the group of Sanz.

With the use of phenyl-imidazole (**52**), the groups of Tang and Wang implemented a nitrogen in 1-position of the ullazine (Scheme 14). Therefore, they used a Rh-catalyzed CH-activation similar to Saá's approach (Scheme 7).[57,58] 1-Azaullazine (**53**) has quiet similar optical properties as **21**.[57] Thus, the quantum yields have the same value ($\Theta_{PL} = 0.19$ (**53**)), the emission and absorption spectra exhibit similar fine structures only with a small blue shift of about 10 nm for **53**. Furthermore, the researchers explored the potential impact on optical properties through protonation of the peripheral nitrogen, resulting in a blue shift of absorption and emission spectra (~30 nm). Additionally, structures featuring imidazolium salts and polymers containing this structural motif are documented.[58,60–62]

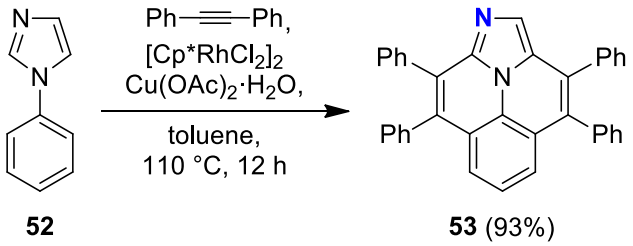

Scheme 14: Synthesis of 1-azaullazine by the groups of Tang and Wang.

The groups of Macgregor and Davies investigated the synthesis of cationic ullazine **55** (Scheme 15).[63] Therefore, they extended the synthesis of pyrazoloquinoline **54**, which was already synthesized by the groups of Sato and Miura, by a Rh-catalyzed oxidative coupling of phenylpyrazole (**54**) with diphenylethyne.[64] The construction of the ullazine core in the final step was accomplished through the same method: a Rh-catalyzed CH-activation of diphenylethyne incorporating a C-N-coupling. In the final step **56** was produced in moderate yields. However, studies on the properties were not conducted.

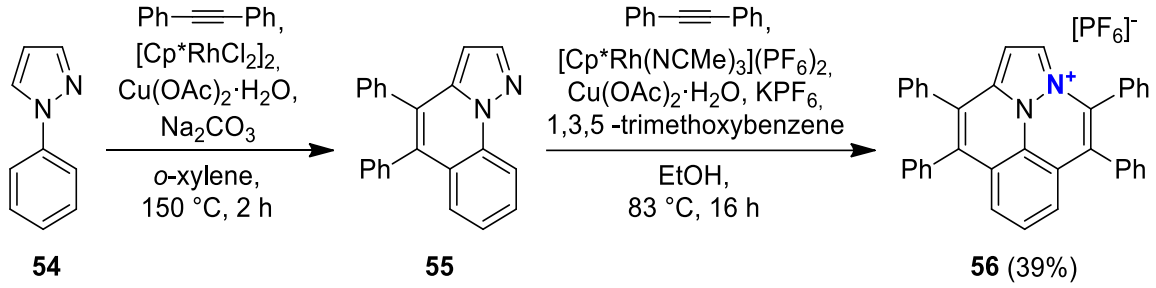

Scheme 15: Synthesis of cationic azaullazine by the groups of Macgregor and Davies.

The groups of Langer (**41** and **42**) and Gros (**41**) were able to introduce an additional nitrogen into the ullazine backbone by starting with halogenated amino-pyridines (**57**).[31–33,65] Synthesis-wise they used the protocol of Grätzel (Scheme 3), however the group of Langer used BRØNSTED- instead of LEWIS-acids in the final step (Scheme 16).[31,33] Furthermore, they were able to synthesize asymmetrically substituted **61** by means of an ACM reaction in the final step.[65] Compared to **21**, the introduction of nitrogen in position 6, as in **59**, has hardly any effect on the optical properties as the nitrogen is located in the existing nodal plane. However the quantum yield is remarkably lower ($\Theta_{PL} = 0.07$).[32] Computational studies revealed stabilization of the HOMO and LUMO energies with introduction of nitrogen.[33] This stabilization is even more enhanced when introducing the nitrogen in 5-position. Moreover, there is a greater influence on the optical properties. Thus, **60** has a blue shifted and different shaped emission as well as higher quantum yield ($\Theta_{PL} = 0.27$) than **21** and **59**.[31,33] The asymmetrically substituted 6-azaullazine (**61**) exhibit a similar quantum yield ($\Theta_{PL} = 0.08$) but

red shifted emission compared to its symmetrical counterpart **60** and undoped ullazine **21**. Nitrogen doping in the 6-position, like substitution, has only a minor influence on the optical properties, whereas a change in the nodal plane due to non-symmetric substitution or the incorporation of a nitrogen outside this plane leads to a significant alteration of the properties.

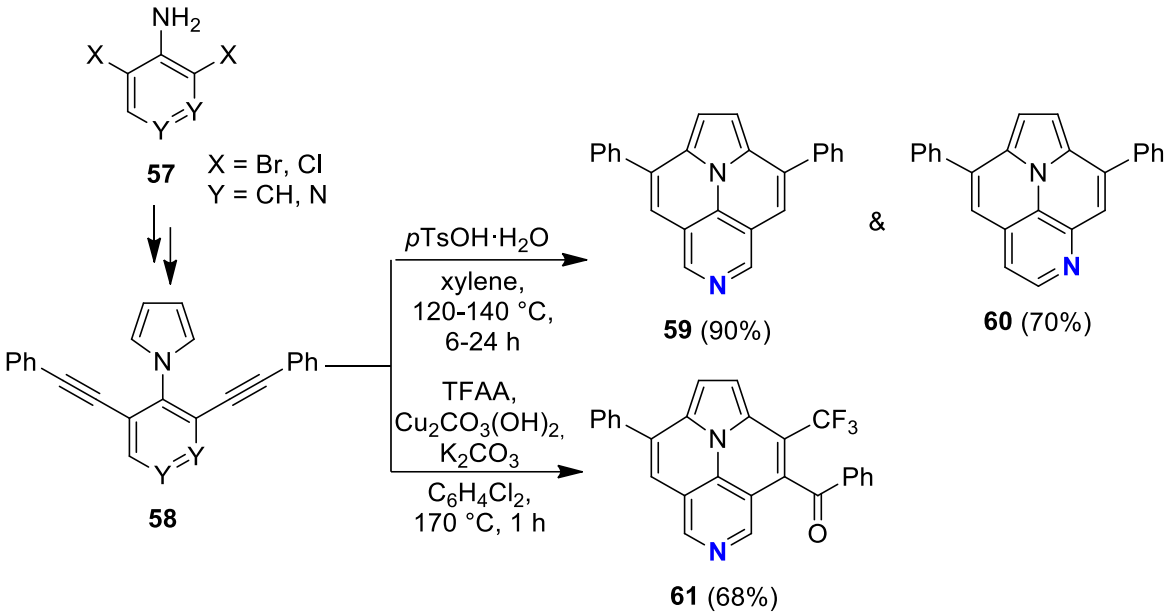

Scheme 16: Synthesis of N-doped ullazines by the group of Langer.

Additionally, the group of Gros investigated the bromination of 6-azaullazine with NBS and was able to isolate 5-bromo-6-azaullazines which can react further with NBS in a second bromination to 5,7-dibromo-6-azaullazine.[66] Functionalization with SUZUKI-MIYAURA and SONOGASHIRA reaction showed great potential with optimized photophysical properties especially for the 5-substituted derivatives similar to substitution of undoped ullazines.

In addition to the use of nitrogen, several examples are known in which a combination of different heteroatoms (boron, oxygen, nitrogen) is used (Scheme 17).[38,67] Liu's research group has been investigating this topic. In 2018, they successfully demonstrated the synthesis of BN-ullazines (**64**).[38] The isoelectronic BN-ullazine is formed by exchanging the C=C bond with a B-N unit. Synthesis wise they obtained **64** through two-fold borylative cyclization of 1,3-diamino-phenylpyrroles (**62**). The molecule exhibits an intense blue shift compared to **21** with approx. 100 nm for both the absorption and emission spectra, along with a slightly lower quantum yield (Θ_{PL} = 0.14). Furthermore, this modification results in a notable stabilization of the HOMO energy, while the LUMO remains largely unaffected. With the successful synthesis of **65** and **66** they expanded their research in 2021.[67] They formed either BN/BO-ullazine (**65**) or BO-ullazine (**66**) through borylative cyclization by replacing either one or two amino groups

with a methoxy group in the starting material (**62**). The incorporation of an oxygen atom leads to further small blue shifts in the absorption and emission spectra of approx. 10 nm for **65** and **66**, along with increased quantum yields (Θ_{PL} = 0.29 (**65**); Θ_{PL} = 0.27 (**66**)) compared to BN-ullazine (**64**). Furthermore, this modification achieved stabilization of both HOMO and LUMO.

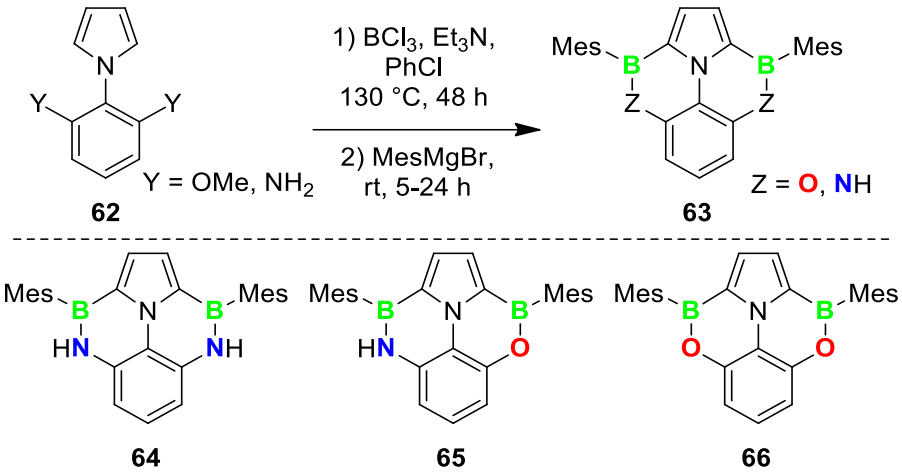

Scheme **17**: Synthesis of B-, N- and O-doped ullazines by the working group of Liu.

1.2.3 π-Expansion

Expansion of the π–system of PAHs offers a powerful tool to alter their properties.[68–70] Enhanced electronic conductivity, intensified absorption and emission within the visible and near-infrared spectrum make this modification compelling for applications in optoelectronic devices. π-Expansions of ullazines are easily accessible through a variety of reactions.[71–75]

In 2012 the first π-expansion of ullazines was published by Ren and coworkers (Scheme 18).[71] The strategy is based on an intramolecular FRIEDL-CRAFTS-arylation of aryl-triazene (**67**) to form the dibenzoullazine **68**. Herein, **67** is easily accessible through a Suzuki-Miyaura reaction of the dibromo-phenylpyrrole precursor. However, the impact on the properties was not studied.

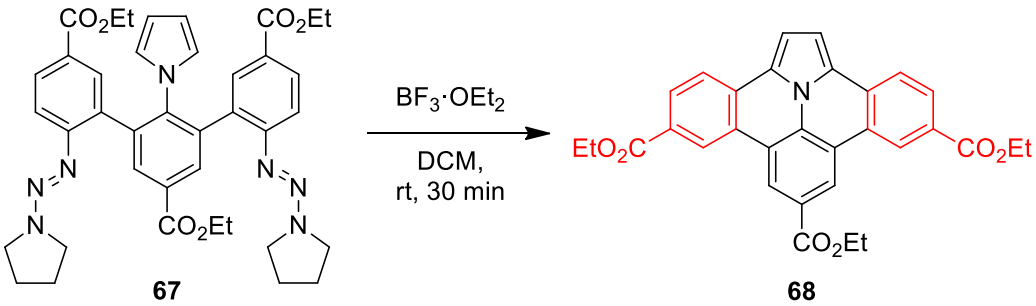

Scheme 18: First synthesis of π-expanded ullazine by Ren.

The most common way to extend the π-system is a strategy based on azomethine ylides (Scheme 19).[75–96] With dipolarophiles they undergo 1,3-dipolar cycloaddition to form dihydropyrroles. To convert these structures into the π-expanded ullazines oxidative dehydrogenation is performed, most commonly with DDQ.[76,77] The expansion occurs at the 3,4- and 8,9-positions of the ullazine due to the azomethine ylide precursors, forming dibenzoullazines, for example **71-76**.[75–94]

Despite being rare, some examples are known using varying azomethine ylides. The research group of Wang revealed a method to synthesize aryl-substituted benzoullazines (**69**).[95] Stupp's research group introduced a method to synthesize dithienoullazine (**70**) by incorporating thiophene moieties into the azomethine ylide.[96] The incorporation of the thieno-units result in a bathochromic shifted absorbance compared to its dibenzoullazine derivative which has also been synthesized by the same group. Furthermore, a high fluorescence quantum yield ($\Theta_{PL} = 0.58$) was determined making it promising for diverse photophysical applications. In comparison to **21** it reveals only a slight shift of the lowest energy band by 9 nm however the

intensity is way more pronounced for **70**, whereby the higher quantum yield could be explained. Additionally, they investigated the photocatalytic reduction of CO_2 to CO and CH_4 using the supramolecular π-extended ullazines **70** and its dibenzoullazine derivative. The acids undergo aqueous self-assembly by treatment with NaOH and NaCl, forming ullazine hydrogels. These hydrogels serve as photosensitizers, absorbing light and transferring electrons to a Co-complex catalyst which then reduces CO_2 to CO and CH_4. The efficiency of ullazine-based sensitizers is comparable to that of precious metal complexes in mixed organic-aqueous solutions. Remarkably, compared to a Ru-based sensitizer in aqueous media, the turnover rate is even higher. Moreover, these sensitizers maintained their activity for more than six days.

Furthermore, the implemented dipolarophiles have the potential to extend or modify the system in the 1,2-positions. The groups of Müllen and Feng synthesized a variety of π-expanded ullazines (**71-73**).[76] By employing various substituted alkynes they were able to synthesize diverse 1,2-substituted dibenzo-ullazines (**71**). More interestingly, with using benzoquinone they were able to generate both the monomer **72** and, with modified reaction conditions, the dimer **73**. These compounds display a bathochromically shifted absorption compared to **21**, with **72** exhibiting a loss of fine structure. Additionally, the emission spectra of **72** reveal a blue shift in contrast to **73**, which, although unshifted, displays a distinctly different structure compared to **21**.

Further interesting π−expanded dibenzo-ullazines were synthesized utilizing this approach with the use of dipolarophiles like corannulene[77,90], pyrene[88], naphtoquinones[76,80,81,85], *N*-phenylmaleimide[76], and acenaphthylenes[73]. The use of nitriles as dipolarophiles makes it possible to combine the π-extension with nitrogen doping to form an imidazole unit incorporated into the ullazine backbone.[83,84]

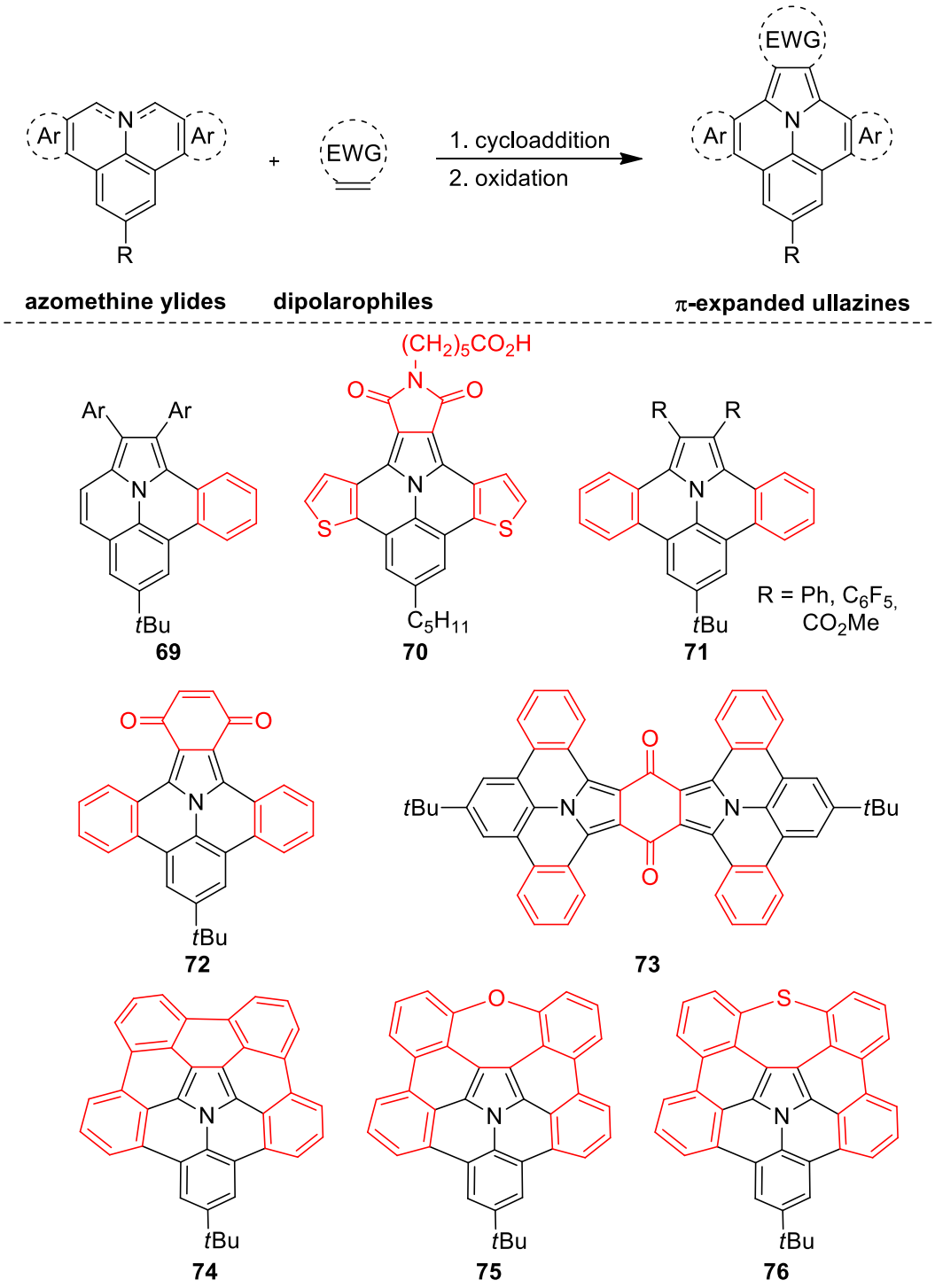

Scheme 19: Examples of π-expanded ullazines trough 1,3-dipolar cycloaddition.

Nozaki's research group combined the strategy of 1,3-dipolar cycloaddition with a subsequent Pd-catalyzed intramolecular arylative cyclization.[78] To introduce chlorine atoms during the 1,3-dipolar cycloaddition, they utilized 2,2',6-trichlorodiphenylethyne. Bowl shaped **74** was produced with three-fold intramolecular cyclization in the final step. This molecule exhibits weak and broadened absorption within the range of 300 nm to 500 nm, with the lowest energy

band at 466 nm showing a slight bathochromic shift compared to **21**. Conversely, the fluorescence spectrum displays a slight blue shift (~25 nm). Moreover, a quantum yield of $\Theta_{Pl} = 0.24$ was determined. In the same manner, the groups of Yasuda and Ito prepared the π-expanded ullazines **75** and **76** and investigated their OFET performance.[89] They fabricated single crystal OFETs from both compounds. The oxygen-containing molecule (**75**) revealed poor OFET performance with a maximum hole mobility (μ_{max}) of 0.002 $cm^2V^{-1}s^{-1}$. Crystal diffraction analysis attributed this poor performance to the slipped π-π stacking in the crystal. However, ullazine **76** achieved a promising μ_{max} of 1.05 $cm^2V^{-1}s^{-1}$ with an on/off current ratio of 10^3. This performance is significantly higher than other reported thiepine OFETs and is comparable to other organic semiconductors and amorphous silicon.[97–99] Similar to these examples the combination of 1,3-dipolar cycloaddition with subsequent reactions is extensively utilized to further extend the π-system of ullazines.[80–84,87–94]

In addition to being used to further expand the π-system following a 1,3-dipolar cycloaddition, Pd-catalyzed reactions are used to create such systems.[72,73,100–102] Particularly, the method of Gao's working group is noteworthy. They developed a Pd-catalyzed annulation of arynes with dibromo phenyl-pyrroles (**77**) (Scheme 20).[72] Initially, the arynes are generated *in situ* from 2-(trimethylsilyl)aryl triflates (**78**) using fluorine anions. Subsequent oxidative addition of the aryne and dibromo phenyl-pyrroles (**77**) on the Pd-catalyst, followed by intramolecular CH-activation and reductive elimination, resulted in the formation of products **79**. In particular, the variety of substitution on **78** has the potential to introduce different substituents, for example **81** and **82**. Furthermore, this method is able to produce unsubstituted dibenzo-ullazine (**80**). The investigated optical properties demonstrate a subtle impact of the substituents in **81** in contrast to the unsubstituted **80**. However, the extension of the π-system (**82**) induces a notable bathochromic shift and increased absorption. Additionally, the emission is red shifted by 53 nm ($\lambda_{em} = 497$ nm) in comparison to **80** ($\lambda_{em} = 444$ nm). Nevertheless, in comparison to the reference substance **21** the maxima of **80** and **81** are relatively similar, merely **82** exhibits a red shift. The emission of **80** and **81** are blue shifted by approx. 65 nm, 16 nm for **82**. Moreover, the determined quantum yields ($\Theta_{PL} = 0.25$-0.35) of the π-expanded ullazines surpass those of **21**.

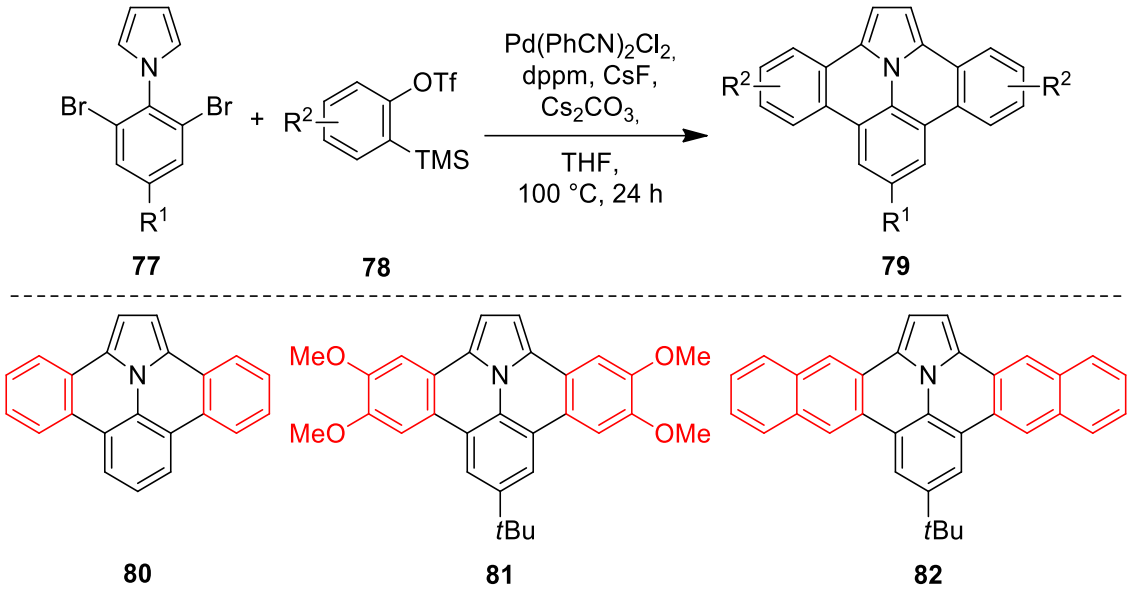

Scheme 20: Examples of π-expanded ullazines through Pd-catalyzed CH-activation by the group of Gao.

A photochemical strategy was introduced by the research group of Morin (Scheme 21).[74,103] The precursors (**83**) were easy accessible through a SUZUKI-MIYAURA coupling with differently halogenated thiophenes, pyridines or benzene. In the final step a photochemical cyclodehydrochlorination achieved yields above 90% for all derivatives (**85-89**). Besides the expansion of the ullazine, the use of thiophene and pyridine made it possible to dope the π-expanded ullazines with either nitrogen or sulfur atoms.[74] However, the influence on the optical properties of heteroatoms in these positions are rather small.

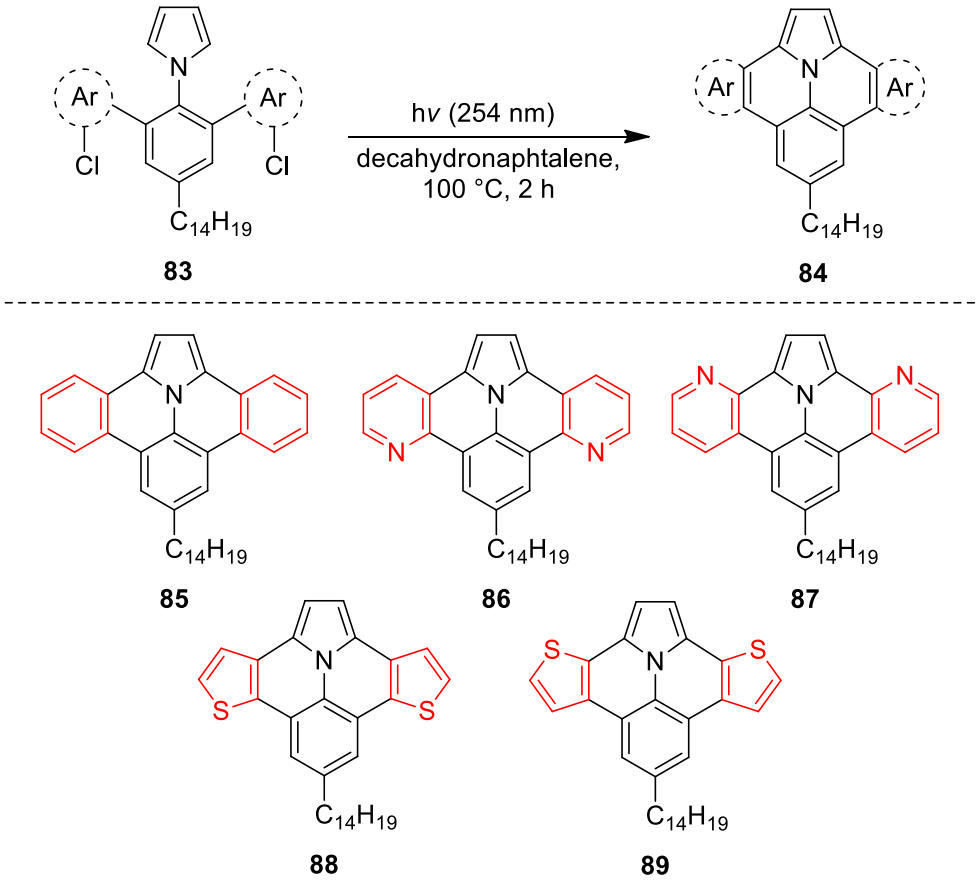

Scheme 21: Photochemical synthesis of π-expanded ullazines by the research group of Morin.

Ullazine typically undergoes expansion in the 3,4- and/or 8,9-positions, as exemplified. Additionally, combinations with expansion in the 1,2-position have been documented. Nevertheless, selective expansions in the 1,2-positions are uncommon.[104,105]

The groups of Li and Müllen synthesized carbonyl functionalized or dicyanomethylene substituted π-extended ullazines (**91** and **92**) (Scheme 22).[104] First, **90** was synthesized through imidization between the respective anhydride and dibromo-aniline followed by a STILLE coupling to introduce acetyl groups. In the key step, intramolecular aldol-condensations were performed to create the ullazine core (**91**). Further functionalization was achieved through a KNOEVENAGEL reaction using malononitrile replacing either one (**94**) or two (**95** and **96**) oxygen atoms with a dicyanomethylene group. In the same manner, the π-system could be extended by a naphthalene unit (**96**).

The emission spectra of **93-95** exhibit a pronounced influence of the different substituents. For **93** the lowest energy absorption is at 449 nm. With introduction of one cyanomethylene group the maximum gets bathochromically shifted to 553 nm and a second cyanomethylene (**95**) shifts the maximum to 629 nm. Additionally, the absorption is significantly enhanced, and the fine

structure is intensified. Unlike most ullazines, these derivatives do not exhibit fluorescence. However, the expansion with a naphthalene group (**96**) instead of a phenyl ring has only marginal effects on the optical properties.

Nevertheless, compound **96** is noteworthy as the authors observed two reversible reduction waves and one oxidation wave during CV measurements, with LUMO levels around -4 eV for molecules **95** and **96**, making them promising for application in *n*-channel thin film transistors (TFTs). The TFT device based on compound **95** achieved electron mobilities of 0.02 $cm^2V^{-1}s^{-1}$ immediately after fabrication, decreasing to 0.006 $cm^2V^{-1}s^{-1}$ after 30 months in air. Remarkably, the TFT based on compound **96** exhibited stability, maintaining electron mobilities of 0.06 $cm^2V^{-1}s^{-1}$ immediately after fabrication as well as after 30 months in air. Compared to other organic *n*-type TFT devices, this durability is notable, as most values significantly reduce after prolonged exposure to ambient air.[106]

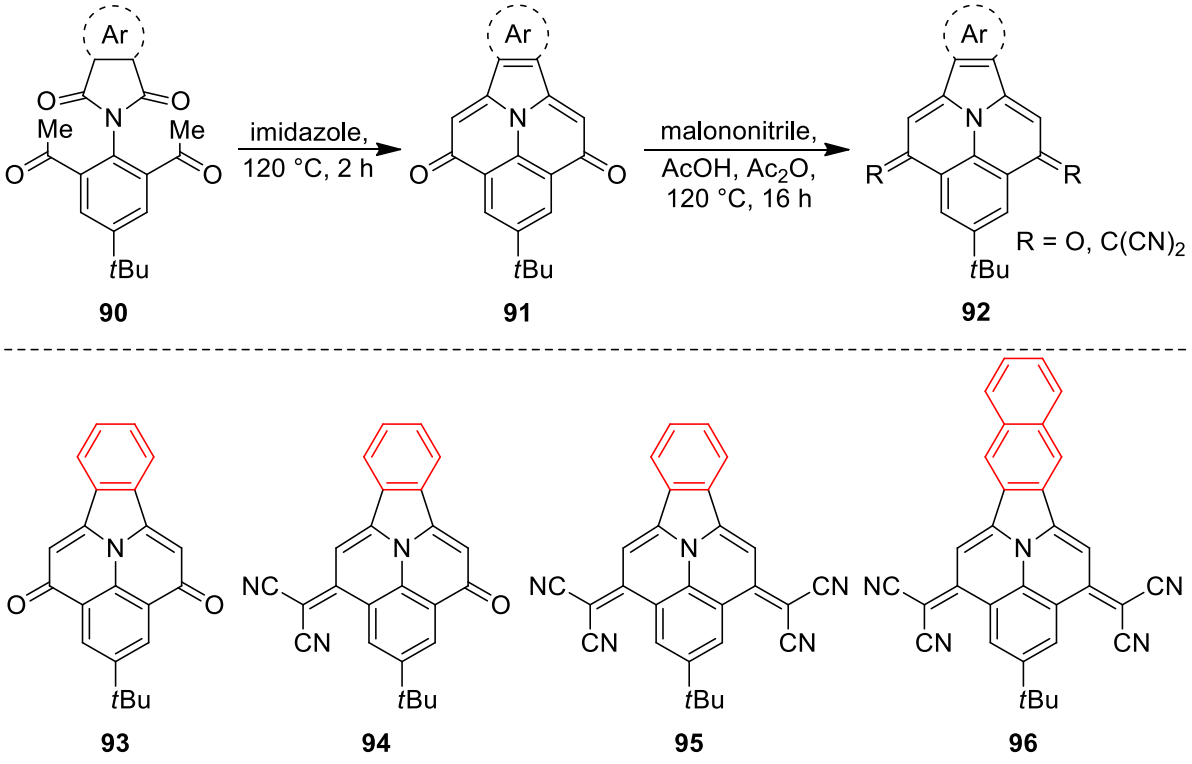

Scheme 22: Synthesis of 1,2-π-expanded ullazines by the groups of Li and Müllen.

Just recently, Matsumoto's and Funabiki's research groups also succeeded in synthesizing 1,2-expanded ullazines (Scheme 23).[105] They began with a DESS-MARTIN oxidation followed by an intramolecular aldol condensation to form **98**. The 1,2-π-extended ullazines were generated through reductive ring closure reaction with hydrazine hydrate and were able to extend the system by a benzene (**100**) or a thiophene (**101**). They studied the impact of benzene fusion by

measuring absorption and emission spectra. Fusion of a benzene ring in 1,2-position (**100**) leads to an augmented absorption with a similar fine structure compared to **21**. However, the peaks of absorbance exhibit a red shift of approx. 50 nm. Similar results can be inferred from the PL spectrum. Thus, the fine structure closely resembles that of **21**. Nonetheless, the emission spectrum demonstrates broadening and a red shift exceeding 100 nm. Conversely, the quantum yield is notably low ($\Theta_{PL} = 0.03$).

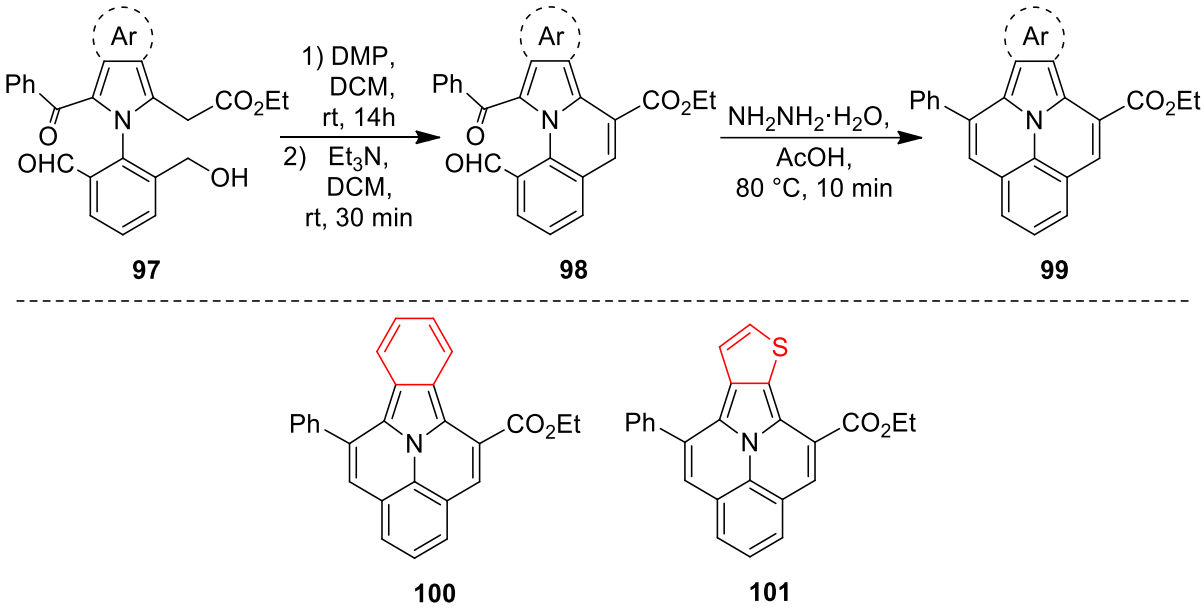

Scheme 23: Synthesis of 1,2-π-expanded ullazines by the groups of Matsumoto and Funabiki.

Also noteworthy is the innovative approach of Langer's research group, who extended aza-doped ullazines to the 6,7-position (Scheme 24).[33] First, they generated alkynylated pyrrolo-quinolines (**103**) from chlorinated amino-quinoline (**102**) with CLAUSSON-KAAS and SONOGASHIRA reactions. The synthesis of **104** was achieved *via* BRØNSTED-acid mediated cycloisomerization reaction in the final step similar to their approach for the synthesis of 5- and 6-azaullazines (Scheme 16).[31,33] Compared to the 5-azaullazine (**60**) π-expanded **95** has a notably finer structured absorption for the low energy band with a bathochromic shift of 65 nm. **95** features a red shift in the PL spectrum compared to the non-expanded azaullazines, but in comparison to **21** a blue shift. Additionally, quantum yields between 0.14 and 0.43 were determined.

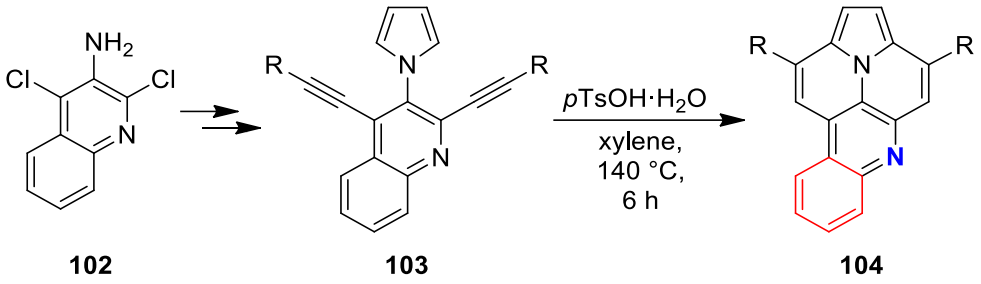

102 **103** **104**

Scheme 24: Synthesis of N-doped and π-expanded ullazines by the working group of Langer.

2 Results and Discussion

In this chapter, the results of the publications are briefly summarized, and key findings are presented to provide an overview of the respective work. The detailed results, such as optimization tables, graphics, synthesized derivatives, X-Ray structures, and more, can be found in the respective publications (chapter 4).

2.1 Synthesis and Properties of 5,7-Diazaullazines

In this publication we first focused on the synthesis of novel nitrogen-doped 5,7-diazaullazines (**108**) (Scheme 25). Therefore, we started with a CLAUSSON-KAAS reaction of commercially available **105** to form chlorinated pyrrolo-pyrimidine (**106**) in excellent yield. Following this, we performed an optimization of the SONOGASHIRA reaction and were able to synthesize five differently substituted derivates (**107**). In the final step we used a BRØNSTED-acid mediated cycloisomerization reaction to generate the N-doped ullazine core (**108**). Through optimization of the reaction conditions, we were able to carry out the assembly in good to excellent yields depending on the residues on the alkynes.

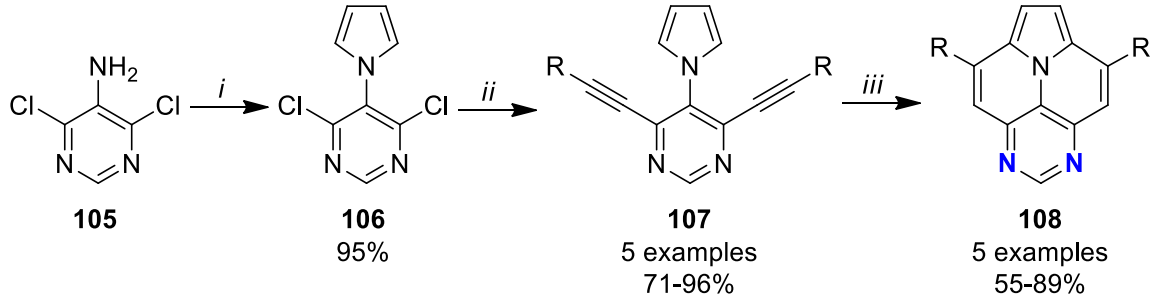

Scheme 25: Synthesis of 5,7-diazaullazines. *i*: 2,5-dimethoxytetrahydrofuran (1.05 eq.), AcOH, 1,2-dichloroethane, reflux, 3 h. *ii*: alkyne (3 eq.), $Pd(CH_3CN)_2Cl_2$ (6 mol%), XPhos (12 mol%), CuI (4 mol%), 1,4-dioxane, HN^iPr_2, 90 °C, 24 h . *iii*: *p*-TsOH·H_2O (30 eq.), xylene, 140 °C, 6 h.

We investigated the optical properties of three derivatives, noting that the influence of the substituents is rather small, except for the introduction of a dimethylaniline (DMA) group. The DMA derivative displays pronounced solvatochromism, unlike the phenyl derivative. Interestingly, the quantum yield ($\Theta_{PL} = 0.56$) is significantly higher than that of the Ph-derivative ($\Theta_{PL} = 0.35$). Furthermore, CV measurements revealed earlier oxidation due to the attached donor-group.

Additionally, we thoroughly examined the incorporation of two nitrogen atoms into the ullazine framework and compared it with 3,9-diphenylullazine (**21**), 3,9-diphenyl-6-azaullazine (**59**),

and 3,9-diphenyl-5-azaullazine (**60**). DFT studies revealed a stabilization of the HOMO and LUMO energies depending on the number and position of the nitrogen atoms, with the most pronounced stabilization observed for 5,7-diazaullazine, followed by 5- and 6-azaullazines, with unmodified ullazine (**21)** exhibiting the least stabilization. Experimentally, we investigated the azaullazines by comparing UV-vis and PL spectra (as mentioned earlier the optical properties of 6-azaullazine and **21** are nearly the same), as well as fluorescence lifetime measurements. **108** shows a bathochromic shift in both the short and long wavelength regions with the highest molar absorption for the lowest energy band. The lowest energy band for both 6- and 5-azaullazines, on the other hand, is characterized as a shoulder. Additionally, the compounds exhibit a blue shift in emission spectra with **108** having the most impact and 6 aza-ullazine (**59**) the least. Consequently, there is a decrease in the stoke shift from 6-azaullazine to 5-azaullazine to 5,7-diazaullazine.

Furthermore, the fluorescence lifetime measurements revealed a long natural lifetime ($\tau_0 \sim$ 129 ns) and the slowest radiative decay for 6-azaullazine, typical for a forbidden transition. A shorter lifetime was determined for 5-azaullazine ($\tau_0 \sim$ 24 ns) and the shortest for 5,7-diazaullazine ($\tau_0 \sim$ 11 ns), which on the other hand exhibits the highest radiative decay rate. These differences clarify the lower absorption values for the first transition and the increasing quantum yields of 6-azaullazine ($\Theta_{PL} = 0.07$), 5-azaullazine ($\Theta_{PL} = 0.23$) and 5,7-diazaullazine ($\Theta_{PL} = 0.35$).

We further examined the transitions of the lowest energy band using electron-hole maps. The illustrations revealed an excited-state electron density rearrangement for ullazines **21**, **59**, and **60**. The density shifts from the periphery to the inner rings and the internal nitrogen atom, which indicates a short-range charge transfer. However, the novel 5,7-diazaullazine does not exhibit this rearrangement. Instead, the electron-holes remain exclusively delocalized along the diazaullazine perimeter. These findings strongly supported the results of the experimental comparison and further explained the solvatochromic properties of the DMA derivative, which on the other hand were not observed for the DMA derivatives of 6- and 5-aza ullazine. The incorporation of two nitrogen atoms in the 5- and 7-positions changes the donor ability in the excited state (as seen in **21**, **59**, and **60**) into an acceptor, a phenomenon also reflected by the CV measurements.

2.2 π-Expanded Azaullazines: Synthesis of Quinolino-Azaullazines by Povarov Reaction and Cycloisomerisation

In this publication, we combined the modification of nitrogen doping, which we examined in previous publications with π-expansion of the ullazine core (Scheme 26). Therefore, we employed two synthetic strategies: the cycloisomerization reaction and the POVAROV reaction, which has never been used in the construction of ullazines. Starting with the literature-known compound **109**, we performed a VILSMEIER-HAACK reaction to introduce an aldehyde at the 2-position of the pyrrole unit (**110**). Subsequently, we optimized the SONOGASHIRA reaction to establish favorable conditions, successfully synthesizing five derivatives (**111**) in good to very good yields. The combination of the two different reactions required optimization and was carried out in two independent steps, leading to the construction of novel quinolino-6-azaullazines (**112**) in moderate to good yields.

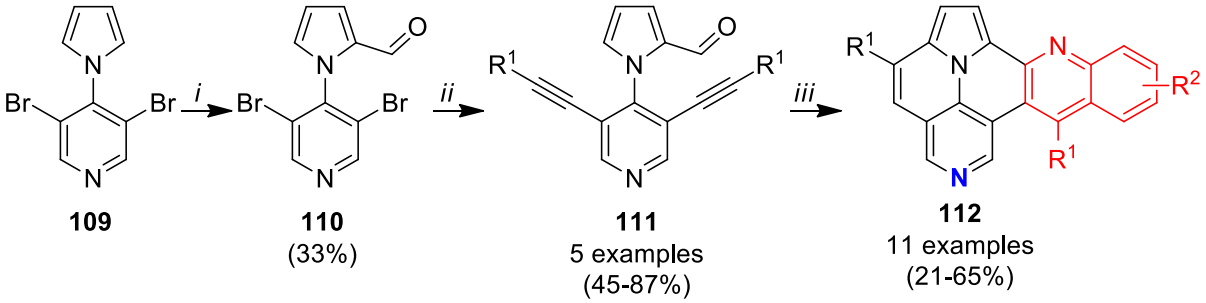

Scheme 26: Synthesis of quinolino-6-azaullazines. *i*: $POCl_3$ (2 eq.), DMF, 100 °C, 3 h. *ii*: alkyne (3 eq.), $PdCl_2(PPh_3)_2$ (5 mol%), cataCXium A (10 mol%), CuI (5 mol%), 1,4-dioxane, HN^iPr_2, 90 °C, 24 h. *iii*: 1) $FeCl_3$ (10 mol %), aniline (1.2 eq.), toluene, 100 °C, 2 h. 2) *p*-TsOH·H_2O (20 eq.), xylene, 120 °C, 6 h.

We conducted a detailed study on the optical properties by measuring absorption and emission spectra, as well as investigated solvatochromism and acidochromism for selected compounds. It became evident that the aryl residues (R^1) introduced during the SONOGASHIRA reaction have almost no influence on the optical properties. However, the introduction of a DMA unit significantly alters the spectra, causing a bathochromic shift and a loss of fine structure. The substituents directly attached to the aromatic skeleton through employed anilines (R^2) have a much stronger influence. All derivatives exhibit moderate quantum yields between 0.19 and 0.35. Compared to known π-expanded ullazines, this novel heterocycle shows significantly red shifted absorption and emission with comparable quantum yields.

Solvatochromic investigations revealed similar behavior regardless of the substituents. A loss of fine structure was observed in more polar solvents, accompanied by a red shift of the emission. However, DMA-substituted compound additionally showed strong fluorescence quenching, which potentially could be attributed to a twisted intramolecular charge transfer (TICT). These observations were further supported by DFT calculations, revealing enhanced dipole moments in the excited state for the investigated compounds, with the highest enhancement determined for the DMA-substituted derivative. The ground state dipole moment is μ_{S0} = 4.4193 D and the excited state dipole moment is μ_{S1} = 26.2043 D.

Protonation studies with TFA in DCM demonstrated the possibility of nitrogen protonation, which further modifies the optical properties. This results in a red shift of the absorption maxima (~63 nm) and emission maxima (~71 nm), along with simultaneous quenching of the fluorescence intensity.

In addition, we investigated the aromaticity of the quinolino-6-azaullazine by calculation of nuclear-independent chemical shift (NICS) values and the bond currents. The aromaticity is divided into two parts: the quinoline unit and the pyrroloquinoline moiety which are connected by a benzene ring exhibiting non-aromaticity.

2.3 Divergent Synthesis of 5,7-Diazaullazines Derivatives through a Combination of Cycloisomerization with Povarov or Alkyne–Carbonyl Metathesis

Based on the previous publications, we decided to combine the efficient modification of the 5,7-diazaullazines (**108**) with the π-expansion shown in the synthesis of quinolino-6-azaullazines (**112**) (Scheme 27). We knew from previous publications that the starting materials (**114**) for the POVAROV/cycloisomerization reaction, could also undergo an ACM reaction to form non-symmetrically substituted 5,7-diazaullazines (**116**). We began our synthetic strategy with chlorinated pyrrolo-pyrimidine (**106**), which we already had in hand, and performed a VILSMEIER-HAAK reaction to introduce an aldehyde on the pyrrole moiety. The introduced aldehyde did not significantly affect the yields of the products **114** during SONOGASHIRA reaction, so we decided to use the same conditions as previously employed for the synthesis of products **107**. Subsequently, we optimized the final reactions: the combination of POVAROV/cycloisomerization and ACM/cycloisomerization. The optimized conditions were sufficient to produce ten examples of the quinolino-5,7-diazaullazines (**115**) in poor to moderate yields and six examples of the non-symmetrically 3,8-substituetd-5,7-diazaullazines (**116**) in good yields.

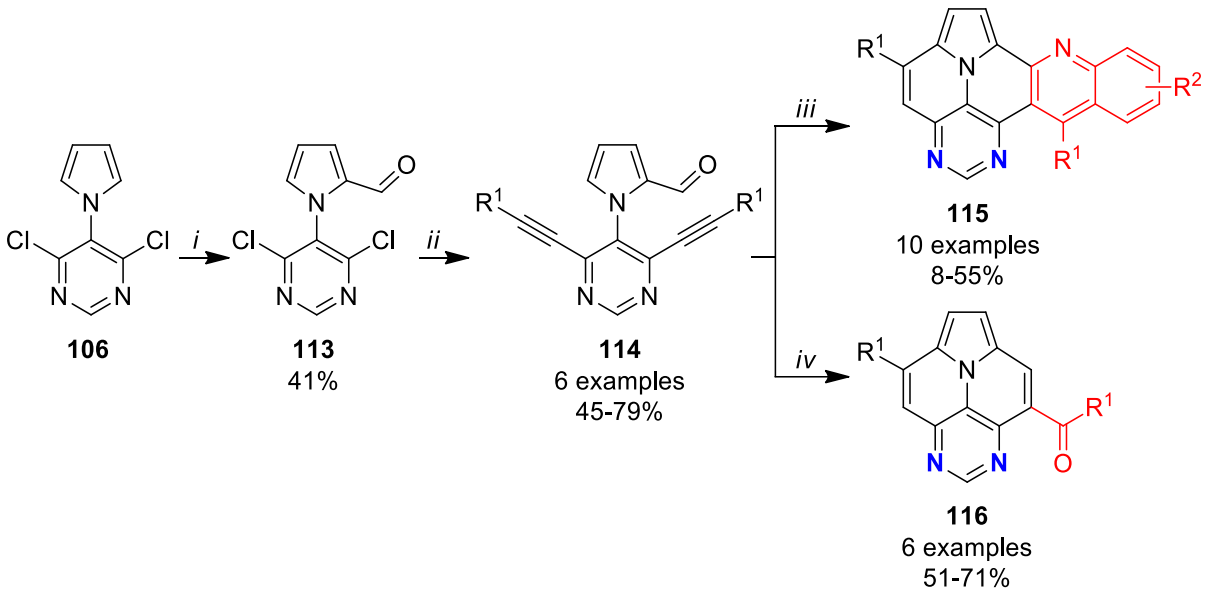

Scheme 27: Synthesis of quinolino-5,7-diazaullazines and asymmetrically substituted 5,7-diazaullazines. *i*: $POCl_3$ (2 eq.), DMF, 100 °C, 3 h. *ii*: alkyne (3 eq.), $Pd(CH_3CN)_2Cl_2$ (6 mol%), XPhos (12 mol%), CuI (4 mol%), 1,4-dioxane, HN^iPr_2, 90 °C, 24 h . *iii*: 1) $FeCl_3$ (1 eq.), aniline (1.2 eq.), xylene, 140 °C, 3 h. 2) *p*-TsOH·H_2O (30 eq.), xylene, 140 °C, 6 h. *iv*: *p*-TsOH·H_2O (20 eq.), xylene, 120 °C, 6 h.

During UV-vis and PL measurements, we focused on the investigation of differently substituted quinolino-5,7-diazaullazines directly attached on the core structure (R^2), as the effect of the SONOGASHIRA residues (R^1) was negligible in the previous study. It was found that only the introduction of a dimethylamino group has a significant impact, resulting in a broadened, unstructured, and bathochromically shifted absorption with dramatically lower extinction coefficients, as well as a red shifted emission compared to the other derivatives. This particular derivative also exhibits a remarkably low quantum yield of 0.29 compared to the other derivatives (Θ_{PL} = 0.52-0.53). Compared to the previous publication, the introduced pyrimidine moiety alters the properties of the quinolino-ullazine core, resulting in higher oxidation potential, quantum yield, and red shifted absorption and emission spectra (Table 3).

On the other hand, the absorption and emission of compound **116** is clearly blue shifted in comparison to compound **115**, with higher extinction coefficients for the lowest energy band. However, a significantly lower quantum yield was determined (Θ_{PL} = 0.10). The properties of compound **116** are very similar to its symmetrically substituted derivatives (**108**). However, the introduction of a benzoyl group leads to the stabilization of HOMO and LUMO energies, a slight red shift in fluorescence, and lower quantum yields.

Table 3: Comparison of properties of the three publications.

	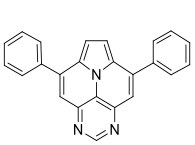	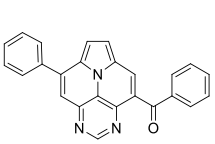	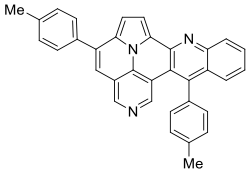	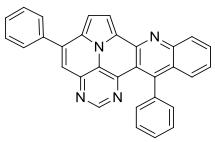
	108a	**116a**	**112a**	**115a**
$\lambda_{1,abs}$ [nm]	422	420	471	497
$\varepsilon_{\lambda 1}$ [10^4 L·mol^{-1}cm^{-1}]	1.7	2.0	1.1	0.8
$\lambda_{1,em}$ [nm]	439	462	515	530
Θ_{PL}	0.35	0.10	0.26	0.52
$E_{Ox.}$ [V vs. Fc/Fc$^+$]	1.00	1.08	0.72	0.95
$E_{HOMO/CV}$ [eV]	-5.69	-5.76	-5.41	-5.65
$E_{HOMO/DFT}$ [eV]	-5.60	-5.73	-5.22	-5.53
$E_{LUMO/DFT}$ [eV]	-1.90	-2.04	-2.09	-2.43
E_{gap} [eV]	3.69	3.69	3.13	3.10

3 References

[1] E. Reizer, B. Viskolcz, B. Fiser, *Chemosphere* **2022**, *291*, 132793.

[2] A. B. Patel, S. Shaikh, K. R. Jain, C. Desai, D. Madamwar, *Front. Mircobiol.* **2020**, *11*, 562813.

[3] K. Kozak, M. Ruman, K. Kosek, G. Karasiński, Ł. Stachnik, Ż. Polkowska, *Water* **2017**, *9*, 42.

[4] B. M. Sahoo, B. V. V. Ravi Kumar, B. K. Banik, P. Borah, *Curr. Org. Synth.* **2020**, *17*, 625.

[5] Y.-C. Lin, Y.-C. Li, S. Shangdiar, F.-C. Chou, Y.-T. Sheu, P.-C. Cheng, *Chemosphere* **2019**, *226*, 502.

[6] J. Wu, W. Pisula, K. Müllen, *Chem. Rev.* **2007**, *107*, 718.

[7] A. Narita, X.-Y. Wang, X. Feng, K. Müllen, *Chem. Soc. Rev.* **2015**, *44*, 6616.

[8] T. M. Figueira-Duarte, K. Müllen, *Chem. Rev.* **2011**, *111*, 7260.

[9] F. P. Kinik, A. Ortega-Guerrero, D. Ongari, C. P. Ireland, B. Smit, *Chem. Soc. Rev.* **2021**, *50*, 3143.

[10] X. Feng, J.-Y. Hu, C. Redshaw, T. Yamato, *Chem. Eur. J.* **2016**, *22*, 11898.

[11] Q. Li, Y. Zhang, Z. Xie, Y. Zhen, W. Hu, H. Dong, *J. Mater. Chem. C* **2022**, *10*, 2411.

[12] G. Hong, X. Gan, C. Leonhardt, Z. Zhang, J. Seibert, J. M. Busch, S. Bräse, *Adv. Mater.* **2021**, *33*, e2005630.

[13] C. W. Lee, O. Y. Kim, J. Y. Lee, *J. Ind. Eng. Chem.* **2014**, *20*, 1198.

[14] H. Dong, X. Fu, J. Liu, Z. Wang, W. Hu, *Adv. Mater.* **2013**, *25*, 6158.

[15] J. E. Anthony, A. Facchetti, M. Heeney, S. R. Marder, X. Zhan, *Adv. Mater.* **2010**, *22*, 3876.

[16] Z.-G. Zhang, Y. Li, *Angew. Chem., Int. Ed.* **2021**, *60*, 4422.

[17] A. Mateo-Alonso, *Chem. Soc. Rev.* **2014**, *43*, 6311.

[18] J. Liu, X. Feng, *Synlett* **2020**, *31*, 211.

[19] X. Wang, G. Sun, P. Routh, D.-H. Kim, W. Huang, P. Chen, *Chem. Soc. Rev.* **2014**, *43*, 7067.

[20] A. Borissov, Y. K. Maurya, L. Moshniaha, W.-S. Wong, M. Żyła-Karwowska, M. Stępień, *Chem. Rev.* **2022**, *122*, 565.

[21] L. Ji, A. Friedrich, I. Krummenacher, A. Eichhorn, H. Braunschweig, M. Moos, S. Hahn, F. L. Geyer, O. Tverskoy, J. Han et al., *J. Am. Chem. Soc.* **2017**, *139*, 15968.

[22] M. Takase, V. Enkelmann, D. Sebastiani, M. Baumgarten, K. Müllen, *Angew. Chem., Int. Ed.* **2007**, *46*, 5524.

[23] P. Langer, *Synlett* **2022**, *33*, 1707.

[24] J. H. Delcamp, A. Yella, T. W. Holcombe, M. K. Nazeeruddin, M. Grätzel, *Angew. Chem., Int. Ed.* **2013**, *52*, 376.

[25] C. Cebrián, *J. Mater. Chem. C* **2018**, *6*, 11943.

[26] H. Balli, M. Zeller, *Helv. Chim. Acta* **1983**, *66*, 2135.

[27] N. Clauson-Kaas, Z. Tyle, M. Rottenberg, E. Stenhagen, S. Östling, *Acta Chem. Scand.* **1952**, *6*, 667.

[28] K. Kanno, Y. Liu, A. Iesato, K. Nakajima, T. Takahashi, *Org. Lett.* **2005**, *7*, 5453.

[29] N. A. Drigo, S. Paek, A. J. Huckaba, P. A. Schouwink, N. Tabet, M. K. Nazeeruddin, *Chem. Eur. J.* **2017**, *23*, 17209.

[30] G. Zhang, P. Gautam, J. M. W. Chan, *Org. Chem. Front.* **2020**, *7*, 787.

[31] S. Boldt, S. Parpart, A. Villinger, P. Ehlers, P. Langer, *Angew. Chem., Int. Ed.* **2017**, *56*, 4575.

[32] P. Pierrat, S. Hesse, C. Cebrián, P. C. Gros, *Org. Biomol. Chem.* **2017**, *15*, 8568.

[33] S. Janke, S. Boldt, P. Nakielski, A. Villinger, P. Ehlers, P. Langer, *J. Org. Chem.* **2023**, *88*, 10470.

[34] D. Wan, X. Li, R. Jiang, B. Feng, J. Lan, R. Wang, J. You, *Org. Lett.* **2016**, *18*, 2876.

[35] A. Das, I. Ghosh, B. König, *Chem. Commun.* **2016**, *52*, 8695.

[36] Y. Hu, Y. Jia, Z. Tuo, W. Zhou, *Org. Lett.* **2023**, *25*, 1845.

[37] S. Otero-Riesgo, J. A. Varela, C. Saá, *Adv. Synth. Catal.* **2024**.

[38] C. Li, Y. Liu, Z. Sun, J. Zhang, M. Liu, C. Zhang, Q. Zhang, H. Wang, X. Liu, *Org. Lett.* **2018**, *20*, 2806.

[39] F. Gerson, A. Metzger, *Helv. Chim. Acta* **1983**, *66*, 2031.

[40] A. K. Verma, S. P. Shukla, J. Singh, V. Rustagi, *J. Org. Chem.* **2011**, *76*, 5670.

[41] S. Mathew, N. A. Astani, B. F. E. Curchod, J. H. Delcamp, M. Marszalek, J. Frey, U. Rothlisberger, M. K. Nazeeruddin, M. Grätzel, *J. Mater. Chem. A* **2016**, *4*, 2332.

[42] H. Qiao, Y. Deng, R. Peng, G. Wang, J. Yuan, S. Tan, *RSC Adv.* **2016**, *6*, 70046.

[43] Y. Zhang, H. Cheema, L. McNamara, L. A. Hunt, N. I. Hammer, J. H. Delcamp, *Chem. Eur. J.* **2018**, *24*, 5939.

[44] A. Hagfeldt, G. Boschloo, L. Sun, L. Kloo, H. Pettersson, *Chem. Rev.* **2010**, *110*, 6595.

[45] F. Bureš, *RSC Adv.* **2014**, *4*, 58826.

[46] A. Dualeh, R. Humphry-Baker, J. H. Delcamp, M. K. Nazeeruddin, M. Grätzel, *Adv. Energy Mater.* **2013**, *3*, 496.

[47] J. Xia, M. Cavazzini, C. Igci, C. Momblona, S. Orlandi, B. Ding, Y. Zhang, H. Kanda, N. Klipfel, S. B. Khan et al., *Sol. RRL* **2022**, *6*.

[48] J. Feng, Y. Jiao, W. Ma, M. K. Nazeeruddin, M. Grätzel, S. Meng, *J. Phys. Chem. C* **2013**, *117*, 3772.

[49] J. Huang, L. Yang, Z. Chen, Y. Zhou, S. Zeng, *New J. Chem.* **2023**, *47*, 11030.

[50] Y. Li, X. Li, Y. Xu, *Sol. Energy* **2020**, *196*, 146.

[51] J. H. Delcamp, Y. Shi, J.-H. Yum, T. Sajoto, E. Dell'Orto, S. Barlow, M. K. Nazeeruddin, S. R. Marder, M. Grätzel, *Chem. Eur. J.* **2013**, *19*, 1819.

[52] M. Stępień, E. Gońka, M. Żyła, N. Sprutta, *Chem. Rev.* **2017**, *117*, 3479.

[53] U. H. F. Bunz, J. Freudenberg, *Acc. Chem. Res.* **2019**, *52*, 1575.

[54] M. Karuppusamy, V. S. K. Choutipalli, D. Vijay, V. Subramanian, *J. Chem. Sci.* **2020**, *132*, 1.

[55] D. Hou, H. Balli, *Helv. Chim. Acta* **1992**, *75*, 2608.

[56] R. Rubio-Presa, M. A. R. Pedrosa, M. A. Fernández-Rodríguez, F. J. Arnáiz, R. Sanz, *Org. Lett.* **2017**, *19*, 5470.

[57] K. Wang, S. Yan, T. Han, Q. Wu, N. Yan, M. Kang, J. Ge, D. Wang, B. Z. Tang, *J. Am. Chem. Soc.* **2022**, *144*, 11788.

[58] Q. Ge, B. Li, B. Wang, *Org. Biomol. Chem.* **2016**, *14*, 1814.

[59] R. Hernández-Ruiz, R. Rubio-Presa, S. Suárez-Pantiga, M. R. Pedrosa, M. A. Fernández-Rodríguez, M. J. Tapia, R. Sanz, *Chem. Eur. J.* **2021**, *27*, 13613.

[60] D. Ghorai, J. Choudhury, *ACS Catal.* **2015**, *5*, 2692.

[61] R. Li, Y. Hu, R. Liu, R. Hu, B. Li, B. Wang, *Adv. Synth. Catal.* **2015**, *357*, 3885.

[62] Q. Ge, B. Li, H. Song, B. Wang, *Org. Biomol. Chem.* **2015**, *13*, 7695.

[63] D. L. Davies, C. E. Ellul, S. A. Macgregor, C. L. McMullin, K. Singh, *J. Am. Chem. Soc.* **2015**, *137*, 9659.

[64] N. Umeda, K. Hirano, T. Satoh, N. Shibata, H. Sato, M. Miura, *J. Org. Chem.* **2011**, *76*, 13.

[65] S. Parpart, S. Boldt, P. Ehlers, P. Langer, *Org. Lett.* **2018**, *20*, 122.

[66] D. Ibrahim, P. Boulet, P. C. Gros, P. Pierrat, *Eur. J. Org. Chem.* **2021**, *2021*, 3331.

[67] Y. Guo, L. Zhang, C. Li, M. Jin, Y. Zhang, J. Ye, Y. Chen, X. Wu, X. Liu, *J. Org. Chem.* **2021**, *86*, 12507.

[68] M. Iyoda, H. Shimizu, *Chem. Soc. Rev.* **2015**, *44*, 6411.

[69] M. Tasior, D. Kim, S. Singha, M. Krzeszewski, K. H. Ahn, D. T. Gryko, *J. Mater. Chem. C* **2015**, *3*, 1421.

[70] J. Ramakrishna, P. Venkatakrishnan, *Chem. Asian J.* **2017**, *12*, 181.

[71] J. Zhou, W. Yang, B. Wang, H. Ren, *Angew. Chem., Int. Ed.* **2012**, *51*, 12293.

[72] D. Wang, Y. Liu, L. Wang, H. Cheng, Y. Zhang, G. Gao, *Chin. Chem. Lett.* **2021**, *32*, 1407.

[73] J. Hager, S. Kang, P. J. Chmielewski, T. Lis, D. Kim, M. Stępień, *Org. Chem. Front.* **2022**, *9*, 3179.

[74] D. Miao, C. Aumaitre, J.-F. Morin, *J. Mater. Chem. C* **2019**, *7*, 3015.

[75] S. Ito, Y. Tokimaru, K. Nozaki, *Chem. Commun.* **2015**, *51*, 221.

[76] R. Berger, M. Wagner, X. Feng, K. Müllen, *Chem. Sci.* **2015**, *6*, 436.

[77] Y. Tokimaru, S. Ito, K. Nozaki, *Angew. Chem., Int. Ed.* **2017**, *56*, 15560.

[78] S. Ito, Y. Tokimaru, K. Nozaki, *Angew. Chem., Int. Ed.* **2015**, *127*, 7364.

[79] R. Berger, A. Giannakopoulos, P. Ravat, M. Wagner, D. Beljonne, X. Feng, K. Müllen, *Angew. Chem., Int. Ed.* **2014**, *53*, 10520.

[80] M. Richter, K. S. Schellhammer, P. Machata, G. Cuniberti, A. Popov, F. Ortmann, R. Berger, K. Müllen, X. Feng, *Org. Chem. Front.* **2017**, *4*, 847.

[81] D. Skidin, F. Eisenhut, M. Richter, S. Nikipar, J. Krüger, D. A. Ryndyk, R. Berger, G. Cuniberti, X. Feng, F. Moresco, *Chem. Commun.* **2019**, *55*, 4731.

[82] M. Richter, Y. Fu, E. Dmitrieva, J. J. Weigand, A. Popov, R. Berger, J. Liu, X. Feng, *ChemPlusChem* **2019**, *84*, 613.

[83] Q.-Q. Li, K. Ochiai, C.-A. Lee, S. Ito, *Org. Lett.* **2020**, *22*, 6132.

[84] Q.-Q. Li, Y. Hamamoto, C. C. H. Tan, H. Sato, S. Ito, *Org. Chem. Front.* **2022**, *9*, 4128.

[85] M. Richter, S. Hahn, E. Dmitrieva, F. Rominger, A. Popov, U. H. F. Bunz, X. Feng, R. Berger, *Chem. Eur. J.* **2019**, *25*, 1345.

[86] M. Richter, M. Borkowski, Y. Fu, E. Dmitrieva, A. Popov, J. Ma, T. Marszalek, W. Pisula, X. Feng, *Org. Mater.* **2021**, *03*, 198.

[87] H. Han, G. W. Z. Goh, Y. Li, N. Yoshikai, S. Ito, *Chin. J. Chem.* **2024**, *42*, 1079.

[88] X. Zhang, M. R. Mackinnon, G. J. Bodwell, S. Ito, *Angew. Chem., Int. Ed.* **2022**, *61*, e202116585.

[89] W. Wang, F. Hanindita, Y. Tanaka, K. Ochiai, H. Sato, Y. Li, T. Yasuda, S. Ito, *Angew. Chem., Int. Ed.* **2023**, *62*, e202218176.

[90] Y. Tokimaru, S. Ito, K. Nozaki, *Angew. Chem., Int. Ed.* **2018**, *57*, 9818.

[91] W. Wang, F. Hanindita, Y. Hamamoto, Y. Li, S. Ito, *Nat. Commun.* **2022**, *13*, 1498.

[92] K. Nakamura, K. Ochiai, A. Yubuta, D. He, D. Miyajima, S. Ito, *Precis. Chem.* **2023**, *1*, 29.

[93] T. Nagano, K. Nakamura, Y. Tokimaru, S. Ito, D. Miyajima, T. Aida, K. Nozaki, *Chem. Eur. J.* **2018**, *24*, 14075.

[94] Y. Hamamoto, K. Ochiai, Y. Li, E. Tapavicza, S. Ito, *Angew. Chem., Int. Ed.* **2024**, *63*, e202319022.

[95] L. Dong, F. Saraci, K. Yuan, X. Wang, S. Wang, *Org. Biomol. Chem.* **2019**, *17*, 6470.

[96] O. Dumele, L. Đorđević, H. Sai, T. J. Cotey, M. H. Sangji, K. Sato, A. J. Dannenhoffer, S. I. Stupp, *J. Am. Chem. Soc.* **2022**, *144*, 3127.

[97] Z. Cai, H. Zhang, H. Geng, Z. Liu, S. Yang, H. Luo, L. Jiang, Q. Peng, G. Zhang, J. Chen et al., *Chem. Eur. J.* **2013**, *19*, 14573.

[98] W. Wu, Y. Liu, D. Zhu, *Chem. Soc. Rev.* **2010**, *39*, 1489.

[99] C. Wang, H. Dong, W. Hu, Y. Liu, D. Zhu, *Chem. Rev.* **2012**, *112*, 2208.

[100] X. Guo, Z. Yuan, Y. Zhu, Z. Li, R. Huang, Z. Xia, W. Zhang, Y. Li, J. Wang, *Angew. Chem., Int. Ed.* **2019**, *131*, 17122.

[101] H. Yokoi, Y. Hiraoka, S. Hiroto, D. Sakamaki, S. Seki, H. Shinokubo, *Nat. Commun.* **2015**, *6*, 8215.

[102] H. Yokoi, S. Hiroto, D. Sakamaki, S. Seki, H. Shinokubo, *Chem. Sci.* **2018**, *9*, 819.

[103] D. Miao, V. Di Michele, F. Gagnon, C. Aumaître, A. Lucotti, M. Del Zoppo, F. Lirette, M. Tommasini, J.-F. Morin, *J. Am. Chem. Soc.* **2021**, *143*, 11302.

[104] A. Skabeev, U. Zschieschang, Y. Zagranyarski, H. Klauk, K. Müllen, C. Li, *Org. Lett.* **2018**, *20*, 1409.

[105] T. Kawazoe, H. Yanai, Y. Hagiyama, K. Funabiki, T. Matsumoto, *Eur. J. Org. Chem.* **2023**, *29*, e202301703.

[106] J. T. E. Quinn, J. Zhu, X. Li, J. Wang, Y. Li, *J. Mater. Chem. C* **2017**, *5*, 8654.

4 Publications

4.1 Synthesis and Properties of 5,7-Diazaullazines

Jonas Polkaehn, Ricardo Molenda, Miguel A. Cordero, Stefan Lochbrunner, Sebastian Boldt, Peter Ehlers, Alexander Villinger, Peter Langer

J. Org. Chem. **2024**, 89, 2169-2211.

DOI: 10.1021/acs.joc.3c01772

Contribution to this work: **65%**

I did most of the synthetic work and most of the measurements, calculations and wrote the manuscript. Ricardo Molenda carried out the synthetic work and measurements for the reference substances and wrote the comparison with them. Miguel A. Cordero and Stefan Lochbrunner conducted the fluorescence lifetime measurements. Alexander Villiger contributed with the measurement and evaluation of the single crystal X-ray experiment. Sebastian Boldt started the synthetic work during his doctoral thesis with the optimization of the Sonogashira reaction and the first synthesis of one final product. Peter Ehlers and Peter Langer supervised the entire project and performed revision and proof reading of the manuscript.

JOC The Journal of Organic Chemistry

pubs.acs.org/joc Article

Synthesis and Properties of 5,7-Diazaullazines

Jonas Polkaehn, Ricardo Molenda, Miguel A. Cordero, Stefan Lochbrunner, Sebastian Boldt, Peter Ehlers, Alexander Villinger, and Peter Langer*

Cite This: J. Org. Chem. 2024, 89, 2169−2181 Read Online

ACCESS | Metrics & More | Article Recommendations | Supporting Information

ABSTRACT: Hitherto unknown 5,8-substituted-pyrimido[4,5,6-*ij*]pyrrolo[2,1,5-*de*]quinolizines (5,7-diazaullazines) were prepared by a three-step synthesis via Clauson-Kaas, Sonogashira, and cycloisomerization reactions with diverse functionalization. The properties, including cyclovoltammetry and UV−vis and fluorescence spectroscopy, as well as solvatochromism, were studied for selected derivatives and supported by density functional theory calculations. Results were compared in detail with previously reported 5- and 6-azaullazines, and the impact of introduced nitrogen atoms was analyzed.

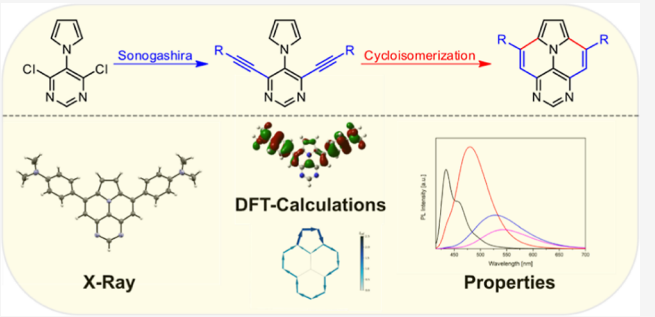

INTRODUCTION

Over the last decades, polycyclic aromatic hydrocarbons (PAHs) as well as hetero-PAHs have emerged as a promising field of organic chemistry. After initial attention on the synthesis, the fascinating and well-studied properties of these compounds came into focus, which is due to their wide range of applications as organic electronics.[1] A well-described example is ullazine, first synthesized by Balli in 1983.[2a] This 16-π-conjugated hetero-PAH, isoelectronic to pyrene, shows interesting electronic and photophysical properties, which are the reason for applications in organic light-emitting diodes (OLEDs),[3,4] organic photovoltaic cells (OPVs),[5,6] organic field-effect transistors (OFETs),[4,7] and other applications. Modifying the ullazine backbone by introducing additional heteroatoms leads to variations of the optoelectronic properties.[3,8,9] Particularly, nitrogen-doping has proven to be a powerful tool for the modification of the properties due to its ability to be added into the framework without changing the structure.[8,10,11] Furthermore, the combination of boron with nitrogen and oxygen atoms has been reported (Figure 1).[3,9]

In addition to the structural advantages, imine-like nitrogen atoms, as in pyridine, have the ability to reduce the LUMO level and HOMO−LUMO gap of hetero-PAHs and amplify the electron-accepting properties.[12] Besides the use of pyridine subunits, the use of pyrimidine units for pyrene-like structures is promising. For example, the group of Gade has shown that tetraazapyrenes, containing two pyrimidine subunits, can potentially act as n-type semiconductors.[13] Moreover, it is known that pyrimidine-containing molecules can exhibit efficient deep blue emission as well as other interesting photophysical properties, such as solvatochromism, and are also suitable for applications as thermally activated delayed fluorescence emitters.[14]

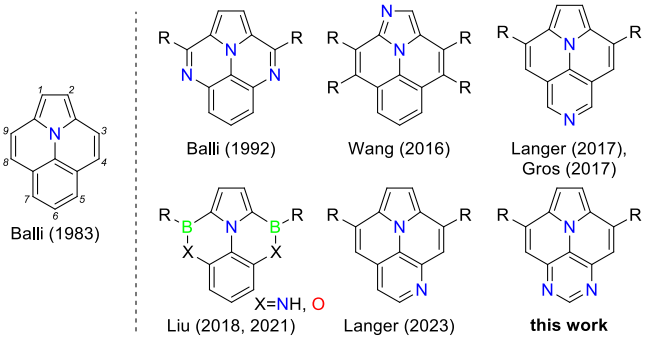

Figure 1. Examples of N-doped ullazine structures.

In order to prepare the core structure of ullazines, several strategies have been described in the literature. The first approach by Balli (1983) used hydrolysis of dithianes in MeOH/H_2O with HgCl, which resulted in double ring closure.[2] In 2005, Takahashi reported a chromium-mediated [4 + 2] cycloaddition of lithiated 1-phenylpyrrole with alkynes.[15] The palladium-catalyzed annulation of 1-(2,6-dibromophenyl)-1*H*-pyrrole with internal alkynes to form various substituted ullazines was shown by You in 2016.[16] Moreover, a photochemical pathway was described by König in 2016 using blue light irradiation in the presence of catalytic amounts of rhodamine 6G and *N*,*N*-diisopropylethylamine, 1-

Received: August 7, 2023
Revised: November 22, 2023
Accepted: January 17, 2024
Published: January 29, 2024

(2,6-dibromophenyl)-1*H*-pyrrole, and aromatic alkynes to produce substituted ullazines. Another possibility, which was described by Grätzel in 2013, relies on cycloisomerization.[5] The key intermediates are prepared by the Sonogashira reaction and subsequently cyclized by a Lewis acid. Using a Brønsted acid-mediated cycloisomerization reaction, in 2017, we reported the synthesis of 6-azaullazines.[8] Recently, we studied the synthesis of 5-azaullazines and the effect of the position of the nitrogen on the optoelectronic properties of the azaullazine system.[17] Herein, we report the first synthesis of various substituted pyrimido[4,5,6-*ij*]pyrrolo[2,1,5-*de*]-quinolizines (5,7-diazaullazines), in which we combined the excellent electronic properties of ullazine with those of electron-deficient pyrimidine. In addition, we have investigated photophysical and electrochemical properties as well as density functional theory (DFT) studies of selected products.

RESULTS AND DISCUSSION

Synthesis. Our synthetic approach started from commercial 4,6-dichloropyrimidin-5-amine (**1**). Known Clauson-Kaas conditions could be successfully transferred to our synthesis, producing starting material **2** in an excellent yield of 95% (Scheme 1).[17]

Scheme 1. Synthesis of Starting Material 2; (i): 2,5-Dimethoxytetrahydrofuran, Acetic Acid, 1,2-Dichloroethane, Reflux, 3 h

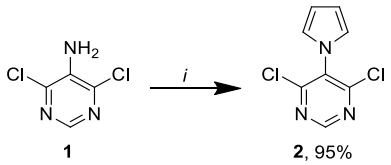

Subsequently, an optimization of the 2-fold Sonogashira reaction was studied for the synthesis of **3a** (Table 1). For the initial test reaction, we used the conditions previously applied during the synthesis of 5-azaullazine, providing **3a** in 82% yield.[17] The yield of **3a** was improved by performing the reaction in 1,4-dioxane at an elevated temperature of 90 °C after 24 h. A shorter reaction time of 12 h caused a diminished yield.

With the conditions of entry 2, various 4,6-bis(arylethynyl)-5-(1*H*-pyrrol-1-yl)pyrimidines **3a**−**e** were synthesized in good to excellent yields (Table 2).

Based on the successful synthesis of precursors **3a**−**e**, it was possible to optimize the final step, i.e., the cycloisomerization (Table 3). The optimization was carried out using derivative **3a**. First, the reaction was performed in the presence of *p*-TsOH·H_2O (30 equiv) at 120 °C in xylene as a solvent. Similar reaction conditions showed good to excellent results in related molecular structures previously published by our group.[8,18] The desired 5,7-diazaullazine (**3a**) could be successfully obtained under these conditions, albeit, in only 38% yield. An increase of the temperature to 140 °C resulted in a better yield of 55% (entry 2). Changing the acid to MsOH (30 equiv) resulted in a lower yield of 34%. The use of TfOH (5 equiv) led to significant decomposition. A further improvement was not achieved using Lewis acids, like $Bi(OTf)_3$ and $In(OTf)_3$. In the case of $In(OTf)_3$, the reaction time had to be increased to 20 h since, after 6 h, the starting material was still present (TLC control). Increasing the temperature to 170 °C using 1,2-dichlorobenzene as a solvent yielded **3a** in 57%. However, the slightly improved yield, as compared to entry 2, does not justify the significantly enhanced temperature. Therefore, the scope was studied using reaction conditions: *p*-TsOH·H_2O (30 equiv) in xylene at 140 °C for 6 h.

The optimized reaction conditions were applied for the conversion of 4,6-bis(arylethynyl)-5-(1*H*-pyrrol-1-yl)-pyrimidines **3a**−**e** to the desired 5,7-diazaullazines **4a**−**e**. The reaction tolerates various functional groups and produces the products in good to very good yields (Table 4). Thereby, electron-donating substituents (**4c** and **4e**) gave better yields compared to those of electron-withdrawing groups like **4b** and **4d.** This can be explained by the stabilization of the cationic transition state (Figure S1).[19]

The structure **4c** was independently confirmed by X-ray crystal structure analysis. Crystallization was performed from a mixture of heptane and EtOAc. The cocrystallized heptane is removed in Figure 2. The phenyl rings are twisted out of the plane of the core structure by dihedral angles of 35°. Furthermore, the crystal lattice exhibits an antiparallel face-to-face $\pi-\pi$-stacking with a spacing of 3.556 Å.

Photophysical Properties. UV−vis absorption and photoluminescence (PL) spectra of 5,7-diazaullazines **4** were measured in dilute dichloromethane (DCM) solutions (Figure 3 and Table 5). Previous studies have shown that functionalized aryl groups at the 3,9-positions of the (aza)ullazine core generally induce minor spectral changes.[5,8,17,28] Therefore, only compounds **4b** and **4c** with more potent donor and

Table 1. Optimization of the Sonogashira Reaction for 3a

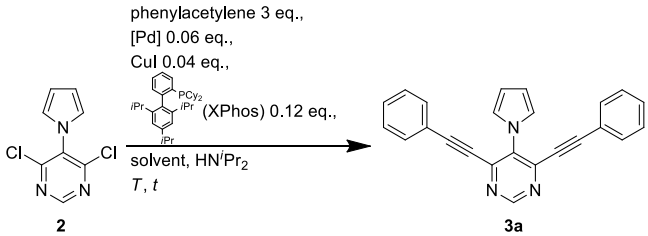

	acid (3 equiv)	ligand	solvent	T [°C]	t [h]	yield[a] [%]
1	$PdCl_2(CH_3CN)_2$	XPhos	MeCN	70	24	82
2	**$PdCl_2(CH_3CN)_2$**	**XPhos**	**1,4-dioxane**	**90**	**24**	**96**
3	$PdCl_2(CH_3CN)_2$	XPhos	1,4-dioxane	90	12	79

[a]Isolated yield.

https://doi.org/10.1021/acs.joc.3c01772
J. Org. Chem. 2024, 89, 2169−2181

Table 2. Synthesis of 3a–e[a]

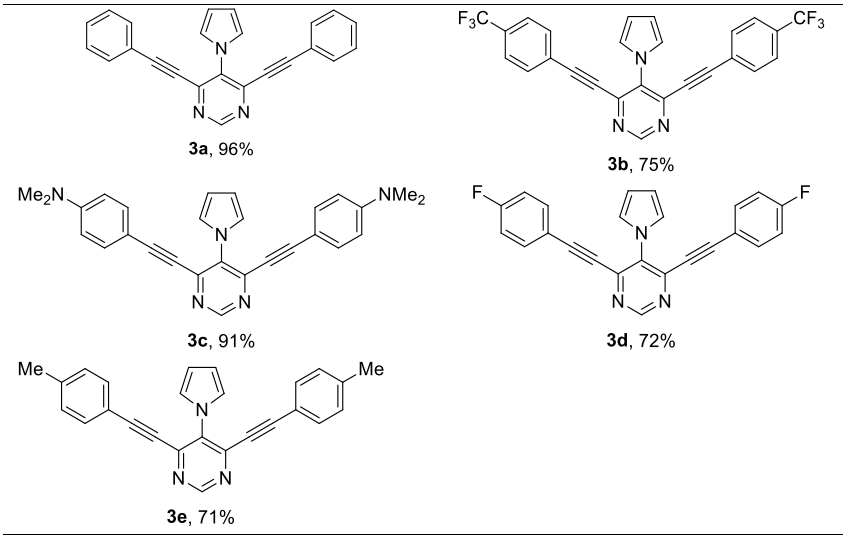

[a]Conditions: alkyne (3 equiv), $Pd(CH_3CN)_2Cl_2$ (6 mol %), XPhos (12 mol %), CuI (4 mol %).

Table 3. Optimization of the Synthesis of 4a

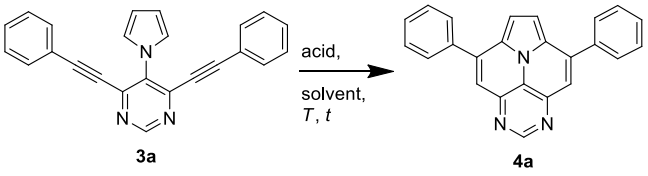

	acid (eq)	solvent	T [°C]	t [h]	yield[a] [%]
1	*p*-TsOH·H_2O (30)	xylene	120	6	38
2	***p*-TsOH·H_2O (30)**	**xylene**	**140**	**6**	**55**
3	MsOH (30)	xylene	140	6	34
5	TfOH (5)	xylene	140	6	17
4	$In(OTf)_3$ (2)	xylene	140	20	27
3	$Bi(OTf)_3$ (2)	xylene	140	6	30
6	*p*-TsOH·H_2O (30)	1,2-dichlorobenzene	170	6	57

[a]Isolated yield.

acceptor groups were studied in addition to the diphenyl derivative **4a**.

As shown in Figure 3, the absorption spectrum of **4a** exhibits well-resolved bands resulting from the rigid 5,7-diazaullazine core. Three prominent absorption bands with maxima at 422 nm (ε = 17,328 M^{-1} cm^{-1}), 338 nm (ε = 11,150 M^{-1} cm^{-1}), and 290 nm (ε = 47,811 M^{-1} cm^{-1}) can be observed. The corresponding extinction coefficients indicate that these are optically allowed transitions and therefore assigned to π–π^* transitions. The emission spectrum with a maximum at 439 nm shows mirror symmetry with respect to the lowest energy absorption band, indicating that the band corresponds to the S_1 state. The intensity distribution of the vibronic sub-bands and the small Stokes shift ($\Delta\lambda$) of 17 nm further suggest only a slight displacement between the ground (S_0) and first excited (S_1) state potential energy surfaces (PES) and thus a small reorganization energy.

Fluorinated **4b** shows an absorption and emission profile comparable to **4a** with lower molar absorptivity and a slight red shift of the absorption and emission maxima by 4 and 10 nm, respectively. In contrast, the introduction of dimethylamino donor moieties at the peripheral phenyl groups leads to remarkable changes in the optical properties. For instance, the lowest energy absorption band of **4c** increases in intensity with respect to **4a**, while $\lambda_{max}^{(abs)}$ remains at 422 nm (ε = 23,805 M^{-1} cm^{-1}). Moreover, broad absorption bands in the range of ~411 to 330 nm with peaks around 395 and 372 nm are observed. These bands are absent in **4a** and **4b** and are therefore associated with transitions involving the amino substituents, for which charge transfer (CT) character can be expected. In addition, the maxima of the higher energy absorption bands show a blue shift relative to **4a** and **4b** along with a significant decrease in molar absorptivity for the high energy band at λ = 285 nm (ε = 27,365 M^{-1} cm^{-1}). Thus, a strong modulation of the electronic transitions with distinct solute–solvent interactions by the introduction of amino donor groups becomes apparent. This is even more evident in the PL spectrum, which displays a broadened unstructured emission band with a maximum at 480 nm, corresponding to a red shift of 41 nm with respect to **4a**. These spectral features indicate an intramolecular charge transfer (ICT) for **4c** upon photoexcitation.

All three 5,7-diazaullazine derivatives exhibit distinct fluorescence in DCM solution with fluorescence quantum yields (Φ_F) in the range of 33–56% using coumarin 153 in cyclohexane as a reference.[20] Compounds **4a** and **4b** emit fluorescence in the deep blue region of the electromagnetic spectra with similar quantum yields of 35 and 33%, respectively, while **4c** emits blue-cyan fluorescence with an enhanced quantum efficiency of Φ_F = 56%. The optical bandgaps determined from the intersection of the normalized absorption and emission spectra are similar and range between 2.84 and 2.88 eV, with the lowest being determined for **4c** (Table 5).

To confirm the ICT nature of the lowest energy excited state of **4c**, solvatochromic studies were performed and compared with **4a** (Figure 4). As can be seen in the spectra of **4a** in various solvents, the solvent polarity shows a negligible effect on the position of the maxima and the fine structure of the

https://doi.org/10.1021/acs.joc.3c01772
J. Org. Chem. 2024, 89, 2169–2181

Table 4. Synthesis of 4a–e[a]

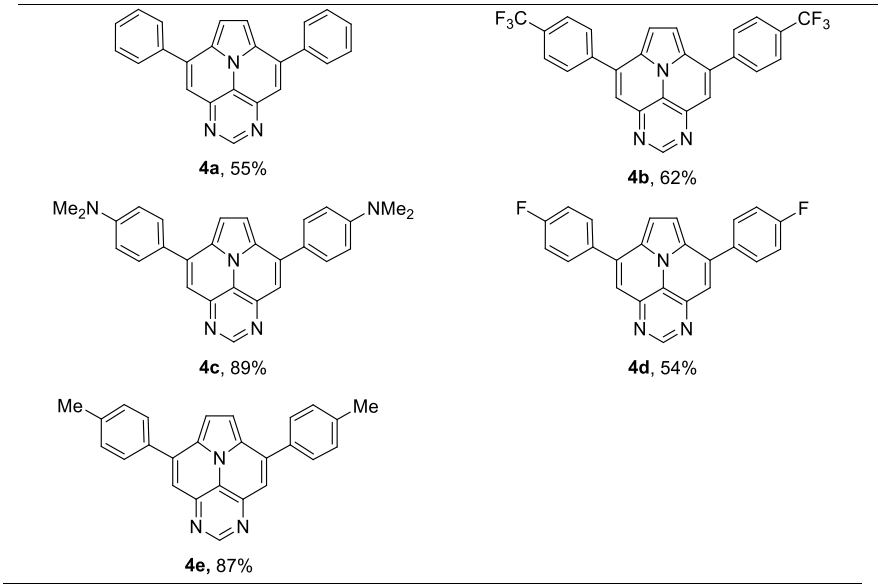

[a]Conditions: *p*-TsOH·H_2O (30 equiv), xylene, 140 °C, 6 h.

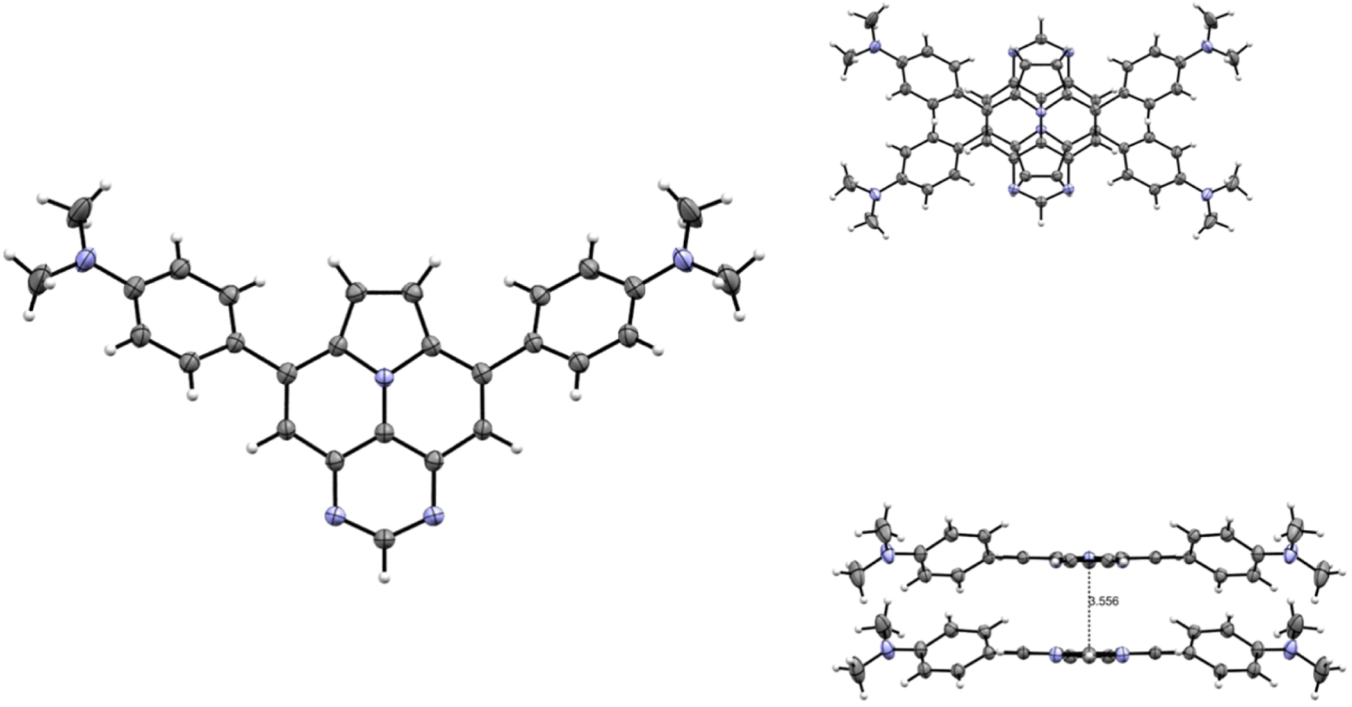

Figure 2. X-ray structure of **4c**. Left: top view. Right top: top view of the packing structure. Right bottom: side view of the packing structure. Thermal ellipsoids are drawn at the 50% probability level.

absorption and emission bands. Therefore, it can be concluded that the dipole moment of **4a** does not change significantly upon excitation, which is supported by the time-dependent DFT (TD-DFT) calculated change of the dipole moment between the S_0 and S_1 states (**4a**: μ_{S0} = 6.1846 D μ_{S1} = 7.6453). In contrast, **4c** shows pronounced solvatochromic behavior. For instance, the extinction coefficient of the lowest energy transition is significantly higher in more polar solvents (DCM: ε = 23,805 M^{-1} cm^{-1}, MeCN: ε = 21,084 M^{-1} cm^{-1}, ethanol: ε = 33,000 M^{-1} cm^{-1}) as compared to that of toluene (ε = 15,724 M^{-1} cm^{-1}), and polarity-specific solute–solvent effects on the absorption profiles at shorter wavelengths become apparent. However, the energy of the S_1 transition changes only marginally in the different solvents, implying that solvent-mediated stabilization of the S_0 state is not significant.

In the emission spectra, a gradual red shift of the emission band with inhomogeneous broadening is observed with increasing solvent polarity. The emission maximum shifts bathochromically from 434 nm in toluene to 542 nm in ethanol along with a large Stokes shift of $\Delta\lambda$ = 118 nm, resulting in a modulation of the emission color from deep blue to yellow. This confirms the ICT character of the lowest

https://doi.org/10.1021/acs.joc.3c01772
J. Org. Chem. 2024, 89, 2169–2181

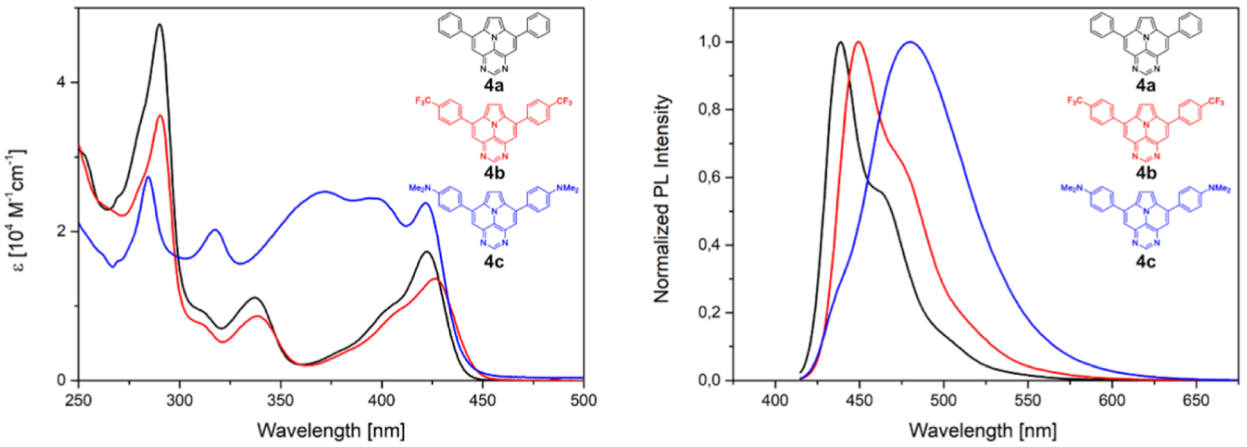

Figure 3. UV/vis (left) and PL spectra (right, λ_{ex} = 400 nm) of **4a–c** in DCM ($c = 10^{-5}$ M) at 20 °C.

Table 5. Spectroscopic Data of 4a–c in DCM ($c = 10^{-5}$ M) at 20 °C

	4a	4b	4c
λ_{abs1} [nm] (ε_1 [10^4 $M^{-1}cm^{-1}$])	290 (4.8)	290 (3.6)	285 (2.7)
λ_{abs2} [nm] (ε_2 [10^4 $M^{-1}cm^{-1}$])	311 (0.9)	311 (0.7)	317 (2.0)
λ_{abs3} [nm] (ε_3 [10^4 $M^{-1}cm^{-1}$])	338 (1.1)	338 (0.9)	372 (2.5)
λ_{abs4} [nm] (ε_4 [10^4 $M^{-1}cm^{-1}$])	402 (1.7)	405 (0.9)	395 (2.5)
λ_{abs5} [nm] (ε_5 [10^4 $M^{-1}cm^{-1}$])	422 (1.7)	426 (1.4)	422 (2.4)
λ_{em1} [nm]	439	449	480
λ_{em2} [nm]	462[b]	473[b]	
E_g(opt.) [eV]	2.88	2.86	2.84
Φ_F[a] [%]	35	33	56

[a]Fluorescence standard: coumarin 153 in cyclohexane (Φ = 0.9).[20] [b]Indicates a shoulder.

electronic transition in **4c**, driven by a large, enhanced dipole moment in the excited state ($\mu_{cal.}$(**4c**): μ_{S0} = 9.9618 D, μ_{S1} = 18.3813 D) and an associated stabilization of the ^{1}CT state by the solvent polarity.[21] In this context, the vibrationally resolved PL spectrum in toluene with a small Stokes shift of $\Delta\lambda$ = 14 nm indicates that the ^{1}CT state is not sufficiently stabilized in low-polar solvents so that emission in toluene arises from the locally excited (^{1}LE) state.

The determined quantum yields in different solvents using coumarin 153 in cyclohexane as ref 20 gave similar values for **4a**: toluene (Φ_F = 40%), DCM (Φ_F = 35%), MeCN (Φ_F = 32%), and ethanol (Φ_F = 39%), with the increase of the latter possibly due to hydrogen bonding effects. On the other hand, the quantum yields for **4c**: toluene (Φ_F = 44%), DCM (Φ_F = 56%), MeCN (Φ_F = 29%), and ethanol (Φ_F = 18%) show a significant decrease for more polar solvents, as is common for CT states. However, the improved quantum efficiency in CH_2Cl_2 and the relatively high Φ_F values retained in acetonitrile and ethanol render **4c** with interesting CT properties, and, to the best of our knowledge, a donor-substituted (aza)ullazine with such CT features has not been reported before.

Next, the redox properties of **4a** and **4c** were explored by means of cyclic voltammetry (CV) (Figure 5). Measurements were carried out in DCM with 0.1 M *n*-Bu_4NPF_6 as a supporting electrolyte, a glassy carbon working electrode, a platinum counter electrode, ferrocene as a standard, and a scan rate of 100 mV/s. Thereby, **4a** shows a distinct oxidation potential at 1.00 V vs Fc^+/Fc with an onset potential of 0.85 V vs Fc^+/Fc, whereas **4c** shows a rather broadened oxidation potential with a peak at 0.89 V vs Fc^+/Fc and an onset potential of 0.40 V vs Fc^+/Fc. The voltammograms reveal that these are irreversible oxidation processes. In comparison, the onset potential of **4c** is significantly lower than that of **4a** and most likely attributed to the oxidation of the amino donor moieties. Using the determined onset potentials, the HOMO level of **4a** and **4c** was calculated. Thereby, the HOMO level of ferrocene is considered to be 4.80 eV below the vacuum level.[22] The calculated HOMO energies are −5.69 eV (**4a**) and −5.20 eV (**4c**).

To gain further insight into the electronic properties and transition characters, DFT and TD-DFT calculations were performed with Gaussian09[23] at the B3LYP/6-31G(d,p) level of theory in combination with a polarizable continuum model (PCM) of dichloromethane using the integral equation formalism variant (IEFPCM) to include solvent effects. As depicted in Figure 6, the HOMO and LUMO of **4a** are mainly distributed along the diazaullazine periphery, with the LUMO extending further into the aryl side groups. In contrast, the HOMO of **4c** is predominantly located at the *N*,*N*-dimethylaniline units, while the LUMO is primarily located at the central diazaullazine core, thus showing the spatial separation between the donor and acceptor. Additionally, compound **4a** shows lower HOMO and LUMO energy levels and a larger band gap compared to those of **4c**. The energies and trends from the calculations are in very good agreement with the experimental results from the UV/vis and CV measurements.

Comparison of the HOMO and LUMO energies and band gaps of ullazine (**5**) with those of singly N-doped 6-azaullazine (**6**) and 5-azaullazine (**7**) further demonstrate that the introduction of nitrogen atoms leads to considerable stabilization of the HOMO and LUMO energy levels with respect to ullazine **5**. The band gap, on the other hand, is hardly affected. Furthermore, the stabilization is significantly stronger when nitrogen is introduced in the 5-position than in the 6-position. This can be explained by the larger orbital coefficients in the 5-position compared to those in the 6-position, which is placed on the nodal planes of both the HOMO and LUMO of ullazine. Consequently, the doping of nitrogen in both the 5- and 7-positions results in the largest stabilization effect on the HOMO and LUMO energies with a slightly larger band gap.

https://doi.org/10.1021/acs.joc.3c01772
J. Org. Chem. 2024, 89, 2169−2181

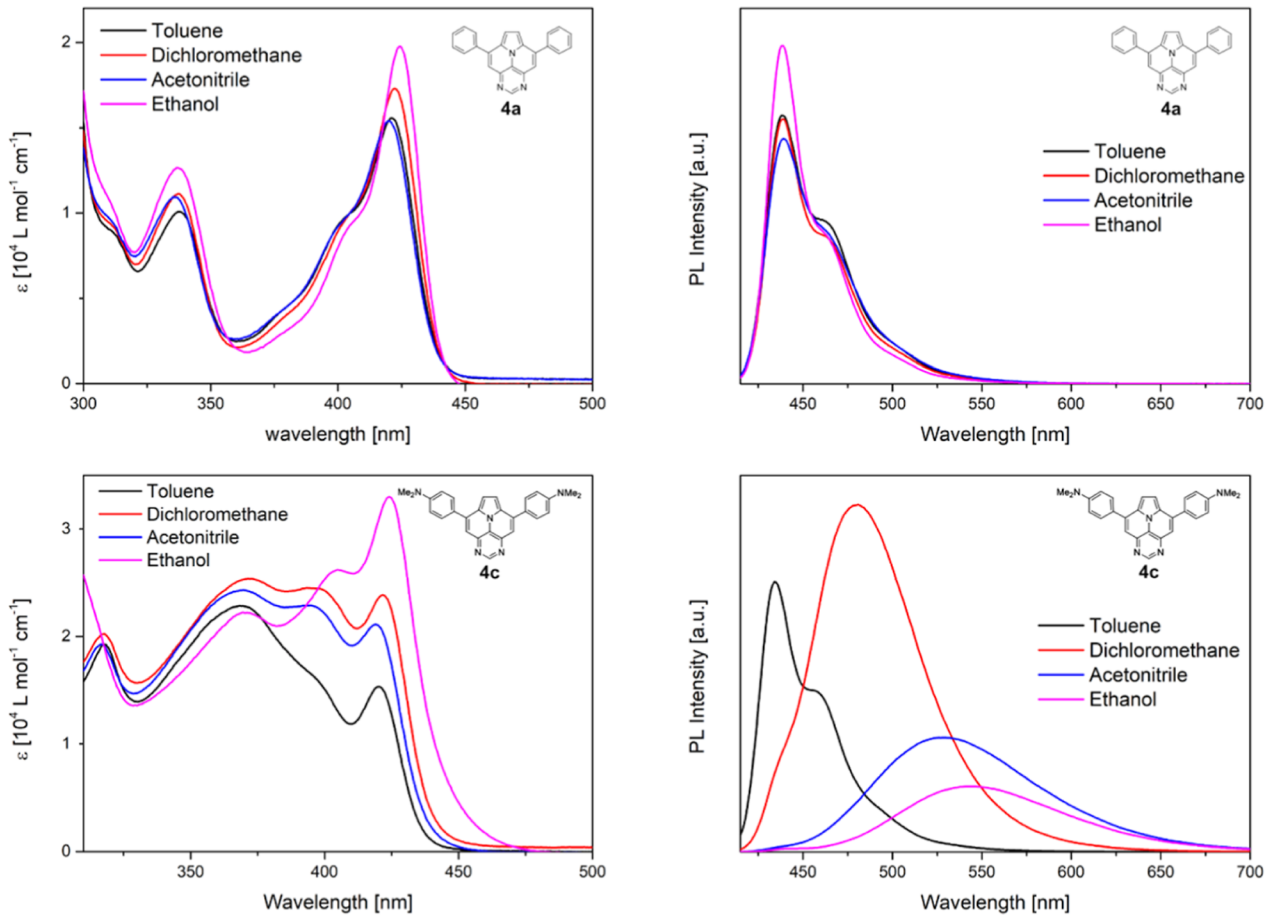

Figure 4. Top: UV/vis (left) and emission spectra (right, λ_{ex} = 400 nm) of **4a**; bottom: UV/vis (left) and emission spectra (right, λ_{ex} = 400 nm) of **4c**; spectra measured in toluene, dichloromethane, acetonitrile, and ethanol ($c = 10^{-5}$ M at 20 °C).

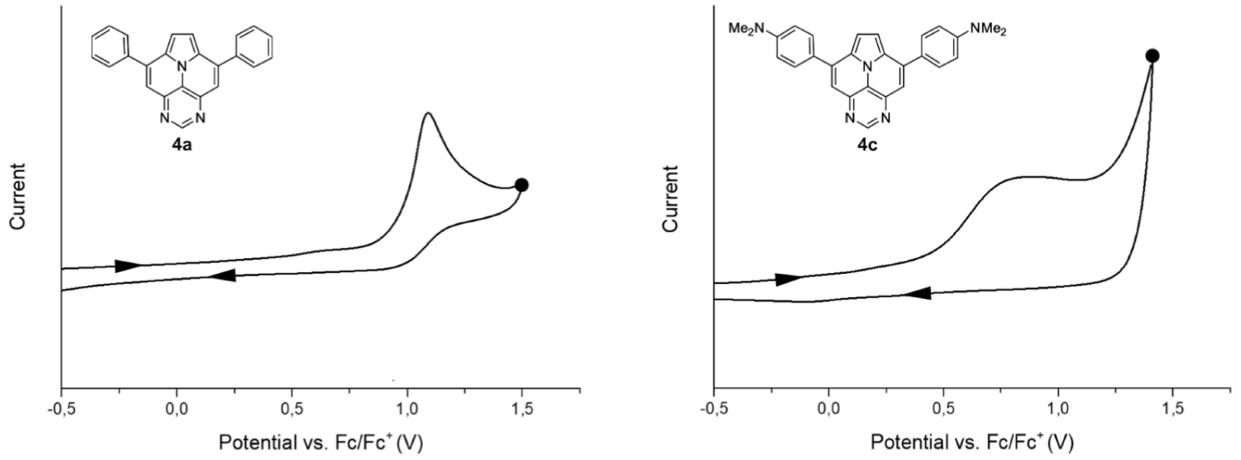

Figure 5. Cyclic voltammograms of **4a** and **4c**, which were measured in DCM ($c = 10^{-3}$ M) with 0.1 M *n*-Bu_4NPF_6 as a supporting electrolyte, a glassy carbon working electrode, and a Pt counter electrode with ferrocene as a standard at a scan rate of 100 mV/s. The direction of the scan is reductive with a starting potential of 1.5 V and a switching potential of −1.5 V. CVs are plotted using the IUPAC convention and shown in the anodic range between −0.5 and 1.5 V.

The calculated $S_1 \leftarrow S_0$ excitation energies of **4a** and **4c** gave excellent agreement for **4c** (λ_{cal} = 424 nm, λ_{exp} = 422 nm), while the B3LYP functional significantly overestimates the experimental value for **4a** (λ_{exp} = 422 nm) by 0.31 eV (λ_{cal} = 381 nm). Better agreement with the experiment is obtained with the PBE functional predicting the S_1 transition of **4a** at 413 nm, which reduces the error to 0.06 eV. Regardless of the accuracy of the excitation energy, both functionals provide the same qualitative result for the $S_1 \leftarrow S_0$ transition of **4a**, which is predicted to be dipole-allowed and dominated by the HOMO → LUMO excitation (Tables 14 and 17). The same dominant MO contribution is given for **4c** (f = 0.6870), thus confirming the LE character in **4a** and the ICT in **4c** (Table S16). In addition, the higher energy transitions of **4c** are also predicted

https://doi.org/10.1021/acs.joc.3c01772
J. Org. Chem. 2024, 89, 2169−2181

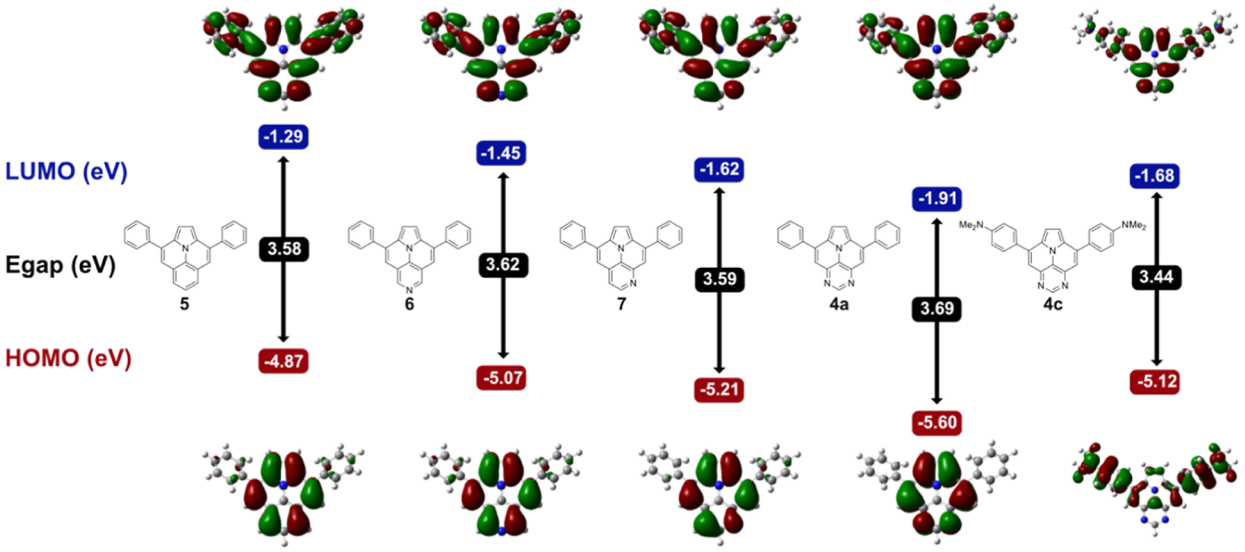

Figure 6. Frontier molecular orbitals, energy levels, and corresponding energy gaps of ullazine (**5**) and various aza-ullazines calculated at the B3LYP/6-31G(d,p) level of theory in DCM.

Table 6. Photophysical, Electrochemical, and Theoretical Data of 6-Azaullazine (6), 5-Azaullazine (7), and 5,7-Diazaullazine (4a) in DCM

	UV−vis/fluorescence									CV		DFT[j]		
	λ_{abs} [nm]	λ_{em}[a] [nm]	$\Delta\lambda$ [nm]	$E_g^{(opt)}$[b] [eV]	Φ_F[c,d] [%]	τ_{fl}[d] [ns]	τ_0[f] [ns]	k_r [10^7 s^{-1}]	k_{nr}[10^7 s^{-1}]	HOMO[h] [eV]	$E_{(ox)}$[i] [V]	HOMO [eV]	LUMO [eV]	E^g [eV]
6	430	487	57	2.75	7[8]	9.0[e]	128.6[g]	0.7	10.3	−5.26	0.46[8]	−5.07	−1.48	3.59
7	443	469	26	2.76	23	5.6	24	4.1	13.7	−5.36	0.56[17]	−5.21	−1.62	3.59
4a	422	439	17	2.88	35	3.7	11	9.5	17.6	−5.69	1.00	−5.60	−1.91	3.69

[a]Excited at λ = 400 nm. [b]Determined from the intersection of the normalized absorption and emission spectra. [c]Fluorescence standard: coumarin 153 in cyclohexane.[20] [d]Measured in air. [e]Amplitude-weighted average lifetime (τ_m). [f]Natural lifetime. [g]Estimated using τ_m. [h]Estimated from $E_{(HOMO)} = -e(4.8 + E_{ox}^{(onset)})$. [i]Potential vs Fc^+/Fc. [j]Calculated at the B3LYP/6-31G(d,p) level of theory in CH_2Cl_2.

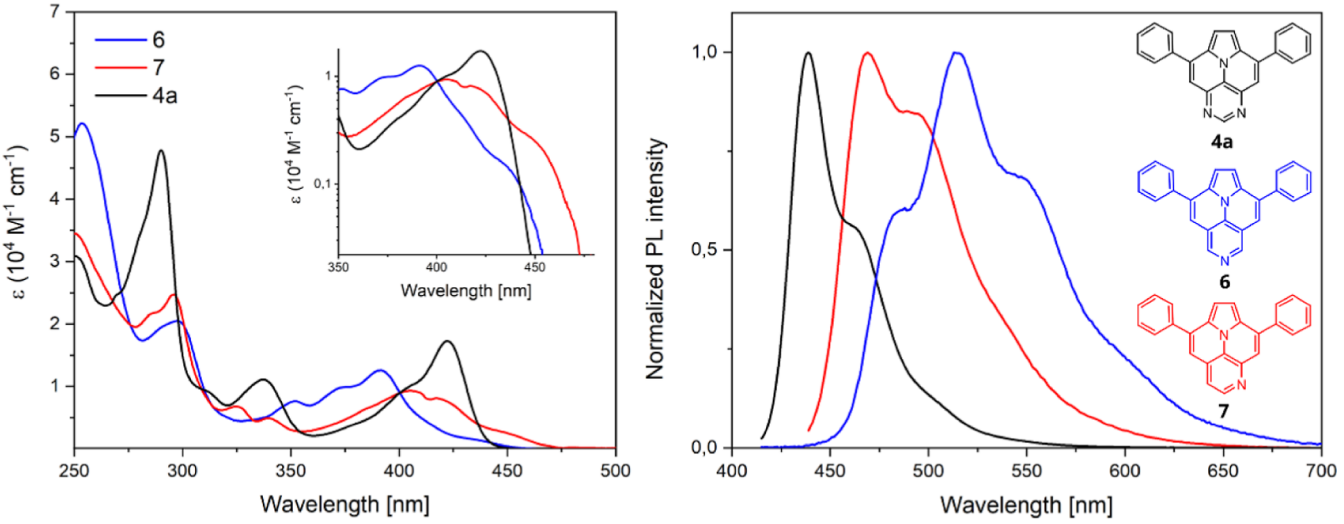

Figure 7. Comparison of UV/vis (left) and PL spectra (right, λ_{ex} = 400 nm) of **4a**, **6**, and **7** in DCM ($c = 10^{-5}$ M) at 20 °C. Inset in UV/vis spectra: lowest energy absorption bands of **4a**, **6**, and **7** in logarithmic scale.

with CT properties, of which the $S_2 \leftarrow S_0$ (f = 0.1945) and $S_5 \leftarrow S_0$ (f = 0.2904) transitions are dipole-allowed at 400 and 362 nm, respectively, which is in good agreement with the experimentally observed absorption bands at 395 and 372 nm.

To illustrate the impact of the position and number of nitrogen atoms in the ullazine backbone on the optoelectronic properties, singly doped ullazines **6**, **7**, and diazaullazine **4a** were compared. The corresponding photophysical, electrochemical, and theoretical data are summarized in Table 6. The absorption and PL spectra of the three aza-ullazine derivatives in CH_2Cl_2 are depicted in Figure 7. Compared to 6-azaullazine **6**, which has been shown to have nearly identical spectral

https://doi.org/10.1021/acs.joc.3c01772
J. Org. Chem. 2024, 89, 2169−2181

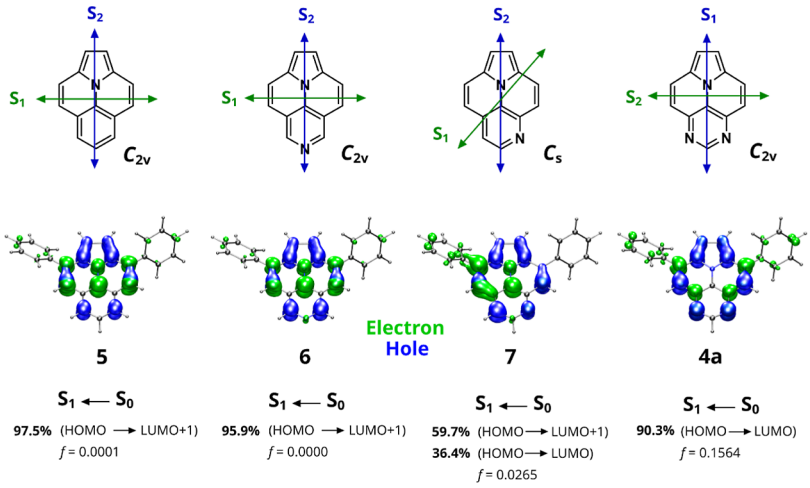

Figure 8. Top: structures of ullazine (**5**), 6-azaullazine (**6**), 5-azaullazine (**7**), and 5,7-diazaullazine (**4a**) with point group symmetry and transition dipole moment directions for the two lowest-lying singlet excited states. Bottom: hole−electron maps for the $S_1 \leftarrow S_0$ transition of (aza)ullazines **5**, **6**, **7**, and **4a**. Dominant orbital contributions for the individual transitions with percentages and corresponding oscillator strengths. Calculated at the B3LYP/6-31+G(d,p) level with the B3LYP/6-31G(d,p)-optimized S_0 geometry. Blue and green isosurfaces represent hole and electron distributions, respectively (isovalue 0.003 au).

properties to ullazine **5**,[8,11,29] 5-azaullazine **7** exhibits red shifts in the long wavelength region with a decrease in molar absorptivity, while the positions of the short wavelength absorption bands change only marginally. 5,7-diazaullazine **4a**, on the other hand, shows red shifts in both the short- and long-wavelength regions of the absorption spectrum and the highest molar absorptivity for the lowest energy absorption band among the nitrogen-doped ullazines. Accordingly, the $S_1 \leftarrow S_0$ absorption in **4a** (λ_{abs} = 422 nm, ε = 17,328 M^{-1} cm^{-1}) is intense, while weak bands are seen for the singly doped ullazines, with extinction coefficients increasing from **6** (λ_{abs} = ∼ 430 nm, ε = 1781 M^{-1} cm^{-1}) to **7** (λ_{abs} = ∼ 443 nm, ε = 3024 M^{-1} cm^{-1}). The Stokes shift decreases from a relatively large value for **6** (57 nm) to **7** (26 nm) to **4a** (17 nm) with a gradual blue shift of the emission maxima and a change in the vibronic intensity distribution with a narrowing of the emission bands. This leads to an emission color change from green for **6** to deep blue for **4a** and shows the strong impact on the optical properties by the position and the number of nitrogen atoms within the ullazine backbone.

This is further elucidated by time-resolved measurements (for details, see Supporting Information), which show that the radiative decay rate ($k_r = 1/(\tau_{fl} \times \Phi_F)$) for **6** determined from the fluorescence lifetime τ_{fl} and quantum yield Φ_F (see Table 6) is fairly slow (k_r = 0.7 × 10^7 s^{-1}) and thus typical of a forbidden transition by the Strickler−Berg relation, which is also fully in line with the long natural lifetime of τ_0 ∼ 129 ns.[30] Compared to **6**, lower-symmetry 5-azaullazine **7** shows a more than 5 times shorter lifetime (τ_0 = 24 ns) with an approximately 6-fold increase of the radiative decay rate (k_r = 4.1 × 10^7 s^{-1}). These values are similar to those of isoelectronic 2-azapyrene (τ_0 = ∼ 28 ns, k_r = 3.6 × 10^7 s^{-1} in DCM), for which the weak $S_1 \leftarrow S_0$ absorption band increases in intensity due to the symmetry-lowering by nitrogen doping of pyrene.[31] On the other hand, the incorporation of nitrogen in positions 5 and 7 of the ullazine core (**4a**) results in the shortest lifetime (τ_0 = 11 ns) and the highest radiative decay rate (k_r = 9.5 × 10^7 s^{-1}) among the three aza-ullazine derivatives.

Consequently, the intensities of the $S_1 \leftarrow S_0$ absorption should be weak for **6** and **7** and increase in the order **6** < **7** < **4a**, which fully agrees with that of the extinction coefficients of the lowest energy absorption bands in the UV−vis spectra. Thus, the position and number of nitrogen atoms in the ullazine backbone determine how allowed the $S_1 \leftarrow S_0$ transition is, which also explains the increasing quantum yields from **6** (7%[8]) over **7** (23%) to **4a** (35%). Nevertheless, the Φ_F value remains moderate even for **4a** as the nonradiative decay rates (k_{nr}) are higher than the k_r rates in all aza-ullazines (Table 6). Moreover, from the above results, it is further derived that the λ_{max} values of **6** (391 nm, ε = 12,571 M^{-1} cm^{-1}) and **7** (405 nm, ε = 9450 M^{-1} cm^{-1}) for the low-energy absorption bands must correspond to the $S_2 \leftarrow S_0$ transition, as was previously suggested for **6**.[11]

These results are fully consistent with TD-DFT calculations, which are in accordance with ullazine **5** the $S_1 \leftarrow S_0$ transition of 6-azaullazine (**6**) with vanishing oscillator strength (f = 0.0000) polarized along the short molecular axis and nearly fully represented by the singly excited configuration of HOMO → LUMO + 1 (95.9%), while the long axis polarized dipole-allowed HOMO → LUMO excitation (f = 0.2800) corresponds to the $S_2 \leftarrow S_0$ transition (Tables S18 and S19). Incorporation of nitrogen in position 5 of the ullazine core adds a HOMO → LUMO contribution to the $S_1 \leftarrow S_0$ transition, and the lowest energy electronic transition in **7** is described by a combination of HOMO → LUMO + 1 (59.7%) and HOMO → LUMO (36.4%) excitations with a slightly increased oscillator strength (f = 0.0265) as compared to that of **6**. Upon doping of nitrogen in the 5- and 7-position, the two lowest singlet excited states in ullazine switch the energetic order, and the $S_1 \leftarrow S_0$ transition of **4a** corresponds to the long axis polarized dipole-allowed HOMO → LUMO excitation (90.3%) (f = 0.1564).

The electron−hole maps[24] of the corresponding $S_1 \leftarrow S_0$ transitions (Figure 8) illustrate that the excited-state electron density rearrangement in **5**, **6**, and **7** leads to electron-rich regions within the two central rings of the short molecular axis including the inner nitrogen. However, compared to **5** and **6**, an asymmetry in the electron density reorganization and the

https://doi.org/10.1021/acs.joc.3c01772
J. Org. Chem. 2024, 89, 2169−2181

resulting spatial distribution of hole-rich and electron-rich regions is shown for **7**, which can be attributed to the mixed double excitation character with the HOMO → LUMO contribution as a result of the lower molecular symmetry. In contrast to the excited-state electron density rearrangement in **5**, **6**, and **7**, the electron−holes in **4a** are exclusively delocalized along the diazaullazine perimeter, without the participation of the central nitrogen and carbon atoms localized in the nodal plane.

Consequently, the $S_1 \leftarrow S_0$ transition of **5**, **6**, and **7** is interpreted as a short-range CT (SRCT)-like excitation of the $\pi\pi^*$ character. Since electron redistribution occurs within short distances, the SRCT retains the local emission nature and thus differs strongly from the long-range charge transfer (LRCT) observed for **4c** with pronounced solvatochromism. This is nicely illustrated by comparing the dimethylaniline derivatives of 6-azaullazine (**8**) and 5-azaullazine (**9**) with 5,7-diazaullazine **4c**, where the SRCT (HOMO → LUMO+1 for **8**, HOMO → LUMO+1/HOMO → LUMO for **9**) is predicted to dominate over the LRCT (HOMO → LUMO) in the S_1 state for **8** and **9**, while the reverse order applies to **4c** (Tables S21−22). These predictions are in full agreement with the experimental results of the solvatochromic studies, which confirm that, unlike **4c**, the emission wavelengths of **8** and **9** are virtually independent of the solvent polarity (Figures S5−6).

From the combined experimental and theoretical studies, the change in the vibronic intensity distribution with narrowing of the emission bands can be rationalized by the different transition characteristics of the $S_1 \leftarrow S_0$ transition, for which the relaxation energy, and thus, the relative shift of the potential energy surface (PES) between the S_0 and S_1 states decrease in the order **6** > **7** > **4a**. Comparative results from the dimethylaniline donor derivatives of the different aza-ullazines further highlight the intriguing changes of the photophysical properties caused by the doping of nitrogen in the 5,7-positions, switching the ullazine donor moiety[5] into an acceptor unit in the excited state. This is also reflected in the CV data, where the typical donor strength of ullazine **5** ($E_{1/2}$ = 0.38 V vs Fc^+/Fc)[2b] is less affected in **6** (0.46 V vs Fc^+/Fc) and **7** (0.56 V vs Fc^+/Fc), while the donating properties strongly decrease in 5,7-diazaullazine **4a** (1.00 V vs Fc^+/Fc), as shown by the more than 2-fold higher oxidation potential as compared to that of ullazine **5**.

Finally, an investigation of the magnetic behavior was performed using the nuclear-independent chemical shift (NICS) method as a criterion of aromaticity.[25,26] The calculations were performed at the GIAO/B3LYP/6-311+G-(d,p) level of theory with the B3LYP/6-311G(d,p) gas-phase optimized ground-state structures. $NICS(1.25)_{ZZ}$ values were determined to describe the "local aromaticity".[25] Additionally, the ring currents were calculated and visualized to perform a more detailed analysis of the aromaticity. Visualization of the bond current (NICS2BC) was performed using the BC-Wizard program (Figures 9 and 10).[26]

5,7-Diazaullazine (**4′**) has negative $NICS(1.7)_{ZZ}$ values in all rings, with a stronger aromaticity predicted for the pyrrole moiety (Figure 9). This is also reflected in the ring current map, where a clear local diatropic ring current can be seen in the pyrrole unit, whereas the other rings do not exhibit any local ring currents. However, a global diatropic ring current is shown along the perimeter of **4′**, which also displays a stronger current strength in the pyrrole moiety. From the X-ray

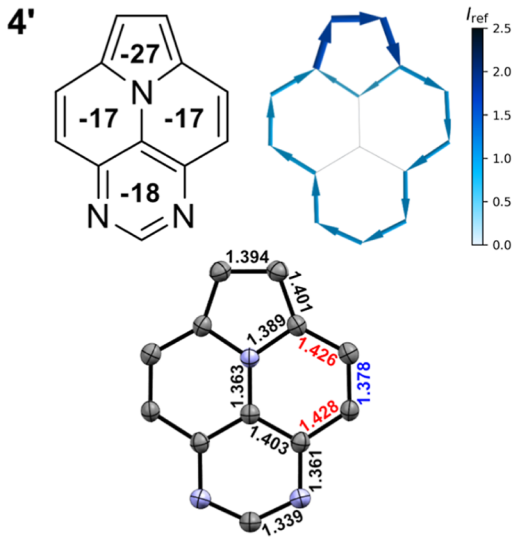

Figure 9. NICS calculations and bond current map for 5,7-diazaullazine (**4′**). Top left: structure of **4′** with respective $NICS(1.7)_{ZZ}$ values in the center of each ring. Top right: NICS2BC bond current graph (current was calculated from $NICS(1.25)_{ZZ}$, strength relative to I_{ref} (ring current of benzene, 11.5 nA T^{-1})). Bottom center: crystal structure of **4c** and bond lengths. Peripheral aryl groups and hydrogen atoms have been omitted for clarity. Thermal ellipsoids are drawn at the 50% probability level.

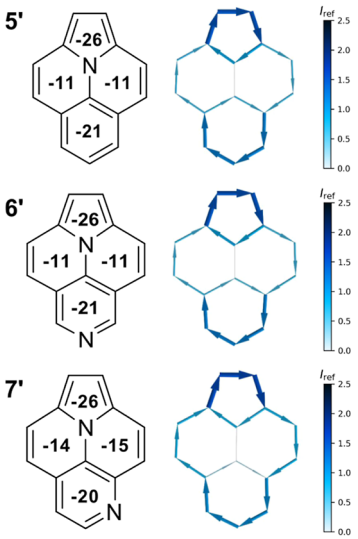

Figure 10. NICS and bond current maps for ullazine (**5′**), 6-azaullazine (**6′**), and 5-azaullazine (**7′**); left: structures of **5′**, **6′**, and **7′** with respective $NICS(1.7)_{ZZ}$ values in the center of each ring. Right: NICS2BC bond current graphs (currents were calculated from $NICS(1.25)_{ZZ}$, strength relative to I_{ref} (ring current of benzene, 11.5 nA T^{-1})).

structure, it can be deduced that the longest C−C bonds (marked in red) as well as the shortest C−C bond (marked in blue) are located in the central ring. These results indicate the lower conjugation/aromaticity in these rings, which also emerge from the calculations.

For comparison, the $NICS(1.7)_{ZZ}$ values and bond currents of ullazine (**5′**), 6-azaullazine (**6′**), and 5-azaullazine (**7′**) were calculated. Herein, both **5′** and **6′** show identical $NICS(1.7)_{ZZ}$ values and bond currents, highlighting that the introduction of nitrogen in the 6-position does not alter the aromaticity of the

https://doi.org/10.1021/acs.joc.3c01772
J. Org. Chem. 2024, 89, 2169−2181

ullazine core. Moving the nitrogen to the 5-position leads to slightly increased aromaticity in the central rings, as indicated by the NICS(1.7)$_{ZZ}$ values, while the pyridine and pyrrole rings are hardly affected. Moreover, the ring currents of 7′ differ from those of **5′** and **6′** in which a decrease of the local ring current is observed in the pyridine unit, while the global ring current is more pronounced. This trend continues for **4′**, leading to an even stronger effect on the global ring current and comparable NICS values in the central rings and the pyrimidine moiety. Overall, doping by nitrogen in the 5- and 7-positions leads to an enhanced global diatropic ring current. Thus, the aromaticity of **4′** differs from the other (aza)ullazine core structures, which emphasizes the modification potential by the introduction of nitrogen in the 5,7-positions.

CONCLUSIONS

A series of diversely functionalized 5,7-diazaullazines were synthesized via a three-step synthesis consisting of Clauson-Kaas, Sonogashira, and Brønsted acid-mediated cycloisomerization reactions in good yields. The electrochemical and photophysical behavior due to the introduction of nitrogen atoms in the 5,7-positions of the ullazine core is remarkable and differs strongly from that of singly doped 5- and 6-azaullazines. In evaluation of the excited-state dynamics, the natural lifetimes decrease from a quite long lifetime in 6-azaullazine **6** ($\tau_0 \sim 129$ ns) to 5-azaullazine **7** ($\tau_0 = 24$ ns) to 5,7-diazaullazine **4a** ($\tau_0 = 11$ ns), while the k_r and Φ_F values increase steadily. TD-DFT calculations indicate that the energy of the "dark" S_1 state in ullazine, originating from a $\pi\pi^*$ transition with the expected local short-range charge transfer character, becomes destabilized as a function of the position and number of nitrogen atoms in the ullazine backbone and finally switches the energetic order with the "bright" $\pi\pi^*$-state in 5,7-diazaullazine. DFT calculations and electrochemical measurements further show that the HOMO and LUMO energies are successively stabilized depending on the position and number of nitrogen atoms and are most pronounced by the incorporation of nitrogen atoms in the 5,7-positions. As a result, the usually strong donor properties of ullazine are strongly reduced in 5,7-diazaullazine, turning the ullazine donor into an acceptor in the excited state, as demonstrated by the strong ICT with pronounced solvatochromism of donor-substituted diazaullazine **4c**. Aromaticity investigations also reveal improved global ring currents by the doping of nitrogen in the 5,7-positions of the ullazine scaffold. Thus, the incorporation of a pyrimidine unit into the ullazine backbone gives rise to strongly modulated optoelectronic properties.

EXPERIMENTAL SECTION

General Information. The nuclear magnetic resonance spectra (^{1}H/^{13}C/^{19}F NMR) were recorded on a Bruker AVANCE 300 III, 250 II, or 500. The analyzed chemical shifts δ are referenced to the residual solvent signals of the deuterated solvent $CDCl_3$ ($\delta = 7.26$ ppm/77.0 ppm). Multiplicities due to spin−spin correlation are reported as follows: s = singlet, d = doublet, dd = double doublet, t = triplet, m = multiplet, and further described through their coupling constants *J*. Infrared spectra (IR) were measured as attenuated total reflection (ATR) experiments with a Nicolet 380 FT-IR spectrometer. The signals were characterized through their wavenumbers $\tilde{\nu}$ and their corresponding absorption as very strong (vs), strong (s), medium (m), or weak (w). UV/vis spectra were recorded on a Cary 60 UV−vis spectrophotometer and emission spectra with an Agilent Cary Eclipse fluorescence spectrophotometer. Time-resolved fluorescence signals were recorded with a streak camera (Streakscope C10627, HAMAMATSU PHOTONICS). The excitation pulses with a wavelength of ∼380 nm were generated with a noncollinear optical parametric amplifier (NOPA). The NOPA was pumped with laser pulses at 775 nm from a Ti:sapphire laser system (CPA 2001, CLARK MXR, INC.) with a repetition rate of 1 kHz. Cyclic voltammograms were measured at room temperature in DCM ($c = 10^{-3}$ M) with 0.1 M *n*-Bu_4NPF_6 as a supporting electrolyte, a glassy carbon working electrode, ANE2 ($Ag/AgNO_3$ 0.01 M in CH_3CN) as a reference electrode, and a Pt counter-electrode (0.5 mm diameter platinum wire) with ferrocene ($c = 10^{-3}$ M in CH_3CN) as an external standard at a scan rate of 100 mV/s. The potentiostat used was an EmStat 3 blue from PalmSense. The working electrode was a 3 mm diameter (length 80, 6.35 mm outer diameter) glassy carbon disk electrode in a KeI-F coating that was polished on a polishing pad in aqueous alumina slurry (0.03 μm alumina powder). The solvents were deoxygenated by purging them with argon. The potential was given vs Fc/Fc+. The direction of the scan was reductive with a starting potential of 1.5 V and a switching potential of −1.5 V. Cyclic voltammograms were plotted using the IUPAC convention and are shown in the anodic range between −0.5 and 1.5 V. Basic and high-resolution mass spectra (MS/HRMS) were measured on instruments which were paired with a preceding gas chromatograph or liquid chromatograph. The samples were ionized through electron impact ionization (EI) on an Agilent 6890/5973 or Agilent 7890/5977 GC−MS system equipped with a HP-5 capillary column using helium carrier gas or by applying electron spray ionization (ESI) on an Agilent 1200/6210 Time-of-Flight (TOF) LC−MS spectrophotometer. Melting points (mp) were determined by Micro-Hot-Stage GalenTM III Cambridge Instruments and are not corrected. X-ray single-crystal structure analysis was performed on a Bruker Apex Kappa-II CCD diffractometer.

Analytical Data. *4,6-Dichloro-5-(1H-pyrrol-1-yl)pyrimidin (**2**).* One equiv (30.5 mmol, 5 g) of 4,6-dichloropyrimidin-5-aminen (**1**) was dissolved in 25 mL of acetic acid and 25 mL of 1,2-dichloroethane. Then, 2,5-dimethoxy-tetrahydrofuran (1.05 equiv, 32 mmol, 4.2 mL) was added. The solution was heated for 3 h under reflux in an oil bath. After cooling to room temperature, the reaction solution was extracted three times with dichloromethane. The combined organic phases were dried over Na_2SO_4, the solvent was distilled off in vacuo, and the residue was purified by column chromatography (heptane/EtOAc 5:1) to give the colorless product in 95% (28.9 mmol, 6.18 g) yield. The NMR data agree with the already published NMR data.[27] ^{1}H NMR (300 MHz, $CDCl_3$): δ = 8.79 (s, 1H), 6.75−6.72 (m, 2H), 6.45−6.43 (m, 2H). ^{13}C{^{1}H} NMR (75 MHz, $CDCl_3$): δ = 160.2, 156.3, 132.7, 121.5, 111.0.

*General Procedure A for the Synthesis of 4,6-Bis(phenylethynyl)-5-(1H-pyrrol-1-yl)pyrimidine (**3a**−**e**).* In a pressure tube, 1 equiv (0.94 mmol, 200 mg) of 4,6-dichloro-5-(1*H*-pyrrol-1-yl)pyrimidine (**2**), 0.06 equiv (0.06 mmol, 15 mg) of $PdCl_2(CH_3CN)_2$, 0.04 equiv (0.04 mmol, 7 mg) of CuI, and 0.12 equiv (0.11 mmol, 54 mg) of XPhos were dissolved in HN^iPr_2 (1 mL/200 mg) and 1,4-dioxane (2 mL/200 mg) under argon counter current. Then, 3 equiv (2.82 mmol) of the respective alkyne was added to the solution with stirring. The pressure tube was sealed with a Teflon cap, and the solution was stirred for 24 h at 90 °C in a heating block. The reaction solution was cooled to room temperature, quenched with distilled water, and extracted three times with ethyl acetate. The combined organic phases were dried over Na_2SO_4, the solvent was distilled off in vacuo, and the residue was purified by column chromatography (Hep/EtOAc) to give the desired products (**3a**−**e**).

*4,6-Bis(phenylethynyl)-5-(1H-pyrrol-1-yl)pyrimidine (**3a**).* According to general procedure A, title compound **3a** was obtained as a brown solid in 96% (0.90 mmol, 311 mg) yield. mp 103−105 °C. R_f = 0.39 (Hep/EtOAc 3:1). ^{1}H NMR (300 MHz, $CDCl_3$): δ = 9.09 (s, 1H), 7.47−7.31 (m, 10H), 7.11−7.09 (m, 2H), 6.49−6.47 (m, 2H). ^{13}C{^{1}H} NMR (75 MHz, $CDCl_3$): δ = 156.7, 147.7, 137.5, 132.6, 130.3, 128.5, 122.5, 120.8, 109.9, 99.2, 84.3. IR (ATR, cm^{-1}): $\tilde{\nu}$ = 2213 (s), 1539 (s), 1492 (s), 1484 (s), 1440 (s), 1409 (s), 1348 (s), 962 (m), 917 (m), 752 (s), 727 (vs), 684 (vs). MS (EI, 70 eV): *m*/*z* (%) = 345 (100, M^+), 344 (75), 343 (22), 342 (10), 319 (6), 318

https://doi.org/10.1021/acs.joc.3c01772
J. Org. Chem. 2024, 89, 2169−2181

(16), 317 (14), 316 (16), 315 (6), 268 (5), 158 (5), 144 (6). HRMS (ESI-TOF): calcd for $C_{24}H_{16}N_3$ ([M + H]$^+$), 346.1344; found, 346.1352.

*5-(1H-Pyrrol-1-yl)-4,6-bis((4-(trifluoromethyl)phenyl)ethynyl)-pyrimidine (**3b**).* According to general procedure A, title compound **3b** was obtained as a yellow solid in 75% (0.70 mmol, 339 mg) yield. mp 149−151 °C. R_f = 0.45 (Hep/EtOAc 2:1). ^{1}H NMR (300 MHz, $CDCl_3$): δ = 9.15 (s, 1H), 7.64−7.53 (m, 8H), 7.10−7.07 (m, 2H), 6.51−6.47 (m, 2H). ^{13}C{^{1}H} NMR (126 MHz, $CDCl_3$): δ = 157.0, 147.5, 138.2, 132.8, 131.9 (q, J = 33.0 Hz), 125.5 (q, J = 3.7 Hz), 124.4, 123.6 (q, J = 272.5 Hz), 122.5, 110.3, 97.1, 85.7. ^{19}F{^{1}H} NMR (282 MHz, $CDCl_3$): δ = −63.16. IR (ATR, cm^{-1}): $\tilde{\nu}$ = 2213 (m), 1319 (vs), 1164 (s), 1123 (s), 1107 (vs), 1065 (vs), 1012 (s), 962 (s), 843 (vs), 734 (vs), 723 (s). MS (EI, 70 eV): m/z (%) = 481 (100, M$^+$), 480 (50), 479 (8), 454 (11), 412 (8), 411 (9), 410 (5), 384 (6), 206 (5), 192 (6), 182 (6). HRMS (ESI-TOF): calcd for $C_{26}H_{14}F_6N_3$ ([M + H]$^+$), 482.1092; found, 482.1098.

*4,4′-((5-(1H-Pyrrol-1-yl)pyrimidine-4,6-diyl)bis(ethyne-2,1-diyl))-bis(N,N-dimethylaniline) (**3c**).* According to general procedure A, title compound **3c** was obtained as an orange solid in 91% (0.86 mmol, 371 mg) yield. mp 198−201 °C. R_f = 0.38 (Hep/EtOAc 1:1). ^{1}H NMR (250 MHz, $CDCl_3$): δ = 8.95 (s, 1H), 7.35−7.28 (m, 4H), 7.11−7.07 (m, 2H), 6.64−6.56 (m, 4H), 6.46−6.42 (m, 2H), 3.00 (s, 12H). ^{13}C{^{1}H} NMR (63 MHz, $CDCl_3$): δ = 156.6, 151.3, 147.8, 136.0, 134.2, 122.5, 111.5, 109.2, 107.0, 102.3, 84.1, 40.0. IR (ATR, cm^{-1}): $\tilde{\nu}$ = 2188 (s), 2174 (s), 1601 (s), 1527 (vs), 1362 (vs), 1350 (vs), 1230 (s), 1183 (s), 1160 (vs), 1094 (s), 1067 (s), 964 (vs), 921 (s), 818 (vs), 795 (s), 727 (vs). MS (EI, 70 eV): m/z (%) = 431 (100, M$^+$), 430 (31), 381 (30), 216 (40), 215 (44), 208 (23), 207 (26), 185 (29), 147 (20), 134 (22), 109 (22), 107 (20). HRMS (ESI-TOF): calcd for $C_{28}H_{26}N_5$ ([M + H]$^+$), 432.2188; found, 432.2184.

*4,6-Bis((4-fluorophenyl)ethynyl)-5-(1H-pyrrol-1-yl)pyrimidine (**3d**).* According to general procedure A, title compound **3d** was obtained as a brown solid in 72% yield (0.68 mmol, 258 mg) mp 129−133 °C. R_f = 0.38 (Hep/EtOAc 3:1). ^{1}H NMR (300 MHz, $CDCl_3$): δ = 9.09 (s, 1H), 7.47−7.40 (m, 4H), 7.09−7.00 (m, 6H), 6.49−6.45 (m, 2H). ^{13} C{^{1}H} NMR (75 MHz, $CDCl_3$): δ = 163.7 (d, J = 253.3 Hz), 156.8, 147.7, 137.5, 134.8 (d, J = 8.9 Hz), 122.5, 116.9 (d, J = 3.5 Hz), 116.0 (d, J = 22.3 Hz CH), 110.0, 98.2, 84.0 (d, J = 1.6 Hz). ^{19}F{^{1}H} NMR (282 MHz, $CDCl_3$): δ = −106.70. IR (ATR, cm^{-1}): $\tilde{\nu}$ = 2215 (m), 1537 (s), 1506 (s), 1484 (s), 1230 (s), 1222 (s), 1156 (s), 832 (vs), 800 (s), 719 (s), 530 (s), 501 (s). MS (EI, 70 eV): m/z (%) = 381 (100, M$^+$), 380 (98), 379 (55), 378 (12), 355 (13), 354 (32), 353 (25), 352 (31), 290 (13), 180 (14), 176 (21). HRMS (ESI-TOF): calcd for $C_{24}H_{14}F_2N_3$ ([M + H]$^+$), 382.1156; found, 382.1165.

*5-(1H-Pyrrol-1-yl)-4,6-bis(p-tolylethynyl)pyrimidine (**3e**).* According to general procedure A, title compound **3e** was obtained as a yellow solid in 71% (0.67 mmol, 250 mg) yield. mp 94−97 °C. R_f = 0.39 (Hep/EtOAc 3:1). ^{1}H NMR (250 MHz, $CDCl_3$): δ = 9.06 (s, 1H), 7.39−7.31 (m, 4H), 7.17−7.12 (m, 4H), 7.11−7.08 (m, 2H), 6.49−6.42 (m, 2H), 2.36 (s, 6H). ^{13}C{^{1}H} NMR (63 MHz, $CDCl_3$): δ = 156.7, 147.7, 140.9, 137.2, 132.5, 129.2, 122.4, 117.7, 109.8, 99.7, 84.0, 21.7. IR (ATR, cm^{-1}): $\tilde{\nu}$ = 2209 (s), 1541 (s), 1510 (s), 1482 (s), 1418 (s), 1348 (s), 816 (vs), 729 (vs), 532 (vs), 503 (s). MS (EI, 70 eV): m/z (%) = 373 (100, M$^+$), 371 (5), 370 (4), 358 (3), 357 (5), 356 (3), 186 (4), 185 (12), 178 (10), 171 (3). HRMS (ESI-TOF): calcd for $C_{26}H_{20}N_3$ ([M + H]$^+$), 374.1657; found, 374.1665.

*General Procedure B for the Synthesis of 4,6-Bis(phenylethynyl)-5-(1H-pyrrol-1-yl)pyrimidine (**4a**−**e**).* In a pressure tube, 1 equiv (100 mg) of 4,6-bis(phenylethynyl)-5-(1*H*-pyrrol-1-yl)pyrimidine (**3a**−**e**) and 30 equiv of *p*-TsOH·H_2O were dissolved in xylene (3 mL/100 mg). The pressure tube was sealed with a Teflon cap, and the solution was stirred for 6 h at 140 °C in a heating block. The reaction solution was cooled to room temperature, neutralized with saturated $NaHCO_3$ solution, and extracted three times with DCM. The combined organic phases were dried over Na_2SO_4, the solvent was distilled off in vacuo, and the residue was purified by column chromatography (Hep/EtOAc) to give the desired products (**4a**−**e**).

*mmol-Scale Procedure for the Synthesis of 5,8-Diphenylpyrimido[4,5,6-ij]pyrrolo[2,1,5-de]quinolizine (**4a**).* In a round-bottom flask, 355 mg (1.03 mmol) of 4,6-bis(phenylethynyl)-5-(1*H*-pyrrol-1-yl)pyrimidine (**3a**) and 30 equiv (30.9 mmol, 3.88 g) of *p*-TsOH·H_2O were dissolved in 10.7 mL of xylene. The solution was stirred for 6 h at 140 °C in an oil bath. The reaction solution was cooled to room temperature, neutralized with saturated $NaHCO_3$ solution, and extracted three times with DCM. The combined organic phases were dried over Na_2SO_4, the solvent was distilled off in vacuo, and the residue was purified by column chromatography (R_f = 0.24, Hep/EtOAc 1:5) to give title compound 5,8-diphenylpyrimido[4,5,6-*ij*]pyrrolo[2,1,5-*de*]quinolizine (**4a**) as a yellow solid in 43% (0.44 mmol, 153 mg) yield.

*5,8-Diphenylpyrimido[4,5,6-ij]pyrrolo[2,1,5-de]quinolizine (**4a**).* According to general procedure B, title compound **4a** was obtained as a yellow solid in 55% (0.16 mmol, 55 mg) yield. mp 234−236 °C. R_f = 0.24 (Hep/EtOAc 1:5). ^{1}H NMR (500 MHz, $CDCl_3$): δ = 9.16 (s, 1H), 7.88−7.85 (m, 4H), 7.84 (s, 2H), 7.67 (s, 2H), 7.63−7.54 (m, 6H). ^{13}C{^{1}H} NMR (126 MHz, $CDCl_3$): δ = 155.3, 146.7, 140.4, 137.3, 129.4, 129.1, 129.0, 127.0, 124.1, 118.5, 112.1. IR (ATR, cm^{-1}): $\tilde{\nu}$ = 1504 (m), 1449 (s), 1344 (s), 1321 (s), 1045 (m), 773 (s), 754 (m), 690 (vs), 674 (s), 612 (s), 560 (s). MS (EI, 70 eV): m/z (%) = 345 (100, M$^+$), 344 (18), 343 (10), 342 (5), 316 (5), 267 (3), 173 (4), 77 (5), 51 (4). HRMS (ESI-TOF): calcd for $C_{24}H_{16}N_3$ ([M + H]$^+$), 346.1344; found, 346.1339.

*5,8-Bis(4-(trifluoromethyl)phenyl)pyrimido[4,5,6-ij]pyrrolo[2,1,5-de]quinolizine (**4b**).* According to general procedure B, title compound **4b** was obtained as a yellow solid in 62% (0.13 mmol, 62 mg) yield. mp 192−194 °C. R_f = 0.26 (Hep/EtOAc 1:5). ^{1}H NMR (300 MHz, $CDCl_3$): δ = 9.21 (s, 1H), 8.01−7.97 (m, 4H), 7.91−7.87 (m, 6H), 7.65 (s, 2H). ^{13}C{^{1}H} NMR (75 MHz, $CDCl_3$): δ = 155.5, 146.7, 140.7, 139.0, 131.6 (q, J = 32.9 Hz), 129.3, 126.8, 126.2 (q, J = 3.7 Hz), 124.5, 123.9 (q, J = 272.4 Hz), 119.3, 112.0. ^{19}F{^{1}H} NMR (282 MHz, $CDCl_3$): δ = −62.69. IR (ATR, cm^{-1}): $\tilde{\nu}$ = 1317 (vs), 1183 (s), 1170 (s), 1125 (s), 1113 (s), 1100 (vs), 1069 (vs), 1055 (s), 1016 (s), 851 (s), 837 (vs), 779 (s), 624 (s). MS (EI, 70 eV): m/z (%) = 481 (100, M$^+$), 480 (14), 462 (5), 412 (4), 411 (5), 240 (3), 231 (3), 196 (3). HRMS (ESI-TOF): calcd for $C_{26}H_{14}F_6N_3$ ([M + H]$^+$), 482.1092; found, 482.1092.

*4,4′-(Pyrimido[4,5,6-ij]pyrrolo[2,1,5-de]quinolizine-5,8-diyl)bis-(N,N-dimethylaniline) (**4c**).* According to general procedure B, title compound **4c** was obtained as an orange solid in 89% (0.21 mmol, 89 mg) yield. mp 135−137 °C. R_f = 0.17 (EtOAc + 1% NEt_3). ^{1}H NMR (300 MHz, $CDCl_3$): δ = 9.08 (s, 1H), 7.82−7.76 (m, 6H), 7.73−7.71 (m, 2H), 6.93−6.86 (m, 4H), 3.08 (s, 6H), 3.08 (s, 6H). ^{13}C{^{1}H} NMR (75 MHz, $CDCl_3$): δ = 155.1, 151.1, 146.5, 140.4, 129.9, 127.1, 124.9, 116.8, 112.4, 112.0, 40.3. IR (ATR, cm^{-1}): $\tilde{\nu}$ = 1515 (vs), 1436 (s), 1348 (s), 1317 (vs), 1230 (s), 1193 (s), 1173 (s), 822 (vs), 806 (vs), 556 (s). MS (EI, 70 eV): m/z (%) = 431 (100, M$^+$), 415 (12), 215 (23), 214 (14), 193 (10), 78 (11), 63 (12), 57 (14), 55 (10), 44 (40), 43 (13). HRMS (ESI-TOF): calcd for $C_{28}H_{26}N_5$ ([M + H]$^+$), 432.2188; found, 432.2192.

*5,8-Bis(4-fluorophenyl)pyrimido[4,5,6-ij]pyrrolo[2,1,5-de]-quinolizine (**4d**).* According to general procedure B, title compound **4d** was obtained as a yellow solid in 54% (0.14 mmol, 54 mg) yield. mp 332−334 °C. R_f = 0.32 (Hep/EtOAc 1:10). ^{1}H NMR (300 MHz, $CDCl_3$/TFA): δ = 9.22 (s, 1H), 8.50 (s, 2H), 8.39 (s, 2H), 7.96−7.89 (m, 4H), 7.50−7.39 (m, 4H). ^{13}C{^{1}H} NMR (75 MHz, $CDCl_3$): δ = 165.0 (d, J = 254.7 Hz), 147.3, 144.2, 137.6, 132.0 (d, J = 9.0 Hz), 130.9, 130.4 (d, J = 3.4 Hz), 121.1, 117.5 (d, J = 22.3 Hz), 116.6. ^{19}F{^{1}H} NMR (282 MHz, $CDCl_3$): δ = −107.4. IR (ATR, cm^{-1}): $\tilde{\nu}$ = 1506 (vs), 1438 (s), 1346 (s), 1323 (s), 1226 (vs), 1164 (s), 1049 (s), 832 (vs), 804 (s), 773 (s), 729 (s), 622 (s), 556 (s), 507 (s). MS (EI, 70 eV): m/z (%) = 381 (100, M$^+$), 380 (17), 379 (8), 352 (4), 190 (14), 189 (4), 180 (4). HRMS (ESI-TOF): calcd for $C_{24}H_{14}F_2N_3$ ([M + H]$^+$), 382.1156; found, 382.1158.

*5,8-Di-p-tolylpyrimido[4,5,6-ij]pyrrolo[2,1,5-de]quinolizine (**4e**).* According to general procedure B, title compound **4e** was obtained as a yellow solid in 87% (0.23 mmol, 87 mg) yield. mp 283−285 °C. R_f = 0.33 (Hep/EtOAc 1:4). ^{1}H NMR (300 MHz, $CDCl_3$): δ = 9.14

https://doi.org/10.1021/acs.joc.3c01772
J. Org. Chem. 2024, 89, 2169−2181

(s, 1H), 7.81 (s, 2H), 7.76 (d, J = 7.9 Hz, 4H), 7.66 (s, 2H), 7.40 (d, J = 7.8 Hz, 4H), 2.49 (s, 6H). $^{13}C\{^1H\}$ NMR (75 MHz, $CDCl_3$): δ = 155.2, 146.7, 140.3, 139.5, 134.5, 129.8, 128.8, 127.0, 124.0, 118.2, 112.1, 21.4. IR (ATR, cm^{-1}): $\tilde{\nu}$ = 1611 (s), 1587 (s), 1508 (s), 1434 (s), 1348 (s), 1321 (vs), 814 (s), 806 (s), 767 (s), 748 (vs), 721 (s), 624 (s), 596 (s), 560 (s), 484 (s). MS (EI, 70 eV): m/z (%) = 373 (100, M^+), 372 (49), 371 (10), 370 (7), 358 (13), 357 (15), 356 (6), 346 (12), 345 (7), 343 (6), 179 (6), 158 (6). HRMS (ESI-TOF): calcd for $C_{26}H_{20}N_3$ ($[M + H]^+$), 374.1657; found, 374.1659.

4,4′-((4-(1H-Pyrrol-1-yl)pyridine-3,5-diyl)bis(ethyne-2,1-diyl))bis-(N,N-dimethylaniline) (8-pcr). According to a previously described literature method,[8] unknown compound **8-pcr** was obtained as a yellow solid in 81% (0.54 mmol, 233 mg) yield. mp 166−176 °C. ^1H NMR (300 MHz, $CDCl_3$): δ = 8.65 (s, 2H), 7.35−7.28 (m, 6H), 6.66−6.59 (m, 4H), 6.42−6.37 (m, 2H), 2.99 (s, 12H). ^{13}C NMR$\{^1H\}$ (75 MHz, $CDCl_3$): δ = 151.6, 150.5, 146.8, 132.8, 122.1, 116.8, 111.6, 109.0, 108.8, 98.4, 81.7, 40.1. IR (ATR, cm^{-1}): $\tilde{\nu}$ = 2916 (m), 2811 (w), 2199 (m), 1607 (s), 1484 (s), 1360 (s), 1222 (m), 1183 (s), 1061 (s), 814 (vs), 719 (s). MS (EI, 70 eV): m/z (%) = 430 (M^+, 100), 429 (13), 415 (12), 414 (36), 398 (14), 215 (25), 214 (37), 192 (16), 171 (12), 170 (13). HRMS (ESI-TOF): calcd for $C_{29}H_{26}N_4$ ($[M + H]^+$), 431.2236; found, 431.2242.

*4,4′-(Indolizino[6,5,4,3-ija][1,6]naphthyridine-5,8-diyl)bis(N,N-dimethylaniline) (**8**).* According to a previously described literature method,[8] unknown compound **8** was obtained as a greenish solid in 57% (0.13 mmol, 57 mg). mp 260−265 °C. ^1H NMR (300 MHz, $CDCl_3$): δ = 8.72 (s, 2H), 7.78−7.66 (m, 4H), 7.24 (s, 2H), 7.22 (s, 2H), 6.95−6.80 (m, 4H), 3.05 (s, 12H). $^{13}C\{^1H\}$ NMR (75 MHz, $CDCl_3$): δ = 150.7, 138.9, 134.9, 134.6, 129.0, 127.1, 126.0, 120.9, 114.3, 112.3, 107.6, 40.4. IR (ATR, cm^{-1}): $\tilde{\nu}$ = 2920 (m), 2852 (m), 2800 (m), 1603 (s), 1502 (s), 1354 (s), 1195 (s), 1053 (s), 880 (s), 820 (vs), 793 (vs), 713 (s), 517 (s). MS (EI, 70 eV): m/z (%) = 430 (M^+, 100), 414 (31), 398 (15), 215 (19), 214 (28), 206 (13). HRMS (ESI): calcd for $C_{29}H_{26}N_4$ ($[M + H]^+$), 431.2236; found, 431.2234.

*4,4′-(Indolizino[6,5,4,3-ija][1,5]naphthyridine-5,8-diyl)bis(N,N-dimethylaniline) (**9**).* The title compound was synthesized according to a previously described method.[17]

■ ASSOCIATED CONTENT

Data Availability Statement

The data underlying this study are available in the published article and its Supporting Information.

Supporting Information

The Supporting Information is available free of charge at https://pubs.acs.org/doi/10.1021/acs.joc.3c01772.

Optimization of starting material synthesis; photophysical and electrochemical data; single-crystal X-ray data; experimental procedures and data; 1-H, 19-F, and 13C NMR spectra of isolated compounds; and computational details (PDF)

Accession Codes

CCDC 2286780 (**4c**) contains the supplementary crystallographic data for this paper. These data can be obtained free of charge via www.ccdc.cam.ac.uk/data_request/cif, by emailing data_request@ccdc.cam.ac.uk, or by contacting the Cambridge Crystallographic Data Centre, 12 Union Road, Cambridge CB2 1EZ, UK; fax: + 44 1223 336033.

■ AUTHOR INFORMATION

Corresponding Author

Peter Langer − *Institute of Chemistry, University Rostock, 18059 Rostock, Germany; Leibniz Institute of Catalysis (LIKAT) at the University Rostock, 18059 Rostock, Germany;* orcid.org/0000-0002-7665-8912; Phone: +49 381 498 6410; Email: peter.langer@uni-rostock.de; Fax: +49 381 498 6412

Authors

Jonas Polkaehn − *Institute of Chemistry, University Rostock, 18059 Rostock, Germany*

Ricardo Molenda − *Institute of Chemistry, University Rostock, 18059 Rostock, Germany*

Miguel A. Cordero − *Institute for Physics and Department of Life, Light and Matter, University of Rostock, 18059 Rostock, Germany*

Stefan Lochbrunner − *Institute for Physics and Department of Life, Light and Matter, University of Rostock, 18059 Rostock, Germany;* orcid.org/0000-0001-9729-8277

Sebastian Boldt − *Institute of Chemistry, University Rostock, 18059 Rostock, Germany*

Peter Ehlers − *Institute of Chemistry, University Rostock, 18059 Rostock, Germany;* orcid.org/0000-0001-6444-7563

Alexander Villinger − *Institute of Chemistry, University Rostock, 18059 Rostock, Germany;* orcid.org/0000-0002-0868-9987

Complete contact information is available at: https://pubs.acs.org/10.1021/acs.joc.3c01772

Notes

The authors declare no competing financial interest.

■ ACKNOWLEDGMENTS

Financial support by the State of Mecklenburg-Vorpommern is gratefully acknowledged.

■ REFERENCES

(1) (a) Facchetti, A. π-Conjugated Polymers for Organic Electronics and Photovoltaic Cell Applications. *Chem. Mater.* **2011**, *23*, 733−758. (b) Figueira-Duarte, T. M.; Müllen, K. Pyrene-based materials for organic electronics. *Chem. Rev.* **2011**, *111*, 7260−7314. (c) Aumaitre, C.; Morin, J.-F. Polycyclic Aromatic Hydrocarbons as Potential Building Blocks for Organic Solar Cells. *Chem. Rec.* **2019**, *19*, 1142−1154.

(2) (a) Balli, H.; Zeller, M. Neue Heteroarene: Synthese und spektrale Daten von Indolizino[6,5,4,3-*aij*]chinolin (≪Ullazin≫) und einigen Derivaten. *Helv. Chim. Acta* **1983**, *66*, 2135−2139. (b) Gerson, F.; Metzger, A. The Radical Ions of Indolizino [6,5,4,3-*aij*]quinoline and Some of its Derivatives. *Helv. Chim. Acta* **1983**, *66*, 2031−2043.

(3) Guo, Y.; Zhang, L.; Li, C.; Jin, M.; Zhang, Y.; Ye, J.; Chen, Y.; Wu, X.; Liu, X. BN/BO-Ullazines and Bis-BO-Ullazines: Effect of BO Doping on Aromaticity and Optoelectronic Properties. *J. Org. Chem.* **2021**, *86*, 12507−12516.

(4) Cebrián, C. Ullazine-based materials: towards novel opportunities in organic electronics. *J. Mater. Chem. C* **2018**, *6*, 11943−11950.

(5) Delcamp, J. H.; Yella, A.; Holcombe, T. W.; Nazeeruddin, M. K.; Grätzel, M. The molecular engineering of organic sensitizers for solar-cell applications. *Angew. Chem., Int. Ed.* **2013**, *52*, 376−380.

(6) (a) Qiao, H.; Deng, Y.; Peng, R.; Wang, G.; Yuan, J.; Tan, S. Effect of π-spacers and anchoring groups on the photovoltaic performances of ullazine-based dyes. *RSC Adv.* **2016**, *6*, 70046−70055. (b) Feng, J.; Jiao, Y.; Ma, W.; Nazeeruddin, M. K.; Grätzel, M.; Meng, S. First Principles Design of Dye Molecules with Ullazine Donor for Dye Sensitized Solar Cells. *J. Phys. Chem. C* **2013**, *117*, 3772−3778.

(7) Skabeev, A.; Zschieschang, U.; Zagranyarski, Y.; Klauk, H.; Müllen, K.; Li, C. Carbonyl-Functionalized Cyclazines as Colorants and Air-Stable n-Type Semiconductors. *Org. Lett.* **2018**, *20*, 1409−1412.

(8) Boldt, S.; Parpart, S.; Villinger, A.; Ehlers, P.; Langer, P. Synthesis and Properties of Aza-ullazines. *Angew. Chem., Int. Ed.* **2017**, *56*, 4575−4578.

(9) Li, C.; Liu, Y.; Sun, Z.; Zhang, J.; Liu, M.; Zhang, C.; Zhang, Q.; Wang, H.; Liu, X. Synthesis, Characterization, and Properties of Bis-BN Ullazines. *Org. Lett.* **2018**, *20*, 2806−2810.
(10) (a) Hou, D.; Balli, H. A Novel Heterocyclic Ring System: Synthesis and Spectral Data of 4,8,9b-Triazacyclopenta[c,d]-phenalene. *Helv. Chim. Acta* **1992**, *75*, 2608−2612. (b) Rubio-Presa, R.; Pedrosa, M. R.; Fernández-Rodríguez, M. A.; Arnáiz, F. J.; Sanz, R. Molybdenum-Catalyzed Synthesis of Nitrogenated Poly-heterocycles from Nitroarenes and Glycols with Reuse of Waste Reduction Byproduct. *Org. Lett.* **2017**, *19*, 5470−5473. (c) Ge, Q.; Li, B.; Wang, B. Synthesis of substituted benzoijimidazo2,1,5-dequinolizine by rhodium(III)-catalyzed multiple C-H activation and annulations. *Org. Biomol. Chem.* **2016**, *14*, 1814−1821.
(11) Pierrat, P.; Hesse, S.; Cebrián, C.; Gros, P. C. Controlling charge-transfer properties through a microwave-assisted mono- or bis-annulation of dialkynyl-N-(het)arylpyrroles. *Org. Biomol. Chem.* **2017**, *15*, 8568−8575.
(12) (a) Mateo-Alonso, A. Pyrene-fused pyrazaacenes: from small molecules to nanoribbons. *Chem. Soc. Rev.* **2014**, *43*, 6311−6324. (b) Omura, Y.; Tachi, Y.; Okada, K.; Kozaki, M. Synthesis and Properties of Nitrogen-Containing Pyrenes. *J. Org. Chem.* **2019**, *84*, 2032−2038.
(13) Geib, S.; Martens, S. C.; Zschieschang, U.; Lombeck, F.; Wadepohl, H.; Klauk, H.; Gade, L. H. 1,3,6,8-Tetraazapyrenes: synthesis, solid-state structures, and properties as redox-active materials. *J. Org. Chem.* **2012**, *77*, 6107−6116.
(14) (a) Itami, K.; Yamazaki, D.; Yoshida, J. Pyrimidine-core extended pi-systems: general synthesis and interesting fluorescent properties. *J. Am. Chem. Soc.* **2004**, *126*, 15396−15397. (b) Komatsu, R.; Ohsawa, T.; Sasabe, H.; Nakao, K.; Hayasaka, Y.; Kido, J. Manipulating the Electronic Excited State Energies of Pyrimidine-Based Thermally Activated Delayed Fluorescence Emitters To Realize Efficient Deep-Blue Emission. *ACS Appl. Mater. Interfaces* **2017**, *9*, 4742−4749. (c) Sohn, S.; Ha, M. W.; Park, J.; Kim, Y.-H.; Ahn, H.; Jung, S.; Kwon, S.-K.; Kim, Y.-H. High-Efficiency Diphenylpyrimidine Derivatives Blue Thermally Activated Delayed Fluorescence Organic Light-Emitting Diodes. *Front. Chem.* **2020**, *8*, 356.
(15) Kanno, K.; Liu, Y.; Iesato, A.; Nakajima, K.; Takahashi, T. Chromium-mediated synthesis of polycyclic aromatic compounds from halobiaryls. *Org. Lett.* **2005**, *7*, 5453−5456.
(16) Wan, D.; Li, X.; Jiang, R.; Feng, B.; Lan, J.; Wang, R.; You, J. Palladium-Catalyzed Annulation of Internal Alkynes: Direct Access to π-Conjugated Ullazines. *Org. Lett.* **2016**, *18*, 2876−2879.
(17) Janke, S.; Boldt, S.; Nakielski, P.; Villinger, A.; Ehlers, P.; Langer, P. Synthesis and Properties of 5-Azaullazines. *J. Org. Chem.* **2023**, *88*, 10470−10482.
(18) (a) Vardanyan, A.; Boldt, S.; Villinger, A.; Ehlers, P.; Langer, P. Synthesis and Properties of 1-Azapyrenes. *J. Org. Chem.* **2022**, *87*, 11296−11308. (b) Molenda, R.; Boldt, S.; Villinger, A.; Ehlers, P.; Langer, P. Synthesis of 2-Azapyrenes and Their Photophysical and Electrochemical Properties. *J. Org. Chem.* **2020**, *85*, 12823−12842.
(19) Gicquiaud, J.; Hacıhasanoğlu, A.; Hermange, P.; Sotiropoulos, J.-M.; Toullec, P. Y. Brønsted Acid-Catalyzed Carbocyclization of 2-Alkynyl Biaryls. *Adv. Synth. Catal.* **2019**, *361*, 2025−2030.
(20) Brouwer, A. M. Standards for photoluminescence quantum yield measurements in solution (IUPAC Technical Report). *Pure Appl. Chem.* **2011**, *83*, 2213−2228.
(21) (a) Nigam, S.; Rutan, S. Principles and Applications of Solvatochromism. *Appl. Spectrosc.* **2001**, *55*, 362A−370A. (b) Marini, A.; Muñoz-Losa, A.; Biancardi, A.; Mennucci, B. What is solvatochromism? *J. Phys. Chem. B* **2010**, *114*, 17128−17135.
(22) Pommerehne, J.; Vestweber, H.; Guss, W.; Mahrt, R. F.; Bässler, H.; Porsch, M.; Daub, J. Efficient two layer leds on a polymer blend basis. *Adv. Mater.* **1995**, *7*, 551−554.
(23) Frisch, M. J.; Trucks, G. W.; Schlegel, H. B.; Scuseria, G. E.; Robb, M. A.; Cheeseman, J. R.; Scalmani, G.; Barone, V.; Petersson, G. A.; Nakatsuji, H.; Li, X.; Caricato, M.; Marenich, A. V.; Bloino, J.; Janesko, B. G.; Gomperts, R.; Mennucci, B.; Hratchian, H. P.; Ortiz, J. V.; Izmaylov, A. F.; Sonnenberg, J. L.; Williams; Ding, F.; Lipparini, F.; Egidi, F.; Goings, J.; Peng, B.; Petrone, A.; Henderson, T.; Ranasinghe, D.; Zakrzewski, V. G.; Gao, J.; Rega, N.; Zheng, G.; Liang, W.; Hada, M.; Ehara, M.; Toyota, K.; Fukuda, R.; Hasegawa, J.; Ishida, M.; Nakajima, T.; Honda, Y.; Kitao, O.; Nakai, H.; Vreven, T.; Throssell, K.; Montgomery, J. A., Jr; Peralta, J. E.; Ogliaro, F.; Bearpark, M. J.; Heyd, J. J.; Brothers, E. N.; Kudin, K. N.; Staroverov, V. N.; Keith, T. A.; Kobayashi, R.; Normand, J.; Raghavachari, K.; Rendell, A. P.; Burant, J. C.; Iyengar, S. S.; Tomasi, J.; Cossi, M.; Millam, J. M.; Klene, M.; Adamo, C.; Cammi, R.; Ochterski, J. W.; Martin, R. L.; Morokuma, K.; Farkas, O.; Foresman, J. B.; Fox, D. J. *Gaussian 16*. Rev. C.01: Wallingford, CT, 2016.
(24) Lu, T.; Chen, F. Multiwfn: a multifunctional wavefunction analyzer. *J. Comput. Chem.* **2012**, *33*, 580−592.
(25) *Aromaticity: Modern computational methods and applications*; Fernández, I., Ed.; Elsevier: Amsterdam, 2021.
(26) Paenurk, E.; Gershoni-Poranne, R. Simple and efficient visualization of aromaticity: bond currents calculated from NICS values. *Phys. Chem. Chem. Phys.* **2022**, *24*, 8631−8644.
(27) Xiang, J.; Zheng, L.; Chen, F.; Dang, Q.; Bai, X. A cascade reaction consisting of Pictet-Spengler-type cyclization and Smiles rearrangement: application to the synthesis of novel pyrrole-fused dihydropteridines. *Org. Lett.* **2007**, *9*, 765−767.
(28) Zhang, G.; Gautam, P.; Chan, J. M. W. Symmetrical and Unsymmetrical Fluorine-Rich Ullazines via Controlled Cycloaromatizations. *Org. Chem. Front.* **2020**, *7*, 787−795.
(29) Drigo, N. A.; Paek, S.; Huckaba, A. J.; Schouwink, P. A.; Tabet, N.; Nazeeruddin, M. K. Approaches for Selective Synthesis of Ullazine Donor−Acceptor Systems. *Chem.—Eur. J.* **2017**, *23*, 17209−17212.
(30) Strickler, S. J.; Berg, R. A. Relationship between Absorption Intensity and Fluorescence Lifetime of Molecules. *J. Chem. Phys.* **1962**, *37*, 814−822.
(31) Molenda, R.; Polkaehn, J.; Argüello Cordero, M. A.; Villinger, A.; Ehlers, P.; Lochbrunner, S.; Langer, P. Synthesis and Properties of Thieno[2′,3′,4′:4,5]naphtho[1,8-*cd*]pyridines. *J. Org. Chem.* **2023**, *88*, 8802−8824.

https://doi.org/10.1021/acs.joc.3c01772
J. Org. Chem. 2024, 89, 2169−2181

4.2 π-Expanded azaullazines: synthesis of quinolino-azaullazines by Povarov reaction and cycloisomerisation

Jonas Polkaehn, Richard Thom, Peter Ehlers, Alexander Villinger, Peter Langer

Org. Biomol. Chem. **2024**, 22, 2027-2042.

DOI: doi.org/10.1039/D4OB00091A

Contribution to this work: **70%**

Richard Thom performed most of the synthetic work and most of the measurements during his master thesis under my supervision. I performed some extended synthetic work and measurements. Furthermore, I conducted the computational calculations and wrote the manuscript. Alexander Villiger contributed with the measurement and evaluation of the single crystal X-ray experiment. Peter Ehlers and Peter Langer supervised the entire project and performed revision and proof reading of the manuscript.

Organic & Biomolecular Chemistry

ROYAL SOCIETY OF CHEMISTRY

PAPER

View Article Online
View Journal | View Issue

Cite this: *Org. Biomol. Chem.*, 2024, **22**, 2027

π-Expanded azaullazines: synthesis of quinolino-azaullazines by Povarov reaction and cycloisomerisation†

Jonas Polkaehn,[a] Richard Thom,[a] Peter Ehlers,[a] Alexander Villinger[a] and Peter Langer *[a,b]

Received 17th January 2024,
Accepted 2nd February 2024

DOI: 10.1039/d4ob00091a

rsc.li/obc

Doping and extension of polycyclic aromatic hydrocarbons (PAHs) by simple and efficient synthetic methods is of increased demand for the development of novel and improved organic electronics. Diarylindolizino[6,5,4,3-*ija*]quinolino[2,3-*c*][1,6]naphthyridines (quinolino-azaullazines) were prepared by combination of Pd catalyzed cross-coupling with Povarov and cycloisomerisation reactions. The products contain an electron-rich ullazine and an electron-poor quinoline moiety and show intramolecular charge transfer properties that can be tuned by the substitution pattern. The optical properties were studied experimentally and further elaborated by (TD)DFT calculations.

Introduction

Indolizino[6,5,4,3-*ija*]quinolines (ullazines), first synthesized and studied by Balli *et al.* in 1983,[1] are of considerable current interest in the field of materials science, due to their application as organic light emitting diodes (OLEDs), organic field-effect transistors (OFETs) or dye-sensitized solar cells (DSSC).[2,3] Due to the electronic influence of the pyrrole moiety, ullazines represent electron-rich molecules that exhibit strong intramolecular charge transfer (ICT).[2] Several synthetic methods have been developed in recent decades to further modify the properties of ullazines. Various approaches are based on the modification of the ullazine core structure by doping with heteroatoms.[4,5] Other methods are focused on the variation of the substitution pattern and substituents.[6] Furthermore, the expansion of the π-system represents a promising approach to modify the optical and electronic properties of ullazines (Fig. 1).[7,8–15] In 2012, Ren and co-workers published the synthesis of dibenzoullazines by Friedel–Crafts arylation of aryl triazenes.[8] Similarly substituted dibenzoullazines were obtained by Pd-catalyzed twofold annulation reactions of arynes in 2021.[9] Müllen *et al.* and Nozaki *et al.* reported in 2015 the synthesis of π-extended ullazines by cycloaddition of polycyclic aromatic azomethine ylides.[10,11] The most common strategy for the synthesis of π-expanded ullazines is based on employment of azomethine ylides. Other examples have been reported by Feng *et al.*,[12] Nozaki *et al.*[13] and Stępień *et al.*[14] Moreover, Stępień *et al.* were able to synthesize such compounds by cyclodehydrohalogenation of α,α-disubstituted *N*-arylpyrroles.[14] Using photochemical cyclodehydrochlorination, Morin and coworkers synthesized π-extended ullazines annulated to two pyridine or two thiophene moieties in 3,4- and 8,9-position.[15]

A well-known methodology for the preparation of polycyclic aromatic heterocycles is the Povarov reaction, a hetero-Diels–Alder reaction that was developed in 1967.[16] In recent years, there has been renewed interest in this methodology.[17] In 2020, Jana *et al.* reported the application of the Povarov reaction for the synthesis of dibenzo[*a*,*c*]acridines from 2′-alkynylbiaryl-2-carbaldehydes using catalytic amounts of $FeCl_3$ (Fig. 2).[18] Recently, we reported the synthesis of benzo[*j*]naphtho[2,1,8-*def*][2,7]phenanthrolines, π-expanded azapyrenes, by combination of a Povarov with a cycloisomerization reaction.[19] Herein, we wish to report the synthesis of what are, to the best of our knowledge, hitherto unknown diarylindolizino[6,5,4,3-*ija*]quinolino[2,3-*c*][1,6]naphthyridines by combination of Povarov and cycloisomerization reactions. The incorporation of an electron-rich, five-membered pyrrole ring will alter the optoelectronic properties of this polycyclic aromatic scaffold and will be studied in detail by experimental and theoretical methods. In addition, the non-symmetric π-expansion of azaullazines will be studied in comparison to previously reported symmetric dibenzoullazines.

[a]*Institute of Chemistry, University Rostock, Albert-Einstein-Str. 3a, 18059 Rostock, Germany. E-mail: peter.langer@uni-rostock.de; Fax: +49 381 498 6412; Tel: +49 381 498 6410*

[b]*Leibniz Institute for Catalysis (LIKAT) at the University Rostock, Albert-Einstein-Str. 29a, 18059 Rostock, Germany*

† Electronic supplementary information (ESI) available: Single crystal X-ray data, ^{1}H-, ^{19}F, ^{13}C-NMR spectra of isolated compounds; computational details. CCDC 2292306. For ESI and crystallographic data in CIF or other electronic format see DOI: https://doi.org/10.1039/d4ob00091a

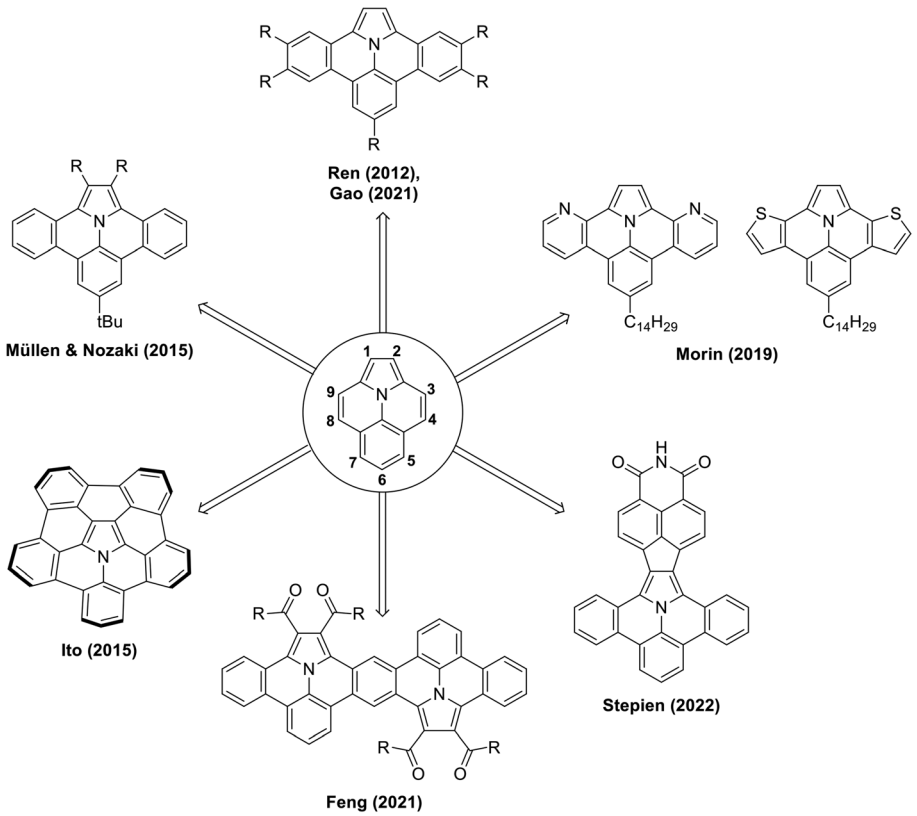

Fig. 1 Examples of π-expanded ullazines.

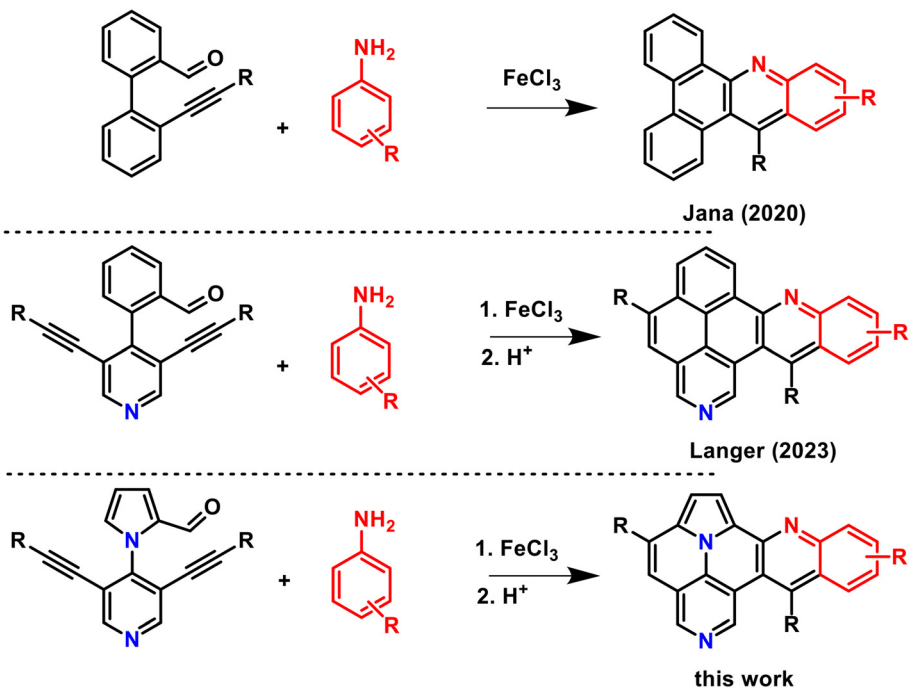

Fig. 2 Recent examples of Povarov reactions.

Synthesis

Vilsmeier–Haack reaction of 3,5-dibromo-4-(1*H*-pyrrol-1-yl)pyridine (**1**)[5] afforded formylated products **2a** and **2b** in 33% and 62% isolated yields, respectively (Scheme 1). During the optimization of, different reaction conditions were tested (ESI, Table 1†). It turned out that the use of 2 eq. of $POCl_3$ in DMF at 100 °C and 3 h reaction time provided the best results. The regiosiomeric mixture could be readily separated by column chromatography. Therefore, although the desired regioisomer **2a** was formed as the minor product, the method was useful in our hands to prepare sufficient material to continue the synthesis.

With **2a** in hand, an optimization of the following double Sonogashira reaction was carried out for the synthesis of **3a** (ESI, Table 2†). The best yields were obtained by using $PdCl_2(PPh_3)_2$ (0.05 eq.) as the catalyst and cataCXium A (0.1 eq.) as the ligand. These conditions were then applied for the synthesis of Sonogashira products **3a–e** were obtained in moderate to very good yields (Scheme 2).

Subsequently, the Povarov reaction of **3a** with aniline was studied to give product **4** (Table 1). We initially applied the conditions reported by Jana *et al.* ($FeCl_3$, toluene, 100 °C) and obtained **4** in a very good yield of 86%.[18] In contrast, employment of $In(OTf)_3$ gave a diminished yield (41%) and Brønsted acids were completely ineffective for this reaction.

Subsequently, we studied the cycloisomerization of **4** to give quinolino-azaullazine **5a** and tested *p*-toluenesulfonic acid (*p*-TsOH) and methanesulfonic acid (MsOH) which were previously used for related reactions (Table 2).[5,20] Employment of *p*-TsOH gave a better yield of 62% as compared to MsOH under the same concentration of acid (30 eq.). Reducing the amount of acid from 30 to 20 equivalents resulted in a slightly improved yield of 67%, further reduction to 10 equivalents resulted in diminished yield (43%). During the purification of **4**, we observed an alkyne-carbonyl-metathesis (ACM) reaction as competitive side reaction of the Povorav reaction.[21] Purification from this side-product was very difficult and, hence, we attempted to directly convert **3b** to **5a** in a one-pot procedure without isolation of Povarov product **4**. To our delight, this idea proved to be successful and allowed to isolate the desired quinolino-azaullazine **5a** in 47% overall yield.

Next, we were interested in the preparative scope of our methodology. Hence, the substitution pattern of the arylacety-

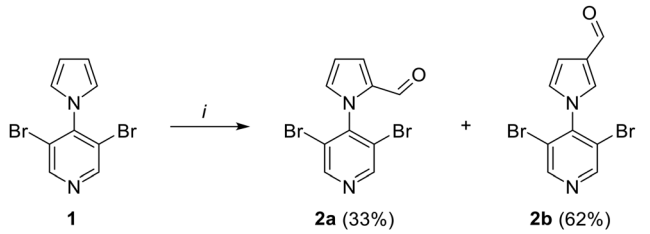

Scheme 1 Synthesis of **2a** and **2b**; (i): $POCl_3$ (2.0 eq.), DMF, 100 °C, 3 h.

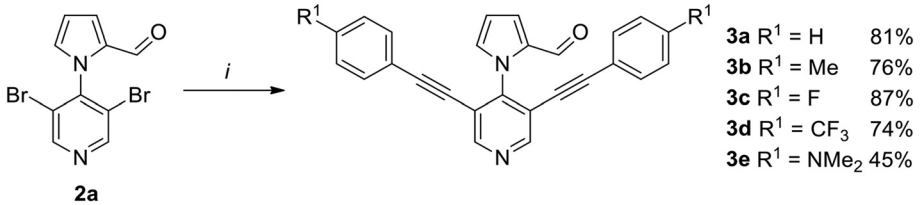

Scheme 2 Synthesis of **3a–e**; (i): alkyne (3 eq.), $PdCl_2(PPh_3)_2$ (0.05 eq.), cataCXium A (0.1 eq.), CuI (0.05 eq.), HN^iPr_2, 1,4-dioxane, 90 °C, 24 h.

Table 1 Optimization of the synthesis of **4**

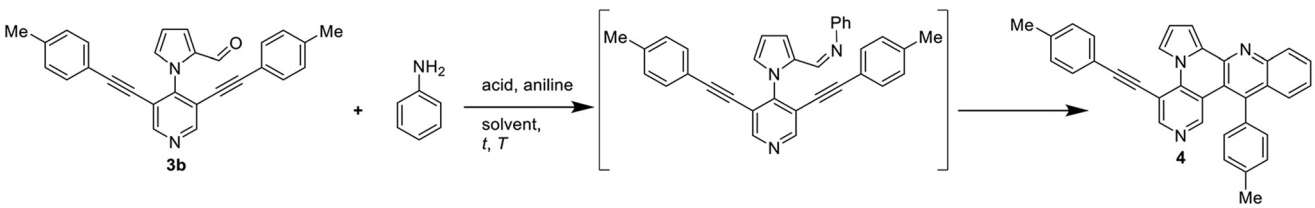

Entry	Reagent (eq.)	Eq. aniline	Solvent	*T* [°C]	*t* [h]	Yield[a] [%]
1[b]	**$FeCl_3$ (0.1)**	**1.2**	**Toluene**	**100**	**2**	**86**
2	$In(OTf)_3$ (0.1)	1.2	Toluene	100	3	41
3	*p*-TsOH·H_2O (0.1)	1.2	Toluene	100	3	0
4	TfOH (0.1)	1.2	Toluene	100	24	0

[a] Isolated yield. [b] Conditions of Jana *et al.*[18]

Table 2 Optimization of the synthesis of **5a**

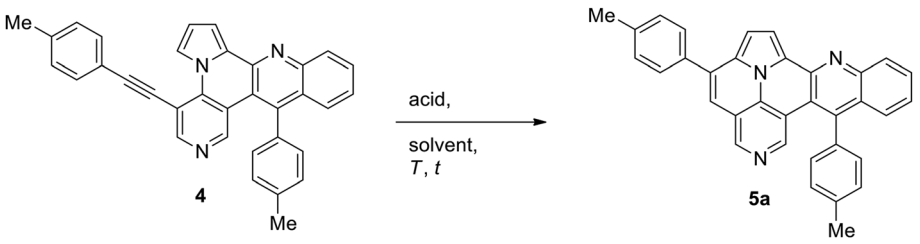

Entry	Reagent (eq.)	Solvent	T [°C]	t [h]	Yield[a] [%]
1	*p*-TsOH·H_2O (30)	Xylene[b]	120	6	62
2	MsOH (30)	Xylene[b]	120	6	40
3	***p*-TsOH·H_2O (20)**	**Xylene[b]**	**120**	**6**	**67**
4	*p*-TsOH·H_2O (10)	Xylene[b]	120	6	43

[a] Isolated yield. [b] Isomeric mixture.

lene and of the aniline were varied (Table 3). The reaction of **3a–e** with various anilines afforded quinolino-azaullazines **5a–f,h–l** in mostly moderate to good yields. All yields refer to a one-pot process in which four new bonds were formed in a single step without the need of purification of intermediates (formation of the imine, Povarov reaction and cycloisomerization). The reaction of aniline with **3e**, containing the strongly electron donating NMe_2 substituent, gave product **5c** in a reduced yield of 21%. However, the reaction of **3e** with reaction with 4-fluoroaniline afforded the corresponding product **5k** in a better yield of 39%. The best yield (product **5l**, 65%) was observed for the reaction of **3c**, containing an electron-withdrawing fluoride substituent, with 4-fluoroaniline. Heterocyclic 4-aminopyridine did not undergo a Povarov reaction (**5g**). The use of 1-naphthylamine provided product **5h** in good yield. Comparison of the yields of products derived from different substituents attached to the alkyne (**5a**, **5j** and **5k**) did not reveal a significant influence of the substitution pattern, except from the fact that the reaction of 4-fluoroaniline with **3d**, containing a trifluoromethyl group, proved to be entirely unsuccessful. In summary, the aniline has a higher influence on the yield that the substituent attached to the alkyne.

The structure of **5d** was independently confirmed by X-ray crystal structure analysis (Fig. 3). Crystallization was carried out in a mixture of heptane and dichloromethane (DCM). For a better visualization, the co-crystallized DCM has been removed. Both *p*-tolyl residues are twisted out of plane of the core structure by dihedral angles of 45° and 78°. Moreover, the crystal lattice shows a slipped antiparallel π–π-stacking with a spacing of 3.44 Å and 3.41 Å between the core structures, respectively.

Physical properties

The photophysical properties of selected derivatives were determined by steady-state absorption and photoluminescence spectra (PL) (Fig. 4). The UV/VIS-spectra indicate strong absorption bands at approx. 250–300 nm and weaker bands at approx. 450–500 nm for all compounds. Comparing the different aniline-derived moieties, a slight influence of the substituents is evident. Thus, **5a** and **5d** show very similar absorption values and shapes of the absorption bands while π-extended compound **5h** exhibits somewhat higher extinction coefficients. In contrast, **5c** has a visibly lower absorption intensity accompanied with loss of fine structure. Additionally, a red shift of the maxima is observed, which can be attributed to the strong donor properties of the *N*,*N*-dimethylamio unit. Compounds **5d**, **5j** and **5k** provide almost identical absorption spectra, due to the twisted orientation of the phenyl rings. Incorporation of a strong donor substituent, as present in **5k**, leads to an altered absorption spectrum as well as loss of fine structure. The redshift, on the other hand, is not as pronounced as for **5c**.

The PL-spectra, **5d**, **5j** and **5k** also show identical band structures and an emission maximum at 525 nm. Only donor-substituted derivative **5k** exhibits a red shift by 14 nm as compared to the other derivatives. Similar to the absorption properties, variation of the substituents directly attached to the heterocyclic core structure alters the PL-spectra to a greater extent. Compared to unsubstituted derivative **5a** (λ_{em} = 515 nm), *N*,*N*-dimethylamino-substituted compound **5c** shows the strongest red shift (λ_{em} = 539 nm), followed by fluorine-substituted **5d** (λ_{em} = 525 nm), while the strongest blue shift occurs for **5h** (λ_{em} = 505 nm).

Most compounds show quantum yields between 19% and 28%. The highest value was determined for **5h** (Φ = 0.35). In contrast, the two *N*,*N*-dimethylamino-compounds **5c** (Φ = 0.19) and **5k** (Φ = 0.20) show the lowest quantum yields. The spectroscopic data are presented in Table 4.

Since the absorption and emission spectra of **5c** and **5k** indicated the strongest influence of the substituents on the core structure, these compounds as well as reference compound **5a** were additionally investigated by time-dependent density functional theory (TD-DFT) calculations using

Table 3 Synthesis of **5a–m**

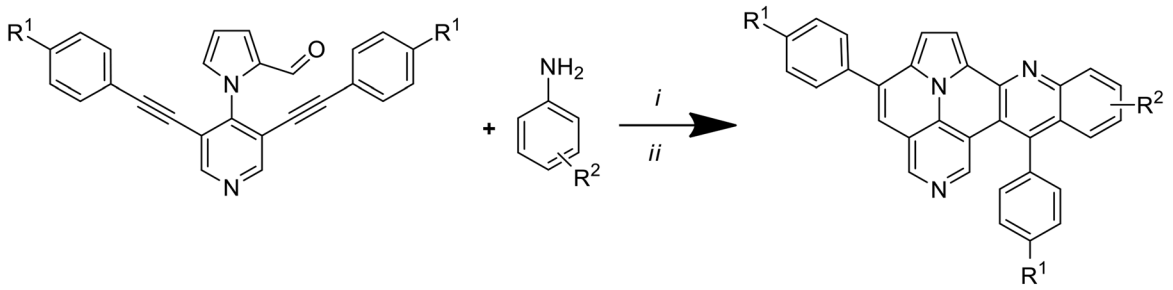

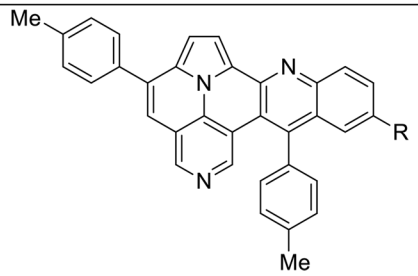

5a R = H 47 %
5b R = Me 44%
5c R = NMe_2 21%[a]
5d R = F 50%

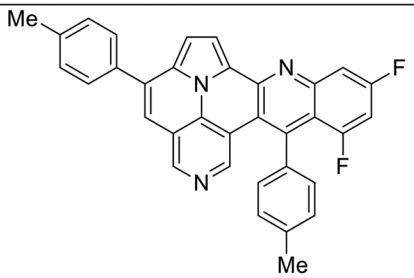

5e 46%

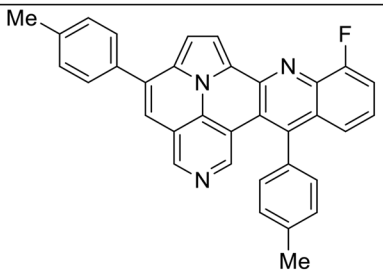

5f 41%

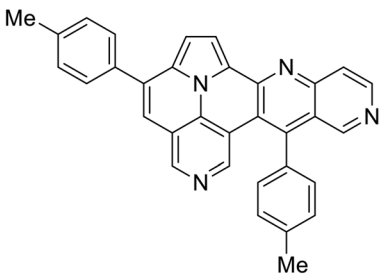

5g 0%

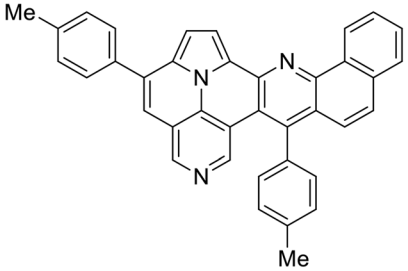

5h 46%

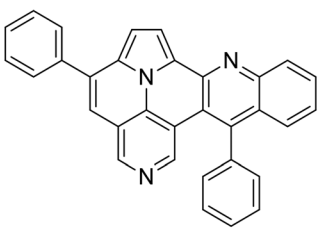

5i 32%[b]

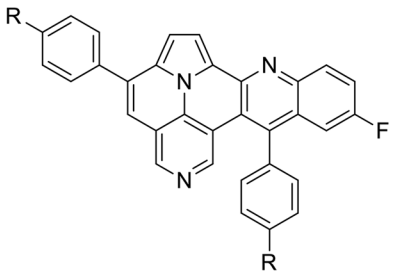

5j R = H 35%
5k R = NMe_2 39%
5l R = F 65%
5m R = CF_3 0%

(*i*): $FeCl_3$ (0.1 eq.), corresponding aniline (1.2 eq.), toluene, 100 °C, 2 h; (*ii*): *p*-TsOH·H_2O (20 eq.), xylene, 120 °C, 6 h. [a] (i): $FeCl_3$ (1.0 eq.); (ii): 20 h. [b] Longer reaction time: (i): 4 h; (ii): 20 h.

Gaussian 09 to get insight into transition characters.[23] The results show that the $S_1 \leftarrow S_0$ excitation for **5a** and **5c** is described by a HOMO → LUMO transition with high oscillator strength. The same applies to **5k**, but with additional minor contribution of HOMO−1 → LUMO and lower oscillator strength for this transition. However, the $S_2 \leftarrow S_0$ transition, which for **5k** again consisted of a HOMO → LUMO and HOMO−1 → LUMO transition, has a significantly higher oscil-

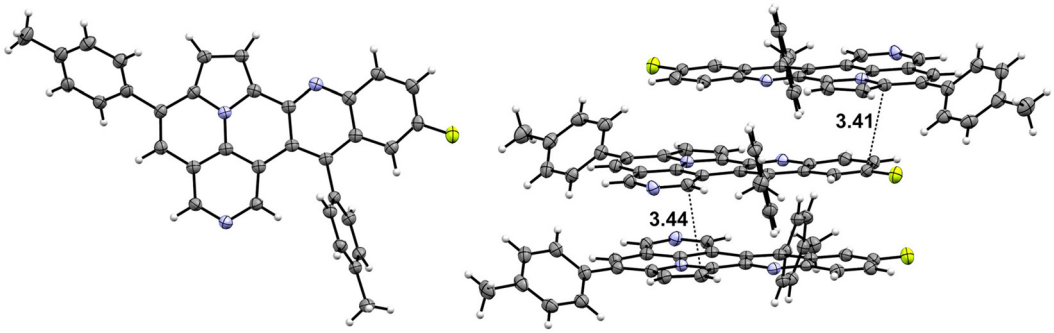

Fig. 3 X-ray structures of **5d**.

lator strength as compared to **5a** and **5c**. Hence, the orbital contribution of these transitions is reversed. In agreement with the experimental results, TD-DFT calculations reveal the greatest impact for derivative **5k**, containing a strong π-donor attached to the heterocyclic core structure.

Comparison of non-symmetric quinolino-azaullazine **5a** with symmetric dibenzoullazines of Gao and Morin and of isoelectronic quinolino-azapyrene reveal further insights into the optical properties of **5a** (Table 5).[9,15,19] Absorption and emission maxima of **5a** are both strongly, bathochromically shifted compared to all three structurally related compounds. The quantum yield of **5a** is reduced to approximately half of the value of quinolino-azapyrene, while extinction coefficients are rather similar for both compounds. A similar trend is observed for 2-aza-pyrene and 2-aza-ullazine without fused quinoline moieties.[5,20] In a smaller extend, quantum yield of **5a** is also reduced compared to symmetric dibenzoullazine reported by Gao and co-workers.[9] However, in impact on the quantum yield of **5a** by the presence of additional tolyl groups and hence increased non-radiative decay compared to dibenzoullazine can currently not ruled out.

To get an understanding of the redox properties, compound **5a** was studied by cyclic voltammetry (CV) (Fig. S1 and S2†). Compound **5a** possesses an irreversible oxidation potential at 0.72 V with an onset potential of 0.61 V, as well as a quasi-reversible oxidation potential at 1.09 V. An irreversible reduction potential was detected at −2.09 V with an onset potential of 1.90 V and a second reduction potential at 3.11 V. The HOMO energy was calculated from the onset potential and is with −5.41 eV somewhat higher than that of previously reported quinolino-azapyrene **6** which is a result of the donor-capacity of the ullazine substructure of **5a**.[19] The determined LUMO energy is −2.90 eV.

We performed density functional theory (DFT) calculations to obtain further insights into the electronic structures and transition characters. The calculations were performed for compounds **5a**, **5c**, **5i** and **5k**. Quinolino-azapyrene **6** and quinolino-ullazine **7** were additionally studied to compare the impact of different core structures (Fig. 5). The calculated HOMO–LUMO gap of the quinolino-azapyrene system is considerably larger, which is mainly due to increased HOMO energies, whereas the LUMO-energies are largely unchanged, highlighting the donating ability of the involved ullazine and azaullazine moiety. Similar HOMO–LUMO-gap energies were determined both for ullazine and azaullazine based structures **5a**, **5i** and **7**. However, an improved stabilization of both HOMO and LUMO orbitals is observed in case of azaullazines **5a** and **5i** with respect to ullazine **7**, which is obviously a result of the presence of the additional nitrogen atom. The NMe_2-groups attached to the heterocyclic core structure (**5c**) as well as the NMe_2-groups attached to the phenyl ring (**5k**) lead to reduced band gaps and elevated HOMO and LUMO energies. A more distinct effect is observed for **5c** as compared to **5k**. However, HOMO and LUMO energies are more destabilized by incorporation of one NMe_2-group directly to the core structure (**5c**) than it does for **5k** with NMe_2-groups attached to each of the two phenyl rings. Furthermore, an ICT character for **5k** can be assumed from its frontier orbitals, derived from its certain push–pull substitution pattern and its optical properties.

The potential occurrence of ICT properties was further validated by solvatochromic studies. Hence, the optical properties in solvents of different polarity were studied for NMe_2-containing compounds **5c** and **5k**, as well as for **5a** (Fig. 6). All absorption spectra show similar behavior in non-polar cyclohexane. A definite fine structure of the absorption bands, as typical for various acenes[24] and acridines,[25] can be observed for all investigated derivatives. This fine structure is lost when the polarity of the solvents increases. This indicates the presence of an ICT effect in all three derivatives **5a**,**c**,**k** and suggests that the ICT character is already present in the heterocyclic core structure, regardless of the substituent. This assumption is supported by the emission spectra, in which all compounds show two maxima and one shoulder at higher wavelength in cyclohexane. In more polar solvents, the emissions appear broadened with a single maximum. Furthermore, a bathochromic shift of emission maxima is visible for these solvents. The shift is ~40 nm for **5a** and for

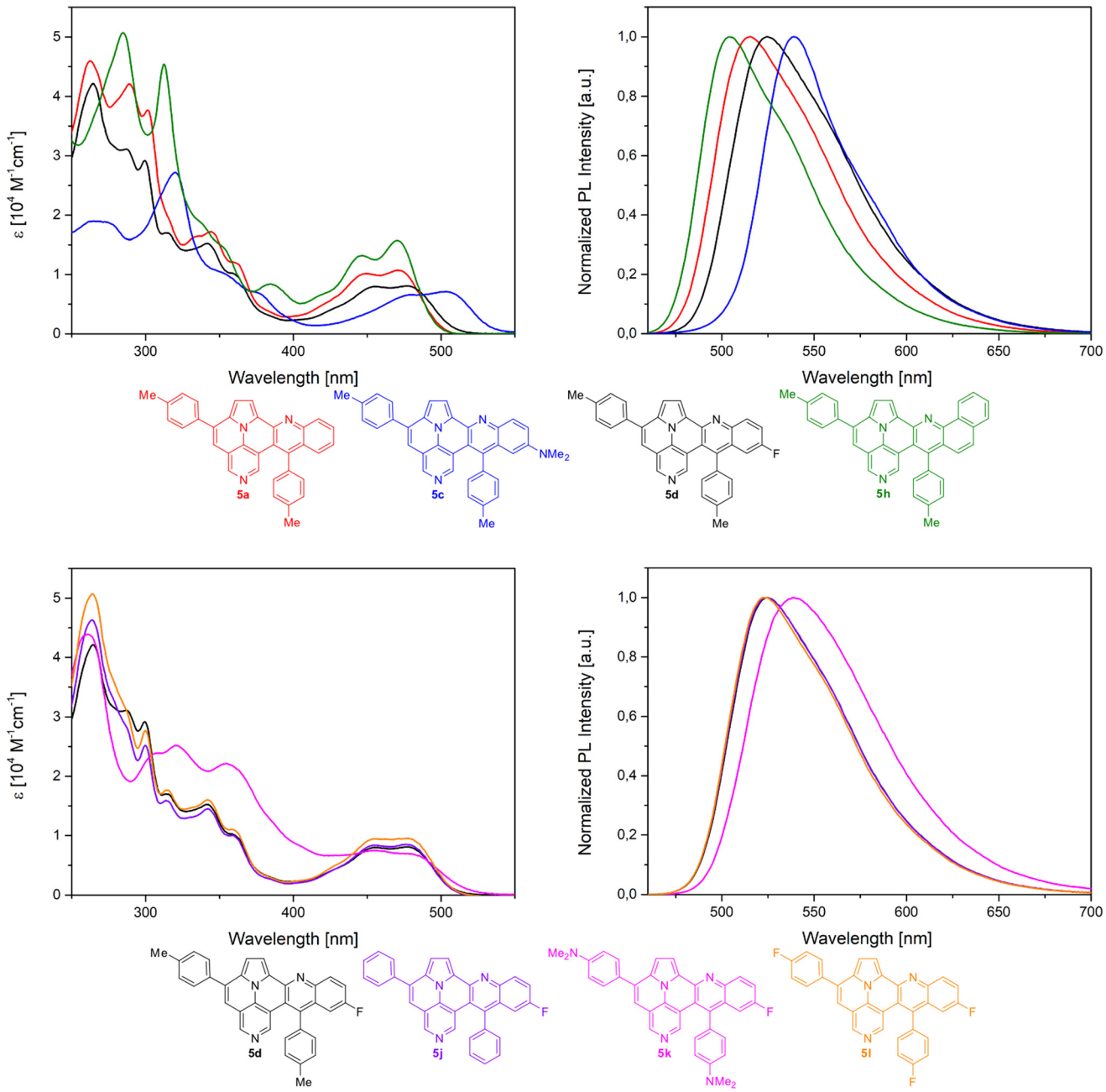

Fig. 4 UV/Vis- (top/bottom, left) and PL-spectra (top/bottom, right, λ_{ex} = 450 nm) of shown compounds in DCM (c = 10^{-5} M) at 20 °C.

Table 4 Spectroscopic data of **5a**, **5c**, **5d**, **5h**, **5j**, **5k** and **5l** in DCM (c = 10^{-5} M) at 20 °C

	5a	**5c**	**5d**	**5h**	**5j**	**5k**	**5l**
$\lambda_{1,abs}$ [nm]	471	503	477	470	477	482	480
ε_{λ_1} [10^4 L mol^{-1} cm^{-1}]	1.1	0.7	0.8	1.6	0.8	0.7	0.9
$\lambda_{2,abs}$ [nm]	448	480	454	447	477	455	455
ε_{λ_2} [10^4 L mol^{-1} cm^{-1}]	1.0	0.7	0.8	1.3	0.8	0.7	0.9
$\lambda_{1,em}$ [nm]	515	539	525	505	524	539	524
E_g^{opt} [eV] [a]	2.56	2.42	2.53	2.59	2.53	2.50	2.53
Φ [b]	0.26	0.19	0.27	0.35	0.25	0.20	0.28

[a] Determined from the intersection of the normalized absorption and emission spectra. [b] Fluorescence standard: quinine hemisulfate monohydrate in 0.05 M H_2SO_4 (Φ = 0.52).[22]

5c between cyclohexane and ethanol, indicating that the NMe_2-group of **5c** has only negligible effect on the ICT character of the core structure. In contrast, a stronger shift of 59 nm can be observed for **5k**. For all compounds, a decrease of the emission in more polar solvents is observed and accompanied by a reduction of their quantum yields (ESI, Table 5†). However, **5k** again behaves quite differently from **5a** and **5c** and shows only very weak fluorescence in acetonitrile and ethanol with quantum yields ≤ 1%, what might be explained by the occurrence of a twisted intramolecular charge transfer (TICT). This effect appears in polar acetonitrile and ethanol, suggesting that the polarity of the solvent

Table 5 Comparison of optical properties with related molecular structures

	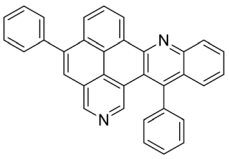 Quinolino-azapyrene[19]	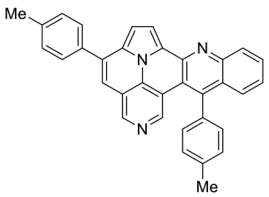 **5a**	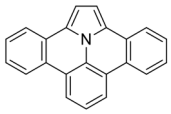 Dibenzo-ullazine[9]	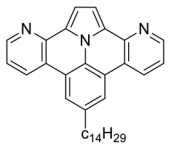 Dipyrido-ullazine[15]
$\lambda_{1,abs}$ [nm]	415	471	~420[a]	~425[a]
ε_{λ_1} [10^4 L mol^{-1} cm^{-1}]	1.0	1.1	—	—
$\lambda_{1,em}$ [nm]	430	515	444	~450[a]
Φ	0.47	0.26	0.35	—

[a] Estimated from the graphs.

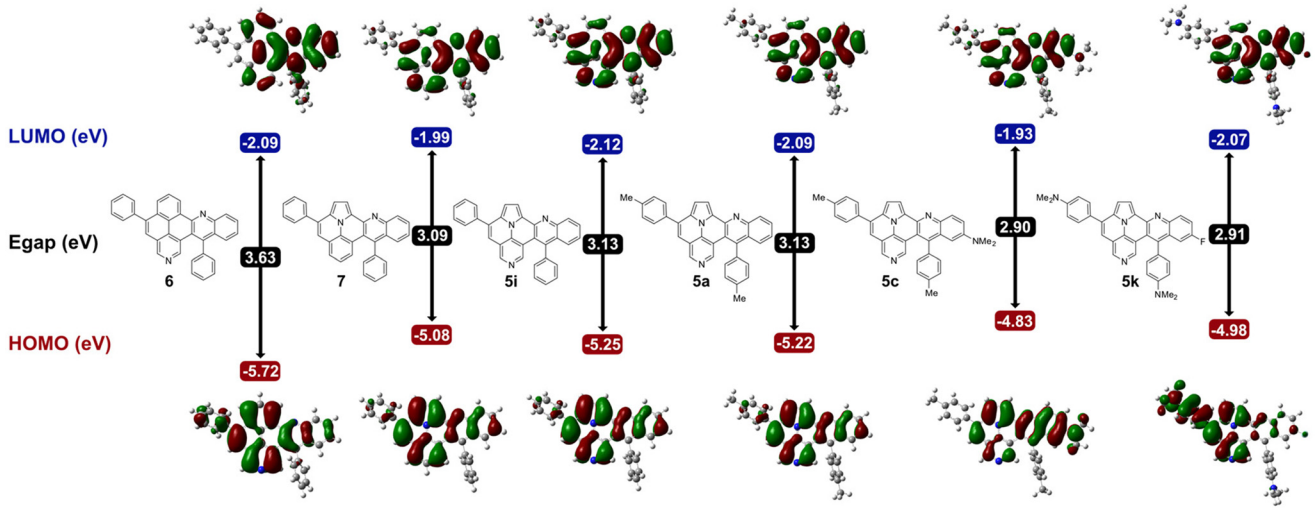

Fig. 5 Frontier orbitals of selected compounds and energy levels calculated at the B3LYP/6-31G(d,p) level of theory within IEFPCM in DCM.

may sufficient to stabilize a TICT. This twisted structure may explain the quenching of the fluorescence through the radiation-free TICT-relaxation.[26]

Further investigations of the ICT-character were performed by calculations of the dipole moments of the ground (S_0) and excited state (S_1) of **5a**, **5c** and **5k**. These calculations confirm the results of the studies related to solvatochromism. Compound **5k** (μ_{S_0} = 4.4193; μ_{S_1} = 26.2043) indicates the strongest increase in the dipole moment, followed by **5a** (μ_{S_0} = 1.0280; μ_{S_1} = 10.6564) and **5c** (μ_{S_0} = 4.1596; μ_{S_1} = 6.0825).

In addition, we performed protonation studies with trifluoromethanesulfonic acid (TFA) in DCM for compound **5a**. As shown in Fig. 7, protonation of **5a** results in a bathochromic shift in the absorption and emission spectra. The first absorption maximum shifts from 471 nm for the free base **5a** to 534 nm for protonated species and an isosbestic point at a wavelength of 482 nm can be detected. The PL-spectra show similar results: the emission maximum shifts from 515 nm to 586 nm, with the first emission maximum decreasing and the second increasing simultaneously. In addition, protonation results, beside the bathochromic shift, also in a decrease of fluorescence. However, changes and shapes of the absorption and PL spectra during the protonation experiments prohibit conclusion whether only one or both pyridinic nitrogen are protonated.

Finally, we performed nuclear-independent chemical shift (NICS) calculations for the quinolino-azaullazine core structure (**5′**) to gain insight into the aromatic behavior of the compound. Therefore, NICS(1.25)$_{zz}$ values were calculated for each ring to investigate the local aromaticity.[27] Furthermore, ring currents were calculated using the BC-Wizard program developed by Gershoni-Poranne *et al.*[28] The calculations were performed in comparison to quinolino-azapyrene **6′** and quinolino-ullazine **7′** (Fig. 8).[19] All three compounds display a global diatropic ring current, as well as negative NICS$_{zz}$ values in all rings. In addition, all studied compounds exhibit two semiglobal ring currents, one in the quinoline moiety, the other in the benzo-isoquinoline or pyrrolo-quinoline moiety. However, the

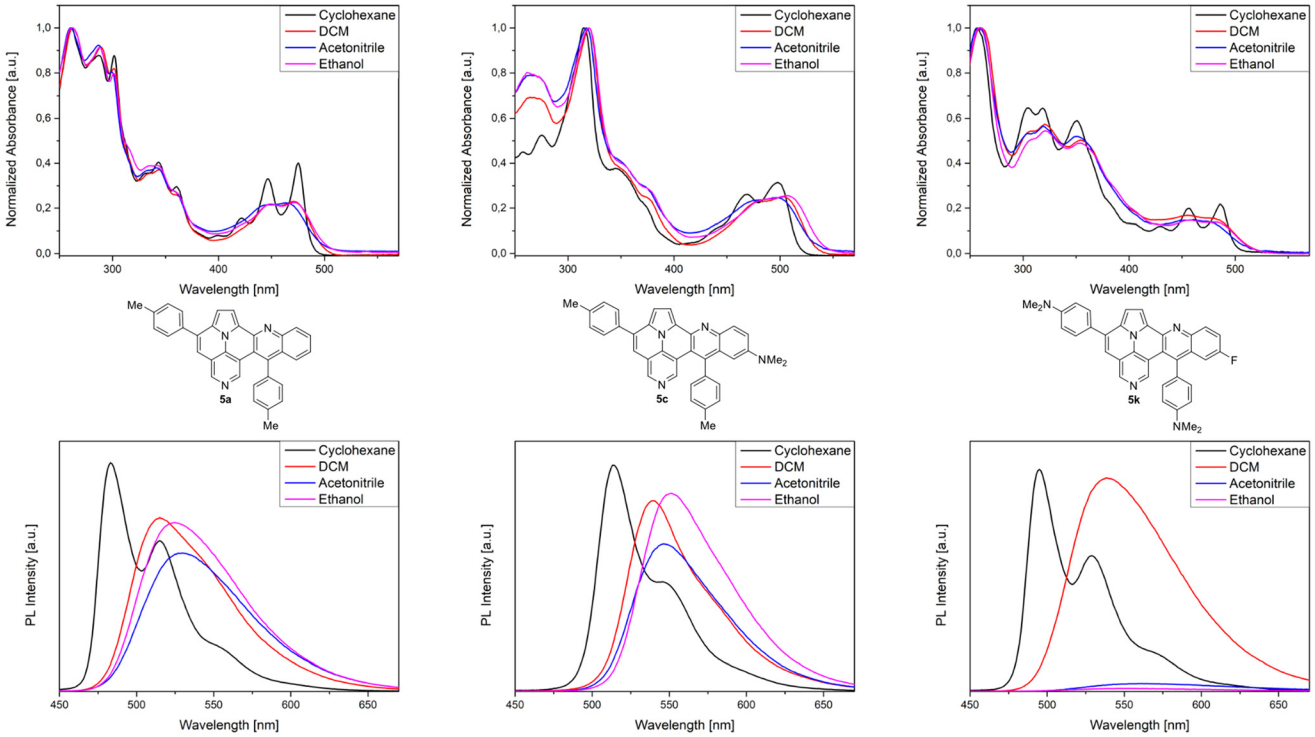

Fig. 6 Top: UV/Vis-spectra of **5a** (left), **5c** (middle), **5k** (right); Bottom: PL-spectra **5a** (left), **5c** (middle), **5k** (right), *t*, λ_{ex} = 340 nm; spectra measured with toluene, dichloromethane, acetonitrile and ethanol ($c = 10^{-5}$ M at 20 °C).

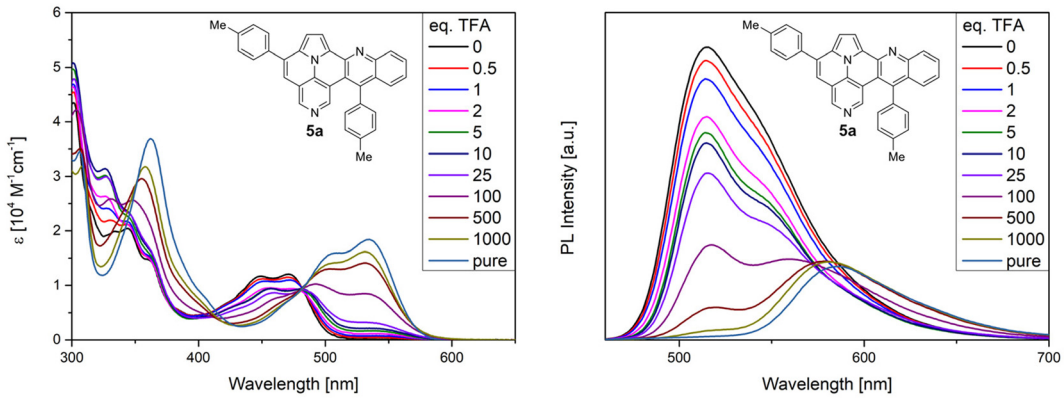

Fig. 7 Absorption and PL spectra of **5a** in dependence of the TFA concentration.

connecting ring of both moieties is not involved in any semi-global ring current, thus the molecules consist of two aromatic subunits connected by a ring with non-aromaticity in case of **5′** and **7′**, and low aromaticity for **6′**, which is confirmed by the $NICS_{zz}$ values. In the two ullazine structures, this ring shows even lower aromaticity than in the aza-pyrene structure. In addition, the ring current maps show that there is a difference mainly in the benzoisoquinoline or pyrroloquinoline moiety, which is due to the different molecular structure. Thus, **6′** shows a stronger semiglobal current, whereas **5′** and **7′** exhibit a stronger local ring current focused on the pyrrole unit. Comparing the structures of ullazine **7′** and azaullazine **5′**, only negligible differences are noticed, as both have almost the same ring currents and similar $NICS_{zz}$ values. Hence, the impact on aromaticity by the presence of an additional nitrogen of **7′** as compared to **5′** is very small. However, a pronounced influence is observed by incorporation of an ullazine as compared to a related azapyrene sub-structure.

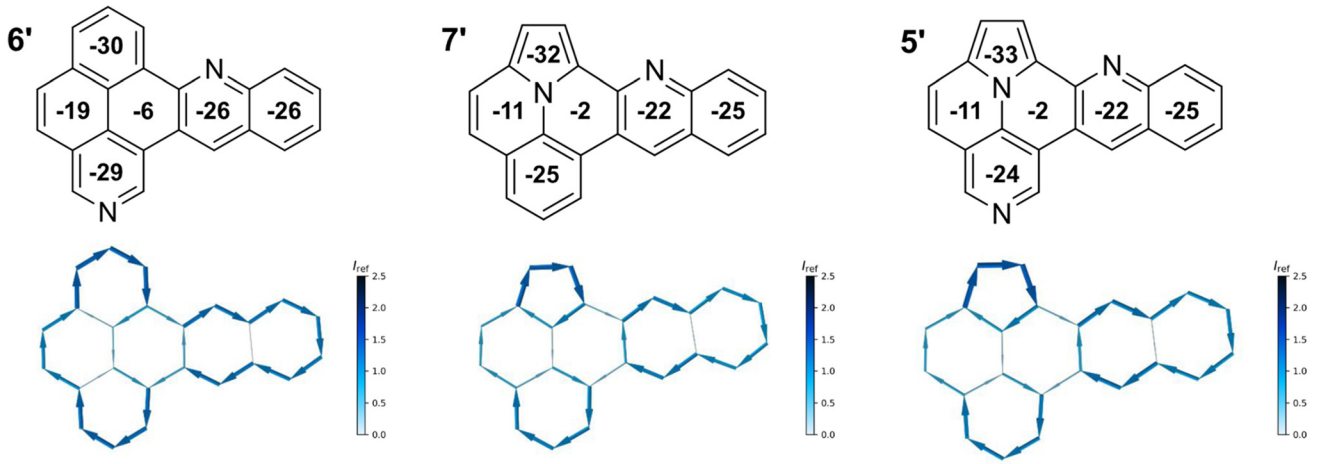

Fig. 8 NICS calculations for benzo[*j*]naphtho[2,1,8-*def*][2,7]phenanthroline (**6'**); indolizino[6,5,4,3-*ija*]quinolino[2,3-*c*]quinoline (**7'**); indolizino[6,5,4,3-*ija*]quinolino[2,3-*c*][1,6]naphthyridine (**5'**). Top: Scheme of molecule with respective NICS(1.25)$_{zz}$ values in the center of each ring. Bottom: NICS2BC graphs (current was calculated form NICS(1.25)$_{zz}$ strength relative to I_{ref} (ring current of benzene, 11.5 nA T^{-1})).[28]

Conclusion

Hitherto unknown quinolino-azaullazines were prepared by combination of Pd catalyzed cross-coupling with Povarov reactions. The synthetic strategy provides a convenient access to various functionalized molecules, which allowed for a fine-tuning of the optical properties. Especially the variation of the aniline component in the Povarov reaction has an important impact on the optoelectronic properties of the products. All investigated compounds exhibit strong absorption in visible light as well as greenish fluorescence with quantum yields between 19% and 35%. Noteworthy is the introduction of strongly donating NMe_2-substituents, which cause extensive alternation of the optical properties not only attached to the core structure, but also on the phenyl substituents. Solvatochromism studies revealed that an ICT character is already present in the core structure, independently from the substitution pattern. However, the presence of a NMe_2-group at the phenyl groups even improved the ICT properties, which suggests the presence of TICT. Further modification of the optical properties was achieved by protonation, which causes a red shift of both absorption and emission. Cyclic voltammetry investigation revealed a more facile oxidation as compared to quinolinoazapyrenes, due to the strong donor capacity of the azaullazine core structure. These observations were confirmed by DFT calculations. NICS calculations disclosed that the novel aza-PAHs prepared have a weak global ring current and can be best described by the presence of two independent aromatic systems consisting of a pyrroloquinoline and a quinoline unit connected by a non-aromatic ring. Further studies will focus on the synthesis of related heteroatom doped PAHs by means of the Povarov reaction.

Experimental section

General information

The nuclear magnetic resonance spectra (^{1}H/^{13}C/^{19}F NMR) were recorded on a Bruker AVANCE 300 III, 250 II, or 500. The analyzed chemical shifts δ are referenced to residual solvents signals of the deuterated solvents $CDCl_3$ (δ = 7.26 ppm/77.0 ppm). Multiplicities due to spin–spin correlation are reported as follows, s = singlet, d = doublet, dd = double doublet, ddd = doublets of doublets, m = multiplet, and further described through their coupling constants *J*. Infrared spectra (IR) were measured as attenuated total reflection (ATR) experiments with a Nicolet 380 FT-IR spectrometer. The signals have been characterized through their wave numbers $\tilde{\nu}$ and their corresponding absorption as very strong (vs), strong (s), medium (m) or weak (w). UV/Vis spectra were recorded on a Cary 60 UV-vis spectrophotometer and emission spectra with an Agilent Cary Eclipse fluorescence spectrophotometer. Cyclic voltammograms were measured at room temperature in DCM or THF ($c = 10^{-3}$ M) with 0.1 M *n*-Bu_4NPF_6 as a supporting electrolyte, glassy carbon working electrode, ANE2 ($Ag/AgNO_3$ 0.01 M in CH_3CN) as reference electrode and Pt counter-electrode (0.5 mm diameter platinum wire) with ferrocene ($c = 10^{-3}$ M, in CH_3CN) as an external standard at a scan rate of 100 mV s^{-1} or 200 mV s^{-1}. The potentiostat used was a PalmSense EmStat 3 blue or a Parstat 4000 from Ametek. The working electrode is a 3 mm diameter (length 80, 6.35 mm outer diameter) glassy carbon disk electrode in a KeI-F coating that was polished on a polishing pad in aqueous alumina slurry (0.03 μm alumina powder). The solvents were deoxygenated by purging with argon. The potential is given *vs.* Fc/Fc^+. The direction of scan is reductive with a starting potential of 1.5 V and a switching potential of −1.5 V for DCM and for THF a starting potential of 0 V and a switching potential of −3.2 V. CVs are plotted using the IUPAC. Basic and high-resolution mass spectra (MS/HRMS) were measured on instruments which are paired with a preceding gas chromatograph (GC) or liquid chromatograph (LC). The samples have been ionized through electron impact ionization (EI) on an Agilent 6890/5973 or Agilent 7890/5977 GC-MS equipped with a HP-5 capillary column using helium carrier gas or by applying electron spray ionization (ESI) on an

Agilent 1200/6210 Time-of-Flight (TOF) LC-MS. Melting points (mp) were determined by a Micro-Hot-Stage GalenTM III Cambridge Instruments and are not corrected. X-ray single-crystal structure analysis was performed on a Bruker Apex Kappa-II CCD diffractometer.

Analytical data

3,5-Dibromo-4-(1*H*-pyrrol-1-yl)pyridine (1). Starting from 4-aminopyridine, **1** could be synthesized according to the literature-known procedure in a yield of 77% (5.14 g) yield.[5] The NMR data agree with the published NMR data. **^{1}H NMR** (250 MHz, $CDCl_3$) δ = 8.77 (s, 2H), 6.74–6.72 (m, 2H), 6.47–6.38 (m, 2H). **^{13}C NMR** (63 MHz, $CDCl_3$) δ = 151.7 (CH), 146.5, 121.0 (C), 120.9, 110.3 (CH).

1-(3,5-Dibromopyridin-4-yl)-1*H*-pyrrole-2-carbaldehyde (2a). 3,5-Dibromo-4-(1*H*-pyrrol-1-yl)pyridine (**1**, 1.00 g, 3.31 mmol) was suspended in 5 ml DMF in a Schlenk flask under an argon atmosphere. 2 eq. $POCl_3$ (6.62 mmol, 0.63 ml) were added dropwise at 0 °C. The solution was stirred at 100 °C for 3 h, cooled to room temperature, neutralized with $NaHCO_3$ and extracted with DCM. The combined organic phases were dried with Na_2SO_4, the solvent was removed *in vacuo* and the residue was purified by column chromatography to give **2a** as a colourless solid (0.364 g, 33%). **Mp** 129 °C. R_f 0.22 (heptane/ethyl acetate 3 : 1). **^{1}H NMR** (300 MHz, $CDCl_3$) δ = 9.49 (d, ^4J = 1.0 Hz, 1H), 8.69 (s, 2H), 7.09 (dd, ^3J = 3.9 Hz, ^4J = 1.6 Hz, 1H), 6.81 (ddd, ^3J = 2.7 Hz, ^4J = 1.6 Hz, ^4J = 1.0 Hz, 1H), 6.49 (dd, ^3J = 4.0 Hz, ^3J = 2.7 Hz, 1H). **^{13}C NMR** (75 MHz, $CDCl_3$) δ = 178.2 (CHO), 151.3 (CH), 145.9, 131.7 (C), 129.1, 123.6 (CH), 121.2 (C), 112.3 (CH). **IR** (ATR, cm^{-1}): $\tilde{\nu}$ = 1661 (s), 1484 (m), 1399 (m), 1356 (s), 1199 (m), 1037 (m), 999 (m), 886 (m), 779 (s), 750 (s), 715 (m), 610 (m), 577 (s). **MS** (EI, 70 eV): *m*/*z* (%) = 330 ([M]$^+$, 1), 252 (11), 251 (98), 250 (15), 249 (100), 170 (21), 142 (8), 130 (5), 115 (9), 114 (7). **HRMS** (EI): calculated for $C_{10}H_6{}^{79}Br_2N_2O$ ([M]$^+$) 327.88414, found 327.88451; calculated for $C_{10}H_6{}^{79}Br^{81}BrN_2O$ ([M]$^+$) 329.88209, found 329.88255; calculated for $C_{10}H_6{}^{81}Br_2N_2O$ ([M]$^+$) 331.88005, found 331.88075.

1-(3,5-Dibromopyridin-4-yl)-1*H*-pyrrole-3-carbaldehyde (2b). Using the reaction conditions as for **2a**, the main product **2b** was obtained after column chromatography (3 : 1 heptane : ethyl acetate) as a colourless solid (0.673 g, 62%). **Mp** 100–110 °C. R_f 0.14 (heptane/ethyl acetate 3 : 1). **^{1}H NMR** (300 MHz, $CDCl_3$) δ = 9.89 (dd, ^4J = 0.4 Hz, 1H), 8.81 (s, 2H), 7.34 (dd, ^4J = 2.1 Hz, ^4J = 1.6 Hz, 1H), 6.87 (ddd, ^3J = 3.1 Hz, ^4J = 1.6 Hz, ^4J = 0.4 Hz, 1H), 6.74 (ddd, ^3J = 3.0 Hz, ^4J = 2.1 Hz, ^4J = 0.7 Hz, 1H). **^{13}C NMR** (75 MHz, $CDCl_3$) δ = 185.2 (CHO), 152.0 (CH), 145.1 (C), 128.9 (CH), 128.3 (C), 123.6 (CH), 120.5 (C), 109.3 (CH). **IR** (ATR, cm^{-1}): $\tilde{\nu}$ = 1675 (s), 1508 (s), 1467 (s), 1294 (m), 1257 (m), 1210 (m), 1152 (m), 1084 (m), 1041 (s), 816 (m), 732 (s), 618 (m), 591 (m). **MS** (EI, 70 eV): *m*/*z* (%) = 332 (34), 331 (54), 330 ([M]$^+$, 69), 329 (100), 328 (36), 327 (50), 142 (7), 141 (10), 130 (6), 128 (6), 114 (7). **HRMS** (ESI-TOF): calculated for $C_{10}H_7Br_2N_2O$ ([M + H]$^+$) 328.8925, found 328.8931.

General procedure A for the synthesis of 1-(3,5-bis(arylethynyl)pyridin-4-yl)-1*H*-pyrrole-2-carbaldehyde (3a–e). In a pressure tube, 200 mg of 1-(3,5-dibromopyridin-4-yl)-1*H*-pyrrole-2-carbaldehyde (**2a**), 0.05 eq. $PdCl_2(PPh_3)_2$, 0.05 eq. CuI, 0.1 eq. cataCXium A were dissolved in 0.5 ml HN^iPr_2 and 3 mL of 1,4-dioxane under argon counter current. Then, 3 eq. of the respective alkyne was added to the solution with stirring. The pressure tube was sealed with a Teflon cap and the solution was stirred for 24 h at 90 °C. The reaction solution was cooled to room temperature, quenched with distilled water and extracted three times with DCM. The combined organic phases were dried over Na_2SO_4, the solvent was distilled off *in vacuo*, and the residue was purified by column chromatography (Hep/EtOAc) to give the desired products (**3a–e**).

1-(3,5-Bis(phenylethynyl)pyridin-4-yl)-1*H*-pyrrole-2-carbaldehyde (3a). According to general procedure A, the title compound **3a** was obtained as a yellow-orange solid in 80% yield (181 mg). **Mp** 118–122 °C. R_f 0.14 (heptane/ethyl acetate 5 : 1). **^{1}H NMR** (300 MHz, $CDCl_3$) δ = 9.60 (d, ^4J = 0.8 Hz, 1H), 8.80 (s, 2H), 7.34–7.28 (m, 10H), 7.24 (dd, ^3J = 3.9 Hz, ^4J = 1.6 Hz, 1H), 7.19 (ddd, ^3J = 2.6 Hz, ^4J = 1.6 Hz, ^4J = 0.9 Hz, 1H), 6.58 (dd, ^3J = 3.9 Hz, ^3J = 2.7 Hz, 1H). **^{13}C NMR** (75 MHz, $CDCl_3$) δ = 178.2 (CHO), 151.8 (CH), 148.2, 132.9 (C), 131.6, 130.5, 129.2, 128.3, 122.4 (CH), 121.7, 118.8 (C), 111.3 (CH), 97.2, 81.6 (C≡C). **IR** (ATR, cm^{-1}): $\tilde{\nu}$ = 1659 (s), 1480 (m), 1403 (m), 1354 (m), 1036 (m), 890 (m), 781 (s), 748 (s), 686 (s), 573 (m), 548 (m). **MS** (EI, 70 eV): *m*/*z* (%) = 372 ([M]$^+$, 19), 345 (25), 344 (100), 343 (47), 342 (40), 341 (11), 340 (14), 316 (8), 315 (9), 266 (10), 171 (5), 158 (4). **HRMS** (ESI-TOF): calculated for $C_{26}H_{17}N_2O$ ([M + H]$^+$) 373.1341, found 373.1349.

1-(3,5-Bis(*p*-tolylethynyl)pyridin-4-yl)-1*H*-pyrrole-2-carbaldehyde (3b). According to general procedure A, the title compound **3b** was obtained as a yellow-orange solid in 76% yield (193 mg). **Mp** 123–125 °C. R_f 0.21 (heptane/ethyl acetate 5 : 1), **^{1}H NMR** (500 MHz, $CDCl_3$) δ = 9.59 (d, ^4J = 0.8 Hz, 1H), 8.77 (s, 2H), 7.23 (dd, ^3J = 4.0 Hz, ^4J = 1.6 Hz, 1H), 7.20 (d, ^3J = 8.2 Hz, 4H), 7.18–7.17 (m, 1H), 7.11 (d, ^3J = 7.9 Hz, 4H), 6.56 (dd, ^3J = 4.0 Hz, ^3J = 2.7 Hz, 1H), 2.34 (s, 6H). **^{13}C NMR** (126 MHz, $CDCl_3$) δ = 178.2 (CHO), 151.5 (CH), 147.9, 139.5 (C), 132.9, 131.5, 130.4, 129.1 (CH), 119.0, 118.7 (C), 111.2 (CH), 97.6, 81.1 (C≡C), 21.5 (CH_3). **IR** (ATR, cm^{-1}): $\tilde{\nu}$ = 1657 (s), 1508 (m), 1484 (m), 1407 (s), 1356 (m), 1030 (m), 886 (m), 814 (s), 785 (s), 754 (s), 743 (s), 577 (s), 528 (s). **MS** (EI, 70 eV): *m*/*z* (%) = 400 ([M]$^+$, 14), 373 (29), 372 (100), 371 (23), 370 (11), 369 (9), 357 (10), 356 (17), 178 (9), 177 (9). **HRMS** (ESI-TOF): calculated for $C_{28}H_{21}N_2O$ ([M + H]$^+$) 401.1654, found 401.1643.

1-(3,5-Bis((4-fluorphenyl)ethynyl)pyridin-4-yl)-1*H*-pyrrole-2-carbaldehyde (3c). According to general procedure A, the title compound **3c** was obtained as yellow solid in 87% yield (216 mg). **Mp** 129–132 °C. R_f 0.19 (heptane/ethyl acetate 5 : 1). **^{1}H NMR** (300 MHz, $CDCl_3$) δ = 9.54 (d, ^4J = 0.8 Hz, 1H), 8.73 (s, 2H), 7.27–7.17 (m, 5H), 7.12 (ddd, ^3J = 2.6 Hz, ^4J = 1.6 Hz, ^4J = 0.9 Hz, 1H), 6.98–6.91 (m, 4H), 6.53 (dd, ^3J = 3.9 Hz, ^3J = 2.7 Hz, 1H). **^{13}C NMR** (75 MHz, $CDCl_3$) δ = 178.2 (CHO), 163.0 (d, ^1J = 251.4 Hz, C), 151.7 (CH), 148.1 (C), 133.6 (d, ^3J = 8.6 Hz, CH), 132.9 (C), 130.4, 122.4 (CH), 118.7 (C), 117.8 (d, ^4J = 3.5 Hz, C), 115.8 (d, ^2J = 22.2 Hz, C), 111.3 (C), 96.2 (C≡C), 81.4 (d, ^5J = 1.5 Hz, C≡C). **^{19}F NMR** (282 MHz, $CDCl_3$): δ = −108.8.

IR (ATR, cm^{-1}): $\tilde{\nu}$ = 1667 (s), 1504 (s), 1407 (s), 1226 (s), 1154 (m), 1092 (m), 832 (s), 783 (m), 742 (s), 575 (m), 528 (s), 492 (s). **MS** (EI, 70 eV): *m*/*z* (%) = 408 ([M]$^+$, 17), 381 (26), 380 (100), 379 (43), 378 (36), 377 (7), 376 (9), 352 (6), 351 (7), 313 (4), 284 (9), 189 (4). **HRMS** (ESI-TOF): calculated for $C_{26}H_{15}F_2N_2O$ ([M + H]$^+$) 409.1152, found 409.1149.

1-(3,5-Bis((4-(trifluoromethyl)phenyl)ethynyl)pyridin-4-yl)-1*H*-pyrrole-2-carbaldehyde (3d). According to general procedure A, the title compound **3d** was obtained as a yellow solid in 74% yield (228 mg). **Mp** 135–142 °C. R_f 0.10 (heptane/ethyl acetate 10 : 1). **^{1}H NMR** (300 MHz, $CDCl_3$) δ = 9.52 (d, ^4J = 0.9 Hz, 1H), 8.75 (s, 2H), 7.48 (d, ^3J = 8.1 Hz, 4H), 7.30 (d, ^3J = 7.9 Hz, 4H), 7.17 (dd, ^3J = 3.9 Hz, ^4J = 1.6 Hz, 1H), 7.10 (ddd, ^3J = 2.6 Hz, ^4J = 1.6 Hz, ^4J = 0.9 Hz, 1H), 6.52 (dd, ^3J = 3.9 Hz, ^3J = 2.7 Hz, 1H). **^{13}C NMR** (75 MHz, $CDCl_3$) δ = 178.2 (CHO), 152.4 (CH), 148.9, 132.9 (C), 131.9 (CH), 130.9 (q, ^2J = 32.8 Hz, C), 130.5 (CH), 125.4 (C), 125.3 (q, ^3J = 3.8 Hz, CH), 123.6 (q, ^1J = 272.2 Hz, C), 123.0 (CH), 118.3 (C), 111.5 (CH), 95.6, 83.6 (C≡C). **^{19}F NMR** (282 MHz, $CDCl_3$): δ = −63.0. **IR** (ATR, cm^{-1}): $\tilde{\nu}$ = 1663 (s), 1613 (m), 1484 (m), 1405 (m), 1319 (s), 1164 (s), 1102 (s), 1063 (s), 1016 (s), 839 (s), 781 (m), 740 (s), 575 (m). **MS** (EI, 70 eV): *m*/*z* (%) = 508 ([M]$^+$, 23), 481 (27), 480 (100), 479 (30), 478 (13), 461 (7), 411 (9), 410 (19), 363 (5), 334 (6), 195 (7). **HRMS** (ESI-TOF): calculated for $C_{28}H_{15}F_6N_2O$ ([M + H]$^+$) 509.1089, found 509.1096.

1-(3,5-Bis((4-(dimethylamino)phenyl)ethynyl)pyridin-4-yl)-1*H*-pyrrole-2-carbaldehyde (3e). According to general procedure A, the title compound **3e** was obtained as a yellow-brown solid in 45% yield (125 mg). **Mp** 175–183 °C. R_f 0.13 (heptane/ethyl acetate 3 : 1). **^{1}H NMR** (300 MHz, $CDCl_3$) δ = 9.57 (d, ^4J = 0.7 Hz, 1H), 8.68 (s, 2H), 7.23 (dd, ^3J = 3.9 Hz, ^4J = 1.6 Hz, 1H), 7.20–7.14 (m, 5H), 6.59–6.53 (m, 5H), 2.95 (s, 12H). **^{13}C NMR** (75 MHz, $CDCl_3$) δ = 178.2 (CHO), 150.4 (C), 150.3 (CH), 146.4, 132.8 (C), 132.8, 132.5, 130.4 (CH), 119.5 (C), 111.5, 110.8 (CH), 108.2 (C), 99.1, 80.2 (C≡C), 39.9 (CH_3). **IR** (ATR, cm^{-1}): $\tilde{\nu}$ = 1667 (s), 1603 (s), 1564 (s), 1519 (s), 1480 (s), 1360 (s), 1232 (m), 1168 (s), 806 (s), 783 (s), 740 (s), 577 (m), 523 (m). **MS** (EI, 70 eV): *m*/*z* (%) = 458 ([M]$^+$, 100), 457 (23), 431 (15), 430 (57), 429 (22), 414 (22), 229 (14), 215 (12), 214 (25), 206 (12), 192 (11). **HRMS** (ESI-TOF): calculated for $C_{30}H_{27}N_4O$ ([M + H]$^+$) 459.2185, found 459.2189.

14-(*p*-Tolyl)-4-(*p*-tolylethynyl)pyrrolo[1,2-*a*]quinolino[2,3-*c*][1,6]naphthyridine (4). **3a** (150 mg) is dissolved in toluene (3.0 ml) together with aniline (1.2 eq.), then $FeCl_3$ (0.01 eq.) was added. The solution was stirred at 100 °C for 2 h. The reaction solution was cooled to room temperature, quenched with distilled water and extracted three times with DCM. The combined organic phases were dried over Na_2SO_4, the solvent was distilled off *in vacuo*, and the residue was purified by column chromatography (Hep/EtOAc) to give the desired product **4** in 86% (153 mg). **Mp** > 375 °C. R_f 0.26 (heptane/ethyl acetate 5 : 1). **^{1}H NMR** (300 MHz, $CDCl_3$) δ = 9.37 (dd, ^3J = 3.1 Hz, ^4J = 1.5 Hz, 1H), 8.63 (s, 1H), 8.46 (s, 1H), 8.14 (d, ^3J = 8.4 Hz, 1H), 7.71 (ddd, ^3J = 8.4 Hz, ^3J = 6.7 Hz, ^4J = 1.4 Hz, 1H), 7.66 (dd, ^3J = 3.8 Hz, ^4J = 1.5 Hz, 1H), 7.57 (dd, ^3J = 8.6 Hz, ^4J = 1.5 Hz, 1H), 7.54–7.50 (m, 2H), 7.43 (d, ^3J = 7.7 Hz, 2H), 7.37 (ddd, ^3J = 8.4 Hz, ^3J = 6.7 Hz, ^4J = 1.3 Hz, 1H), 7.32–7.19 (m, 4H), 6.80 (dd, ^3J = 3.8 Hz, ^3J = 3.1 Hz, 1H), 2.53 (s, 3H), 2.41 (s, 3H). **^{13}C NMR** (75 MHz, $CDCl_3$) δ = 153.7, 148.2, 145.6, 144.8, 139.6, 138.8, 135.2 (C), 131.3 (C), 131.3, 130.7, 130.2, 129.4, 129.2, 128.8 (CH), 127.1 (C), 126.9, 125.7, 120.3 (CH), 119.3, 115.9 (C), 113.5, 109.5 (CH), 97.9, 85.6 (C≡C), 21.6, 21.5 (CH_3). **IR** (ATR, cm^{-1}): $\tilde{\nu}$ = 1737 (s), 1597 (s), 1504 (s), 1451 (s), 1356 (s), 1205 (s), 1028 (s), 960 (m), 812 (s), 762 (s), 690 (s), 604 (m). **MS** (EI, 70 eV): *m*/*z* (%) = 473 ([M]$^+$, 100), 472 (87), 471 (21), 470 (9), 459 (7), 458 (24), 457 (22), 456 (11), 229 (10), 228 (12). **HRMS** (ESI-TOF): calculated for $C_{34}H_{24}N_3$ ([M + H]$^+$) 474.1970, found 474.1978.

General procedure B for the synthesis of 5,13-di-arylindolizino[6,5,4,3-*ija*]quinolino[2,3-*c*][1,6]naphthyridines (5a–l). 150 mg of **3a–e** together with 1.2 eq. of corresponding aniline and 0.1 eq. $FeCl_3$ (1 eq. for **5c**) were suspended in 3 ml toluene and stirred at 100 °C for 2 h (4 h for **5i**). Subsequently, the solution was diluted with water and extracted with DCM. The combined organic phases were dried over Na_2SO_4, the solvent was distilled off *in vacuo*. The crude product was dissolved in xylene and 20 eq. *p*-TsOH·H_2O were added. The solution was stirred at 120 °C for 6 h (20 h for **5i** and **5k**). The reaction was quenched with $NaHCO_3$-solution, extracted with DCM and dried over Na_2SO_4. The solvent was distilled off *in vacuo* and the residue was purified by column chromatography (Hep/EtOAc) to give the desired products (**5a–l**).

mmol-scale procedure for the synthesis 5,13-di-*p*-tolylindolizino[6,5,4,3-*ija*]quinolino[2,3-*c*][1,6]naphthyridine (5a). 480 mg (1.2 mmol) of **3a** together with 1.2 eq. aniline (131 µl) and 0.1 eq. $FeCl_3$ (19 mg) were suspended in 10 ml toluene and stirred at 100 °C for 2 h. Subsequently, the solution was diluted with water and extracted with DCM. The combined organic phases were dried over Na_2SO_4, the solvent was distilled off *in vacuo*. The crude product was dissolved in xylene and 20 eq. *p*-TsOH·H_2O (4.55 g) were added. The solution was stirred at 120 °C for 6 h. The reaction was quenched with $NaHCO_3$-solution, extracted with DCM and dried over Na_2SO_4. The solvent was distilled off *in vacuo* and the residue was purified by column chromatography (Hep/EtOAc) to give desired products **5a** in 47% (224 mg) yield.

5,13-Di-*p*-tolylindolizino[6,5,4,3-*ija*]quinolino[2,3-*c*][1,6]naphthyridine (5a). According to general procedure B, the title compound **5a** was obtained as a orange solid in 47% yield (83 mg). **Mp** 242–247 °C; R_f 0.29 (heptane/ethyl acetate 2 : 1). **^{1}H NMR** (300 MHz, $CDCl_3$) δ = 8.74 (s, 1H), 8.13 (ddd, ^3J = 8.5 Hz, ^4J = 1.3 Hz, ^5J = 0.6 Hz, 1H), 8.03 (s, 1H), 7.95 (d, ^3J = 4.2 Hz, 1H), 7.73–7.64 (m, 3H), 7.52–7.46 (m, 3H), 7.39–7.27 (m, 5H), 7.14 (s, 1H), 7.09 (d, ^3J = 4.2 Hz, 1H), 2.57 (s, 3H), 2.47 (s, 3H). **^{13}C NMR** (75 MHz, $CDCl_3$) δ = 148.1, 146.4 (C), 145.0, 144.8 (CH), 144.8, 138.9, 138.7, 135.3, 134.8, 134.3, 134.0 (C), 130.9, 130.3, 129.5 (CH), 129.2 (C), 128.6, 128.0 (CH), 127.3 (C), 127.0 (CH), 126.2 (C), 125.7 (CH), 119.8, 117.5, 117.2 (C), 115.3, 111.2, 107.1 (CH), 21.6, 21.3 (CH_3). **IR** (ATR, cm^{-1}): $\tilde{\nu}$ = 2920 (m), 1539 (m), 1502 (m), 1445 (m), 1358 (m), 1179 (m), 1109 (m), 1041 (m), 892 (m), 816 (s), 758 (s), 734 (s), 610 (m), 490 (s). **MS** (EI, 70 eV): *m*/*z* (%) = 473 ([M]$^+$, 100), 472 (69), 471 (72), 470

(17), 457 (17), 456 (18), 236 (46), 235 (16), 228 (37), 227 (24), 226 (12), 220 (12). **HRMS** (ESI-TOF): calculated for $C_{34}H_{24}N_3$ ($[M + H]^+$) 474.1970, found 474.1977.

11-Methyl-5,13-di-*p*-tolylindolizino[6,5,4,3-*ija*]quinolino[2,3-*c*][1,6]naphthyridine (5b). According to general procedure B, the title compound **5b** was obtained as a yellow solid in 44% yield (82 mg). **Mp** 271–275 °C; R_f 0.34 (heptane/ethyl acetate 2 : 1). **^{1}H NMR** (300 MHz, $CDCl_3$) δ = 8.74 (s, 1H), 8.05 (d, ^3J = 8.6 Hz, 1H), 7.99 (s, 1H), 7.95 (d, ^3J = 4.2 Hz, 1H), 7.71–7.66 (m, 2H), 7.54 (dd, ^3J = 8.6 Hz, ^4J = 2.0 Hz, 1H), 7.52–7.47 (m, 2H), 7.37–7.32 (m, 2H), 7.32–7.27 (m, 2H), 7.24–7.22 (m, 1H), 7.15 (s, 1H), 7.10 (d, ^3J = 4.1 Hz, 1H), 2.58 (s, 3H), 2.47 (s, 3H), 2.41 (s, 3H). **^{13}C NMR** (75 MHz, $CDCl_3$) δ = 146.8, 145.7 (C), 145.0, 144.7 (CH), 144.1, 138.8, 138.7, 135.7, 135.5, 134.9, 134.3, 134.0 (C), 132.7, 130.9, 129.6 (CH), 129.0 (C), 128.7, 128.4, 128.0 (CH), 127.3, 126.3 (C), 125.6 (CH), 119.8, 117.7, 117.2 (C), 115.2, 110.8, 107.0 (CH), 21.9, 21.6, 21.4 (CH_3). **IR** (ATR, cm^{-1}): $\tilde{\nu}$ = 1502 (m), 1354 (m), 1183 (m), 1109 (m), 1036 (m), 884 (m), 814 (s), 802 (s), 781 (s), 711 (m), 602 (m), 488 (s). **MS** (EI, 70 eV): *m*/*z* (%) = 487 ($[M]^+$, 100), 486 (55), 485 (11), 472 (18), 471 (24), 470 (11), 457 (6), 244 (9), 236 (23). **HRMS** (EI): calculated for $C_{35}H_{25}N_3$ ($[M]^+$) 487.20430, found 487.20439.

***N*,*N*-Dimethyl-5,13-di-*p*-tolylindolizino[6,5,4,3-*ija*]quinolino[2,3-*c*][1,6]naphthyridin-11-amine (5c).** According to modified general procedure B the title compound **5c** was obtained as a red solid in 21% yield (40 mg). **Mp** 272–277 °C; R_f 0.26 (heptane/ethyl acetate 2 : 1). **^{1}H NMR** (500 MHz, $CDCl_3$) δ = 8.73 (s, 1H), 8.05 (d, ^3J = 9.3 Hz, 1H), 8.03 (s, 1H), 7.90 (d, ^3J = 4.1 Hz, 1H), 7.70 (d, ^3J = 8.0 Hz, 2H), 7.47 (d, ^3J = 7.7 Hz, 2H), 7.40 (dd, ^3J = 9.3 Hz, ^4J = 2.8 Hz, 1H), 7.34 (d, ^3J = 7.7 Hz, 2H), 7.31 (d, ^3J = 8.0 Hz, 2H), 7.13 (s, 1H), 7.11 (d, ^3J = 4.1 Hz, 1H), 6.43 (d, ^4J = 2.8 Hz, 1H), 2.91 (s, 6H), 2.56 (s, 3H), 2.47 (s, 3H). **^{13}C NMR** (126 MHz, $CDCl_3$) δ = 147.9 (C), 144.9, 144.4 (CH), 143.6, 142.8, 141.4, 138.6, 138.4, 136.1, 135.0, 134.2, 134.1 (C), 130.9, 129.5, 129.4 (CH), 128.9 (C), 128.6 (CH), 128.5 (C), 128.0 (CH), 126.8 (C), 120.7 (CH), 119.9, 117.9, 117.3 (C), 114.6, 109.6, 106.8, 104.1 (CH), 40.5, 21.6, 21.3 (CH_3). **IR** (ATR, cm^{-1}): $\tilde{\nu}$ = 1613 (s), 1504 (m), 1440 (m), 1341 (m), 1055 (m), 892 (m), 814 (s), 800 (s), 781 (s), 587 (m), 495 (m). **MS** (EI, 70 eV): *m*/*z* (%) = 516 ($[M]^+$, 100), 501 (6), 500 (7), 486 (11), 472 (10), 471 (14), 400 (11), 258 (22), 257 (8). **HRMS** (EI): calculated for $C_{36}H_{28}N_4$ ($[M]^+$) 516.23085, found 516.23130.

11-Fluoro-5,13-di-*p*-tolylindolizino[6,5,4,3-*ija*]quinolino[2,3-*c*][1,6]naphthyridine (5d). According to general procedure B, the title compound **5d** was obtained as a red solid in 50% yield (87 mg). **Mp** 275–280 °C; R_f 0.37 (heptane/ethyl acetate 2 : 1). **^{1}H NMR** (300 MHz, $CDCl_3$) δ = 8.75 (s, 1H), 8.14–8.07 (m, 1H), 8.03 (s, 1H), 7.91 (d, ^3J = 4.2 Hz, 1H), 7.71–7.64 (m, 2H), 7.54–7.41 (m, 3H), 7.38–7.32 (m, 2H), 7.31–7.27 (m, 2H), 7.14 (s, 1H), 7.11–7.03 (m, 2H), 2.57 (s, 3H), 2.47 (s, 3H). **^{13}C NMR** (75 MHz, $CDCl_3$) δ = 160.0 (d, ^1J = 246.9 Hz, C), 145.7 (d, ^3J = 6.1 Hz, C), 145.1 (d, ^3J = 6.7 Hz, CH), 144.3 (d, ^4J = 2.6 Hz, C), 139.2, 138.8, 134.9, 134.7, 134.3, 134.0 (C), 131.1, 131.1, 131.0, 129.6 (CH), 129.2 (C), 128.5 (CH), 128.1 (C), 128.0 (CH), 126.0 (C), 120.7 (d, ^2J = 26.3 Hz, CH), 119.8, 117.7, 117.2 (C), 115.3, 111.1 (CH), 110.1 (d, ^2J = 23.8 Hz, CH), 107.1 (CH), 21.6, 21.3 (CH_3). **^{19}F NMR** (282 MHz, $CDCl_3$): δ = −113.0. **IR** (ATR, cm^{-1}): $\tilde{\nu}$ = 1735 (m), 1541 (m), 1457 (s), 1339 (m), 1230 (m), 1166 (s), 1041 (m), 822 (s), 800 (s), 734 (s), 600 (s), 490 (s). **MS** (EI, 70 eV): *m*/*z* (%) = 491 ($[M]^+$, 100), 490 (71), 489 (18), 487 (13), 476 (18), 475 (19), 245 (10), 238 (18), 237 (10). **HRMS** (EI): calculated for $C_{34}H_{22}N_3F$ ($[M]^+$) 491.17923, found 491.18050.

10,12-Difluor-5,13-di-*p*-tolylindolizino[6,5,4,3-*ija*]quinolino[2,3-*c*][1,6]naphthyridine (5e). According to general procedure B, the title compound **5e** was obtained as a red solid in 46% yield (78 mg). **Mp** 283–293 °C; R_f 0.30 (heptane/ethyl acetate 2 : 1). **^{1}H NMR** (300 MHz, $CDCl_3$) δ = 8.69 (s, 1H), 7.86 (d, ^3J = 4.2 Hz, 1H), 7.73 (s, 1H), 7.66–7.60 (m, 2H), 7.54–7.48 (m, 1H),7.47–7.41 (m, 2H), 7.36–7.30 (m, 4H), 7.12 (s, 1H), 7.02 (d, ^3J = 4.2 Hz, 1H), 6.83–6.73 (m, 1H), 2.56 (s, 3H), 2.47 (s, 3H). **^{13}C NMR** (126 MHz, $CDCl_3$) δ = 162.6 (dd, ^1J = 252.0 Hz, ^3J = 14.2 Hz, C), 159.8 (dd, ^1J = 264.4 Hz, ^3J = 14.4 Hz, C), 149.4 (dd, ^3J = 14.7 Hz, ^4J = 1.8 Hz, C), 146.0 (C), 145.3, 145.1 (CH), 144.7, 138.8 (C), 136.8 (d, ^4J = 4.4 Hz), 134.4, 134.0, 133.9 (C), 130.5 (CH), 129.7 (C), 129.6, 127.9 (CH), 127.3 (d, ^4J = 4.1 Hz, CH), 125.3, 119.6 (C), 117.9, 117.2 (C), 115.8 (CH), 114.7 (dd, ^3J = 6.1 Hz, ^3J = 2.0 Hz, C), 112.2 (CH), 108.6 (dd, ^2J = 20.1 Hz, ^4J = 4.9 Hz, CH), 107.3 (CH), 102.9 (pt, ^2J = 28.4 Hz, CH), 21.6, 21.3 (CH_3). **^{19}F NMR** (282 MHz, $CDCl_3$): δ = −106.5 (d, $^4J_{F,F}$ = 9.0 Hz), −99.9 (d, $^4J_{F,F}$ = 9.0 Hz). **IR** (ATR, cm^{-1}): $\tilde{\nu}$ = 1632 (s), 1543 (s), 1399 (m), 1339 (s), 1205 (s), 1135 (s), 1041 (m), 997 (m), 845 (s), 818 (s), 787 (s), 732 (s), 558 (s), 492 (m). **MS** (EI, 70 eV): *m*/*z* (%) = 509 ($[M]^+$, 100), 508 (84), 507 (12), 494 (21), 493 (29), 420 (6), 329 (7), 247 (13). **HRMS** (EI): calculated for $C_{34}H_{21}N_3F_2$ ($[M]^+$) 509.16981, found 509.17052.

9-Fluor-5,13-di-*p*-tolylindolizino[6,5,4,3-*ija*]quinolino[2,3-*c*][1,6]naphthyridine (5f). According to general procedure B, the title compound **5f** was obtained as an orange solid in 41% yield (67 mg). **Mp** 284–286 °C. R_f 0.28 (heptane/ethyl acetate 2 : 1); **^{1}H NMR** (500 MHz, $CDCl_3$) δ = 8.70 (s, 1H), 7.97 (d, ^3J = 4.2 Hz, 2H), 7.69–7.64 (m, 2H), 7.50 (d, ^3J = 7.7 Hz, 2H), 7.37–7.30 (m, 5H), 7.25–7.20 (m, 2H), 7.11 (s, 1H), 7.05 (d, ^3J = 4.1 Hz, 1H), 2.57 (s, 3H), 2.47 (s, 3H). **^{13}C NMR** (126 MHz, $CDCl_3$) δ = 157.3 (d, ^1J = 256.6 Hz, C), 146.3 (d, ^4J = 2.6 Hz, C), 145.1, 145.0 (CH), 144.8, 139.1, 138.8 (C), 138.5 (d, ^2J = 11.9 Hz, C), 135.1, 134.6, 134.2, 133.9 (C), 131.0, 129.6 (CH), 129.3 (C), 128.9 (d, ^5J = 1.7 Hz, C), 128.5, 128.0 (CH), 125.9 (C), 124.7 (d, ^3J = 7.8 Hz, CH), 122.7 (d, ^4J = 4.5 Hz, CH), 119.7, 117.9, 117.1 (C), 115.4 (CH), 113.9 (d, ^2J = 18.6 Hz, CH), 112.1, 107.3 (CH), 21.6, 21.3 (CH_3). **^{19}F NMR** (282 MHz, $CDCl_3$): δ = −126.0. **IR** (ATR, cm^{-1}): $\tilde{\nu}$ = 1537 (m), 1445 (m), 1339 (m), 1241 (m), 1119 (m), 1041 (m), 892 (m), 816 (s), 760 (s), 579 (m), 486 (m). **MS** (EI, 70 eV): *m*/*z* (%) = 491 ($[M]^+$, 100), 474 (9), 473 (45), 229 (1). **HRMS** (EI): calculated for $C_{34}H_{22}N_3F$ ($[M]^+$) 491.17923, found 491.17838.

5,15-Di-*p*-tolylbenzo[7,8]quinolino[2,3-*c*]indolizino[6,5,4,3-*ija*][1,6]naphthyridine (5h). According to general procedure B, the title compound **5h** was obtained as an orange solid in 41% yield (81 mg). **Mp** 334–339 °C; R_f 0.42 (heptane/ethyl acetate 2 : 1). **^{1}H NMR** (300 MHz, $CDCl_3$) δ = 9.47–9.43 (m, 1H), 8.65 (s, 1H), 7.99 (d, ^3J = 4.1 Hz, 1H), 7.90 (s, 1H), 7.76–7.70 (m, 1H), 7.70–7.60 (m, 4H), 7.51–7.41 (m, 3H), 7.37–7.27 (m, 4H),

7.25–7.21 (m, 1H), 7.08 (d, ^3J = 4.1 Hz, 1H), 7.07 (s, 1H), 2.58 (s, 3H), 2.47 (s, 3H). **^{13}C NMR** (75 MHz, $CDCl_3$) δ = 146.4, 145.8 (C), 144.1, 143.9 (CH), 143.2, 138.7, 138.6, 135.6, 134.8, 134.1, 134.0, 133.6 (C), 130.8 (CH), 130.7 (C), 129.5, 128.7 (CH), 128.6 (C), 128.0, 127.4, 126.8 (CH), 126.6 (C), 126.5, 125.2 (CH), 124.7 (C), 123.6 (CH), 119.9, 117.5, 117.1 (C), 115.1, 110.4, 106.9 (CH), 21.6, 21.3 (CH_3). **IR** (ATR, cm^{-1}): $\tilde{\nu}$ = 1533 (m), 1459 (m), 1356 (m), 1179 (m), 1111 (m), 1039 (m), 882 (m), 820 (s), 795 (s), 762 (s), 719 (m), 488 (m). **MS** (EI, 70 eV): *m*/*z* (%) = 523 ([M]$^+$, 100), 522 (44), 521 (15), 516 (10), 508 (12), 507 (14), 262 (14), 261 (13), 254 (19), 253 (11). **HRMS** (EI): calculated for $C_{38}H_{25}N_3$ ([M]$^+$) 523.20430, found 523.20496.

5,13-Diphenylindolizino[6,5,4,3-*ija*]quinolino[2,3-*c*][1,6]naphthyridine (5i). According to modified general procedure B ((1) *t* = 4 h; (2) *t* = 24 h), the title compound **5i** was obtained as an orange solid in 32% yield (57 mg); **Mp** 297–299 °C. R_f 0.43 (dcm/ethyl acetate 15 : 1). **^{1}H NMR** (300 MHz, $CDCl_3$) δ = 8.73 (s, 1H), 8.16–8.10 (m, 1H), 7.96–7.92 (m, 2H), 7.81–7.75 (m, 2H), 7.73–7.65 (m, 4H), 7.59–7.47 (m, 3H), 7.47–7.39 (m, 3H), 7.39–7.31 (m, 1H), 7.16 (s, 1H), 7.08 (d, ^3J = 4.2 Hz, 1H). **^{13}C NMR** (75 MHz, $CDCl_3$) δ = 148.1, 146.1 (C), 145.1, 145.0 (CH), 144.7, 138.3, 137.6, 134.3, 134.0 (C), 130.3, 130.2 (CH), 129.1 (C), 129.1, 128.9, 128.8, 128.7, 128.6, 128.1 (CH), 127.1 (C), 126.9 (CH), 126.2 (C), 125.8 (CH), 119.7, 117.4, 117.0 (C), 115.7, 111.3, 107.1 (CH). **IR** (ATR, cm^{-1}): $\tilde{\nu}$ = 1541 (m), 1337 (m), 1311 (m), 1183 (m), 1105 (m), 1034 (m), 888 (m), 849 (m), 808 (m), 760 (s), 701 (s), 649 (m), 474 (m). **MS** (EI, 70 eV): *m*/*z* (%) = 445 ([M]$^+$, 100), 444 (80), 443 (43), 442 (20), 441 (15), 418 (8), 367 (8), 223 (10), 222 (22), 221 (14), 207 (7). **HRMS** (ESI-TOF): calculated for $C_{32}H_{20}N_3$ ([M + H]$^+$) 446.1657, found 446.1656.

11-Fluor-5,13-diphenylindolizino[6,5,4,3-*ija*]quinolino[2,3-*c*][1,6]naphthyridine (5j). According to modified general procedure B ((2) 24 h reaction time) the title compound **5j** was obtained as an orange solid in 35% yield (56 mg); **Mp** 275–283 °C. R_f 0.33 (dcm/ethyl acetate 15 : 1). **^{1}H NMR** (300 MHz, $CDCl_3$) δ = 8.77 (s, 1H), 8.13 (dd, ^3J = 9.2 Hz, ^4J = 5.5 Hz, 1H), 7.94 (d, ^3J = 4.2 Hz, 1H), 7.82–7.76 (m, 2H), 7.73–7.66 (m, 3H), 7.59–7.47 (m, 4H), 7.46–7.39 (m, 3H), 7.18 (s, 1H), 7.10 (d, ^3J = 4.2 Hz, 1H), 7.07–7.01 (m, 1H). **^{13}C NMR** (75 MHz, $CDCl_3$/TFA) δ = 162.1 (d, ^1J = 257.8 Hz, C), 158.2 (d, ^4J = 5.8 Hz, C), 139.7 (C), 138.5 (CH), 137.6 (d, ^4J = 2.0 Hz, C), 137.1, 135.2, 134.9 (C), 134.8 (CH), 134.1, 133.5 (C), 132.4, 131.1, 129.8 (CH), 128.7 (d, ^3J = 8.7 Hz, C), 128.5 (d, ^2J = 25.6 Hz, CH), 128.3, 126.7 (CH), 122.5 (C), 122.4 (d, ^3J = 9.3 Hz, CH), 120.5, 118.6 (CH), 118.6, 118.3, 116.3 (C), 114.6 (CH), 113.1 (d, ^2J = 25.1 Hz, CH). **^{19}F NMR** (282 MHz, $CDCl_3$): δ = −112.8. **IR** (ATR, cm^{-1}): $\tilde{\nu}$ = 1539 (m), 1459 (m), 1434 (m), 1356 (m), 1232 (m), 1175 (m), 1107 (m), 828 (m), 800 (m), 725 (m), 696 (s), 604 (m), 565 (m), 474 (m). **MS** (EI, 70 eV): *m*/*z* (%) = 463 ([M]$^+$, 100), 462 (78), 461 (43), 460 (13), 459 (13), 436 (5), 385 (9), 232 (11), 231 (26), 230 (12), 217 (5). **HRMS** (ESI-TOF): calculated for $C_{32}H_{19}FN_3$ ([M + H]$^+$) 464.1563, found 464.1554.

4,4′-(11-Fluorindolizino[6,5,4,3-*ija*]quinolino[2,3-*c*][1,6]naphthyridine-5,13-diyl)bis(*N*,*N*-dimethylaniline) (5k). According to modified general procedure B ((2) 8 h reaction time) the title compound **5k** was obtained as an orange solid in 39% yield (95 mg); **mp** 301–305 °C. R_f 0.34 (dcm/ethyl acetate 3 : 1). **^{1}H NMR** (500 MHz, $CDCl_3$) δ = 8.76 (s, 1H), 8.21 (s, 1H), 8.14 (dd, ^3J = 9.2 Hz, ^4J = 5.5 Hz, 1H), 7.95 (d, ^3J = 4.1 Hz, 1H), 7.73–7.68 (m, 2H), 7.51–7.46 (m, 1H), 7.27–7.23 (m, 1H), 7.22–7.19 (m, 2H), 7.17 (d, ^3J = 4.1 Hz, 1H), 7.14 (s, 1H), 6.99–6.95 (m, 2H), 6.89–6.86 (m, 2H), 3.12 (s, 6H), 3.06 (s, 6H). **^{13}C NMR** (126 MHz, $CDCl_3$) δ = 160.0 (d, ^1J = 246.4 Hz, C), 150.8, 150.7 (C), 146.6 (d, ^4J = 6.0 Hz, C), 145.3 (C), 145.1, 144.7 (CH), 144.6 (d, ^4J = 2.4 Hz, C), 134.4, 133.9 (C), 130.9 (d, ^3J = 8.9 Hz, CH), 129.5 (C), 129.4, 128.9 (CH), 128.8 (d, ^3J = 9.2 Hz, C), 126.0, 125.4, 124.8 (C), 120.5 (d, ^2J = 26.5 Hz, CH), 120.1, 118.3, 117.5 (C), 114.0, 113.5, 112.3, 110.9 (CH), 110.4 (d, ^2J = 23.5 Hz, CH), 107.2 (CH), 40.4, 40.3 (CH_3). **^{19}F NMR** (282 MHz, $CDCl_3$): δ = −113.6. **IR** (ATR, cm^{-1}): $\tilde{\nu}$ = 1607 (s), 1523 (s), 1508 (s), 1428 (m), 1360 (s), 1335 (s), 1230 (m), 1191 (s), 1164 (s), 816 (s), 804 (s), 793 (s), 729 (m), 600 (m). **MS** (EI, 70 eV): *m*/*z* (%) = 550 ([M]$^+$, 62), 549 (100), 548 (19), 535 (15), 534 (32), 520 (15), 518 (11), 479 (19), 274 (18), 252 (12). **HRMS** (EI): calculated for $C_{36}H_{28}FN_5$ ([M]$^+$) 550.2407, found 550.2407.

11-Fluor-5,13-bis(4-fluorphenyl)indolizino[6,5,4,3-*ija*]quinolino[2,3-*c*][1,6]naphthyridine (5l). According to modified general procedure B ((2) 24 h reaction time) the title compound **5l** was obtained as a yellow solid in 65% yield (119 mg); **mp** 318–323 °C. R_f 0.50 (dcm/ethyl acetate 15 : 1). **^{1}H NMR** (300 MHz, $CDCl_3$) δ = 9.40 (s, 1H), 8.77 (d, ^3J = 4.7 Hz, 1H), 8.51 (dd, ^3J = 9.4 Hz, ^4J = 4.5 Hz, 1H), 8.05–7.97 (m, 2H), 7.84 (s, 1H), 7.82–7.75 (m, 2H), 7.71 (d, ^3J = 4.7 Hz, 1H), 7.64–7.56 (m, 2H), 7.50–7.43 (m, 2H), 7.40–7.31 (m, 3H). **^{13}C NMR** (75 MHz, $CDCl_3$) δ = 164.7 (d, ^1J = 256.9 Hz, C), 164.3 (d, ^1J = 252.6 Hz, C), 162.0 (d, ^1J = 258.1 Hz, C), 156.7 (d, ^4J = 5.8 Hz, C), 138.8 (CH), 138.2 (C), 137.4 (d, ^4J = 2.0 Hz, C), 137.0, 135.2 (C), 134.7 (CH), 134.4 (C), 130.2 (d, ^3J = 8.8 Hz, CH), 130.2 (C), 129.2 (d, ^3J = 8.3 Hz. CH), 129.1 (d, ^4J = 4.2 Hz, C), 128.7 (d, ^3J = 9.8 Hz, C), 128.4 (d, ^2J = 26.7 Hz, CH), 122.7 (d, ^3J = 9.2 Hz, CH), 122.3 (C), 120.8 (CH), 119.9 (d, ^2J = 22.3 Hz, CH), 118.6 (CH), 118.3, 118.3 (C), 117.0 (d, ^2J = 22.1 Hz, CH), 116.5 (C), 114.3 (CH), 112.7 (d, ^2J = 24.9 Hz, CH). **^{19}F NMR** (282 MHz, $CDCl_3$): δ = −102.9, −105.2, −108.5. **IR** (ATR, cm^{-1}): $\tilde{\nu}$ = 1502 (s), 1461 (m), 1339 (m), 1224 (s), 1158 (m), 828 (s), 802 (s), 779 (m), 725 (m), 587 (m), 560 (s), 540 (s), 505 (s). **MS** (EI, 70 eV): *m*/*z* (%) = 499 ([M]$^+$, 100), 498 (61), 497 (31), 459 (43), 458 (86), 457 (13), 250 (44), 249 (20), 248 (17), 239 (18), 229 (24). **HRMS** (ESI-TOF): calculated for $C_{32}H_{17}F_3N_3$ ([M + H]$^+$) 500.1375, found 500.1377.

Conflicts of interest

There are no conflicts to declare.

Acknowledgements

Financial support by the State of Mecklenburg-Vorpommern is gratefully acknowledged.

References

1 H. Balli and M. Zeller, Neue Heteroarene: Synthese und spektrale Daten von Indolizino[6,5,4,3-aij]chinolin («Ullazin») und einigen Derivaten, *Helv. Chim. Acta*, 1983, **66**, 2135–2139.

2 J. H. Delcamp, A. Yella, T. W. Holcombe, M. K. Nazeeruddin and M. Grätzel, The molecular engineering of organic sensitizers for solar-cell applications, *Angew. Chem., Int. Ed.*, 2013, **52**, 376–380.

3 (*a*) J. Feng, Y. Jiao, W. Ma, M. K. Nazeeruddin, M. Grätzel and S. Meng, First Principles Design of Dye Molecules with Ullazine Donor for Dye Sensitized Solar Cells, *J. Phys. Chem. C*, 2013, **117**, 3772–3778; (*b*) Q. Le Bao, S. Thogiti, G. Koyyada and J. H. Kim, Synthesis and photovoltaic performance of novel ullazine-based organic dyes for dye-sensitized solar cells, *Jpn. J. Appl. Phys.*, 2019, **58**, 12011; (*c*) C. Cebrián, Ullazine-based materials: towards novel opportunities in organic electronics, *J. Mater. Chem. C*, 2018, **6**, 11943–11950.

4 (*a*) Q. Ge, B. Li and B. Wang, Synthesis of substituted benzoijimidazo-2,1,5-dequinolizine by rhodium(III)-catalyzed multiple C-H activation and annulations, *Org. Biomol. Chem.*, 2016, **14**, 1814–1821; (*b*) Y. Guo, L. Zhang, C. Li, M. Jin, Y. Zhang, J. Ye, Y. Chen, X. Wu and X. Liu, BN/BO-Ullazines and Bis-BO-Ullazines: Effect of BO Doping on Aromaticity and Optoelectronic Properties, *J. Org. Chem.*, 2021, **86**, 12507–12516; (*c*) C. Li, Y. Liu, Z. Sun, J. Zhang, M. Liu, C. Zhang, Q. Zhang, H. Wang and X. Liu, Synthesis, Characterization, and Properties of Bis-BN Ullazines, *Org. Lett.*, 2018, **20**, 2806–2810; (*d*) P. Pierrat, S. Hesse, C. Cebrián and P. C. Gros, Controlling charge-transfer properties through a microwave-assisted mono- or bis-annulation of dialkynyl-N-(het)arylpyrroles, *Org. Biomol. Chem.*, 2017, **15**, 8568–8575; (*e*) S. Janke, S. Boldt, P. Nakielski, A. Villinger, P. Ehlers and P. Langer, Synthesis and Properties of 5-Azaullazines, *J. Org. Chem.*, 2023, **88**, 10470–10482.

5 S. Boldt, S. Parpart, A. Villinger, P. Ehlers and P. Langer, Synthesis and Properties of Aza-ullazines, *Angew. Chem., Int. Ed.*, 2017, **56**, 4575–4578.

6 (*a*) G. Zhang, P. Gautam and J. M. W. Chan, Symmetrical and unsymmetrical fluorine-rich ullazines via controlled cycloaromatizations, *Org. Chem. Front.*, 2020, **7**, 787–795; (*b*) H. Qiao, Y. Deng, R. Peng, G. Wang, J. Yuan and S. Tan, Effect of π-spacers and anchoring groups on the photovoltaic performances of ullazine-based dyes, *RSC Adv.*, 2016, **6**, 70046–70055; (*c*) D. Wan, X. Li, R. Jiang, B. Feng, J. Lan, R. Wang and J. You, Palladium-Catalyzed Annulation of Internal Alkynes: Direct Access to π-Conjugated Ullazines, *Org. Lett.*, 2016, **18**, 2876–2879; (*d*) S. Mathew, N. A. Astani, B. F. E. Curchod, J. H. Delcamp, M. Marszalek, J. Frey, U. Rothlisberger, M. K. Nazeeruddin and M. Grätzel, Synthesis, characterization and ab initio investigation of a panchromatic ullazine–porphyrin photosensitizer for dye-sensitized solar cells, *J. Mater. Chem. A*, 2016, **4**, 2332–2339; (*e*) K. Kanno, Y. Liu, A. Iesato, K. Nakajima and T. Takahashi, Chromium-mediated synthesis of polycyclic aromatic compounds from halobiaryls, *Org. Lett.*, 2005, **7**, 5453–5456.

7 (*a*) E. S. Larsen, G. Ahumada, P. R. Sultane and C. W. Bielawski, Stereoelectronically-induced allosteric binding: shape complementarity promotes positive cooperativity in fullerene/buckybowl complexes, *Chem. Commun.*, 2022, **58**, 6498–6501; (*b*) S. Li, Y. Sun, X. Li, O. Smaga, S. Koniarz, M. Stępień and P. J. Chmielewski, 1,3-Dipolar cycloaddition of polycyclic azomethine ylide to norcorroles: towards dibenzoullazine-fused derivatives, *Chem. Commun.*, 2022, **58**, 6510–6513.

8 J. Zhou, W. Yang, B. Wang and H. Ren, Friedel-Crafts arylation for the formation of $C(sp^2)$–$C(sp^2)$ bonds: a route to unsymmetrical and functionalized polycyclic aromatic hydrocarbons from aryl triazenes, *Angew. Chem., Int. Ed.*, 2012, **51**, 12293–12297.

9 D. Wang, Y. Liu, L. Wang, H. Cheng, Y. Zhang and G. Gao, Synthesis of π-extended dibenzo[d,k]ullazines by a palladium-catalyzed double annulation using arynes, *Chin. Chem. Lett.*, 2021, **32**, 1407–1410.

10 R. Berger, M. Wagner, X. Feng and K. Müllen, Polycyclic aromatic azomethine ylides: a unique entry to extended polycyclic heteroaromatics, *Chem. Sci.*, 2015, **6**, 436–441.

11 S. Ito, Y. Tokimaru and K. Nozaki, Isoquinolino[4,3,2-de]phenanthridine: synthesis and its use in 1,3-dipolar cycloadditions to form nitrogen-containing polyaromatic hydrocarbons, *Chem. Commun.*, 2015, **51**, 221–224.

12 M. Richter, M. Borkowski, Y. Fu, E. Dmitrieva, A. Popov, J. Ma, T. Marszalek, W. Pisula and X. Feng, Synthesis and Self-Assembly Behavior of Double Ullazine-Based Polycyclic Aromatic Hydrocarbons, *Org. Mater.*, 2021, **03**, 198–203.

13 S. Ito, Y. Tokimaru and K. Nozaki, Benzene-Fused Azacorannulene Bearing an Internal Nitrogen Atom, *Angew. Chem., Int. Ed.*, 2015, **54**, 7256–7260.

14 J. Hager, S. Kang, P. J. Chmielewski, T. Lis, D. Kim and M. Stępień, Acenaphthylene-fused ullazines: fluorescent π-extended monopyrroles with tunable electronic gaps, *Org. Chem. Front.*, 2022, **9**, 3179–3185.

15 D. Miao, C. Aumaitre and J.-F. Morin, Photochemical synthesis of π-extended ullazine derivatives as new electron donors for efficient conjugated D–A polymers, *J. Mater. Chem. C*, 2019, **7**, 3015–3024.

16 L. S. Povarov, α,β-Unsaturated Ethers and their analogues in reactions of diene synthesis, *Russ. Chem. Rev.*, 1967, **36**, 656–670.

17 (*a*) J. Clerigué, M. T. Ramos and J. C. Menéndez, Enantioselective catalytic Povarov reactions, *Org. Biomol. Chem.*, 2022, **20**, 1550–1581; (*b*) E. A. Kuznetsova, A. V. Smolobochkin, T. S. Rizbayeva, A. S. Gazizov, J. K. Voronina, O. A. Lodochnikova, D. P. Gerasimova, A. B. Dobrynin, V. V. Syakaev, D. N. Shurpik, I. I. Stoikov, A. R. Burilov, M. A. Pudovik and O. G. Sinyashin, Diastereoselective intramolecular cyclization/Povarov reaction cascade for the one-pot synthesis of polycyclic quinolines, *Org. Biomol. Chem.*, 2022, **20**, 5515–5519.

18 B. Chakraborty, A. Kar, R. Chanda and U. Jana, Application of the Povarov Reaction in Biaryls under Iron Catalysis for the General Synthesis of Dibenzo[a,c]Acridines, *J. Org. Chem.*, 2020, **85**, 9281–9289.

19 F. Spruner von Mertz, R. Molenda, S. Boldt, A. Villinger, P. Ehlers and P. Langer, Synthesis and Properties of Diphenylbenzo[j]naphtho[2,1,8-def][2,7]phenanthrolines, *Chem. – Eur. J.*, 2023, **29**, e202204011.

20 R. Molenda, S. Boldt, A. Villinger, P. Ehlers and P. Langer, Synthesis of 2-Azapyrenes and Their Photophysical and Electrochemical Properties, *J. Org. Chem.*, 2020, **85**, 12823–12842.

21 S. Parpart, S. Boldt, P. Ehlers and P. Langer, Synthesis of Unsymmetrical Aza-Ullazines by Intramolecular Alkynyl-Carbonyl Metathesis, *Org. Lett.*, 2018, **20**, 122–125.

22 A. M. Brouwer, Standards for photoluminescence quantum yield measurements in solution (IUPAC Technical Report), *Pure Appl. Chem.*, 2011, **83**, 2213–2228.

23 M. J. Frisch, G. W. Trucks, H. B. Schlegel, G. E. Scuseria, M. A. Robb, J. R. Cheeseman, G. Scalmani, V. Barone, G. A. Petersson, H. Nakatsuji, X. Li, M. Caricato, A. V. Marenich, J. Bloino, B. G. Janesko, R. Gomperts, B. Mennucci, H. P. Hratchian, J. V. Ortiz, A. F. Izmaylov, J. L. Sonnenberg, J. Williams, F. Ding, F. Lipparini, F. Egidi, J. Goings, B. Peng, A. Petrone, T. Henderson, D. Ranasinghe, V. G. Zakrzewski, J. Gao, N. Rega, G. Zheng, W. Liang, M. Hada, M. Ehara, K. Toyota, R. Fukuda, J. Hasegawa, M. Ishida, T. Nakajima, Y. Honda, O. Kitao, H. Nakai, T. Vreven, K. Throssell, J. A. Montgomery Jr., J. E. Peralta, F. Ogliaro, M. J. Bearpark, J. J. Heyd, E. N. Brothers, K. N. Kudin, V. N. Staroverov, T. A. Keith, R. Kobayashi, J. Normand, K. Raghavachari, A. P. Rendell, J. C. Burant, S. S. Iyengar, J. Tomasi, M. Cossi, J. M. Millam, M. Klene, C. Adamo, R. Cammi, J. W. Ochterski, R. L. Martin, K. Morokuma, O. Farkas, J. B. Foresman and D. J. Fox, *Gaussian 16 Rev. C.01*, Wallingford, CT, 2016.

24 (*a*) D. Bischof, M. W. Tripp, P. E. Hofmann, C.-H. Ip, S. I. Ivlev, M. Gerhard, U. Koert and G. Witte, Regioselective Fluorination of Acenes: Tailoring of Molecular Electronic Levels and Solid-State Properties, *Chem. – Eur. J.*, 2022, **28**, e202103653; (*b*) J. Holec, B. Cogliati, J. Lawrence, A. Berdonces-Layunta, P. Herrero, Y. Nagata, M. Banasiewicz, B. Kozankiewicz, M. Corso, D. G. de Oteyza, A. Jancarik and A. Gourdon, A Large Starphene Comprising Pentacene Branches, *Angew. Chem., Int. Ed.*, 2021, **60**, 7752–7758; (*c*) O. Francesconi, M. Martinucci, L. Badii, C. Nativi and S. Roelens, A Biomimetic Synthetic Receptor Selectively Recognising Fucose in Water, *Chem. – Eur. J.*, 2018, **24**, 6828–6836.

25 M.-L. Tan, S. Tong, S.-K. Hou, J. You and M.-X. Wang, Copper-Catalyzed N,N-Diarylation, of Amides for the Construction of 9,10-Dihydroacridine Structure and Applications in the Synthesis of Diverse Nitrogen-Embedded Polyacenes, *Org. Lett.*, 2020, **22**, 5417–5422.

26 J. Liu, C. Chen and C. Fang, Polarity-Dependent Twisted Intramolecular Charge Transfer in Diethylamino Coumarin Revealed by Ultrafast Spectroscopy, *Chemosensors*, 2022, **10**, 411.

27 P. v. R. Schleyer, C. Maerker, A. Dransfeld, H. Jiao and N. J. R. van Eikema Hommes, Nucleus-Independent Chemical Shifts: A Simple and Efficient Aromaticity Probe, *J. Am. Chem. Soc.*, 1996, **118**, 6317–6318.

28 E. Paenurk and R. Gershoni-Poranne, Simple and efficient visualization of aromaticity: bond currents calculated from NICS values, *Phys. Chem. Chem. Phys.*, 2022, **24**, 8631–8644.

4.3 Divergent Synthesis of 5,7-Diazaullazines Derivatives through a Combination of Cycloisomerization with Povarov or Alkyne–Carbonyl Metathesis

Jonas Polkaehn, Peter Ehlers, Alexander Villinger, Peter Langer

Molecules **2024***,* 29, 2159.

DOI: 10.3390/molecules29092159

Contribution to this work: **85%**

I performed the synthetic work, measurements, computational calculations and wrote the manuscript. Alexander Villiger contributed with the measurement and evaluation of the single crystal X-ray experiment. Peter Ehlers and Peter Langer supervised the entire project and performed revision and proof reading of the manuscript.

Reproduced from J. Polkaehn, P. Ehlers, A. Villinger, P. Langer, *Molecules* **2024***,* 29, 2159. DOI: 10.3390/molecules29092159.

molecules

MDPI

Article

Divergent Synthesis of 5,7-Diazaullazines Derivatives through a Combination of Cycloisomerization with Povarov or Alkyne–Carbonyl Metathesis

Jonas Polkaehn [1], Peter Ehlers [1,*], Alexander Villinger [1] and Peter Langer [1,2,*]

[1] Institute of Chemistry, University Rostock, Albert-Einstein-Str. 3a, 18059 Rostock, Germany
[2] Leibniz Institute for Catalysis (LIKAT), University Rostock, Albert-Einstein-Str. 29a, 18059 Rostock, Germany
* Correspondence: peter.ehlers@uni-rostock.de (P.E.); peter.langer@uni-rostock.de (P.L.); Tel.: +49-381-498-6427 (P.E.); +49-381-498-6410 (P.L.)

Abstract: Ullazines and their π-expanded derivatives have gained much attention as active components in various applications, such as in organic photovoltaic cells or as photosensitizers for CO_2 photoreduction. Here, we report the divergent synthesis of functionalized diazaullazines by means of two different domino-reactions consisting of either a Povarov/cycloisomerization or alkyne–carbonyl metathesis/cycloisomerization protocol. The corresponding quinolino-diazaullazine and benzoyl-diazaullazine derivatives were obtained in moderate to good yields. Their optical and electronic properties were studied and compared to related, literature-known compounds to obtain insights into the impact of nitrogen doping and π-expansion.

Keywords: alkyne-carbonyl-metathesis; cycloisomerisation; polycyclic heteroaromatic hydrocarbons; Povarov reaction; ullazines

Citation: Polkaehn, J.; Ehlers, P.; Villinger, A.; Langer, P. Divergent Synthesis of 5,7-Diazaullazines Derivatives through a Combination of Cycloisomerization with Povarov or Alkyne–Carbonyl Metathesis. *Molecules* **2024**, *29*, 2159. https://doi.org/10.3390/molecules29092159

Academic Editor: Roman Dembinski

Received: 19 February 2024
Revised: 23 April 2024
Accepted: 30 April 2024
Published: 6 May 2024

1. Introduction

Ullazine contains 16-π-electrons, is isoelectronic to pyrene, and is a representative of polycyclic heteroaromatic hydrocarbons (PAHs) [1]. It has been known since its first synthesis in 1983 [2], but has gained much interest for applications in organic electronics during the last decade [1,3–7] since Grätzel et al. disclosed its promising application in dye-sensitized solar cells in 2013 [1]. The aromatic 14-π-electron resonance structure is a key factor, consisting of an electron-accepting iminium center surrounded by an electron-donating annulene. Hence, in the following years, several approaches, such as substitution, π-extension or heteroatom doping, were employed to modify the properties of various applications. Substitutions on the ullazine core are known in each position (1–9) of the ullazine core (Figure 1) [1,2,8–12]. Positions 4, 5, and 7 can be addressed by electrophilic substitution, whereas position 5 is the most active of these three [1,13,14]. Functionalization on the other positions can be achieved through the employment of suitable precursors during ullazine formation, for example, by the double benzannulation of *N*-phenylpyrroles [1,2,8,9]. The expansion of the π-systems is mainly executed by 1,3-dipolar cycloaddition with azomethine ylides, which leads to symmetrical dibenzoullazines with functionalization of positions 1 and 2 [15–20]. Fused dithieno- and dipyridoullazines are obtained by the photochemical cyclization of 3,9-diarylullazines [21]. In addition to the extension of the π-system and variations in the substitution pattern, doping of the scaffold by heteroatoms has been used to alter the inherent properties of ullazines. Several examples of N-, O-, and B-doped ullazines are known in the literature [9,22–29].

Recently, we studied the synthesis of 5,7-diazaullazines [29]. The incorporation of a pyrimidine ring into the ullazine scaffold leads to strongly altered optical properties through the stabilization of the HOMO and LUMO energies with strong intramolecular charge transfer (ICT) properties and improved quantum yields. Moreover, we reported

the synthesis of quinolino-azaullazines, which show bathochromically shifted absorption and emission features compared to their azaullazine subunit or related dibenzoullazines [30]. Hence, we were interested in combining these two approaches, π-expansion and increased N-doping of the ullazine structure, to study the impact of these structural modifications on the photophysical properties. Retrosynthetic analysis revealed that respective quinolino-diazaullazines are accessible by a combination of the Povarov reaction and cycloisomerization, similarly to the synthesis of quinolino-azapyrenes and quinolino-azaullazines [30,31]. Interestingly, the same starting material might also undergo alkyne–carbonyl metathesis (ACM) followed by cycloisomerization for the construction of novel benzoyl-diazaullazine derivatives. Hence, we report a divergent synthesis of quinolino-diazaullazines and benzoyl-diazaullazine from the same precursor through careful choice of the employed reaction conditions. During our studies, the group of Chen reported a related approach for the selective synthesis of pharmaceutically relevant naphthyridinones and quinolinones via either Povarov or ACM reaction, respectively, starting from formyl-phenylpropialamide (Scheme 1) [32].

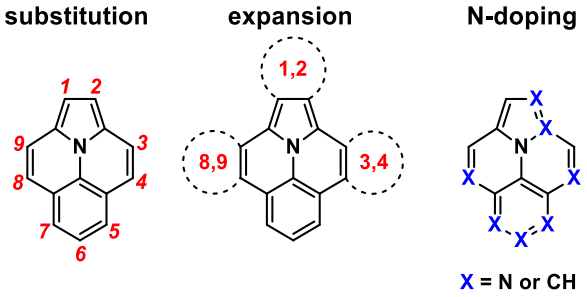

Figure 1. Potential modifications to ullazine.

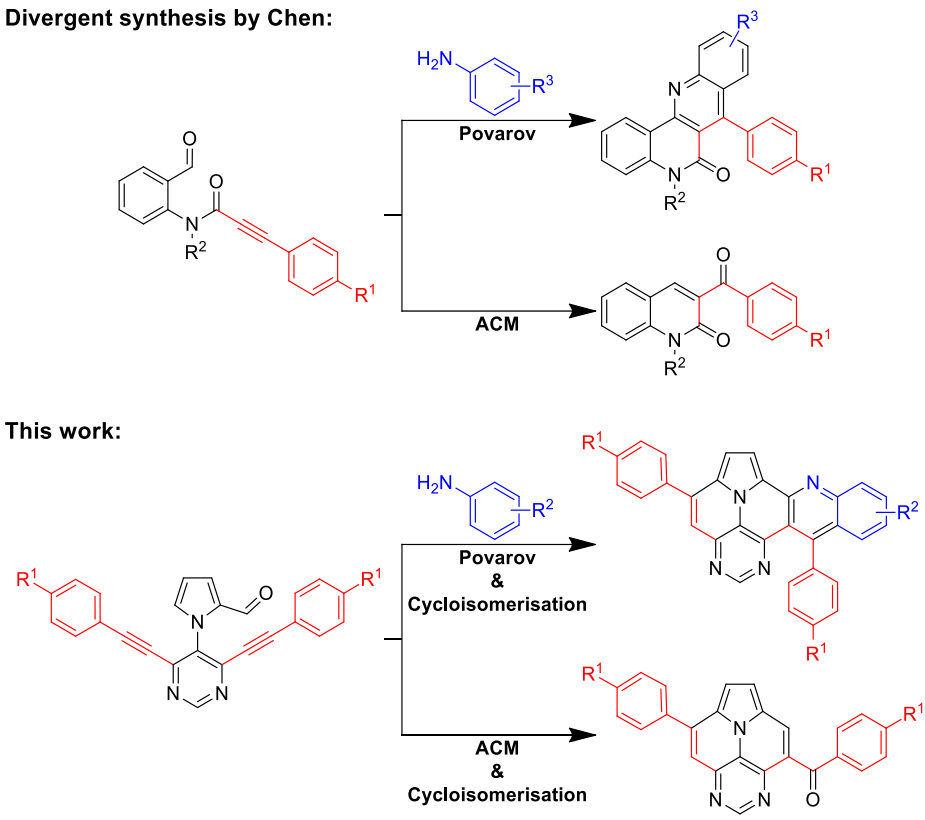

Scheme 1. Divergent synthesis of Chen and our approach with the synthesis quinolino-diazaullazines and benzoyl-diazaullazines.

1.1. Synthesis

Our synthetic methodology started with the synthesis of an eligible pyrrolopyrimidine **4**, which can undergo ACM and Povorav reactions followed by cycloisomerization. Starting from commercially available 4,6-dichloropyrimidin-5-amine (**1**), the Clausson–Kaas reaction gave pyrrolopyrimidine **2** in excellent yield. Subsequent Vilsmeier–Haak reaction proceeded selectively on the pyrrole ring, resulting in a mixture of the 2- and 3-formylpyrrole derivatives from which the respective precursor **3**, with aldehyde function in position 2, was separated in 41% yield. Finally, the desired precursors **4a–f** were obtained by two-fold Sonogashira reaction in good yield (Scheme 2) [29,30].

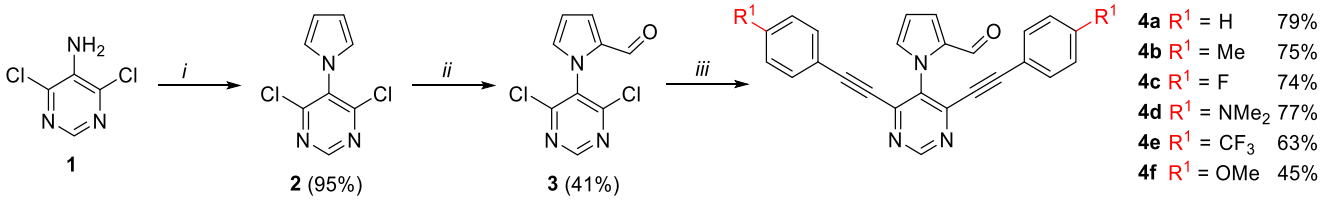

Scheme 2. Synthesis of ACM and Povarov precursors **4a–f**; *i*: 2,5-dimethoxytetrahydrofuran, acetic acid, 1,2-dichloroethane, reflux, 3 h. *ii*: $POCl_3$ (2.0 eq.), DMF, 100 °C, 3 h. *iii*: alkyne (3 eq.), $PdCl_2(CH_3CN)_2$ (0.06 eq.), XPhos (0.12 eq.), CuI (0.04 eq.), HN^iPr_2, 1,4-dioxane, 90 °C, 24 h.

Starting material **4a** was chosen as the model substrate to study the divergent synthesis of quinolino-diazapyrene **5a** and benzoyl-diazaullazine **6a**. At first, we focused on the optimization of the Povarov reaction with subsequent cycloisomerization in a one-pot protocol, as both reactions are typically mediated by strong acids. In particular, product **5a** derives from three individual reaction steps: Schiff-base formation, Povarov reaction and cycloisomerization.

The synthesis of **5a** is initially based on the addition of aniline and $FeCl_3$ [33]. $FeCl_3$ has proven to be a powerful catalyst for the synthesis of PAHs via Povarov reaction [30–33]. After the Povarov reaction has ceased, *p*-TsOH, as a Brønsted acid, is added to the reaction mixture, which initiates the final ring closure through the activation of the second triple bond. As a starting point, we tested the reaction conditions that were recently employed for the synthesis of related quinolino-azaullazine derivatives, but only traces of the desired product **5a** were obtained (Table 1) [30]. Since starting material **4a** was still detected by TLC control, we decided to focus on the first reaction step—the Povarov reaction. The elevation of the reaction temperature and the amount of $FeCl_3$ led to an improvement of 38% in the yield of final product **5a** using 1 eq. of $FeCl_3$ at 140 °C. Interestingly, the formation of **5a** was detected by the TLC control before the addition of Brønsted acid. However, **5a** was isolated in a reduced 21% yield even when access of $FeCl_3$ was employed. Hence, a strong Brønsted acid is required to drive the reaction to completion. Next, we turned our attention to the final cyclization step. The application of *p*-TsOH·H_2O proved to be superior to the employment of methanesulfonic acid (MsOH). Different amounts of *p*-TsOH·H_2O and an increased reaction time improved the overall product yield to 45%, which corresponds to a theoretical yield of more than 75% for each reaction step in this one-pot process.

In the following, we analyzed the synthesis of **6a**. It is known from the literature that both cycloisomerization and the ACM reaction are promoted efficiently by Brønsted acids (Table 2) [24,34]. Hence, we first tested similar conditions as for the Povarov but without the addition of aniline [32]. To our delight, product **6a** was isolated in 59% after 16 h. Reducing the amount of *p*-TsOH to 20 eq. and lowering the reaction temperature to 120 °C gave an improved yield of 68%, while the use of less acid or the employment of MsOH led to inferior results. Finally, we reduced the reaction time to 6 h without compromising the isolated yield.

Table 1. Optimization of one-pot reaction for the synthesis of **5a** consisting of the Schiff base formation, Povarov reaction and cycloisomerization.

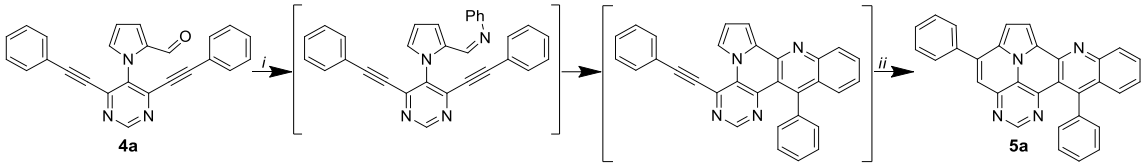

Entry	eq. $FeCl_3$	Acid (eq.)	Solvent	*T* [°C]	t_1 [h]	t_2 [h]	Yield [a] [%]
1	0.1	*p*-TsOH·H_2O (30)	toluene	100	3	2	traces
2	0.3	*p*-TsOH·H_2O (30)	xylene	140	3	2	29
3	0.6	*p*-TsOH·H_2O (30)	xylene	140	3	2	34
4	1	*p*-TsOH·H_2O (30)	xylene	140	3	2	38
5	4	-	xylene	140	3	-	21
6	1	*p*-TsOH·H_2O (10)	xylene	140	3	2	23
7	1	*p*-TsOH·H_2O (20)	xylene	140	3	2	27
8	**1**	***p*-TsOH·H_2O (30)**	**xylene**	**140**	**3**	**6**	**45**
9	1	*p*-TsOH·H_2O (30)	xylene	140	3	16	45
10	1	*p*-TsOH·H_2O (40)	xylene	140	3	6	43
11	1	MsOH (30)	xylene	140	3	6	40

i: aniline (1.2 eq.), $FeCl_3$, *T*, t_1. *ii*: acid, *T*, t_2. [a] isolated yield (bold highlighted line indicates used conditions for scope analysis).

Table 2. Optimization of cycloisomerization and ACM reaction for **6a**.

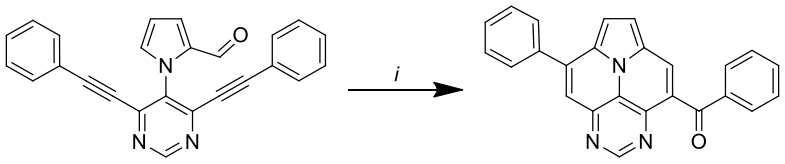

Entry	Acid (eq.)	Solvent	*T* [°C]	*t* [h]	Yield [a] [%]
1	*p*-TsOH·H_2O (30)	-	120	16	57
2	*p*-TsOH·H_2O (30)	xylene	120	16	68
3	*p*-TsOH·H_2O (30)	xylene	140	16	59
4	*p*-TsOH·H_2O (20)	xylene	120	16	67
5	*p*-TsOH·H_2O (10)	xylene	120	16	53
6	MsOH (20)	xylene	120	16	27
7	***p*-TsOH·H_2O (20)**	**xylene**	**120**	**6**	**68**

i: acid, solvent, *T*, *t*. [a] isolated yield (bold highlighted line indicates used conditions for scope analysis).

With optimized reaction conditions for both reactions, we studied the scope and limitations of our developed methodologies through an examination of different precursors, **4a**–**f** and the employed anilines (Scheme 3). Similar yields of the respective quinoline-diazaullazine (**5a**–**c**) were obtained for weak sigma donors or acceptors on the aryl alkyne moiety. However, stronger donors and acceptors led to inferior results (**5d**–**f**). One explanation for this could be the competitive reaction (ACM), as only the product **6d** was obtained during the synthesis of **5d**. In particular, **4d** did not react to product **5d,** and instead ACM product **6d** was detected as the only product. However, whether strong donors/acceptors lead to an enhancement of the ACM or to an inhibition of imine formation/[4 + 2]-cycloaddition cannot be clarified conclusively. Similar effects were observed by changing the substitution pattern of the employed aniline. While 4-methyl or 4-F substituents gave good yields (**5g**, **5j**), the yield dropped when CF_3 or NMe_2 groups were present. Moreover, sterical effects lead to reduced yield (**5h**, **5i**).

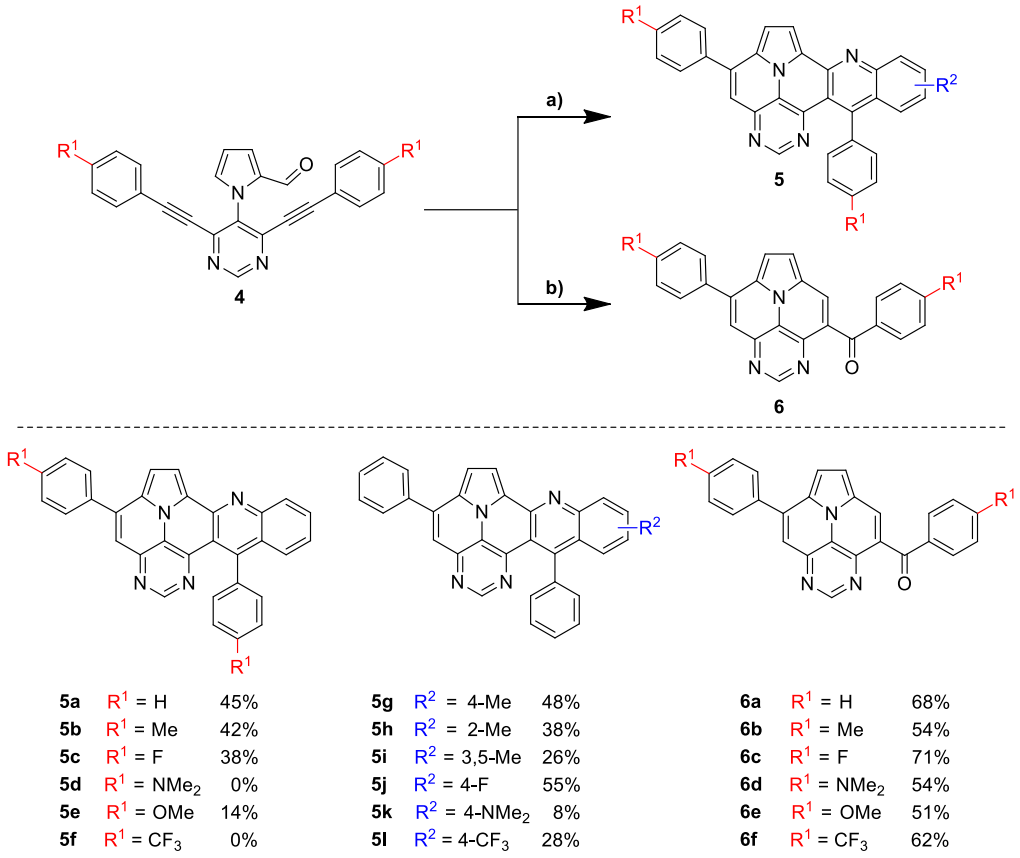

Scheme 3. Synthesis of final products **5a–l** by Povarov/cycloisomerization and **6a–f** by ACM/cycloisomerization. (**a**) 1. $FeCl_3$ (1 eq.), corresponding aniline (1.2 eq.), xylene, 140 °C, 3 h; 2. *p*-TsOH·H_2O (30 eq.), xylene, 140 °C, 6 h. (**b**) *p*-TsOH·H_2O (20 eq.), xylene, 120 °C, 6 h.

The ACM reaction seems to be less sensitive to functional groups and compounds **6a–f** were isolated in moderate to good yields independently from the substitution pattern. However, donor-substituted products (**6b**, **6d**, **6e**) were obtained in slightly lower yields.

Crystals of **5c** were grown via the slow evaporation of its chloroform solution, making them suitable for X-ray crystal structure analysis (Figure 2) [35]. The obtained crystal structure contained two co-crystallized $CHCl_3$ molecules per unit cell, which were omitted for better illustration. Both *p*-tolyl residues were twisted out of plane from the core structure by dihedral angles of 40° on the diazaullazine moiety and 84° on the quinoline part. Moreover, the crystal lattice showed a slipped antiparallel π-π-stacking with a spacing of 3.43 Å and 3.41 Å between the quinoline and diazaullazine entities, respectively. Different stacks within the crystal lattice were stabilized by close F-π (3.14 Å) and F-HC (2.52 Å) contacts.

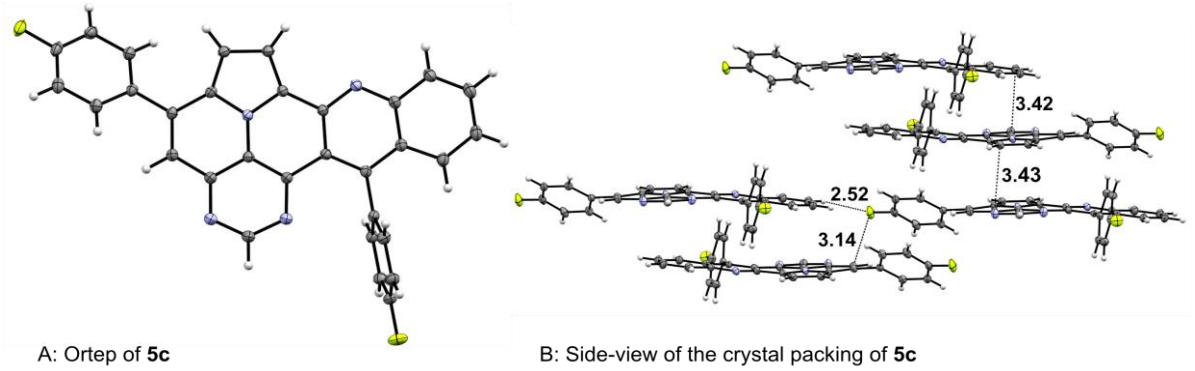

Figure 2. X-ray structures of **5c**.

NICS(1.7)$_{ZZ}$, as a criterion of the local aromaticity, and bond currents, using the BC-Wizard by Gershoni-Poranne et al., were calculated to obtain detailed insights into the aromatic behavior of **5** (Figure 3) [36,37]. A global diatropic ring current is apparent, accompanied by two local diatropic ring currents within the pyrrole and the pyrimidine rings. Furthermore, two diatropic semi-global currents are identifiable for the quinoline and the pyrimido-indolizine units. The central benzene ring connecting both moieties possesses the lowest NICS(1.7)$_{ZZ}$ values of the entire molecule. This observation coincides with the experimentally measured bond lengths. The C-C bond lengths between the quinoline and pyrimido-quinoline moieties are the longest within the molecular scaffold (1.45–1.47 Å; marked in red), indicating a reduced delocalization of π-electrons and leading to a slight curvature between the pyrimido-indolizine and the quinoline moieties by 8.2°. Similar results were observed for the related quinolino-azapirone and quinolino-azaullazine [30,31].

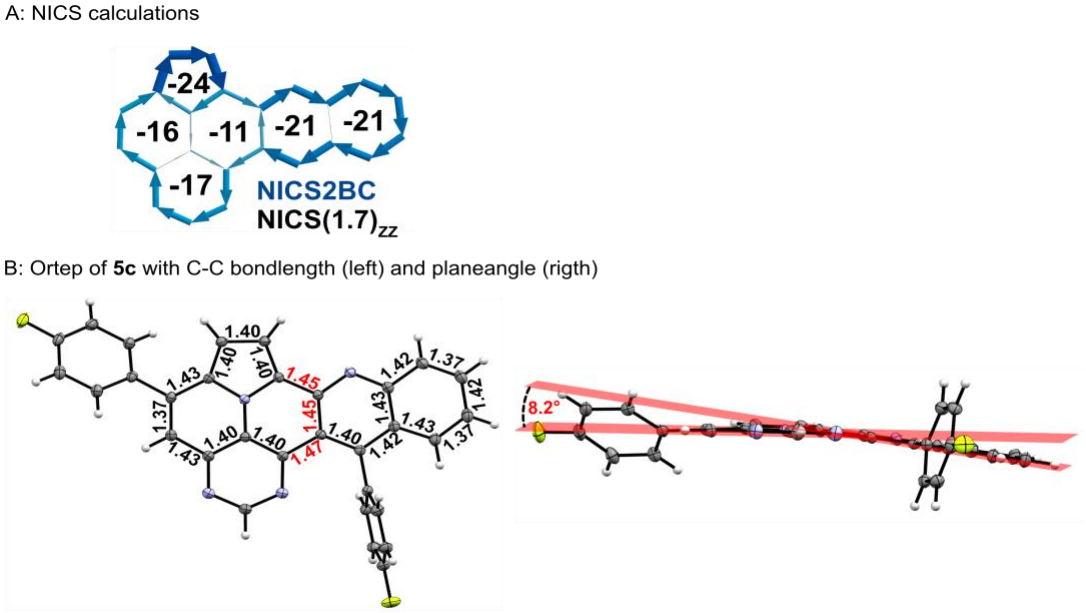

Figure 3. (**A**) NICS calculations for pyrimido[4′,5′,6′:9,1]pyrrolo[2′,1′,5′:4,5,6]quinolizino[3,2-*b*]quinoline: NICS2BC graphs (current was calculated from NICS(1.25)$_{ZZ}$ strength relative to I_{ref} (ring current of benzene, 11.5 nA T^{-1})). In the center of each ring are the respective NICS(1.7)$_{ZZ}$ values. (**B**) Ortep of **5c** with C-C bond length of the core structure (left) and plane angle between the pyrimido-indolizine and the quinoline moieties.

1.2. Photophysical Properties

The optical properties were studied via steady-state absorption- and emission spectroscopy (Figure 4). We focused on products **5a**, **5k**, and **5l**, which differ from the substitution pattern directly on the polycyclic scaffold. The impact of the attached phenyl rings on the optical properties is known to be limited due to its twisted orientation, and will not be further analyzed [30,31]. The results will be compared with ACM product **6a**. The spectroscopic data are shown in Table S2.

Only slight differences between **5a** and **5l** containing an electron-withdrawing CF_3-group are evident. Thus, both exhibit similar extinction coefficients and a fine structure of the absorption spectra, with slightly red-shifted absorption and emission maxima of **5l**. The fluorescence quantum yields of both compounds are also very similar and relatively high, at 53% and 52%, respectively [38]. Compound **5k** displays a broadened, unstructured absorption with smaller extinction coefficients over the entire spectrum, with significantly red-shifted absorption and emission maxima and noticeably reduced quantum yields (29%). These observations could indicate an ICT for compound **5k**.

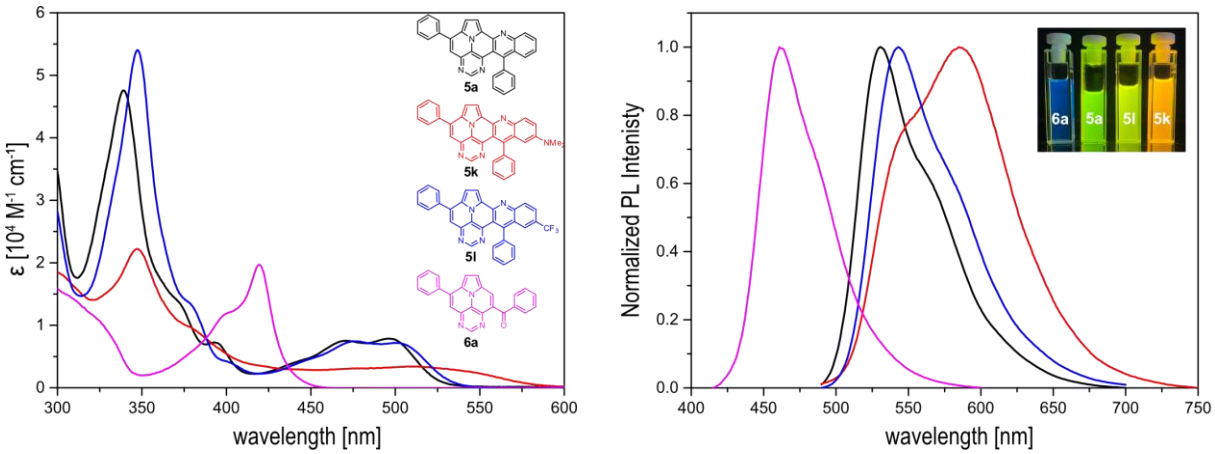

Figure 4. UV/Vis (**left**) and PL spectra ((**right**), λ_{ex} = 480 nm (**5a**,**k**,**l**), λ_{ex} = 400 nm (**6a**)) of the compounds shown in CH_2Cl_2 (c = 10^{-5} M) at 20 °C.

To investigate its potential ICT character, we performed solvatochromic studies with **5a** and **5k** and compared the calculated dipole moments of their S_0 and the S_1 transition states. Only minor changes in the calculated dipole moments, as well as in the absorption and emission features, in solvents of different polarities (toluene, CH_2Cl_2, acetonitrile, ethanol) were determined for both compounds (Figure S1, Supplementary Materials). Hence, the occurrence of ICT properties due to the presence of the NMe_2 group can be neglected.

In contrast, **6a** features a completely different structure of the absorption spectrum and strongly blue-shifted absorption and emission spectra with higher extinction coefficients of the lowest energy band (Figure 4). The fine structure and the location of the lowest energy band is very similar to that of the symmetrically 3,9-substituted 5,7-diazaullazines (**8**) [29]. However, **6a** has a much lower fluorescence quantum yield compared to **8**. A similar impact of benzoyl groups was previously observed for benzoyl functionalized aza-pyrene derivatives [39,40]. Interestingly, the quantum yield is comparable to 2-azaullazines, containing a benzoyl group and an additional CF_3 group, whereby the emission maxima of **5a** are significantly blue-shifted by ~140 nm [41].

To gain insights into the redox properties of the different core structures, **5a** and **6a**, we performed cyclic voltammetry (CV) measurements in dichloromethane (Figure 5). Both compounds exhibit an irreversible oxidation potential, while **5a** is slightly more easily oxidized (0.95 V; onset potential of 0.85 V) than compound **6a** (1.08 V; onset potential of 0.96 V), which corresponds to the experimentally deduced HOMO energies of −5.65 eV (**5a**) and −5.76 eV (**6a**) [42]. As expected, the presence of a withdrawing benzoyl group on the ullazine scaffold leads to a lower oxidation potential compared to diazaullazine **8** [29]. Similarly, the exchange of a pyridine ring of **7** with a more electron-poor pyrimidine ring (**5a**) leads to a reduced oxidation potential (Table 3) [30]. No reduction event is observed within the analyzed potential window of dichloromethane.

Density functional theory (DFT) calculations were performed for **5a**, **5k**, **5l,** and **6a** to obtain an improved understanding of the electronic properties and to disclose the impact of N-doping (Figure 6) [43]. The frontier orbitals of all three quinolino-diazaullazines are very similar and are mainly located on the core structures, with no contribution of the aryl substituents. Localization of the frontier orbitals, as well as the HOMO-LUMO gap, is comparable, as could be assumed from their previously discussed optical properties. The depiction of the HOMO and LUMO reveals no additional contribution by the CF_3 group to either of the frontier orbitals. In contrast, a pertinent contribution by the NMe_2 group of **5k** to the HOMO and, to a lesser extent, to the LUMO is apparent, leading to destabilized HOMO and LUMO energies, with a greater impact on the former. A comparison of **5a** with **7** shows the stabilization of both the HOMO and LUMO by ~0.30 eV due to the incorporation of a pyrimidine instead of a pyridine ring within the ullazine scaffold (Table 3) [30].

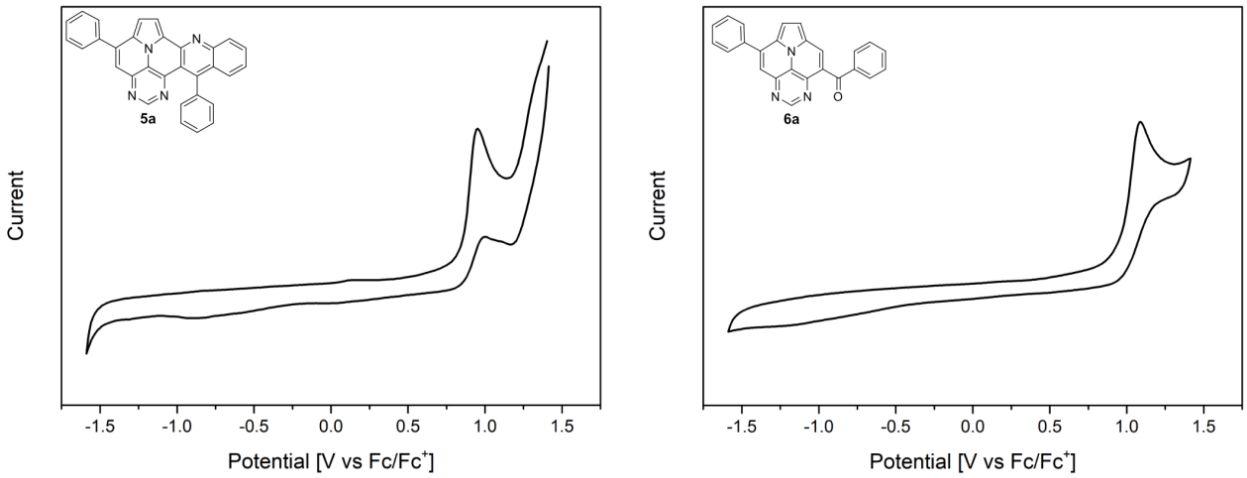

Figure 5. Cyclic voltammograms of **5a** and **6a**. Measured in CH_2Cl_2 (0.001 M) with 0.1 M n-Bu_4NPF_6 as a supporting electrolyte, glassy carbon working electrode, and Pt counter-electrode, with ferrocene as a standard, at a scan rate of 100 mV/s.

Table 3. Comparison of properties with related molecular structures.

	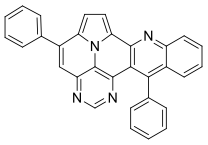	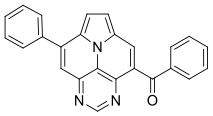	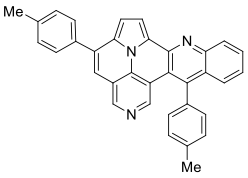	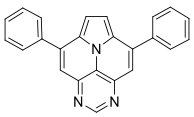
	5a	**6a**	**7** [30]	**8** [29]
$\lambda_{1,abs}$ [nm]	497	420	471	422
$\varepsilon_{\lambda 1}$ [10^4 L·mol^{-1}cm^{-1}]	0.8	2.0	1.1	1.7
$\lambda_{1,em}$ [nm]	530	462	515	439
Φ	0.52	0.10	0.26	0.35
$E_{Ox.}$ [V vs. Fc/Fc$^+$]	0.95	1.08	0.72	1.00
$E_{HOMO/CV}$ [eV]	−5.65	−5.76	−5.41	−5.69
$E_{HOMO/DFT}$ [eV]	−5.53	−5.73	−5.22	−5.60
$E_{LUMO/DFT}$ [eV]	−2.43	−2.04	−2.09	−1.90
E_{gap} [eV]	3.10	3.69	3.13	3.69

6a has an increased HOMO-LUMO gap (3.69 eV), which is due to a destabilized LUMO and a stabilized HOMO compared to product **5**. Interestingly, the HOMO–LUMO gap is exactly the same as for 3,9-substituted 5,7-diazaullazine (**8**), with both the HOMO and LUMO energies stabilized by 0.13 eV [29]. However, both compounds show different contributions to their respective frontier orbitals. While the HOMO and LUMO of **8** are mainly localized on the ullazine core structure, the strong participation of the benzoyl substituent of **6a** is observed on the LUMO.

A comparison of symmetrical (**8**) and unsymmetrical (**6a**) substituted diazaullazines, as well as π-expanded aza-(**7**) and diazaullazines (**5a**), reveal the impact of nitrogen doping, π-expansion, and the substitution pattern on the properties of these ullazine derivatives (Table 3) [29,30].

The absorption and emission properties of **5a** are comparable to those of quinolino-azaullazine (**7**) However, the installment of a pyrimidine moiety instead of a pyridine unit leads to red-shifted absorption and emission spectra. **5a** exhibits the highest quantum yields of the compared substances, which are twice as high as for related compound **7**. The HOMO and LUMO energies are stabilized by ~0.30 eV. Comparing compounds **5a** and **8** reveals significantly red-shifted absorption and emission spectra. The annulation of a

quinoline moiety on the diazaullazine moiety leads to a bathochromical shift of 75 nm for the absorption and 91 nm for the emission spectrum.

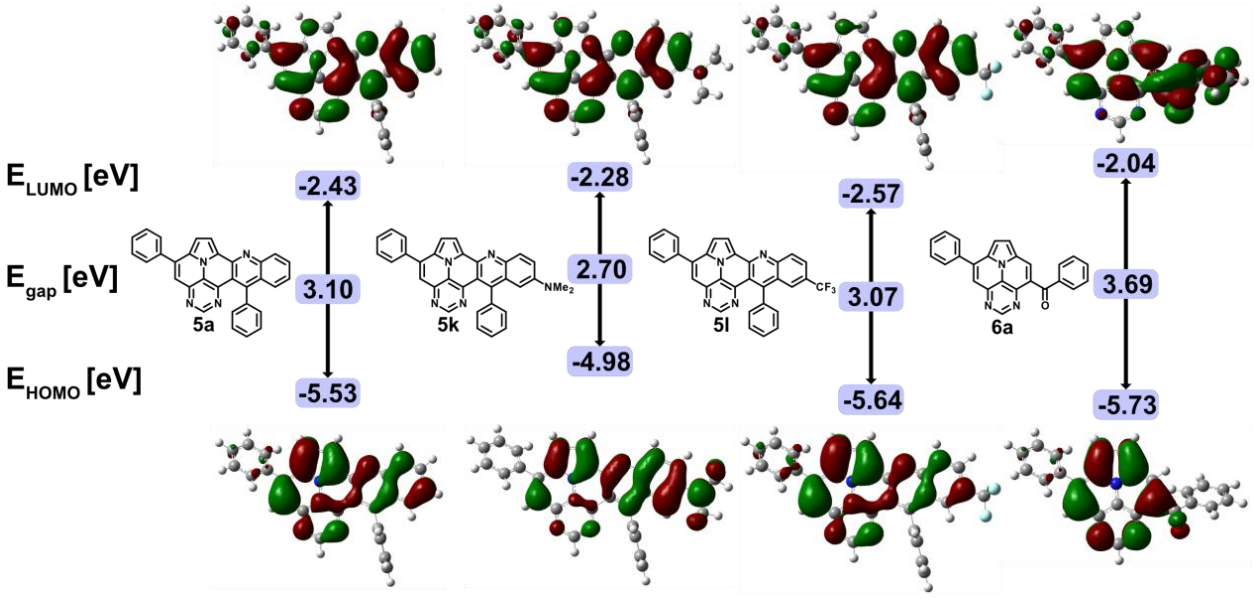

Figure 6. Frontier orbitals of **5a**, **5k**, **5l,** and **6a**, and energy levels calculated at the B3LYP/6-31G(d,p) level of theory within IEFPCM in CH_2Cl_2.

The differences between **6a** and **8** are rather small. Both have similar absorption and emission spectra, as well as similar HOMO and LUMO energies, which differ by 0.13 eV. This can be explained by the fact that these properties are mainly specified by the core structure and the substituents only have a minor influence on this. However, the introduction of a benzoyl function results in a noticeable quenching of the fluorescence and thus **8** has a 3.5 times higher quantum yield than **6a**.

2. Conclusions

We developed a divergent synthesis of π-expanded diazaullazine (quinolinodiazaullazines) and 9-benzoyl-diazaullazines through a one-pot multi-step procedure consisting of a Povarov/cycloisomerization or ACM/cycloisomerization protocol, respectively. Moderate to good yields of the desired products were obtained and selected compounds were studied by UV/Vis, fluorescence, and cyclovoltammetric measurements, which have been underpinned by DFT calculations. A comparison with related compounds offered insights into the impact of the substitution pattern and degree of N-doping on the optical and electrochemical properties. In particular, π-expansion by the fusion of a quinoline moiety leads to bathochromically shifted absorption and emission spectra accompanied by improved quantum yields, while benzoyl substituents lead to blue-shifted absorption and emission bands and reduced quantum yields.

3. Materials and Methods

3.1. General Information

The nuclear magnetic resonance spectra ($^1H/^{13}C/^{19}F$ NMR) were obtained using a Bruker AVANCE 300 III, 250 II, or 500. Chemical shifts (δ) were calibrated with respect to residual solvent signals of deuterated solvents $CDCl_3$ (δ = 7.26 ppm/77.0 ppm). Spin–spin correlation-induced multiplicities were denoted as follows: s = singlet; d = doublet; dd = double doublet; ddd = doublets of doublets; pt = pseudo triplet; m = multiplet, accompanied by their coupling constants (J). Infrared spectra (IR) were measured using attenuated total reflection (ATR) with a Nicolet 380 FT-IR spectrometer. Signal characteristics were described in terms of wavenumbers ($\tilde{\nu}$) and absorption strengths, categorized

as very strong (vs), strong (s), medium (m), or weak (w). UV/Vis spectra were acquired using a Cary 60 UV−vis spectrophotometer, and emission spectra were obtained with an Agilent Cary Eclipse fluorescence spectrophotometer. Cyclic voltammograms (CVs) were conducted at room temperature in CH_2Cl_2 (c = 10^{-3} M) with 0.1 M *n*-Bu_4NPF_6 as the supporting electrolyte, a glassy carbon working electrode, ANE2 ($Ag/AgNO_3$ 0.01 M in CH_3CN), as a reference electrode, and Pt as a counter-electrode (0.5 mm diameter platinum wire). Ferrocene (c = 10^{-3} M, in CH_3CN) served as an external standard at a scan rate of 100 mV/s. The voltammograms were recorded on a PalmSense EmStat 3 blue potentiostat. The working electrode is a 3 mm diameter, glassy, carbon disk electrode coated with KeI-F, polished using aqueous alumina slurry (0.03 µm alumina powder) on a polishing pad. Solvents were deoxygenated by argon purging. Potentials were referenced to as Fc^+/Fc, with a reductive scan direction starting at 1.5 V and a switching potential of −1.5 V, plotted using the IUPAC conventions. Mass spectra (MS/HRMS) were acquired using instruments coupled with preceding gas chromatography (GC) or liquid chromatography (LC). The samples were ionized either by electron impact ionization (EI) using an Agilent 6890/5973 or Agilent 7890/5977 GC-MS with a HP-5 capillary column and helium carrier gas, or by electron spray ionization (ESI) using an Agilent 1200/6210 Time-of-Flight (TOF) LC−MS. Melting points (mp) were determined using a Micro-Hot-Stage GalenTM III Cambridge Instruments without correction. X-ray single-crystal structure analysis was performed using a Bruker Apex Kappa-II CCD diffractometer.

3.2. Analytical Data

3.2.1. General Procedure A for the Synthesis of 5,13-Diphenylpyrimido[4′,5′,6′:9,1] pyrrolo[2′,1′,5′:4,5,6]quinolizino[3,2-*b*]quinoline (**5a–l**)

A total of 100 mg of **4a–f**, 1.2 eq. of the corresponding aniline and 1 eq. $FeCl_3$ were suspended in 4 mL xylene and stirred at 140 °C for 3 h. Subsequently, 20 eq. *p*-TsOH·H_2O were added to the reaction mixture and the solution was stirred at 140 °C for another 6 h. The reaction was quenched with $NaHCO_3$-solution, extracted three times with 50 mL CH_2Cl_2 and dried over Na_2SO_4. The solvent was distilled in vacuo and the residue was purified by column chromatography (CH_2Cl_2/EtOAc) to yield the desired products (**5a–l**).

5,13-diphenylpyrimido[4′,5′,6′:9,1]pyrrolo[2′,1′,5′:4,5,6]quinolizino[3,2-b]quinoline (**5a**)

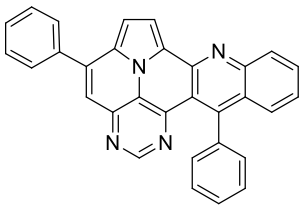

According to general procedure A, the title compound **5a** was obtained as an orange solid in 45% yield (54 mg, 0.121 mmol). R_f 0.50 (CH_2Cl_2/EtOAc 10:1). Mp. 284–286 °C. ^{1}H NMR (500 MHz, $CDCl_3$) δ = 8.83 (s, 1H), 8.31–8.27 (m, 1H), 8.24 (d, *J* = 4.3 Hz, 1H), 7.89–7.86 (m, 2H), 7.84 (ddd, *J* = 8.3 Hz, *J* = 6.6 Hz, *J* = 1.4 Hz, 1H), 7.66 (dd, *J* = 8.6 Hz, *J* = 1.4 Hz, 1H), 7.63–7.54 (m, 7H), 7.46 (ddd, *J* = 8.3 Hz, *J* = 6.7 Hz, *J* = 1.2 Hz, 1H), 7.42 (d, *J* = 4.3 Hz, 1H), 7.40–7.37 (m, 2H). ^{13}C NMR (126 MHz, $CDCl_3$) δ = 153.4, 150.2, 149.6, 146.9, 146.8, 144.5, 140.9, 138.7, 137.3, 131.5, 129.4, 129.1, 128.9, 128.7, 128.2, 127.9, 127.6, 127.5, 127.2, 126.3, 126.1, 122.1, 117.5, 116.8, 112.2, 109.1. IR (ATR, cm^{-1}): $\tilde{\nu}$ = 1605 (s), 1578 (m), 1500 (m), 1449 (m), 1405 (m), 863 (m), 777 (s), 734 (s), 705 (vs), 612 (s), 554 (s). MS (EI, 70 eV): *m*/*z* (%) = 446 (86, M^+), 445 (92), 444 (28), 382 (56), 381 (100), 380 (89), 379 (28), 354 (26), 223 (49), 222 (52), 208 (31). HRMS (ESI-TOF): calculated for $C_{31}H_{19}N_4$ ([M + H]$^+$) 447.1609, found 447.1602.

5,13-di-p-tolylpyrimido[4′,5′,6′:9,1]pyrrolo[2′,1′,5′:4,5,6]quinolizino[3,2-b]quinoline (**5b**)

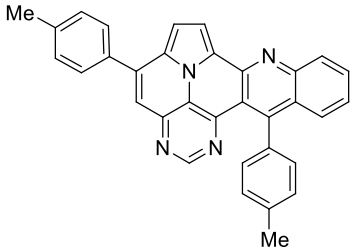

According to general procedure A, the title compound **5b** was obtained as an orange solid in 42% yield (50 mg, 0.105 mmol). R_f 0.78 (CH_2Cl_2/EtOAc 15:1). Mp. 303–306 °C. ^{1}H NMR (250 MHz, $CDCl_3$) δ = 8.83 (s, 1H), 8.22–8.16 (m, 1H), 8.13 (d, *J* = 4.3 Hz, 1H), 7.79–7.69 (m, 3H), 7.64 (ddd, *J* = 8.7 Hz, *J* = 1.5 Hz, *J* = 0.7 Hz, 1H), 7.49 (s, 1H), 7.44–7.35 (m, 5H), 7.33 (d, *J* = 4.3 Hz, 1H), 7.32–7.21 (m, 2H), 2.60 (s, 3H), 2.48 (s, 3H).^{13}C NMR (63 MHz, $CDCl_3$) δ = 153.3, 150.4, 149.4, 146.8, 146.7, 144.4, 140.7, 139.5, 137.0, 135.6, 134.4, 131.3, 129.7, 128.8, 128.8, 128.6, 128.5, 127.9, 127.4, 127.3, 126.1, 125.8, 121.9, 117.0, 116.7, 112.0, 108.9, 21.5, 21.4. IR (ATR, cm^{-1}): $\tilde{\nu}$ = 1603 (s),1498 (m), 820 (s), 771 (m), 748 (vs), 734 (s), 725 (s), 612 (s), 556 (s). MS (EI, 70 eV): *m*/*z* (%) = 474 (92, M^+), 473 (100), 472 (7), 238 (6), 237 (28), 236 (10), 230 (21), 229 (13), 228 (7), 222 (7), 215 (7). HRMS (ESI-TOF): calculated for $C_{33}H_{23}N_4$ ([M + H]$^+$) 475.1923, found 475.1926.

5,13-bis(4-fluorophenyl)pyrimido[4′,5′,6′:9,1]pyrrolo[2′,1′,5′:4,5,6]quinolizino[3,2-b]quinoline (**5c**)

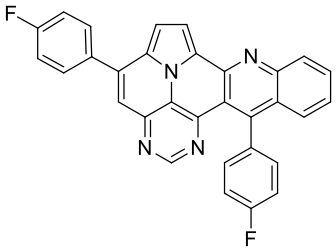

According to general procedure A, the title compound **5c** was obtained as an orange solid in 38% yield (44 mg, 0.091 mmol). R_f 0.78 (CH_2Cl_2/EtOAc 15:1). Mp. 318–320 °C. ^{1}H NMR (500 MHz, $CDCl_3$) δ = 8.86 (s, 1H), 8.32 (d, *J* = 8.5 Hz, 1H), 8.27 (d, *J* = 4.3 Hz, 1H), 7.89–7.84 (m, 3H), 7.68–7.65 (m, 1H), 7.54 (s, 1H), 7.50 (ddd, *J* = 8.3 Hz, *J* = 6.6 Hz, *J* = 1.2 Hz, 1H), 7.38 (d, *J* = 4.3 Hz, 1H), 7.36–7.28 (m, 6H). ^{13}C NMR (126 MHz, $CDCl_3$) δ = 163.5 (d, *J* = 250.0 Hz), 162.6 (d, *J* = 246.3 Hz), 153.4, 149.5, 149.3, 146.8, 146.7, 144.4, 139.9, 134.3 (d, *J* = 3.6 Hz), 133.3 (d, *J* = 3.2 Hz), 131.7, 130.4 (d, *J* = 8.7 Hz), 130.4 (d, *J* = 8.6 Hz),129.0, 127.6, 127.5, 127.2, 126.3, 126.3, 122.1, 117.5, 116.9, 116.2 (d, *J* = 21.8 Hz), 115.3 (d, *J* = 21.6 Hz), 112.4, 109.0. ^{19}F NMR (471 MHz, $CDCl_3$) δ = −111.4, −114.7. IR (ATR, cm^{-1}): $\tilde{\nu}$ = 1603 (vs),1502 (vs), 1228 (vs), 1158 (s), 835 (vs), 802 (s), 769 (s), 748 (s), 736 (s), 610 (s), 563 (vs). MS (EI, 70 eV): *m*/*z* (%) = 482 (67, M^+), 481 (100), 480 (42), 453 (13), 241 (27), 240 (71), 231 (16), 226 (37), 225 (32), 217 (16), 216 (17), 213 (14). HRMS (ESI-TOF): calculated for $C_{31}H_{17}F_2N_4$ ([M + H]$^+$) 483.1421, found 483.1425.

5,13-bis(4-methoxyphenyl)pyrimido[4′,5′,6′:9,1]pyrrolo[2′,1′,5′:4,5,6]quinolizino[3,2-b]quinoline (**5e**)

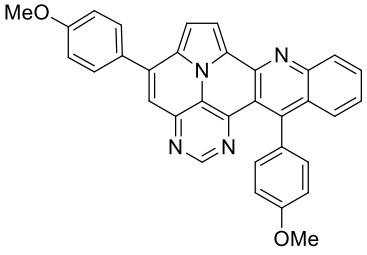

According to general procedure A, the title compound **5e** was obtained as an orange solid in 14% yield (16 mg, 0.032 mmol). R_f 0.85 (CH_2Cl_2/EtOAc 15:1). Mp. 298–301 °C. ^{1}H NMR (250 MHz, $CDCl_3$/TFA) δ = 9.05 (d, *J* = 4.9 Hz, 1H), 8.92 (s, 1H), 8.61 (d, *J* = 8.6 Hz, 1H), 8.44

(ddd, *J* = 8.6 Hz, *J* = 6.9 Hz, *J* = 1.4 Hz, 1H), 8.31–8.18 (m, 3H), 8.03–7.90 (m, 3H), 7.39–7.21 (m, 6H), 4.06 (s, 3H), 4.01 (s, 3H). ^{13}C NMR (63 MHz, $CDCl_3$/TFA) δ = 166.0, 163.3, 161.4, 148.6, 146.7, 145.3, 140.6, 140.3, 138.4, 136.1, 131.4, 131.3, 130.8, 130.1, 129.6, 128.1, 127.0, 126.6, 119.9, 119.7, 119.4, 118.4, 116.0, 115.9, 115.1, 111.1, 55.8, 55.7. IR (ATR, cm^{-1}): $\tilde{\nu}$ = 1601 (s),1498 (s), 1243 (vs), 1175 (vs), 1158 (s), 1024 (vs), 835 (s), 785 (s), 762 (vs), 736 (s), 573 (s), 558 (vs). MS (EI, 70 eV): *m*/*z* (%) = 506 (100, M^+), 505 (99), 463 (5) 462 (13), 420 (4), 419 (8), 254 (7), 253 (19), 232 (8), 231 (5), 210 (9), 197 (5), 196 (5). HRMS (ESI-TOF): calculated for $C_{33}H_{23}N_4O_2$ ([M + H]$^+$) 507.1821, found 507.1828.

11-methyl-5,13-diphenylpyrimido[4′,5′,6′:9,1]pyrrolo[2′,1′,5′:4,5,6]quinolizino[3,2-b]quinoline (**5g**)

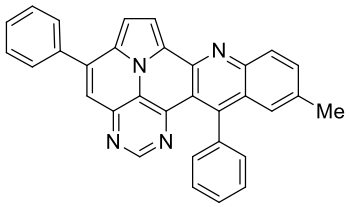

According to general procedure A, the title compound **5g** was obtained as an orange solid in 48% yield (59 mg, 0.128 mmol). R_f 0.75 (CH_2Cl_2/EtOAc 15:1).Mp. 319–322 °C. ^{1}H NMR (500 MHz, $CDCl_3$) δ = 8.80 (s, 1H), 8.17 (d, *J* = 4.3 Hz, 1H), 8.14 (d, *J* = 8.6 Hz, 1H), 7.87–7.84 (m, 2H), 7.64–7.54 (m, 7H), 7.53 (s, 1H), 7.40–7.36 (m, 4H), 2.44 (s, 3H). ^{13}C NMR (126 MHz, $CDCl_3$) δ = 153.3, 149.2, 148.2, 146.7, 143.7, 140.7, 138.8, 137.3, 136.1, 134.0, 129.4, 129.0, 128.7, 128.6, 128.6, 128.1, 127.4, 127.3, 127.1, 126.2, 126.2, 122.0, 117.2, 116.7, 111.8, 109.0, 22.0. IR (ATR, cm^{-1}): $\tilde{\nu}$ = 1607 (s),1554 (m), 1492 (m), 1449 (m), 1403 (m), 1325 (m), 814 (m), 777 (vs), 754 (m), 703 (vs), 596 (m), 556 (s). MS (EI, 70 eV): *m*/*z* (%) = 460 (91, M^+), 459 (100), 458 (11), 457 (7), 230 (28), 229 (29), 228 (15), 222 (18), 215 (8), 214 (13), 208 (7). HRMS (ESI-TOF): calculated for $C_{32}H_{21}N_4$ ([M + H]$^+$) 461.1766, found 461.1771.

9-methyl-5,13-diphenylpyrimido[4′,5′,6′:9,1]pyrrolo[2′,1′,5′:4,5,6]quinolizino[3,2-b]quinoline (**5h**)

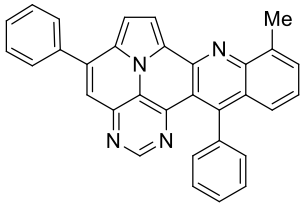

According to general procedure A, the title compound **5h** was obtained as an orange solid in 38% yield (34 mg, 0.074 mmol). R_f 0.80 (CH_2Cl_2/EtOAc 15:1). Mp. 256–259 °C. ^{1}H NMR (300 MHz, $CDCl_3$) δ = 8.83 (s, 1H), 8.26 (d, *J* = 4.3 Hz, 1H), 7.92–7.85 (m, 2H), 7.69 (ddd, *J* = 6.8 Hz, *J* = 1.5 Hz, *J* = 1.0 Hz, 1H), 7.65–7.55 (m, 7H), 7.50 (ddd, *J* = 8.7 Hz, *J* = 1.5 Hz, *J* = 0.7 Hz, 1H), 7.43 (d, *J* = 4.3 Hz, 1H), 7.38–7.32 (m, 3H), 3.0 (s, 3H). ^{13}C NMR (75 MHz, $CDCl_3$) δ = 153.4, 150.1, 148.8, 146.9, 146.8, 143.4, 140.9, 139.1, 137.4, 136.9, 131.3, 129.4, 129.1, 128.7, 128.7, 128.1, 127.4, 127.1, 126.9, 125.8, 125.8, 122.2, 117.2, 116.4, 111.8, 109.0, 18.2. IR (ATR, cm^{-1}): $\tilde{\nu}$ = 1601 (m),1552 (m), 1447 (m), 1428 (s), 1339 (m), 1323 (m), 781 (s), 762 (vs), 701 (vs), 604 (m), 567 (m), 556 (s). MS (EI, 70 eV): *m*/*z* (%) = 460 (81, M^+), 459 (100), 458 (6), 457 (6), 445 (7), 230 (16), 229 (18), 228 (8), 222 (10), 214 (8). HRMS (ESI-TOF): calculated for $C_{32}H_{21}N_4$ ([M + H]$^+$) 461.1766, found 461.1775.

10,12-dimethyl-5,13-diphenylpyrimido[4′,5′,6′:9,1]pyrrolo[2′,1′,5′:4,5,6]quinolizino[3,2-b]quinoline (**5i**)

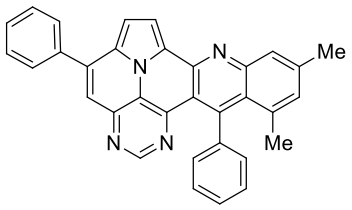

According to general procedure A, the title compound **5i** was obtained as an orange solid in 26% yield (34 mg, 0.072 mmol). R_f 0.82 (CH_2Cl_2/EtOAc 15:1). Mp. 317–320 °C. ^{1}H NMR (500 MHz, $CDCl_3$/TFA) δ = 9.12 (d, *J* = 4.9 Hz, 1H), 8.84 (s, 1H), 8.36 (s, 1H), 8.25 (s, 1H), 8.16 (d, *J* = 4.9 Hz, 1H), 7.95–7.87 (m, 2H), 7.76–7.64 (m, 6H), 7.58 (s, 1H), 7.40–7.35 (m, 2H), 2.77 (s, 3H), 2.15 (s, 3H). ^{13}C NMR (126 MHz, $CDCl_3$/TFA) δ = 165.2, 154.1, 147.5, 147.4, 145.6, 142.6, 142.0, 138.9, 137.5, 136.7, 135.2, 134.2, 132.1, 130.9, 130.4, 130.0, 129.4, 129.3, 127.1, 125.2, 121.3, 119.5, 119.2, 118.1, 117.3, 115.7, 112.8, 25.2, 22.8. IR (ATR, cm^{-1}): $\tilde{\nu}$ = 1605 (s),1578 (m), 1550 (m), 1504 (m), 1451 (s), 1325 (m), 857 (m), 777 (s), 725 (s), 703 (vs), 558 (m). MS (EI, 70 eV): *m*/*z* (%) = 474 (89, M^+), 473 (100), 471 (5), 470 (5), 399 (7), 237 (10), 236 (6), 229 (15), 228 (12), 214 (6). HRMS (ESI-TOF): calculated for $C_{33}H_{22}N_4$ ([M + H]$^+$) 475.1923, found 475.1934.

11-fluoro-5,13-diphenylpyrimido[4′,5′,6′:9,1]pyrrolo[2′,1′,5′:4,5,6]quinolizino[3,2-b]quinoline (**5j**)

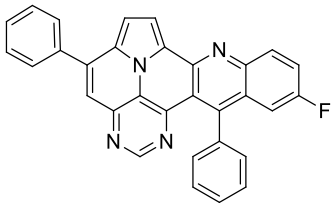

According to general procedure A, the title compound **5j** was obtained as an orange solid in 55% yield (69 mg, 0.148 mmol). R_f 0.79 (CH_2Cl_2/EtOAc 15:1). Mp. 348–350 °C. ^{1}H NMR (500 MHz, $CDCl_3$) δ = 8.85 (s, 1H), 8.32 (dd, *J* = 9.3 Hz, *J* = 5.5 Hz, 1H), 8.24 (d, *J* = 4.3 Hz, 1H), 7.91–7.86 (m, 2H), 7.67–7.55 (m, 8H), 7.44 (d, *J* = 4.3 Hz, 1H), 7.38–7.35 (m, 2H), 7.26 (dd, *J* = 10.3 Hz, *J* = 2.8 Hz, 1H). ^{13}C NMR (126 MHz, $CDCl_3$) δ = 160.1 (d, *J* = 248.7 Hz), 153.5, 149.5, 149.5, 147.0, 146.8, 146.4, 144.1 (d, *J* = 1.9 Hz), 141.1, 138.3, 137.3, 131.5 (d, *J* = 8.9 Hz), 129.5, 129.1, 128.7, 128.5, 128.4, 127.9 (d, *J* = 9.5 Hz), 127.8, 127.6, 126.2, 122.4 (d, *J* = 26.2 Hz), 117.5, 117.2, 112.0, 110.7 (d, *J* = 23.6 Hz), 109.2. ^{19}F NMR (471 MHz, $CDCl_3$) δ = −111.7. IR (ATR, cm^{-1}): $\tilde{\nu}$ = 1488 (s),1175 (s), 830 (s), 777 (vs), 725 (s), 705 (vs), 593 (s), 552 (s), 474 (s), 460 (s), 443 (s). MS (EI, 70 eV): *m*/*z* (%) = 464 (89, M^+), 463 (100), 462 (25), 435 (12), 232 (41), 231 (42), 230 (10), 218 (11), 217 (19). HRMS (ESI-TOF): calculated for $C_{31}H_{18}FN_4$ ([M + H]$^+$) 465.1516, found 465.1524.

N,N-dimethyl-5,13-diphenylpyrimido[4′,5′,6′:9,1]pyrrolo[2′,1′,5′:4,5,6]quinolizino[3,2-b]quinolin-11-amine (**5k**)

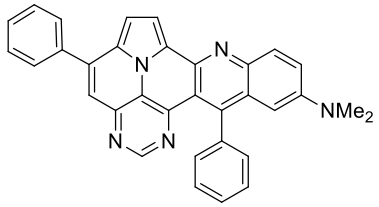

According to general procedure A, the title compound **5k** was obtained as an orange solid in 8% yield (11 mg, 0.021 mmol). R_f 0.82 (CH_2Cl_2/EtOAc 15:1). Mp. 130–134 °C. ^{1}H NMR (500 MHz, $CDCl_3$) δ = 8.81 (s, 1H), 8.25 (s, 2H), 7.91–7.88 (m, 2H), 7.62–7.57 (m, 5H), 7.57–7.55 (m, 3H), 7.45 (d, *J* = 4.3 Hz, 1H), 7.41–7.35 (m, 2H), 6.55 (d, *J* = 2.8 Hz, 1H), 2.96 (s, 6H). ^{13}C NMR (126 MHz, $CDCl_3$/TFA) δ = 148.3, 146.8, 146.7, 145.8, 138.9, 137.4, 134.9, 134.2, 134.0, 132.2, 130.8, 130.3, 130.1, 130.0, 129.8, 129.6, 129.3, 126.8, 122.4, 121.5, 120.4,

118.8, 117.8, 116.6, 112.0, 42.9. IR (ATR, cm^{-1}): $\tilde{\nu}$ = 2920 (s),1607 (s), 1492 (s), 1449 (s), 1323 (s), 1123 (s), 775 (s), 699 (vs), 591 (s), 554 (s).MS (EI, 70 eV): *m*/*z* (%) = 489 (40, M^+), 488 (24), 207 (14), 57 (25), 55 (20), 44 (100), 43 (28), 41 (23). HRMS (ESI-TOF): calculated for $C_{33}H_{24}N_5$ ($[M + H]^+$) 490.3032, found 490.2031.

5,13-diphenyl-11-(trifluoromethyl)pyrimido[4′,5′,6′:9,1]pyrrolo[2′,1′,5′:4,5,6]quinolizino[3,2-b] quinoline (**5l**)

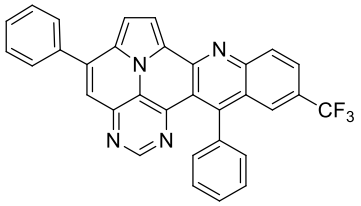

According to general procedure A, the title compound **5l** was obtained as an orange solid in 28% yield (38 mg, 0.075 mmol). R_f 0.85 (CH_2Cl_2/EtOAc 15:1). Mp. 311–313 °C. ^{1}H NMR (500 MHz, $CDCl_3$/TFA) δ = 9.10 (d, *J* = 4.9 Hz, 1H), 8.96 (s, 1H), 8.77 (d, *J* = 8.9 Hz, 1H), 8.56 (dd, *J* = 9.1 Hz, *J* = 1.8 Hz, 1H), 8.37 (s, 1H), 8.31 (s, 1H), 8.28 (d, *J* = 4.9 Hz, 1H), 7.95–7.89 (m, 2H), 7.86–7.82 (m, 1H), 7.81–7.71 (m, 5H), 7.41–7.37 (m, 2H). ^{13}C NMR (126 MHz, $CDCl_3$/TFA) δ = 167.4, 149.3, 147.4, 145.8, 141.4, 138.6, 137.3, 135.9 (q, *J* = 3.1 Hz), 133.8, 133.8, 132.7, 132.2, 132.1 (q, *J* = 34.7 Hz), 131.2, 130.3, 129.8, 129.4, 128.2 (q, *J* = 4.1 Hz), 127.1, 127.0, 122.4 (q, *J* = 273.1 Hz), 121.9, 121.5, 120.6, 119.7, 118.8, 116.9, 113.0. ^{19}F NMR (471 MHz, $CDCl_3$/TFA) δ = −63.8. IR (ATR, cm^{-1}): $\tilde{\nu}$ = 1609 (m), 1311 (s), 1298 (s), 1117 (vs), 1067 (s), 985 (m), 837 (s), 779 (s), 701 (vs), 589 (s), 556 (s). MS (EI, 70 eV): *m*/*z* (%) = 514 (86, M^+), 513 (100), 512 (5), 485 (5), 445 (4), 257 (11), 256 (14), 223 (4), 222 (13), 221 (4), 208 (5), 207 (4). HRMS (ESI-TOF): calculated for $C_{32}H_{18}F_3N_4$ ($[M + H]^+$) 515.1483, found 515.1495.

3.2.2. General Procedure B for the Synthesis of Aryl(8-arylpyrimido[4,5,6-*ij*]pyrrolo[2,1,5-*de*] quinolizin-4-yl)methanone (**6a**–**f**)

In a pressure tube, 100 mg of **4a**–**f** and 20 eq. of *p*-TsOH·H_2O were dissolved in 4 mL of xylene. The pressure tube was sealed with a Teflon cap and the solution was stirred for 6 h at 120 °C. The reaction mixture was cooled to room temperature, quenched with saturated $NaHCO_3$ solution and extracted three times with 50 mL CH_2Cl_2. The combined organic phases were dried over Na_2SO_4; the solvent was distilled off in vacuo. The residue was purified by column chromatography (heptane/EtOAc) to yield the desired products (**6a–f**).

Phenyl(8-phenylpyrimido[4,5,6-ij]pyrrolo[2,1,5-de]quinolizin-4-yl)methanone (**6a**)

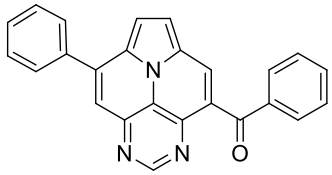

According to general procedure B, the title compound **6a** was obtained as a yellow solid in 68% yield (68 mg, 0.182 mmol). R_f 0.48 (heptane/EtOAc 1:2). Mp. 266–269 °C. ^{1}H NMR (250 MHz, $CDCl_3$) δ = 9.14 (s, 1H), 8.52 (s, 1H), 7.99–7.94 (m, 2H), 7.93 (s, 1H), 7.90–7.84 (m, 2H), 7.75–7.69 (m, 2H), 7.67–7.57 (m, 4H), 7.52–7.44 (m, 2H). ^{13}C NMR (63 MHz, $CDCl_3$) δ = 194.4, 155.1, 147.2, 144.9, 140.6, 137.2, 136.9, 133.5, 130.1, 129.6, 129.2, 128.9, 128.6, 128.1, 127.7, 126.3, 126.3, 124.7, 119.8, 113.9, 113.2. IR (ATR, cm^{-1}): $\tilde{\nu}$ = 1644 (m), 1609 (s), 1455 (s), 1261 (s), 1238 (s), 1045 (s), 795 (s), 779 (s), 684 (vs), 637 (vs), 563 (vs). MS (EI, 70 eV): *m*/*z* (%) = 373 (16, M^+), 372 (29), 346 (7), 345 (28), 344 (100), 316 (5), 240 (10), 187 (16), 172 (8). HRMS (ESI-TOF): calculated for $C_{25}H_{15}N_3O$ ($[M + H]^+$) 374.1293, found 374.1294.

p-tolyl(8-(p-tolyl)pyrimido[4,5,6-ij]pyrrolo[2,1,5-de]quinolizin-4-yl)methanone (**6b**)

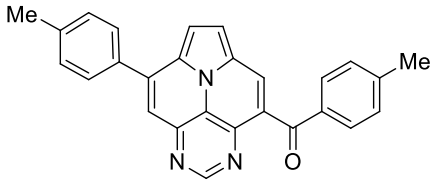

According to general procedure B, the title compound **6b** was obtained as a yellow solid in 54% yield (54 mg, 0.135 mmol). R_f 0.52 (heptane/EtOAc 1:2). Mp. 258–261 °C. ^{1}H NMR (300 MHz, $CDCl_3$) δ = 9.12 (s, 1H), 8.47 (s, 1H), 7.88 (s, 1H), 7.86 (d, *J* = 8.3 Hz, 2H), 7.76 (d, *J* = 8.1 Hz, 2H), 7.73–7.66 (m, 2H), 7.45–7.39 (m, 2H), 7.30–7.21 (m, 2H), 2.50 (s, 3H), 2.43 (s, 3H). ^{13}C NMR (75 MHz, $CDCl_3$) δ = 194.0, 155.1, 147.2, 144.8, 144.5, 140.5, 139.8, 134.6, 134.0, 130.3, 129.9, 129.2, 128.8, 128.4, 127.6, 126.2, 125.9, 124.6, 119.4, 113.6, 113.1, 21.7, 21.3. IR (ATR, cm^{-1}): $\tilde{\nu}$ = 1607 (s), 1457 (s), 1344 (vs), 1267 (s), 1251 (s), 1043 (s), 903 (s), 824 (s), 777 (vs), 756 (s), 723 (s), 563 (vs). MS (EI, 70 eV): *m*/*z* (%) = 401 (19, M^+), 400 (28), 373 (31), 372 (100), 371 (9), 201 (12), 186 (8), 179 (6), 178 (11), 91 (7). HRMS (ESI-TOF): calculated for $C_{27}H_{19}N_3O$ ($[M + H]^+$) 402.1606, found 402.1602.

(4-fluorophenyl)(8-(4-fluorophenyl)pyrimido[4,5,6-ij]pyrrolo[2,1,5-de]quinolizin-4-yl)methanone (**6c**)

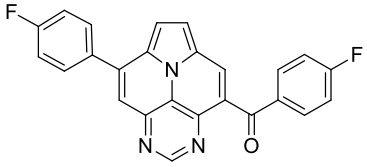

According to general procedure B, the title compound **6c** was obtained as a yellow solid in 71% yield (71 mg, 0.173 mmol). R_f 0.48 (heptane/EtOAc 1:2). Mp. 317–320 °C. ^{1}H NMR (500 MHz, $CDCl_3$/TFA) δ = 9.25 (s, 1H), 9.17 (s, 1H), 8.63 (s, 1H), 8.41 (d, *J* = 5.0 Hz, 1H), 8.35 (d, *J* = 5.0 Hz, 1H), 8.00–7.87 (m, 4H), 7.44 (pt, *J* = 8.3 Hz, 2H), 7.30 (pt, *J* = 8.3 Hz, 2H). ^{13}C NMR (126 MHz, $CDCl_3$/TFA) δ = 193.9, 166.6 (d, *J* = 258.6 Hz), 164.9 (d, *J* = 254.6 Hz), 146.3, 144.6, 143.6, 136.7, 132.8 (d, *J* = 9.7 Hz), 131.9 (d, *J* = 8.9 Hz), 131.7, 130.6, 130.4, 130.3, 129.9, 122.9, 121.9, 121.2, 118.2, 117.5 (d, *J* = 22.1 Hz), 116.7 (d, *J* = 22.3 Hz). ^{19}F NMR (471 MHz, $CDCl_3$/TFA) δ = −101.5, −107.3. IR (ATR, cm^{-1}): $\tilde{\nu}$ = 1609 (s), 1599 (s), 1589 (s), 1508 (s), 1453 (s), 1267 (s), 1243 (vs), 1232 (s), 1158 (s), 847 (s), 837 (s), 783 (vs), 563 (s). MS (EI, 70 eV): *m*/*z* (%) = 409 (14, M^+), 408 (17), 382 (4), 381 (27), 380 (100), 379 (7), 259 (4), 258 (10), 205 (7), 190 (4), 95 (9). HRMS (ESI-TOF): calculated for $C_{25}H_{14}F_2N_3O$ ($[M + H]^+$) 410.1105, found 410.1113.

*(4-(dimethylamino)phenyl)(8-(4-(dimethylamino)phenyl)pyrimido[4,5,6-ij]pyrrolo[2,1,5-de]quinolizin-*4-yl)methanone (**6d**)

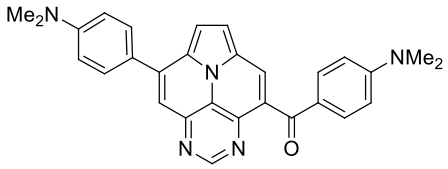

According to general procedure B, the title compound **6d** was obtained as a yellow solid in 54% yield (54 mg, 0.118 mmol). R_f 0.29 (EtOAc). Mp. 255–258 °C. ^{1}H NMR (500 MHz, $CDCl_3$) δ = 9.11 (s, 1H), 8.39 (s, 1H), 7.91–7.75 (m, 6H), 7.63 (d, *J* = 4.6 Hz, 1H), 6.94–6.88 (m, 2H), 6.67–6.61 (m, 2H), 3.09 (s, 6H), 3.07 (s, 6H). ^{13}C NMR (126 MHz, $CDCl_3$) δ = 192.2, 155.0, 153.9, 151.2, 147.2, 144.6, 140.8, 132.7, 130.0, 129.7, 127.4, 126.4, 124.8, 124.7, 124.3, 124.3, 117.5, 113.1, 112.8, 112.4, 110.6, 40.3, 40.0. IR (ATR, cm^{-1}): $\tilde{\nu}$ = 1597 (vs), 1523 (s), 1346 (s), 1284 (s), 1271 (s), 1261 (s), 1189 (s), 1179 (s), 1168 (s), 818 (s), 779 (s), 771 (s), 560 (s). MS (EI, 70 eV): *m*/*z* (%) = 459 (53, M^+), 458 (39), 445 (22), 444 (28), 431 (34), 430 (100), 416 (35), 414 (16), 230 (18), 215 (13). HRMS (ESI-TOF): calculated for $C_{29}H_{26}N_5O$ ($[M + H]^+$) 460.2137, found 460.2148.

(4-methoxyphenyl)(8-(4-methoxyphenyl)pyrimido[4,5,6-ij]pyrrolo[2,1,5-de]quinolizin-4-yl) methanone (**6e**)

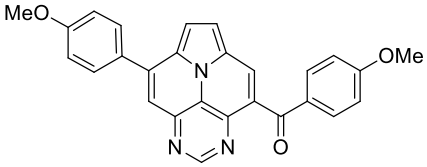

According to general procedure B, the title compound **6e** was obtained as a yellow solid in 51% yield (51 mg, 0.118 mmol). R_f 0.29 (heptane/EtOAc 1:3). Mp. 265–267 °C. ^{1}H NMR (300 MHz, $CDCl_3$) δ = 9.27 (s, 1H), 9.14 (s, 1H), 8.64 (s, 1H), 8.46–8.40 (m, 2H), 7.96–7.84 (m, 4H), 7.26 (d, *J* = 8.9 Hz, 2H), 7.10 (d, *J* = 8.3 Hz, 2H), 3.99 (s, 3H), 3.95 (s, 3H). ^{13}C NMR (75 MHz, $CDCl_3$) δ = 194.3, 165.4, 162.7, 146.3, 145.8, 143.0, 135.7, 133.1, 131.8, 131.7, 130.5, 130.1, 127.8, 126.6, 123.1, 122.9, 122.0, 121.1, 118.1, 115.8, 114.9, 55.8, 55.7. IR (ATR, cm^{-1}): $\tilde{\nu}$ = 1597 (s), 1455 (s), 1253 (vs), 1166 (vs), 1041 (s), 1020 (s), 832 (s), 775 (s), 604 (s), 575 (s), 560 (s), 536 (s). MS (EI, 70 eV): *m*/*z* (%) = 433 (16, M^+), 432 (20), 405 (26), 404 (100), 389 (11), 361 (13), 217 (26), 180 (9), 265 (7). HRMS (ESI-TOF): calculated for $C_{27}H_{20}N_3O_3$ ([M + H]$^+$) 434.1505, found 434.1518.

(4-(trifluoromethyl)phenyl)(8-(4-(trifluoromethyl)phenyl)pyrimido[4,5,6-ij]pyrrolo[2,1,5-de] quinolizin-4-yl)methanone (**6f**)

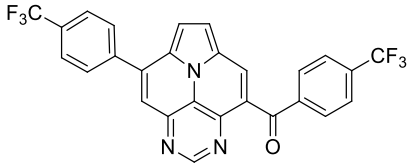

According to general procedure B, the title compound **6f** was obtained as a yellow solid in 62% yield (62 mg, 0.121 mmol). R_f 0.52 (heptane/EtOAc 1:2). Mp. 309–311 °C. ^{1}H NMR (500 MHz, $CDCl_3$/TFA) δ = 9.23 (s, 1H), 9.18 (s, 1H), 8.66 (s, 1H), 8.41 (d, *J* = 5.0 Hz, 1H), 8.30 (d, *J* = 5.0 Hz, 1H), 8.04 (d, *J* = 8.1 Hz, 2H), 8.02–7.94 (m, 4H), 7.85 (d, *J* = 7.9 Hz, 2H). ^{13}C NMR (126 MHz, $CDCl_3$) δ = 194.3, 146.2, 144.1, 143.8, 138.8, 137.6, 137.0, 135.3 (q, *J* = 33.0 Hz), 133.4 (q, *J* = 33.3 Hz), 131.7, 130.9, 130.2, 130.0, 129.9, 126.9 (q, *J* = 3.8 Hz), 126.2 (q, *J* = 3.8 Hz), 123.6, 123.5 (q, *J* = 272.7 Hz), 123.3, 123.3 (q, *J* = 272.9 Hz), 122.6, 120.8, 117.8. ^{19}F NMR (471 MHz, $CDCl_3$) δ = −63.2, −63.5. IR (ATR, cm^{-1}): $\tilde{\nu}$ = 1325 (vs), 1166 (s), 1109 (vs), 1067 (s), 1057 (s), 1049 (s), 1018 (s), 845 (m), 787 (s), 670 (m), 563 (m). MS (EI, 70 eV): *m*/*z* (%) = 509 (12, M^+), 508 (20), 482 (5), 481 (28), 480 (100), 255 (7), 240 (8), 145 (9). HRMS (ESI-TOF): calculated for $C_{27}H_{14}F_6N_3O$ ([M + H]$^+$) 510.1041, found 510.1055.

Supplementary Materials: The following supporting information can be downloaded at: https://www.mdpi.com/article/10.3390/molecules29092159/s1, containing analytical data of starting materials, X-ray chrystallograpfic, UV-Vis data (solvatochromism), Cartesian Coordinates from DFT calculations and NMR-spectra of final products. Reference [44] is cited in the Supplementary Materials.

Author Contributions: Conceptualization, P.E.; formal analysis, A.V.; investigation, J.P.; writing—original draft, J.P.; writing—review and editing, P.E. and P.L.; supervision, P.E. and P.L.; project administration, P.L. All authors have read and agreed to the published version of the manuscript.

Funding: This research received no external funding.

Institutional Review Board Statement: Not applicable.

Informed Consent Statement: Not applicable.

Data Availability Statement: The data underlying this study are available in this article and its Supplementary Materials.

Conflicts of Interest: The authors declare no conflict of interest.

References

1. Delcamp, J.H.; Yella, A.; Holcombe, T.W.; Nazeeruddin, M.K.; Grätzel, M. The molecular engineering of organic sensitizers for solar-cell applications. *Angew. Chem. Int. Ed.* **2013**, *52*, 376–380. [CrossRef] [PubMed]
2. Balli, H.; Zeller, M. Neue Heteroarene: Synthese und spektrale Daten von Indolizino[6,5,4,3-*aij*]chinolin («Ullazin») und einigen Derivaten. *Helv. Chim. Acta* **1983**, *66*, 2135–2139. [CrossRef]
3. Feng, J.; Jiao, Y.; Ma, W.; Nazeeruddin, M.K.; Grätzel, M.; Meng, S. First Principles Design of Dye Molecules with Ullazine Donor for Dye Sensitized Solar Cells. *J. Phys. Chem. C* **2013**, *117*, 3772–3778. [CrossRef]
4. Zhang, Y.; Cheema, H.; McNamara, L.; Hunt, L.A.; Hammer, N.I.; Delcamp, J.H. Ullazine Donor-π bridge-Acceptor Organic Dyes for Dye-Sensitized Solar Cells. *Chem. Eur. J.* **2018**, *24*, 5939–5949. [CrossRef] [PubMed]
5. Cebrián, C. Ullazine-based materials: Towards novel opportunities in organic electronics. *J. Mater. Chem. C* **2018**, *6*, 11943–11950. [CrossRef]
6. Li, Y.; Li, X.; Xu, Y. Theoretical screening of high-efficiency sensitizers with D-π-A framework for DSSCs by altering promising donor group. *Sol. Energy.* **2020**, *196*, 146–156. [CrossRef]
7. Le Bao, Q.; Thogiti, S.; Koyyada, G.; Kim, J.H. Synthesis and photovoltaic performance of novel ullazine-based organic dyes for dye-sensitized solar cells. *Jpn. J. Appl. Phys.* **2019**, *58*, 12011. [CrossRef]
8. Das, A.; Ghosh, I.; König, B. Synthesis of pyrrolo1,2-aquinolines and ullazines by visible light mediated one- and twofold annulation of N-arylpyrroles with arylalkynes. *Chem. Commun.* **2016**, *52*, 8695–8698. [CrossRef] [PubMed]
9. Pierrat, P.; Hesse, S.; Cebrián, C.; Gros, P.C. Controlling charge-transfer properties through a microwave-assisted mono- or bis-annulation of dialkynyl-N-(het)arylpyrroles. *Org. Biomol. Chem.* **2017**, *15*, 8568–8575. [CrossRef]
10. Kanno, K.; Liu, Y.; Iesato, A.; Nakajima, K.; Takahashi, T. Chromium-mediated synthesis of polycyclic aromatic compounds from halobiaryls. *Org. Lett.* **2005**, *7*, 5453–5456. [CrossRef]
11. Drigo, N.A.; Paek, S.; Huckaba, A.J.; Schouwink, P.A.; Tabet, N.; Nazeeruddin, M.K. Approaches for Selective Synthesis of Ullazine Donor-Acceptor Systems. *Chem. Eur. J.* **2017**, *23*, 17209–17212. [CrossRef] [PubMed]
12. Zhang, G.; Gautam, P.; Chan, J.M.W. Symmetrical and unsymmetrical fluorine-rich ullazines via controlled cycloaromatizations. *Org. Chem. Front.* **2020**, *7*, 787–795. [CrossRef]
13. Qiao, H.; Deng, Y.; Peng, R.; Wang, G.; Yuan, J.; Tan, S. Effect of π-spacers and anchoring groups on the photovoltaic performances of ullazine-based dyes. *RSC Adv.* **2016**, *6*, 70046–70055. [CrossRef]
14. Wan, D.; Li, X.; Jiang, R.; Feng, B.; Lan, J.; Wang, R.; You, J. Palladium-Catalyzed Annulation of Internal Alkynes: Direct Access to π-Conjugated Ullazines. *Org. Lett.* **2016**, *18*, 2876–2879. [CrossRef] [PubMed]
15. Richter, M.; Fu, Y.; Dmitrieva, E.; Weigand, J.J.; Popov, A.; Berger, R.; Liu, J.; Feng, X. Polycyclic Aromatic Hydrocarbons Containing A Pyrrolopyridazine Core. *ChemPlusChem* **2019**, *84*, 613–618. [CrossRef]
16. Liu, J.; Feng, X. Bottom-Up Synthesis of Nitrogen-Doped Polycyclic Aromatic Hydrocarbons. *Synlett* **2020**, *31*, 211–222. [CrossRef]
17. Berger, R.; Wagner, M.; Feng, X.; Müllen, K. Polycyclic aromatic azomethine ylides: A unique entry to extended polycyclic heteroaromatics. *Chem. Sci.* **2015**, *6*, 436–441. [CrossRef] [PubMed]
18. Ito, S.; Tokimaru, Y.; Nozaki, K. Isoquinolino4,3,2-dephenanthridine: Synthesis and its use in 1,3-dipolar cycloadditions to form nitrogen-containing polyaromatic hydrocarbons. *Chem. Commun.* **2015**, *51*, 221–224. [CrossRef] [PubMed]
19. Tokimaru, Y.; Ito, S.; Nozaki, K. Synthesis of Pyrrole-Fused Corannulenes: 1,3-Dipolar Cycloaddition of Azomethine Ylides to Corannulene. *Angew. Chem. Int. Ed.* **2017**, *56*, 15560–15564. [CrossRef]
20. Hager, J.; Kang, S.; Chmielewski, P.J.; Lis, T.; Kim, D.; Stępień, M. Acenaphthylene-fused ullazines: Fluorescent π-extended monopyrroles with tunable electronic gaps. *Org. Chem. Front.* **2022**, *9*, 3179–3185. [CrossRef]
21. Miao, D.; Aumaitre, C.; Morin, J.-F. Photochemical synthesis of π-extended ullazine derivatives as new electron donors for efficient conjugated D–A polymers. *J. Mater. Chem. C* **2019**, *7*, 3015–3024. [CrossRef]
22. Hou, D.; Balli, H. A Novel Heterocyclic Ring System: Synthesis and Spectral Data of 4,8,9b-Triazacyclopenta[*c*,*d*]phenalene. *Helv. Chim. Acta* **1992**, *75*, 2608–2612. [CrossRef]
23. Janke, S.; Boldt, S.; Nakielski, P.; Villinger, A.; Ehlers, P.; Langer, P. Synthesis and Properties of 5-Azaullazines. *J. Org. Chem.* **2023**, *88*, 10470–10482. [CrossRef] [PubMed]
24. Boldt, S.; Parpart, S.; Villinger, A.; Ehlers, P.; Langer, P. Synthesis and Properties of Aza-ullazines. *Angew. Chem. Int. Ed.* **2017**, *56*, 4575–4578. [CrossRef]
25. Ge, Q.; Li, B.; Wang, B. Synthesis of substituted benzoijimidazo2,1,5-dequinolizine by rhodium(III)-catalyzed multiple C-H activation and annulations. *Org. Biomol. Chem.* **2016**, *14*, 1814–1821. [CrossRef] [PubMed]
26. Davies, D.L.; Ellul, C.E.; Macgregor, S.A.; McMullin, C.L.; Singh, K. Experimental and DFT Studies Explain Solvent Control of C-H Activation and Product Selectivity in the Rh(III)-Catalyzed Formation of Neutral and Cationic Heterocycles. *J. Am. Chem. Soc.* **2015**, *137*, 9659–9669. [CrossRef] [PubMed]
27. Li, C.; Liu, Y.; Sun, Z.; Zhang, J.; Liu, M.; Zhang, C.; Zhang, Q.; Wang, H.; Liu, X. Synthesis, Characterization, and Properties of Bis-BN Ullazines. *Org. Lett.* **2018**, *20*, 2806–2810. [CrossRef] [PubMed]
28. Guo, Y.; Zhang, L.; Li, C.; Jin, M.; Zhang, Y.; Ye, J.; Chen, Y.; Wu, X.; Liu, X. BN/BO-Ullazines and Bis-BO-Ullazines: Effect of BO Doping on Aromaticity and Optoelectronic Properties. *J. Org. Chem.* **2021**, *86*, 12507–12516. [CrossRef] [PubMed]
29. Polkaehn, J.; Molenda, R.; Cordero, M.A.; Lochbrunner, S.; Boldt, S.; Ehlers, P.; Villinger, A.; Langer, P. Synthesis and Properties of 5,7-Diazaullazines. *J. Org. Chem.* **2024**, *89*, 2169–2181. [CrossRef]

30. Polkaehn, J.; Thom, R.; Ehlers, P.; Villinger, A.; Langer, P. π-Expanded azaullazines: Synthesis of quinolino-azaullazines by Povarov reaction and cycloisomerisation. *Org. Biomol. Chem.* **2024**. [CrossRef]
31. Spruner von Mertz, F.; Molenda, R.; Boldt, S.; Villinger, A.; Ehlers, P.; Langer, P. Synthesis and Properties of Diphenylbenzojnaphtho2,1,8-def2,7phenanthrolines. *Chem. Eur. J.* **2023**, *29*, e202204011. [CrossRef] [PubMed]
32. Chen, J.; Li, J.; Xie, L.; Fan, H.; Sheng, X.; Du, Y.; Liu, G.; Hu, H.; Jiang, Y.; Chen, M. Iron-catalyzed divergent approach to naphthyridinones and quinolinones: Leveraging Povarov and carbonyl-alkyne metathesis reactions of electron deficient alkynes. *Org. Chem. Front.* **2023**, *10*, 5505–5511. [CrossRef]
33. Chakraborty, B.; Kar, A.; Chanda, R.; Jana, U. Application of the Povarov Reaction in Biaryls under Iron Catalysis for the General Synthesis of Dibenzoa, cAcridines. *J. Org. Chem.* **2020**, *85*, 9281–9289. [CrossRef] [PubMed]
34. Sobhani, M.; Frey, A.; Rettmann, A.; Thom, R.; Villinger, A.; Ehlers, P.; Langer, P. Synthesis of Dibenzotropones by Alkyne-Carbonyl Metathesis. *J. Org. Chem.* **2021**, *86*, 14420–14432. [CrossRef]
35. CCDC 2332651 Contains the Supplementary Crystallographic Data for This Paper. Available online: www.ccdc.cam.ac.uk/data_request/cif (accessed on 19 February 2024).
36. Paenurk, E.; Gershoni-Poranne, R. Simple and efficient visualization of aromaticity: Bond currents calculated from NICS values. *Phys. Chem. Chem. Phys.* **2022**, *24*, 8631–8644. [CrossRef]
37. Schleyer, P.v.R.; Maerker, C.; Dransfeld, A.; Jiao, H.; van Eikema Hommes, N.J.R. Nucleus-Independent Chemical Shifts: A Simple and Efficient Aromaticity Probe. *J. Am. Chem. Soc.* **1996**, *118*, 6317–6318. [CrossRef] [PubMed]
38. Brouwer, A.M. Standards for photoluminescence quantum yield measurements in solution (IUPAC Technical Report). *Pure Appl. Chem.* **2011**, *83*, 2213–2228. [CrossRef]
39. Vardanyan, A.; Boldt, S.; Villinger, A.; Ehlers, P.; Langer, P. Synthesis and Properties of 1-Azapyrenes. *J. Org. Chem.* **2022**, *87*, 11296–11308. [CrossRef] [PubMed]
40. Vardanyan, A.; Argüello Cordero, M.A.; Lochbrunner, S.; Villinger, A.; Ehlers, P.; Langer, P. Synthesis and Properties of 4- and 10-Benzoyl-1-azapyrenes. *J. Org. Chem.* **2024**, *89*, 2155–2168. [CrossRef]
41. Parpart, S.; Boldt, S.; Ehlers, P.; Langer, P. Synthesis of Unsymmetrical Aza-Ullazines by Intramolecular Alkynyl-Carbonyl Metathesis. *Org. Lett.* **2018**, *20*, 122–125. [CrossRef]
42. Pommerehne, J.; Vestweber, H.; Guss, W.; Mahrt, R.F.; Bässler, H.; Porsch, M.; Daub, J. Efficient two layer leds on a polymer blend basis. *Adv. Mater.* **1995**, *7*, 551–554. [CrossRef]
43. Frisch, M.J.; Trucks, G.W.; Schlegel, H.B.; Scuseria, G.E.; Robb, M.A.; Cheeseman, J.R.; Scalmani, G.; Barone, V.; Petersson, G.A.; Nakatsuji, H.; et al. *Gaussian 16 Rev. C.01*; Gaussian, Inc.: Wallingford, CT, USA, 2016.
44. Xiang, J.; Zheng, L.; Chen, F.; Dang, Q.; Bai, X. A cascade reaction consisting of Pictet-Spengler-type cyclization and Smiles rearrangement: Application to the synthesis of novel pyrrole-fused dihydropteridines. *Org. Lett.* **2007**, *9*, 765–767. [CrossRef] [PubMed]

Curriculum Vitae

Jonas Polkaehn geboren am 20.02.1997 in Lübeck

Beruflicher Werdegang

10/2021 – 09/2024 **Wissenschaftlicher Mitarbeiter**

- Universität Rostock

10/2020 – 09/2021 **Wissenschaftliche Hilfskraft**

- Universität Rostock

Ausbildung

10/2021 – 06/2025 **Promotionsstudium (Chemie)**

- Universität Rostock, Arbeitsgruppe Prof. Dr. Dr. h.c. mult. Peter Langer
- Dissertation: „Synthesis and Properties of Ullazine Derivatives“

10/2019 – 09/2021 **Master of Science (Chemie)**

- Universität Rostock, Arbeitsgruppe Prof. Dr. Dr. h.c. mult. Peter Langer
- Gesamtnote: 1.3
- Masterarbeit: „Synthese polyzyklischer Heteroaromaten“, Note: 1.0

10/2016 – 08/2019 **Bachelor of Science (Chemie)**

- Universität Rostock, Arbeitsgruppe Prof. Dr. Dr. h.c. mult. Peter Langer
- Gesamtnote: 2.0
- Bachelorarbeit: „Synthese von Thieno[2′,3′,4′:4,5] naphto-[1,8-*cd*]pyridinen“, Note: 1.0

08/2007 – 06/2016 **Allgemeine Hochschulreife**

- Katharineum zu Lübeck

Tagungen

10/2023 **6th Erlangen Symposium on Synthetic Carbon Allotropes**

- Posterbeitrag: Synthesis of π-expanded (aza)-pyrenes by CH-activation and investigations on their optoelectronic properties

Publikationen

(1) Franziska Spruner von Mertz, Jonas Polkaehn, Alexander Villinger, Peter Ehlers, Peter Langer, *J. Org. Chem.* **2025**, *90*, 1024-1035. "π-Expanded and N-Doped Fluoranthenes"

(2) Arpine Vardanyan, Jonas Polkaehn, Marie-Louis Bauder, Alexander Villinger, Peter Ehlers and Peter Langer, *Org. Biomol. Chem*., **2024**, *22*, 8631-8648. " Synthesis and properties of thienonaphtho[bc]pyridines and thienonaphtho[bc]quinolines"

(3) Jonas Polkaehn, Peter Ehlers, Alexander Villinger, Peter Langer, *Molecules* **2024***, 29*, 2159. "Divergent Synthesis of 5,7-Diazaullazines Derivatives through a Combination of Cycloisomerization with Povarov or Alkyne–Carbonyl Metathesis"

(4) Jonas Polkaehn, Richard Thom, Peter Ehlers, Alexander Villinger, Peter Langer, *Org. Biomol. Chem.* **2024**, *22*, 2027-2042. "π-Expanded azaullazines: synthesis of quinolino-azaullazines by Povarov reaction and cycloisomerisation"

(5) Jonas Polkaehn, Ricardo Molenda, Miguel A. Cordero, Stefan Lochbrunner, Sebastian Boldt, Peter Ehlers, Alexander Villinger, Peter Langer, *J. Org. Chem.* **2024**, *89*, 2169-2211. "Synthesis and Properties of 5,7-Diazaullazines"

(6) Jonas Polkaehn, Peter Ehlers, Alexander Villinger, Peter Langer, *Org. Biomol. Chem.* **2023**, *21*, 9669-9676. "Pyrene-bridged acenaphthenes: synthesis and properties of a diacenaphtho[1,2-*e*:1′,2′-*l*]pyrene and its symmetrical nitrogen analogue"

(7) Ricardo Molenda, Jonas Polkaehn, Miguel A. Cordero, Alexander Villinger, Peter Ehlers, Stefan Lochbrunner, Peter Langer, *J. Org. Chem.* **2023**, *88*, 8802–8824. "Synthesis and Properties of Thieno[2′,3′,4′:4,5]naphtho[1,8-*cd*]pyridines"